NOTE TO USERS

This reproduction is the best copy available.

UMI®

Syntheses and Evaluation of Novel Porpholactones for Photonic Applications

Kimberly S.F. Lau

A dissertation submitted in partial fulfillment of the
requirements for the degree of:

Doctor of Philosophy

University of Washington

2006

Program Authorized to Offer Degree:

Department of Chemistry

University of Washington

Graduate School

This is to certify that I have examined this copy of a doctoral dissertation by

Kimberly S.F. Lau

and have found that it is complete and satisfactory in all respects,
and that any and all revisions required by the final
examining committee have been made.

Chair of Supervisory Committee:

_____

Martin P. Gouterman

Reading Committee:

_____

Martin P. Gouterman

_____

Gamal E. Khalil

_____

Christian Brückner

Date: _____

In presenting this dissertation in partial fulfillment of the requirements for the doctoral degree at the University of Washington, I agree that the Library shall make its copies freely available for inspection. I further agree that extensive copying of the dissertation is allowable only for scholarly purposes, consistent with "fair use" as prescribed in the U.S. Copyright Law. Requests for copying or reproduction of this dissertation may be referred to Proquest Information and Learning, 300 North Zeeb Road, Ann Arbor, MI 48106-1346, 1-800-521-0600, to whom the author has granted "the right to reproduce and sell (a) copies of the manuscript in microform and/or (b) printed copies of the manuscript made from microform."

Signature _____

Date _____

University of Washington

Abstract

Syntheses and Evaluation of Novel Porpholactones for Photonic Applications

Kimberly S.F. Lau

Chairperson of the Supervisory Committee:
Professor Martin P. Gouterman
Department of Chemistry

Previous research by our group has led to the development of a platinum porpholactone-based oxygen permeable luminescent coating that was applied as a Pressure Sensitive Paint (PSP). Oxygen partial pressures can be measured through the oxygen-dependent modulation of luminescence intensity or luminescence decay rate (lifetime). Rapid and sensitive oxygen measurements are much sought after in the physical sciences. Particularly for applications in biological systems, near-IR absorbing and emitting chromophores are desired.

We describe here the step-by-step syntheses of a range of novel porpholactones, their dihydroxylation products (dihydroxylactones), and dilactones in which two porphyrinic β,β'-bonds have been replaced with lactone moieties. An OsO_4-mediated dihydroxylation of porphyrins, porpholactone or dihydroxychlorins was followed by an MnO_4^--induced cleavage of the diol moiety under phase transfer catalysis. Both the *meso-* and metallated versions of the tetraphenyl- and -tetrafluorophenyl-series were prepared, each providing their unique synthetic challenges.

Several members of the novel chromophores were characterized by UV-vis and IR spectroscopy, NIR emission and excitation, ^{1}H and ^{13}C NMR, mass spectroscopy, and X-ray crystallography. Further, we report on the unique chemical characteristics of the novel chromophores.

Table of Contents

List of Figures

List of Schemes

List of Tables

Acknowledgements

Dedication

This dissertation is dedicated to my advisor Professor Martin P. Gouterman (aka "Dr. G"). His first PhD graduate became a Nobel laureate. As his last graduate student, I have the privilege of adding the bookend to an era of scientific influence. Thank you Dr. G for being an amazing mentor, advisor, and friend.

Chapter 1 – Introduction

Section 1: Porphyrin Structure and Synthesis

A porphyrin is a heterocyclic macrocycle consisting of four pyrrole subunits linked through four methine bridges. The name *porphyrin* is derived from the Greek word for the color *purple* and was first used in the naming of hematoporphyrin by Hoppe-Seyler.[1, 1978 #28] There is much known about porphyrins and the macrocycle's related chlorins, bacteriochlorins, and isobacteriochlorins. The basic structures of which are shown in Figure 1.1.[1, 2]

A chlorin is produced when one of the four pyrrolic subunits is reduced to a pyrroline. If two of the pyrrolic subunits are reduced, then either a bacteriochlorin or an isobacteriochlorin is formed depending on the relative positions of the reduction sites. Many natural products such as heme and chlorophyll are derived from these basic macrocycles. Synthetic porphyrins are of significant interest because of their many medical and technological applications in, for instance, photodynamic therapy, light harvesting devices, and pressure sensitive paints.[3-9]
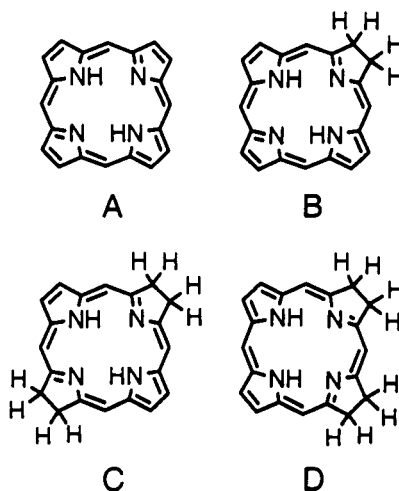
Figure 1.1 Basic macrocycles of A) porphyrins, B) chlorins, C) bacteriochlorins, D) isobacteriochlorins.

The most common naturally occurring porphyrin is hematoporphyrin and its Fe-complex, found as the prosthetic group in hemoglobin, myoglobin, cytochrome C, and the cytochrome P450 family. The main function of hemoglobin and myoglobin is the retention of diatomic oxygen (O_2) and delivering it for enzymatic reactions (Figure 1.2). The iron atom of every heme group can bind one molecule of O_2. Heme groups are also found in cytochromes used in electron transport and cytochrome P450, nature's primary oxidation enzymes.[10]

Chlorophyll, its name derived from the Greek *chloros* for green and *phyllon* for leaf, is a magnesium chlorin complex in plants that harvests light. After absorption, this light is used through photosynthesis to oxidize electrons from water, producing O_2 and energy in the form of ATP and NADPH, which is ultimately used to transform CO_2 to carbohydrates. Found in plants, algae, and cyanobacteria, chlorophyll's intense green color is due to its strong absorption in the blue and weak absorption in the red regions of the electromagnetic spectrum. Other naturally occurring examples of porphyrin-like macrocycles include vitamin B12 and coenzyme F430, which are used in various bio-catalytic processes.[10]
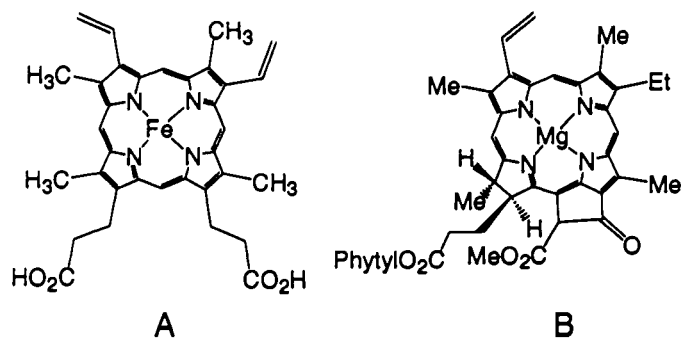
Figure 1.2 Naturally occurring porphyrins and chlorins: A) heme, and B) chlorophyll a.

The numbering and common nomenclature of the ring positions of the porphyrin macrocycle are shown in Figure 1.3. The positions adjacent to the nitrogens on the pyrrole ring are referred to as the α-positions, while the peripheral positions are called the β-positions. The methine bridges are frequently called the *meso*-position.
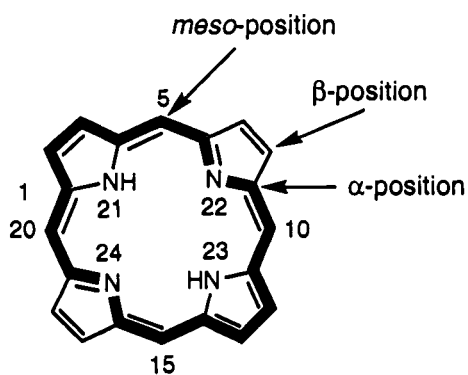
Figure 1.3 Numbering and nomenclature of porphyrinic positions with the porphyrin 18π-electron pathway shown in bold.

The porphyrin macrocycle is an aromatic system containing 22 conjugated π-electrons. To maintain aromaticity, only 18 of them need to be involved in any one delocalization pathway. Porphyrins have been shown by X-ray crystallography to be planar, obeying Hückel's rule of aromaticity, having (4n + 2) π-electrons where n = 0, 1, 2....[11] This allows for the aforementioned chlorins, bacteriochlorins, and isobacteriochlorins, shown in Figure 1.1, to maintain an 18π-aromatic system despite the reduction of one or two β,β'-double bonds. Thus, the electronic structure of the inner 16-membered ring, highlighted in bold in Figure 1.3, is responsible for the photophysical and chemical properties of these macrocycles.

Porphyrins can undergo a number of chemical reactions typical of aromatic compounds. For example, the β-positions often undergo electrophilic aromatic substitution reactions such as formylation, nitration, and halogenation.[3] In addition, the β,β'-double bonds can also undergo some characteristic olefin reactions including dehydroxylation by OsO_4. Furthermore, substituents at the β- and meso-positions on a porphyrin molecule can be introduced. As seen with heme and chlorophyll in Figure 1.2, the β–substituted porphyrins closely mimic natural porphyrin systems. On the other hand, meso-substituted porphyrins have no natural counterparts, but have found wide application as biomimetic models and in materials chemistry.[3, 12] This is due to their relatively facile syntheses.

The common synthesis of meso-substituted porphyrins involves the condensation of aryl aldehydes and pyrrole. These syntheses are characterized by the formation of a porphyrinogen intermediate, which is then converted to the porphyrin through oxidation. In 1936 Rothemund performed this reaction at high temperatures in sealed tubes under basic conditions.[13] Due to resulting low yields, variations of the procedure have since been developed to simplify the reaction and to increase yields and purity. During the 1960's, Adler and Longo increased overall yield of the reaction product by performing the reaction in refluxing acetic acid under aerobic conditions (Scheme 1.1). In this fashion, their meso-tetraphenylporphyrin crystallizes out of solution as the crude reaction

product in approximately 30% yields.[14, 15] Due to its scalability, the Adler method is often used for the synthesis of larger batches of porphyrins. In the 1980's Lindsey developed a higher yielding (up to 60%) method that, however, is only suitable for small scale syntheses.[16, 17]
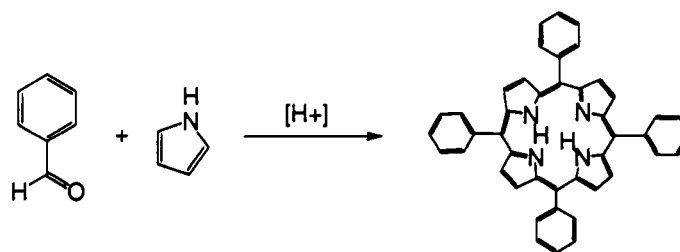
Scheme 1.1 Adler/Longo synthesis of *meso*-substituted porphyrins.

As a result of these advances, the most commonly used *meso*-substituted porphyrin is *meso*-tetraphenylporphyrin (TPP). Other *meso*-substituted porphyrins, such as *meso*-tetrapentafluorophenylporphyrin (TFPP), are also readily available albeit in lower yields.

Section 2: Porpholactones

In 1984, Maxwell Crossley and Lionel King described the formation of tetraphenylporpholactone. Starting with 2-amino-5,10,15,20-tetraphenylporphyrin **1.1**, available by reduction of the corresponding nitroporphyrin, Crossley and co-workers performed oxidative modifications on the periphery of the macrocycle. In their proceedure, **1.1** was photo-oxidized to the 17–imino–18–oxochlorin **1.2**, which was then converted to the 17,18-dioxochlorin **1.3** upon hydrolysis on silica gel. When reacted with MCPBA, **1.1** also gave the novel 18–oxo–17–oxachlorin (porpholactone) **1.4**. Porpholactone is also formed by treatment of **1.2** with MCPBA. Treatment of **1.3** with

MCPBA did not quantitatively form porpholactone, but instead produced the 17,18a-dioxo-18a-homo-17-oxachlorin **1.5** containing a six-membered ring. Porpholactone was again synthesized by base induced ring-opening followed by decarboxylation of **1.5**; however, this procedure did not produce the desired secochlorin derivative.[18] In his later work, Crossley also reported the appearance of **1.4** as an overoxidation product in the cleavage of the cyclic anhydride **1.5** by methanolysis (Scheme 1.2).[19]
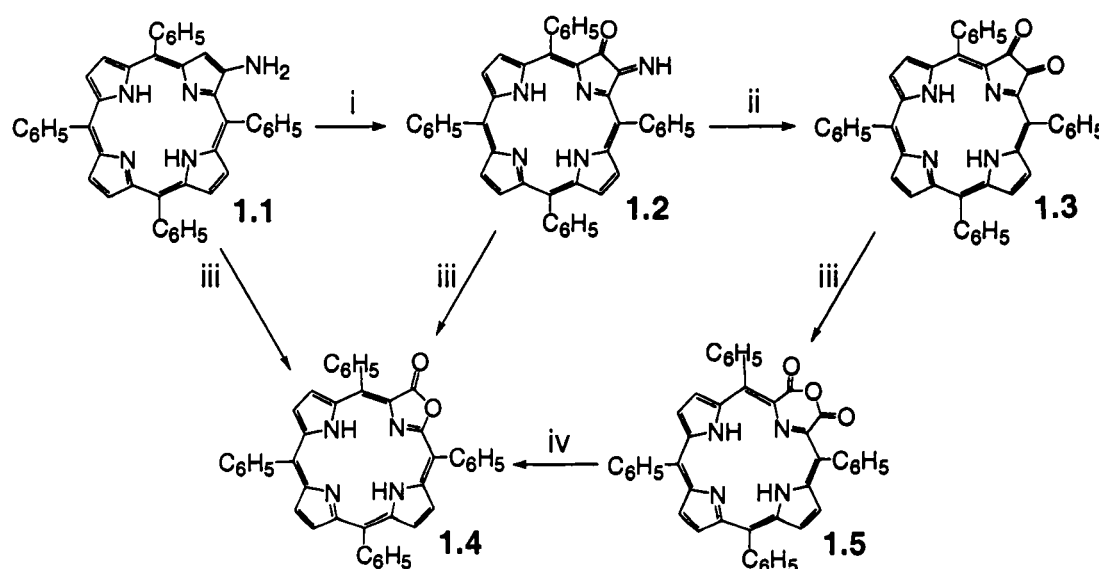
Scheme 1.2 Crossley's introduction of oxygen into the β-position of porphyrins. Conditions: i) hυ, O_2; ii) H+/H_2O or silica gel; iii) MCPBA; iv) NaOH, H_2O, DMF.

In 1986, *meso*-tetra(pentafluorophenyl)porpholactone **1.7** was synthesized by Martin Gouterman, Gamal Khalil, and co-workers in an attempt to synthesize silver *meso*-tetra(pentafluorophenyl)porphyrin (Scheme 1.3). In their procedure, *meso*-tetra(pentafluorophenyl)porphyrin **1.6**, and silver nitrate were heated at reflux in glacial acetic acid for a period of six hours. This reaction did not produce the expected silver tetra(pentafluorophenyl)porphyrin, but instead yielded *meso*-tetra(pentafluorophenyl)porpholactone as shown by ^1H NMR, ^{19}F NMR, and FTIR.[20]
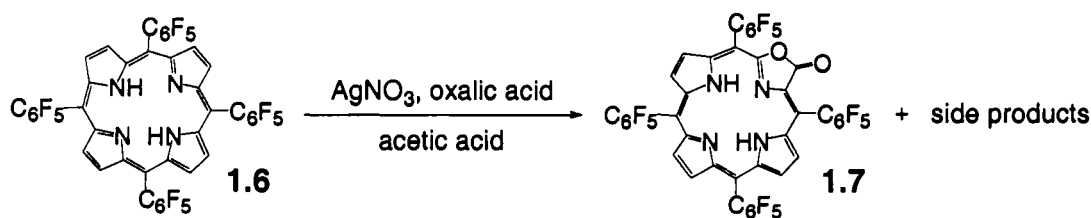
Scheme 1.3 Gouterman - Khalil one-pot reaction to porpholactone.

Here Gouterman and co-workers were able to prepare the lactone **1.7** directly from the free base porphyrin **1.6**, using mild reagents. More recently, Zelelow et. al further refined the synthetic procedure by refluxing **1.6**, $AgNO_3$, glacial acetic acid, and oxalic acid for approximately 3-4 hours in a one pot reaction.[21] However in both these approaches, a multitude of side products decreases the ability for absolute separation and isolation of the desired porpholactone **1.7**, also affecting overall yields.

In 2003, Brückner and co-workers introduced a new series of pyrrole-modified, novel free base porphyrin macrocycles (Scheme 1.4). *meso*-Tetraaryl-2, 3-dihydroxy chlorin **1.9**, was made from the oxidation of *meso*-tetraphenylporphyrin **1.8**, with a stoichiometric amount of OsO_4 in the presence of pyridine. $NaIO_4$ heterogenized on silica gel and supended in a $CHCl_3$ solution of **1.9** produced the secochlorin **1.10**. The reaction of **1.10** under acid catalysis provided the morpholinochlorin **1.11**, with porpholactone **1.12**, as the major isolated side product. The reaction of **1.9** with $NaIO_4$/silica under N_2 in the presence of alcohol also provided **1.11**. Aside from their novel morpholinochlorin synthesis, Brückner and co-workers found that the MnO_4^- induced cleavage of **1.9** under phase transfer catalysis generated the corresponding secochlorin biscarboxylate which spontaneously cyclized and decarboxylated to form porpholactone **1.12**.[22]

Scheme 1.4 Brückner's morpholinochlorin and porpholactone synthesis. i) OsO_4/pyridine, H_2S, ii) $NaIO_4$/silica, in $CHCl_3$, iii) H+, iv) $NaIO_4$/silica under N_2 in alcohol, v) MnO_4^-.

The generalized concept of the "breaking and mending" of porphyrins is shown in Scheme 1.5. As seen in the various porpholactone syntheses, a β-position of one of the pyrroles is activated, followed by the cleavage of the β,β'-bond, forming a secochlorin. With a ring-closure reaction, a new heterocycle is formed by inclusion of a heteroatom or formation of a larger ring. These transformations were the first to show that pyrrole-modified porphyrins can be formed by modifications to the periphery of the macrocycle, as opposed to total porphyrin synthesis.
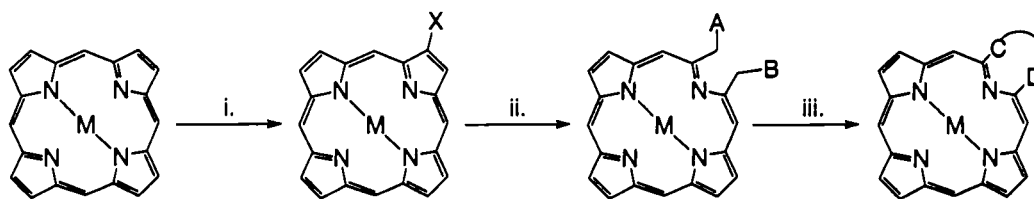
Scheme 1.5 The breaking and mending of porphyrins. i) Activation of the β position. ii) Cleavage of the β,β'-bond. iii) Ring closure and formation of new heterocycle.

Section 3: Metalloporphyrins

An important feature of all porphyrins is their ability to chelate to a wide range of metal ions (e.g. Fe, Zn, Cu, Ni, Pt). A porphyrin with two central hydrogens in its inner cavity is referred to as a *free base* porphyrin whereas the metal complexes are referred to as metalloporphyrins. The porphyrin nucleus is a tetradentate ligand which has a maximum diameter of 3.7 Å of available space for a coordinating metal.[12] Formally, metalloporphyrins are porphyrin derivatives in which at least one of the lone electron pairs residing on the central nitrogen atoms of the porphyrin is shared with a metal ion acting as a Lewis acid.[3] Upon complexation, the metal displaces the two central hydrogens, leaving two negative charges which are distributed equally about the inner ring. Depending upon the size, charge, presence of axial ligands, and preferred coordination geometry by the metal ion, range of metal coordination geometries are found. Metals are commonly used in porphyrin chemistry to induce a conformational or electronic change. They can also be used as protecting or directing groups.
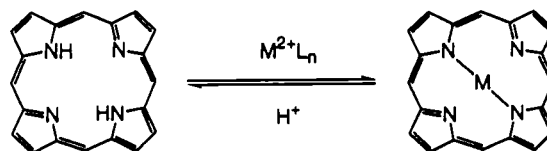
Scheme 1.6 The reversible metallation of the porphyrin macrocycle.

As seen in Scheme 1.6, a common method for metallation involves the addition of a metal acetate to a refluxing solution of porphyrin in an appropriate solvent. Other metal complexes, such as metal acetylacetonates or halides, are also frequently used. More forceful conditions call for higher reflux temperatures and the presence of bases such as pyridine. Porphyrin metallation is potentially a reversible reaction and the metalloporphyrins can be ranked according to the ease of metal removal. This demetalation, can be achieved by treatment with acids of various strengths (Scheme 1.6). One metalloporphyrin is of particular interest to this thesis, the Pt(II) porphyrin.

Platinum insertion into the porphyrin macrocycle induces a heavy atom effect. Because the platinum is in the plane of the porphyrin ring, it is able to interact with the porphyrin π-electron system to increase spin-orbit coupling, thus increasing intersystem crossing from the singlet to triplet excited state. As later discussed in Section 1.4, heavy metal porphyrins tend to have higher triplet yields, shorter triplet lifetimes, and higher phosphorescence yields that increase with the mass of a heavy atom substituent.[2]

Section 4: Photophysics of Porphyrins

Porphyrins are the reason that blood is red and grass is green. They possess planar, rigid, aromatic, π-electron systems that are responsible for many of their electronic and spectroscopic properties. These spectroscopic properties were explained by Gouterman in 1959.[23]

In most species, *electronic transitions* from a ground to an excited state occur between a single highest occupied molecular orbital (HOMO) and a single lowest unoccupied molecular orbital (LUMO) (Figure 1.4A). An *electronic transition* is defined as an electron moving from a filled (HOMO) to an empty (LUMO) orbital which allows for four possible excited states ($\alpha\alpha$, $\beta\beta$, $\alpha\beta + \beta\alpha$ (triplet state), $\alpha\beta - \beta\alpha$ (singlet state)).

These excited states are due to the various electron spin possibilities (α being spin up, β being spin down) in each orbital.

Gouterman's *four orbital theory* shows that porphyrin square planar symmetry leads to the formation of two quasi degenerate HOMOs and two degenerate LUMOs. As with the LUMOs, each HOMO has approximately the same energy (within 1 eV) which is referred to as quasi degeneracy. In Figure 1.4B, the porphyrin is shown to have a total of four excited electronic transitions instead of one. Because of spin degeneracy, for each transition, there are four possible excited states which allow the porphyrin a total of sixteen possible excited states. Each transition also has a polarization since the electric field of the absorbed light has a direction vector. Because porphyrins undergo only $\pi \rightarrow \pi^*$ transitions, light is polarized in only the plane of the molecule, the x- and y-axes. Porphyrin transitions are not polarized along the z-axis because they do not generally undergo $\sigma \rightarrow \pi$ transitions. It has been shown that two porphyrin transitions are polarized along the x-axis while the other two are polarized along the y-axis which pair-wise couple. Figure 1.4D shows that the electronic states resulting from these transitions are split into two high energy, short wavelength (B_x and B_y) and two low energy, long wavelength (Q_x and Q_y) transitions.

More symmetrical or degenerate porphyrins have strongly allowed B transitions and zero probability of Q transitions. Reduction of porphyrin symmetry by ring modifications or addition of substituents lifts degeneracy, changing the distance between the two HOMO-LUMO transitions and increasing the probability of Q transitions (Figure 1.4C, 1.4E). Thus the increased degeneracy of heme allows for its absorption in the blue-green region (490 nm) so that the color red (620 nm) is observed, while the less symmetrical chlorophyll absorbs in the blue (450 nm) and red (650 nm) so that the green/yellow (520-560 nm) of plant species is seen.
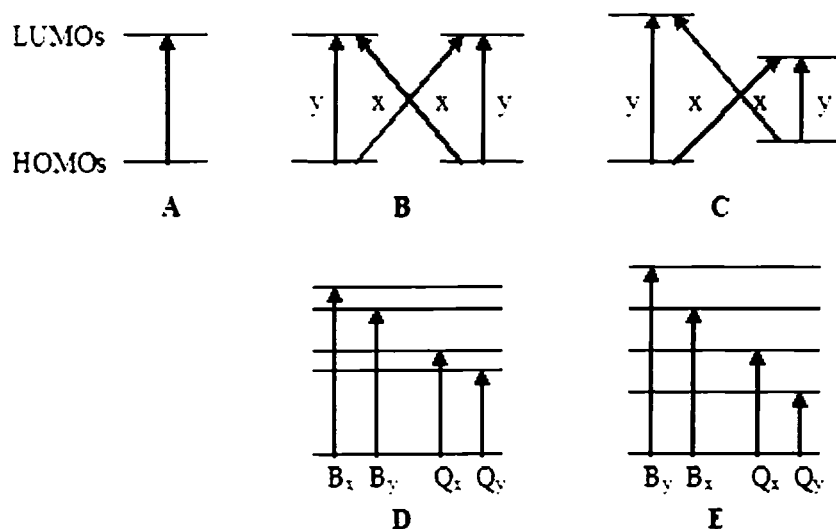
Figure 1.4 A schematic representation of the two highest occupied and two lowest unoccupied molecular orbitals (A-C) and corresponding electrons transitions (D,E) with A) showing undegenerate species, B, D) porphyrins with high degeneracy, and C, E) porphyrins with lower degeneracy.

The absorption spectra of porphyrins and their derivatives are their most characteristic property.[12] All porphyrin and metalloporphyrin absorption spectra contain one very strong absorption band between 400-500 nm. This "Soret" band, also referred to as the "B band", is the most intense absorption band of the porphyrin, with a molar extinction coefficient in the order of 2 to 5 X 10^5, depending on substituents and central metal. Seen above in Figure 1.4, the B_x and B_y transitions in porphyrins are of nearly the same energy, causing a relatively sharp Soret band, while in chlorins these transitions are not of the same energy, which brings about the observed broadening effect.

In addition to the Soret band, porphyrins have multiple less intense visible bands, also referred to as the "Q bands", between 500-800 nm. These Q-bands display more characteristic spectral properties than the Soret band. Q band trends in the UV-vis spectra for free base porphyrins, chlorins, bacteriochlorins, and isobacteriochlorins are shown in Figure 1.5. In free-base porphyrin-like spectra, the four Q-bands decrease in

intensity as the wavelength of absorption increases. On the other hand, the longest wavelength of absorption in chlorin-like spectra is the most intense Q-band. The reduction of one of the β,β'-double bonds in porphyrins causes a bathochromic shift in the UV-vis absorption spectra due to a decrease in the HOMO-LUMO gap. A further long wavelength shift is observed if the porphyrin is reduced to a bacteriochlorin derivative. Absorption maxima for bacteriochlorins are normally above 700 nm. Isobacteriochlorins, on the other hand, have very chlorin-like absorption spectra. Metalloporphyrins also follow the same general trends observed for their free base analogues, but with two Q-bands instead of four.[12, 23]
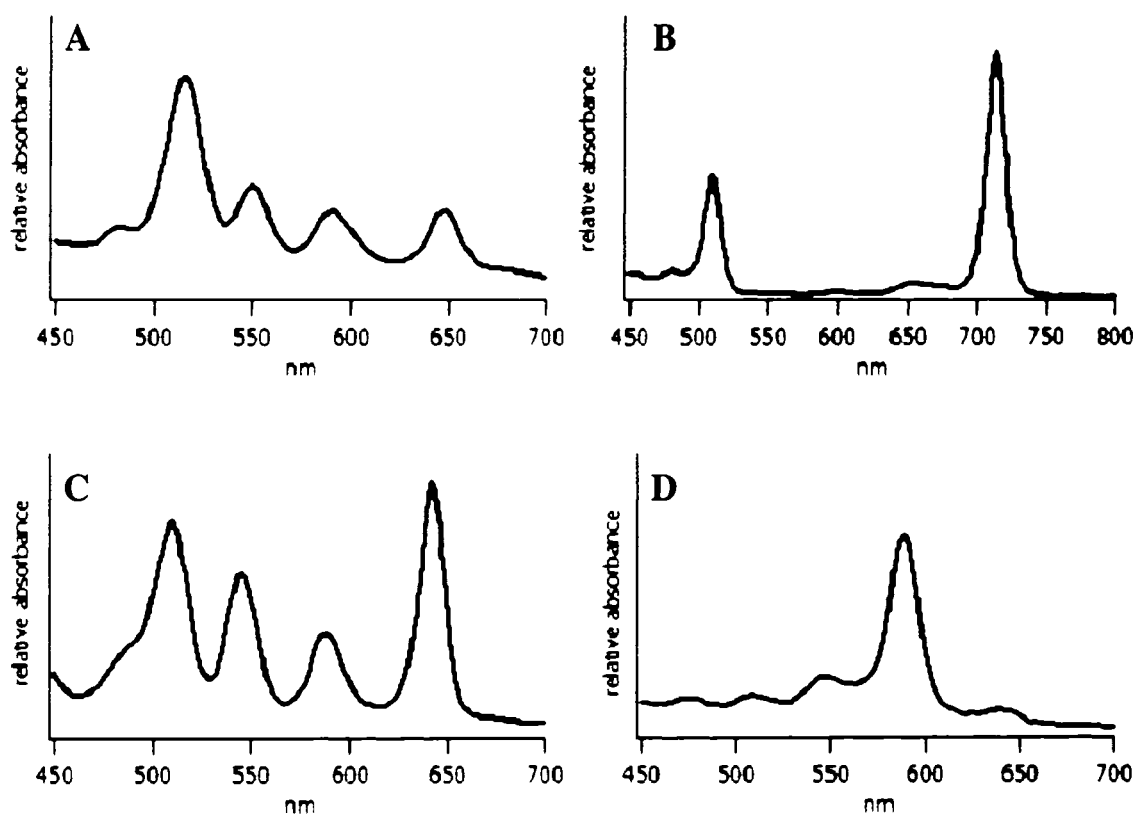
Figure 1.5 Q-bands in the UV-Vis absorbance spectra of various porphyrin derivatives. A) An example of a porphyrin-like UV-Vis spectra. B) An example of a chlorin-like UV-Vis spectra. C) An example of a bacteriochlorin-like UV-Vis spectra. D) An example of an isobacteriochlorin-like UV-Vis spectra.

Porphyrin emission is also an important spectral characteristic. Atoms and molecules have a number of discrete, quantized energy levels dependent on the electron configuration of the species.[24] When a porphyrin is excited by light absorption, relaxation from an excited state down to a lower energy state can result in the emission of light, observed as luminescence. According to the selection rules for electric-dipole transitions, not all transitions between states are allowed based on an examination of the transition dipole moment between the two states of interest. An allowed transition has a transition dipole moment that is nonzero while the transition dipole moment for a forbidden transition is zero.[24]

The energy diagram for porphyrin photoluminescence is depicted in Figure 1.6. Shown is a closed-shell singlet ground state, S_0 with the lowest energy excited singlet state designated as S_1. S_n represents a higher energy excited singlet state containing greater electronic and/or vibrational energy than S_1. T_1 is the lowest energy excited triplet state having a lower energy than S_1 for nearly all closed-shell molecules. Radiationless processes are denoted by dashed arrows while radiative processes are denoted by solid arrows.
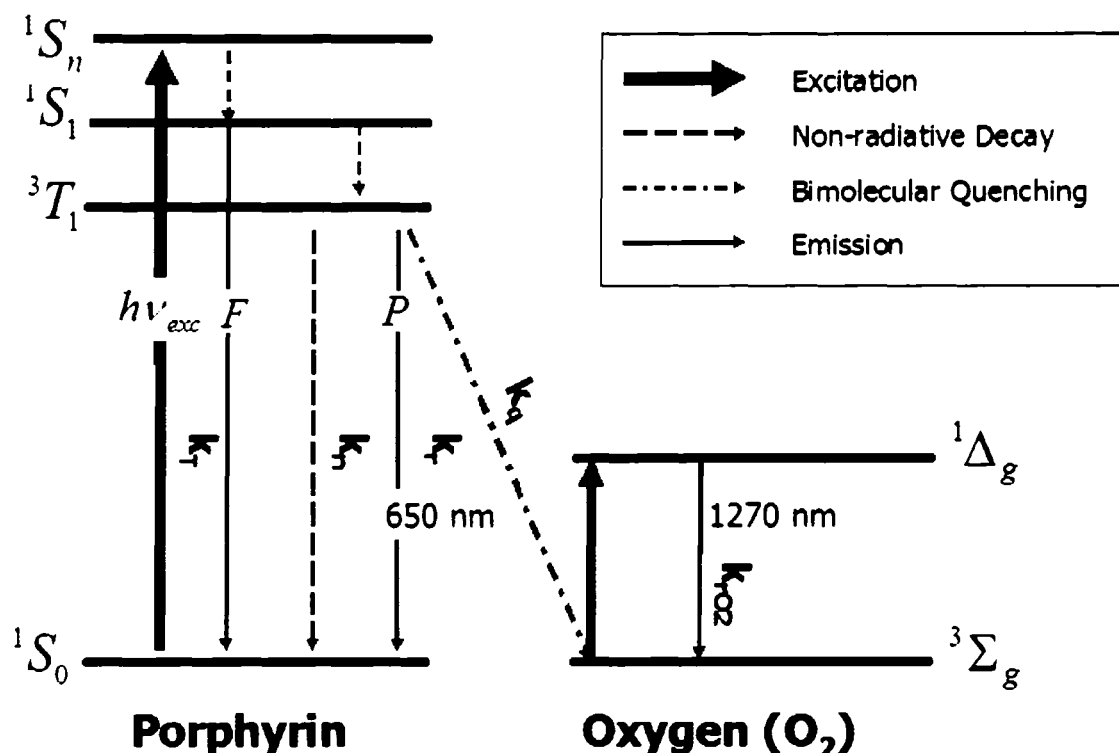
Figure 1.6 Jablonski energy diagram depicting porphyrin interaction with diatomic oxygen.

The term luminescence includes both fluorescence (F) and phosphorescence (P). Fluorescence is the radiative transition of electrons from the first singlet excited state to the singlet ground state ($S_1 \rightarrow S_0$). This produces a relatively short lifetime of the excited state on the order of $10^{-9} - 10^{-7}$ seconds. However, intersystem crossing from the lowest singlet excited state to the triplet state ($S_1 \rightarrow T_1$), attributed to the crossing of the potential energy curves of the two states, can often occur. The process in which an electron radiatively relaxes from this lowest excited triplet state to the singlet ground state ($T_1 \rightarrow S_0$) is referred to as phosphorescence. The phosphorescence quenching of phorphyrins by oxygen occurs through the transfer of energy between the triplet excited state of a porphyrin and the triplet ground state of diatomic oxygen ($T_1 \rightarrow {}^3\Sigma_g$).

The effect of the interaction of a porphyrin in its triplet state with other molecules is referred to as photosensitization (the absorption of visible light by a colored substance which initiates physical or chemical changes in a substrate).[25] When a triplet excited porphyrin, T_1, and triplet ground state oxygen, $^3\Sigma_g$, collide, energy transfer from the porphyrin to the oxygen occurs, creating ground state porphyrin, S_0, and singlet excited oxygen, $^1\Delta_g$. This rapid, spin allowed process is described in Equation 1.1.[26]

$$T_1 + {}^3\Sigma_g \rightarrow S_0 + {}^1\Delta_g \qquad\qquad (1.1)$$

The lowest singlet excited oxygen state, $^1O_2$, is referred to as "singlet oxygen". This bimolecular reaction causes the creation of singlet oxygen while quenching porphyrin phosphorescence.

Singlet oxygen is much more reactive than ground state oxygen and plays a role in the photodegradation of unsaturated or aromatic organic compounds in air. In addition, $^1O_2$ reacts with many organic compounds including olefins, dienes, sulphides, aromatics, hetero-aromatics, terpenes, steroids, fatty acids, flavones, tetracyclines, vitamines, amino acids, proteins, nucleic acids, blood and bile pigments, and synthetic polymers. In the presence of singlet oxygen, many of these compounds can undergo Alder-ene reactions (hydrogen abstraction and oxygen addition), oxygenation, or cycloaddition. The phosphorescence emission of singlet oxygen occurs at 1270 nm. While this luminescence is very weak, it can still be detected.[27]

Phosphorescence is a forbidden transition due to a second electron spin reversal, which contributes to its relatively long lifetimes of 10^{-4} – 10 seconds. In addition, the wavelength of phosphorescence is longer than the wavelength of fluorescence, due to the lower energy of the triplet state. Electron spin reversals can be made allowed by one of two ways:

1) The rotation of the electron around the nucleus in the presence of a heavy atom (e.g. the insertion of Pt(II)) can generate magnetic forces (spin-orbit coupling), which can cause the spin to reverse. (Refer to Section 1.3)

2) Other unpaired electrons (e.g. the unpaired electrons in O_2) lend to the breakdown of spin selection rules.[26]

Because it has two unpaired electrons, O_2 is paramagnetic and unique among the gaseous diatomic molecules. The electron energy level diagram of ground state O_2 is depicted in Figure 1.7. The existence of unpaired valence electrons in a stable molecule is very rare in nature and confers high chemical reactivity. The two electrons least-strongly bound occupy the degenerate π* level and have parallel spins. This degeneracy places diatomic oxygen in a triplet ground state, $^3\Sigma_g$.[28] There are a total of three spin states for O_2, depending on electron occupancy and spin. If the two electrons occupy a single orbital and have opposite spin, a singlet excited state is formed. A second singlet excited state can also be formed if the two electrons occupy separate π* orbitals with opposite spins. These spin states and O_2 energies are shown in Table 1.1.
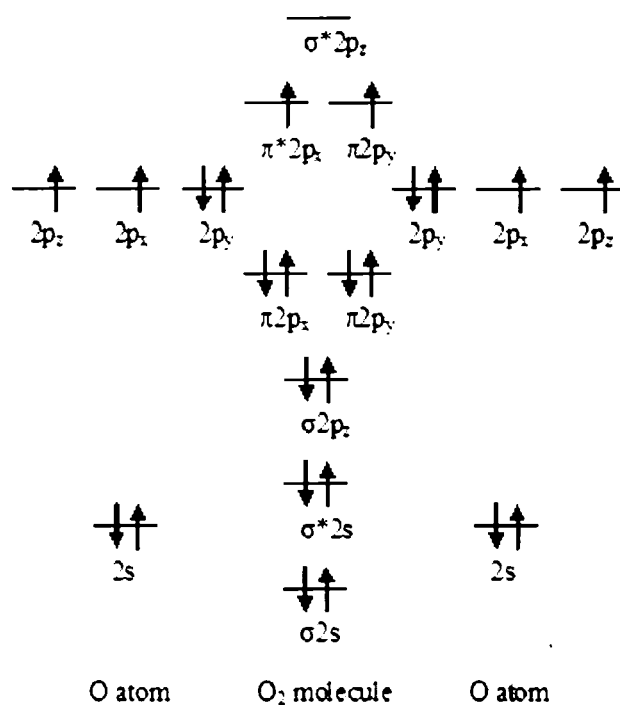
Figure 1.7 Energy level diagram of ground state oxygen, $^3\Sigma_g^-$.

Table 1.1 States and Energies of O_2.

	π_{1+}^*	π_{1-}^*	Energy (kJ/mol)
$^1\Sigma_g^+$	↑	↓	155 [1.61 eV]
$^1\Delta_g$	↓↑		92 [0.95 eV]
$^3\Sigma_g^-$	↑	↑	0 [0 eV] (ground state)

Described by Stern and Volmer, the quenching of both fluorescence and phosphorescence by oxygen is well known.[29-32] The Stern-Volmer relation describes the luminescence of a molecule in solution that is subject to bimolecular quenching by another species such as oxygen. In accordance to the Stern-Volmer relation, the rate of excited state (luminescence) decay in the presence of O_2 is given by,

$$k_T = (k_r + k_n) + k_q p = k_a + k_q p = \tau^{-1} \qquad (1.2)$$

where k_r is the radiative rate of the excited state, k_n is the rate of any intrinsic nonradiative decay process, k_q is the quenching rate due to collisions with oxygen, p is the oxygen pressure, and k_a is the decay rate in the absence of oxygen. τ is the emission lifetime which is the inverse of k_T.

The quantum yield, ϕ of a molecule is defined by,

$$\phi = \frac{k_r}{k_T} \qquad (1.3)$$

where k_r can be described as the rate of luminescence emission, while k is the excited state decay rate.[33, 34] From Equations (1.2) and (1.3), the quantum yield, ϕ_o at a reference pressure, p_o, divided by the quantum yield, ϕ at any other pressure, p is given by,[7, 26, 35]

$$\frac{\phi_o}{\phi} = \frac{k_a + k_q p}{k_a + k_q p_o} \qquad (1.4)$$

Under fixed conditions of excitation and detection, the observed phosphorescence intensity, I is directly proportional to the quantum yield so that Equation 1.4 can be rewritten as,

$$\frac{I_o}{I} = \frac{k_a + k_q p}{k_a + k_q p_o} \qquad (1.5)$$

Thus,

$$\frac{I_o}{I} = A + B\frac{p}{p_o}$$

(1.6)

where $A = \dfrac{k_a}{(k_a + k_q p_o)}$ and $B = \dfrac{k_q p_o}{(k_a + k_q p_o)}$ so that,

$$A + B = 1$$

(1.7)

Section 5: Applications

1.5.a Photodynamic Therapy

meso-Tetraarylporphyrins are generally potent singlet oxygen photosensitizers that have been utilized in the photodynamic destruction of neovascular tissue.[36] Photodynamic therapy (PDT) is a well-recognized treatment for the destruction of tumors, utilizing the ability of a selectively retained photosensitizer, or drug, to elicit an efficient photodynamic reaction upon activation with tissue-penetrating light. The oxidative stress caused by singlet oxygen induces cell apoptosis, or programmed cell death, effectively killing the tumor cell in which the photosensitizer has localized.[3] The most widely used PDT drug, Photofrin is approved in the U.S. for treatment of obstructing cancer of the esophagus and early stage cancer of the bronchus. Clinical trials are also under way using Photofrin for early stage esophageal cancer, head and neck cancers and superficial bladder cancer. In addition, researchers are hoping to use PDT as an adjuvant therapy for brain tumors and intrathoracic and intraperitoneal tumors.[4]

Photofrin and other current porphyrin sensitizers have weak absorbance in the red region of the spectrum (maxima at approximately 630 nm) and induce long-lasting skin photosensitivity. The ideal sensitizer would absorb light strongly in this region of the spectrum and into the near-IR (600-900 nm), where light has greater penetration into

tissue, would have highly efficient photochemistry for killing tumor cells, would localize in or around the tumor and not in normal tissues, and would rapidly clear the system following treatment.[5]

The depth of penetration of light into tissue is limited by optical absorption, due to endogeneous tissue chromophores, mainly hemoglobin, and by optical scattering within the tissue. Both of these parameters differ from tissue to tissue. At the maximum wavelength of Photofrin (approximately 630 nm), light can penetrate the skin to the depths of 0.4 to 3.9 mm to induce cell apoptosis. Increasing the wavelength of absorption from 635 to 700 nm almost doubles the light penetration depth. The increased penetration depth of longer-wavelength light is the major incentive for the development of sensitizers absorbing at wavelengths greater than 700 nm.[4, 5] Much research is currently underway to find a PDT agent with an absorption wavelength greater than 700 nm that will have less detrimental effects than current PDT drugs.

1.5.b Pressure Sensitive Paints

Oxygen quenching of the photo-excited triplet state of Pt(II) complexes of porphyrins is the origin of their utility in pressure-sensitive paints (PSP).[6-9, 37] Previous efforts of our research group have centered on the concept of using porphyrin luminescence quenching to monitor the level of oxygen in order to map the pressure distribution over airfoil surfaces in wind tunnel testing. This research has led to the development of an oxygen permeable luminescent coating that permits continuous mapping of surface pressure. This coating, based upon a luminescent porphyrin dye, is referred to as pressure sensitive paint.

Once synthesized, the porphyrin dyes can be incorporated into a polymer matrix such as polycarbonate or fluoro-acrylic polymer (FIB). As seen in Figure 1.8, sensor films are fabricated by spraying or spin coating samples onto a surface (aluminum, glass, or model). The resulting films have a uniform thickness of ~1 micrometer. This paint is then dried and annealed to the surface at 70° C for thirty minutes. In a wind tunnel, false

color images of pressure distribution can be created based on changes in intensity or lifetime emissions that change with respect to oxygen concentration, as explained in the previous section.
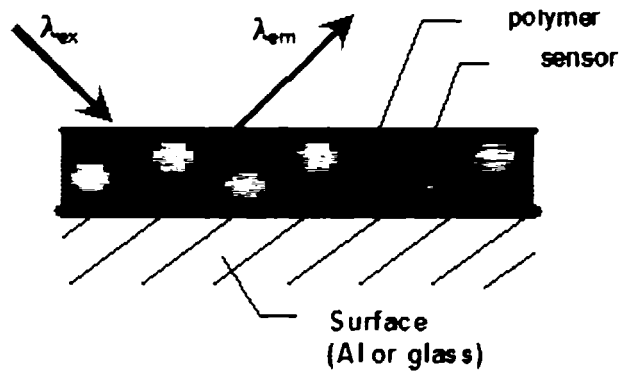
Figure 1.8 The incorporation of porphyrin dye into polymer matrix for use in Pressure Sensitive Paints (PSPs).

PSPs play an important role in aerodynamic testing. Its use provides a number of advantages over the discrete pressure taps traditionally used on conventional wind tunnel models. PSPs allow researchers to obtain continuous quantitative pressure distributions over a surface, visualize dynamic flow processes that measure areas undetectable with conventional pressure taps (e.g., thin trailing edges), as well as acquire real time modeling (Figure 1.9). This has resulted in the more effective integration of experimental and computational fluid dynamics, which has lead to significant reductions in time for the prototyping of new designs.[37]
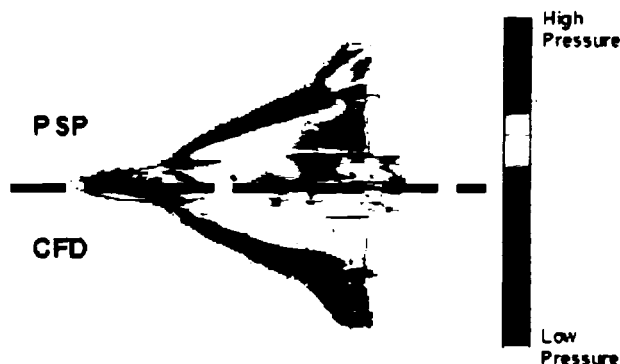
Figure 1.9 Airfoil airplane model comparing PSP measurements and computational fluid dynamics (CFD) in low speed tests on an F-16XL. At an airflow velocity of 100-200 m/s, PSP measurements are comparable to CFD calculations.

We have found that the use of TFPPPt in PSP formulations leads to increased photostability of the coatings, presumably because of the protection the pentafluorophenyl groups provide from singlet-oxygen-mediated oxidative degradation of the chromophore.[6, 9, 38] Pentafluoro substitution on porphyrins was shown to increase photostability by raising the oxidation potential and reducing electron density.[39, 40] Optical stability of fluorinated free base porphyrin was observed in film studies, where meso-tetrakis(perfluorophenyl)porphyrin (TFPPH$_2$) and 5,10,15,20-meso-(tetrakis(heptafluoropropyl)porphyrin (HFPPH$_2$) showed much higher stability in the presence of oxygen. It should be noted that TFPPH$_2$ porphyrin ring is one of the most highly electron deficient porphyrins and has the highest known ionization potential. An optical study of the π-cation concentrations of several porphyrin rings measured in the presence of oxygen and light clearly showed that the TFPPH$_2$ ring had no π-cation presence. This absence of π-cations suggests that no transfer of electrons proceed from the fluorinated porphyrin ring to the oxygen molecule. Further studies consistently show that there is little or no electron transfer from the TFPPH$_2$ porphyrin ring to the metal surface.[20, 41, 42]

Recently our group has developed a luminescent-based *temperature sensitive paint* (TSP) that can be used to accurately measure surface temperature as well as correct for PSP's temperature variations. The temperature sensor is a tris(β-diketonate) phenanthroline europium complex. The two sensors (PSP and TSP) have maximum absorption within the range of 370 – 400 nm, but upon excitation with a broadband illumination at 400 nm, have non-overlapping emission spectra. The PSP platinum tetrakis(perfluorophenyl)porpholactone (TFPLPt) emits at approximately 730 nm while the TSP 1-phenanthren-3-yl-3-phenanthren-9-yl-propane-1, 3-dione (D2) has an emission at approximately 612 nm. As a result, with appropriate band pass optical filters, the two emission lines can be detected separately (Figure 1.10). These luminescent compounds provide a lifetime based dual pressure and temperature sensor when jointly dissolved in a polymer matrix. In addition to the high photostability of the dual system, our studies show that the luminescence properties of one sensor are independent of the presence of the other sensor [6, 43]. A summary of our current PSPs and reference sensors is shown in Tables 1.2 and 1.3.
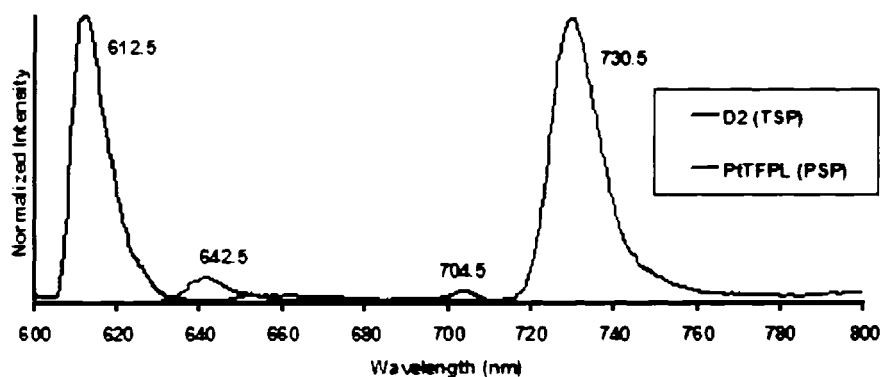
Figure 1.10 Emission spectra of a Temperature Sensitive Paint (TSP) and a PSP showing that the two emissions can be spectrally resolved. Here both sensors can be excited at the same wavelength yet detected separately.

Table 1.2 Absorption wavelengths of current porphyrin PSPs and reference sensors.

Compound Name	Abbreviation	Absorption (nm)		
		B(0,0)	Q(1,0)	Q(0,0)
[meso-tetrakis(pentafluorophenyl)porphyrinato]Mg(II)	TFPPMg	424 (367)	558 (16.7)	594 (1.6)
[meso-tetrakis(pentafluorophenyl)porphyrinato]Pd(II)	TFPPPd	406 (192)	519 (18.2)	552 (15.5)
[meso-tetrakis(pentafluorophenyl)porphyrinato]Y(II)	TFPPY	414 (192)	550 (11.8)	586 (2.5)
[meso-tetrakis(pentafluorophenyl)porphyrinato]Zn(II)	TFPPZn	412 (479)	544 (20.9)	582 (5.4)
[meso-tetrakis(pentafluorophenyl)-2-oxa-3-oxoporphyrinato]Ni(II); Ni-porpholactone	(COO) TFPLNi	404 (143)	550 (10)	592 (47)
[meso-tetrakis(pentafluorophenyl)-2-oxa-3-oxoporphyrinato]Pd(II); Pd-porpholactone	(COO) TFPLPd	412 (120)	544 (9.4)	584 (39.2)
[meso-tetrakis(pentafluorophenyl)-2-oxa-3-oxoporphyrinato]Zn(II); Zn-porpholactone	(COO) TFPLZn	420 (133)	564 (10)	608 (20)

Table 1.3 Emission wavelengths, lifetime measurements, and quantum yields of current porphyrin PSPs and reference sensors.

Abbreviation	Emission (nm) in 3-MP				Lifetime		Quantum Yield
	fluorescence		phosphorescence		τ_f(ns)	τ_p	Φ_f or Φ_f
TFPPMg	596	650	705		5.5		0.08
TFPPPd	562	608	660	736		1.65 ms (660 nm)	
TFPPY	592	646	718		< 1.0		0.01
TFPPZn	586	640	729	816	< 1.0		0.07
(COO)TFPLNi							
(COO)TFPLPd							<0.001
(COO)TFPLZn							0.05

1.5.c Other O₂ Sensors

Recently our laboratory has developed airborne microspheres made of polystyrene beads for pressure measurement in fluid flow.[44] Polystyrene bead microspheres (PSBeads) that contain a dual luminescence from both an oxygen sensitive platinum porphyrin and a pressure insensitive silicon porphyrin are prepared in high uniformity and high synthetic yield. The ratio of the two luminescences responds reversibly in aerodynamic flows over a wide dynamic range of oxygen concentrations and has a response time of < 1 ms.[45] PSBeads are small enough to follow fluid flow accurately and function simultaneously as pressure-sensitive airborne micro-particles. In addition to this, PSP's and our porphyrin sensors have been applied to motor vehicle modeling (Figure 1.11a), insect flight studies (Figure 1.11b), and pancreatic islet cell

maintenance and viability (Figure 1.11c).[46-48] Table 1.4 shows the vast improvements made in our sensor capabilities over the last twenty years.
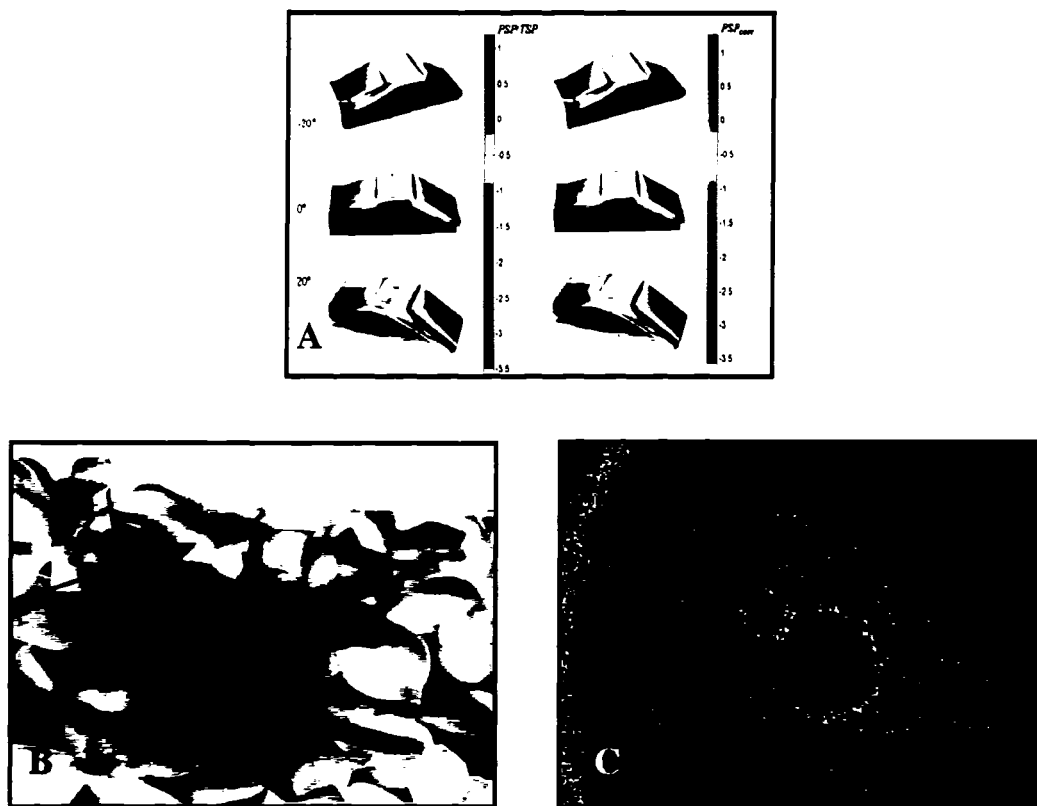
Figure 1.11 A) False color image of pressure distribution over the surface of car models based on emission intensity from PSP. B) A bee's wings coated with PSP. C) Contour map indicating oxygen gradient around two islets.

Table 1.4 Progress in PSP over the Last Twenty Years at the University of Washington.

	1990	2000	2004
Dynamic range for testing Resolution 5 % of range	1.0 bar	50 mbar	1 mbar (=1/1000 atm)
90% Response Time (msec)	2500	10	0.07
Temperature coefficient (% Intensity / degree)	-2.5	-0.6	-0.05
Temperature error (mbar / degree)	34	10	1
Applications M = Mach Re = Reynold's # α turbulence = (air speed x length of plane x air density)/(air viscosity)	High speed (Airplane model) M > 0.3 Re = 106	Low speed (Auto model) M > 0.1 Re = 105	Insect flight M ~ 0.02 Re = 103

Besides monitoring cell viability, oxygen sensing at the cellular level is also important in a multitude of other biological studies. NIR absorbance and emission properties are crucial for any chemosensor to be used for *in vivo* biological systems as tissue does not absorb at these wavelengths. We have also been pursuing the bathochromatic shift of potential sensors into the NIR region because of the increase in analyte spectral detection range and decrease in background signal. The current goal of our research is to develop porphyrin sensors which have the potential to serve as NIR emitters, useful as oxygen (pressure), temperature, and pH sensors.

Section 6: Overview and Goals

To achieve our current goal of a NIR emitting porphyrin sensor, we begin with its synthetic design. Currently we favor the use of the fluorinated platinum porpholactone, (COO)TFPCPt. Tetrapentafluorophenyl (TFPP) porphyrin derivatives have shown to have increased photostability, which increases usefulness for applicaitons. The heavy metal platinum increases the forbidden electronic transition from the singlet excited state to triplet excited state with close to a 100% quantum yield, thus maximizing phosphorescent porphyrin emission. The lactone moiety has also shown to have interesting acid/base characteristics which will be discussed in Section 2.2.3. The goal of this thesis was to determine how to bathochromatically shift this spectral wavelength.

It has been shown that bacteriochlorins are bathochromatically shifted in absorption and thus emission spectra. We deduce that the reduction of an opposite pyrrolic subunit of (COO)TFPCPt could induce such a bacteriochlorin-like spectra. Section 2.1 discusses this feasibility through the use of Density Functional Theory calculations. In Sections 2.2 through 2.4 we discuss the synthetic process towards the synthesis of the novel dilactone. In the following Section 2.5, we present the NIR photochemical properties of our novel porphyrin derivatives. While some predictions were confirmed, some could not be. In due course of this work, we discovered unique fragmentation patterns in the ESI mass spectrometric analysis of pentafluoroporphyrins and porpholactones. These intriguing results are presented in Chapter 3.

Notes to Chapter 1:

1.   *The Porphyrin Handbook.* 1 ed.; Academic Press: New York, 2000; Vol. 6, 7.

2.   Gouterman, M., *Optical spectra and electronic structure of porphyrins and related rings.* Academic Press: New York, 1978; Vol. 3, p 1-165.

3.   McCarthy, J. R. Novel Macrocycles by Modification of the beta, beta'–Position of Porphyrins. PhD, University of Connecticut, Storrs, 2003.

4.   Pandey, R. K., Recent advances in photodynamic therapy. *Journal of Porphyrins and Phthalocyanines* **2000,** 4, 368-373.

5.   Stilts, C. E. N., M.I.; Hilmey, D.G.; Davies, S.R.; Gollnick, S.O.; Oseroff, A.R.; Gibson, S.L.; Hilf, R.; Detty, M.R., Water-Soluble, Core-Modified Porphyrins as Novel, Longer-Wavelength-Absorbing Sensitizers for Photodynamic Therapy. *J. Med. Chem* **2000,** 43, 2403-2410.

6.   Zelelow, B.; Khalil, G. E.; Phelan, G.; Carlson, B.; Gouterman, M.; Callis, J. B.; Dalton, L. R., Dual luminophor pressure sensitive paint II. Lifetime based measurement of pressure and temperature. *Sensors and Actuators, B: Chemical* **2003,** B96, (1-2), 304-314.

7.   Gouterman, M., Oxygen quenching of luminescence of pressure sensitive paint for wind tunnel research. *Journal of Chemical Education* **1997,** 74, (6), 697-702.

8.   Gouterman, M.; Callis, J.; Dalton, L.; Khalil, G.; Mebarki, Y.; Cooper, K. R.; Grenier, M., Dual luminophor pressure-sensitive paint: III. Application to automotive model testing. *Meas. Sci. Technol.* **2004,** 15, (10), 1986-1994.

9.   Khalil, G. E.; Costin, C.; Crafton, J.; Jones, G.; Grenoble, S.; Gouterman, M.; Callis, J. B.; Dalton, L. R., Dual-luminophor pressure-sensitive paint I. Ratio of reference to sensor giving a small temperature dependency. *Sens. Actuators, B* **2004,** 97, (1), 13-21.

10.   Milgrom, L. R., *The Colors of Life.* Oxford University Press: Oxford, 1997.

11.   Ege, S. N., *Organic Chemistry; Structure and Reactivity.* D.C. Health and Company: Lexington, 1994.

12.   Falk, J. E., *Porphyrins and Metalloporphyrins*. Elsevier Publishing Company: Amsterdam, 1964.

13.   Rothemund, P. J., *J. Am. Chem. Soc.* **1936,** 58, 625-627.

14.   Adler, A. D. L., F.R.; Shergalis, W.J., *J. Am. Chem. Soc.* **1964,** 86, 3145-3149.

15.   Adler, A. D. L., F.R.; Finarelli, J.D.; Goldmacher, J.; Assour, J.; Korsakoff, L., A Simplified Synthesis for meso-Tetraphenylporphyrin. *J. Org. Chem.* **1967,** 32, 476.

16.   Lindsey, J. S. S., I.C.; Hsu, H.C.; Kearney, P.C.; Marguerettaz, A.M., *J. Org. Chem.* **1987,** 52, 827-836.

17.   Lindsey, J. S. S., I.C., *Tetrahedron Lett.* **1986,** 27, (4969-4970).

18.   Crossley, M. J. K., Lionel G., Novel Heterocyclic Systems from Selective Oxidation at the beta-Pyrrolic Position of Porphyrins. *J. Chem. Soc., Chem. Commun.* **1984,** 920-922.

19.   Crossley, M. J. H., Trevor W.; King, Lionel G., Conversion of a porphyrin into a 5,6-dihydroporphyrin. Synthesis and X-ray crystal structure of (5RS, 6SR)-5,6-dihydro-6-(methoxycarbonyl)-8-oxo-5,10,15,20-tetraphenyl-8H-7-oxaporphyrin. *Bull. Soc. Chim. Fr.* **1996,** 133, 735-742.

20.   Gouterman, M.; Hall, R. J.; Khalil, G. E.; Martin, P. C.; Shankland, E. G.; Cerny, R. L., Tetra(pentafluorophenyl)porpholactone. *Journal of the American Chemical Society* **1989,** 111, (10), 3702-7.

21.   Zelelow, B., Memorandum. Seattle, 2002.

22.   McCarthy, J., R.; Jenkins, Hilary, A.; Bruckner, Christian, Free Base meso-Tetraaryl-morpholinochlorins and Porpholactone from meso-Tetraaryl-2,3-dihydroxy-chlorin. *Organic Letters* **2003,** 5, (1), 19-22.

23.   Gouterman, M., Study of the Effects of Substituents on the Absorption Spectra of Porphyrins. *The Journal of Chemical Physics* **1959,** 30, (5), 1139-1161.

24.   Atkins, P. W. F., R.S., *Molecular Quantum Mechanics*. 3 ed.; Oxford University Press: Oxford, 1997; p 202-239.

25.   Zhao, L. *Singlet Oxygen*; B-180 ML; University of Iowa, Department of Radiology: Iowa City, February 8, 2001, 2001; pp 1-10.

26.   Kavandi, J. L. Doctoral, University of Washington, Seattle, 1990.

27.   *Singlet Oxygen: Reactions with Organic Compounds and Polymers*. Wiley: Winchester, 1978; p 331.

28.   Greenwood, N. N. E., A, *Chemistry of the Elements*. Pergamon Press: Oxford, 1984; p 14.

29.   Bowen, E. J., *Trans. Faraday Soc.* **1954,** 50, (2), 97.

30.   Cox, G. S. W., D.G., *Chem. Phys. Lett.* **1979,** 67, (2,3), 511.

31.   Phillips, D., *Polymer Photophysics*. Chapman and Hall: London, 1985; p 12.

32.   Stern, O. V., M, *Phys. Z.* **1919,** 20, 183.

33.   Bowen, E. J., *Luminescence in Chemistry*. Van Nostrand: London, 1968; p 13-14.

34.   Skoog, D. A. H., J.F.; Nieman, T.A., *Principles of Instrumental Analysis*. 5 ed.; Harcourt Brace and Company: Philadelphia, 1998; p 365-376.

35.   Kavandi, J. C., J.; Gouterman, M.; Khalil, G.; Wright, D.; Green, E.; Burns, D.; McLachlan, B., *Review of Scientific Instruments* **1990,** 61, 3340.

36.   Sternberg, E. D.; Dolphin, D.; Brückner, C., Porphyrin-based photosensitizers for use in photodynamic therapy. *Tetrahedron* **1998,** 54, (17), 4151-4202.

37.   Khalil, G. C., C.; Crafton, J.; Grenoble, S.; Gouterman, M.; Callis, J.; Dalton, L.R., *Sensor and Actuators* **2002,** (97), 13-21.

38.   Khalil, G.; Gouterman, M.; Ching, S.; Costin, C.; Coyle, L.; Gouin, S.; Green, E.; Sadilek, M.; Wan, R.; Yearyean, J.; Zelelow, B., Synthesis and spectroscopic characterization of Ni, Zn, Pd and Pt tetra(pentafluorophenyl)porpholactone with comparison to Mg, Zn, Y, Pd and Pt metal complexes of tetra(pentafluorophenyl)porphine. *J. Porphyrins Phthalocyanines* **2002,** 6, (2), 135-145.

39.   Dougherty T., J., Photodynamic Therapy. *Photochemistry and Photobiology* **1993,** 58, (6), 895-900.

40.   Khalil, G., Gouterman, M., and Green, E. Method for Measuring Oxygen Concentration. 1989.

41.   Spellane, P. J.; Gouterman, M.; Antipas, A.; Kim, S.; Liu, Y. C., Porphyrins. 40. Electronic spectra and four-orbital energies of free-base, zinc, copper, and palladium tetrakis(perfluorophenyl)porphyrins. *Inorganic Chemistry* **1980**, 19, (2), 386-91.

42.   DiMagno, S. G.; Williams, R. A.; Therien, M. J., Facile Synthesis of *meso*-Tetrakis(perfluoroalkyl)porphyrins: ... *J. Org. Chem.* **1994**, 59, 6943-6948.

43.   Khalil, G. E.; Lau, K.; Phelan, G. D.; Carlson, B.; Gouterman, M.; Callis, J. B.; Dalton, L. R., Europium beta-diketonate temperature sensors: Effects of ligands, matrix, and concentration. *Review of Scientific Instruments* **2004**, 75, (1), 192-206.

44.   Im, S. H. K., G.; Callis, J.; Ahn, B.H.; Xia, Y., Synthesis of Polystyrene Beads Loaded with Dual Luminophors for Self Referenced Oxygen Sensing. *Talanta* **2005**, 67, 492-497.

45.   Kimura, F. K., G.; Zettsu, N.; Xia, Y.; Callis, J.; Gouterman, M.; Dalton, L.; Dabiri, D.; Rodriguez, M., Dual Luminophore Polystyrene Microspheres for Pressure Sensitive Luminescent Imaging. *Measurent Sci. Tech.* **2006**, in press.

46.   McGraw, C., et al., *Rev. Sci. Instruments* **2003**, 74, 5260-66.

47.   Mebarki, Y., The Institute for Aerospace Research, NRC.: Ottawa, Canada, 2004.

48.   Sweet, I., Univ. of Washington: Seattle, WA, 2004.

Chapter 2 - Results and Discussion

Section 1: Overview

Porpholactones are porphyrins in which one of the β,β'-double bonds has been formally replaced by a lactone moiety. Since the serendipitous discovery of *meso*-tetra(pentafluorophenyl)porpholactone (TFPLH$_2$) by our group in 1986, we have been trying to understand the reaction mechanism of this one-pot synthesis (Section 1.2).[20] We have made specific attempts to optimize the reaction conditions such as varying reaction time and temperatures, changing oxygen concentrations of the reaction mixture, as well as irradiating the reaction vessel with various wavelengths of light. These were done to simplify isolation and purification and increase overall yields. TFPLH$_2$ and its platinum complex TFPLPt, have been used as the integral ingredient in our group's most successful pressure sensitive paint (Section 1.5.b). Our aim for improving its synthesis inspired the investigation of the hitherto unknown platinum tetra(pentafluorophenyl)porphodilactones. It was our hopes that with this red shifted porphyrin analogue, our long term goal of creating a NIR-porphyrin sensor would be fulfilled.

The Results and Discussion Section of this thesis is composed of two chapters. In Section 2.1, we will describe the computational studies undertaken to find novel long-wavelength absorbing and fluorescing porphyrinic derivatives. Sections 2.3-2.5 describe the synthetic efforts toward the rational syntheses of these macrocycles. While not all possible isomers could be made, several surprising features of these macrocycles were discovered. In Section 2.6 we will detail the synthesis of other porphyrinic macrocycles not related to the dilactone series. Section 2.7 delineates the photophysical properties of all the novel porphyrinic systems synthesized. A comparison to the properties of a range of known porphyrins highlights the unique characteristics of select members studied.

Section 2: Density Functional Theory (DFT) Calculations

2.1.a Introduction

We have used DFT calculations in order to find porpholactone derivatives with greatly red shifted absorption and emission properties for the applications stated above. In particular, we have computed the structures and optical properties of the possible isomers of porphodilactone, porphyrins in which two of the β,β'-bonds are formally replaced with lactone moieties. Initially considered as a possibility for the structures of side products found in the silver oxidation of porphyrins, they were never isolated or characterized.[20] The following will provide a brief overview over the DFT methods used for the computations. Further information regarding DFT and its use with porphyrin calculations can be found in the appendix.

2.1.b Results and Discussion

Since the synthesis of meso-tetra(pentafluorophenyl)porpholactone by our group in 1986, its platinum complex has been our farthest red shifted PSP emitter at 730 nm. We realized that new synthetic porphyrin species were required to drastically red-shift the emission wavelength. However, we were unsure of the types of substitutions needed to induce this bathochromatic shift, we decided to use DFT to predict which novel prototype porphyrin derivatives would best suit our needs.

As described in Section 1.4, the reduction of one of the β,β'-double bonds of a porphyrin changes the UV-vis absorption spectra, due to a decrease in the HOMO-LUMO gap. This is observed when a porphyrin is altered to the chlorin-like porpholactone. A bathochromatic shift in UV-vis absorption is observed when a porphyrin is reduced to a bacteriochlorin derivative, where opposite β,β'-double bonds of the porphyrin macrocycle are reduced. With this in mind, we hypothesized that a bacteriochlorin dilactone would produce red-shifted absorption and emission spectra and thus chose to investigate these derivatives using DFT methods.

High molecular weight compounds, such as the fluorophenyl substituted porphyrins, decrease the accuracy of DFT calculations. In this study, simpler tetrapyrrole species were used for the actual calculations. These species are shown in Figure 2.1. The structure coordinates for the prototype porphyrins in Figure 2.1 were input into Gaussian, geometry-optimized at the local density approximation (LDA) level and then used to calculate the six lowest excited singlet states of each molecule using DFT/SCI methods.
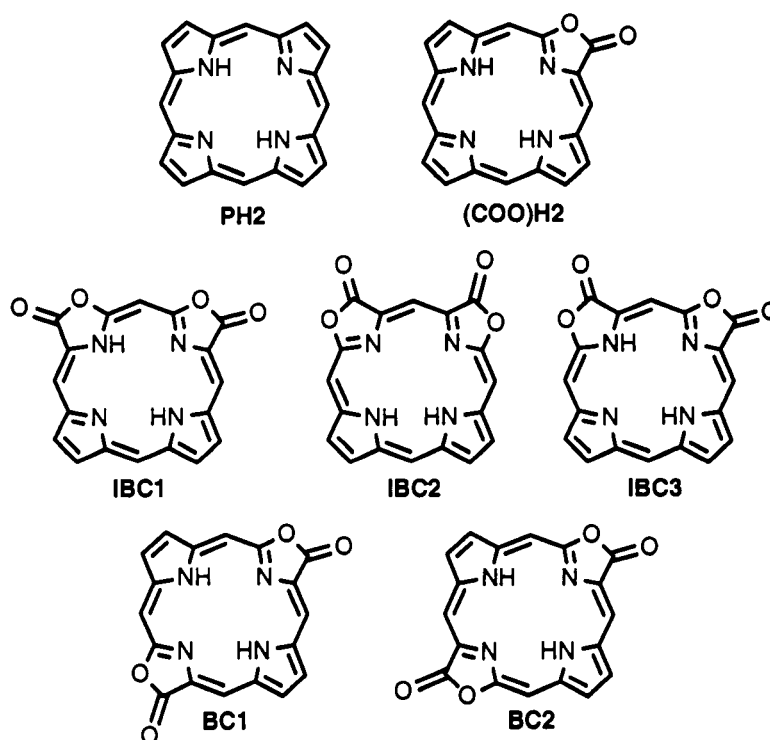
Figure 2.1 Prototype porphyrin species used for DFT/SCI calculations.

Table 2.1 lists the DFT/SCI excitation energies (in eV) of the six lowest singlet energy states of each prototype porphyrin shown in Figure 2.1. Table 2.2 is analogous to Table 2.1, whereby the excitation energies are expressed in nm, corresponding to the excitation wavelengths. The four lowest singlet energy states represent the approximate spectral location of the Q-bands while the fifth and sixth states are representative of the

B-band. The excitation energies calculated here by LDA are approximations. Here the theoretically calculated excitation energies are hypsochromically shifted in comparison to the experimental values for the known TFPPH2 and TFPLH2. In addition, simplified porphyrin prototypes that do not carry any *meso*-substituents were used in these calculations. The interpreted trends in electron volts and wavelength can be seen in Figures 2.2 and 2.3.

Table 2.1 DFT/SCI excitation energies (in eV) of the six the lowest singlet energy states.

Excited State (Energy)	PH2 (eV)	(COO)H2 (eV)	IBC1 (eV)	IBC2 (eV)	IBC3 (eV)	BC1 (eV)	BC2 (eV)
1	2.28	2.27	2.30	2.26	2.31	2.20	2.16
2	2.44	2.43	2.50	2.31	2.39	2.43	2.40
3	3.34	3.30	3.16	3.41	3.18	3.48	3.53
4	3.42	3.42	3.53	3.46	3.37	3.52	3.60
5	3.51	3.61	3.55	3.48	3.62	3.84	3.69
6	3.61	3.76	3.85	3.89	3.66	3.95	3.73
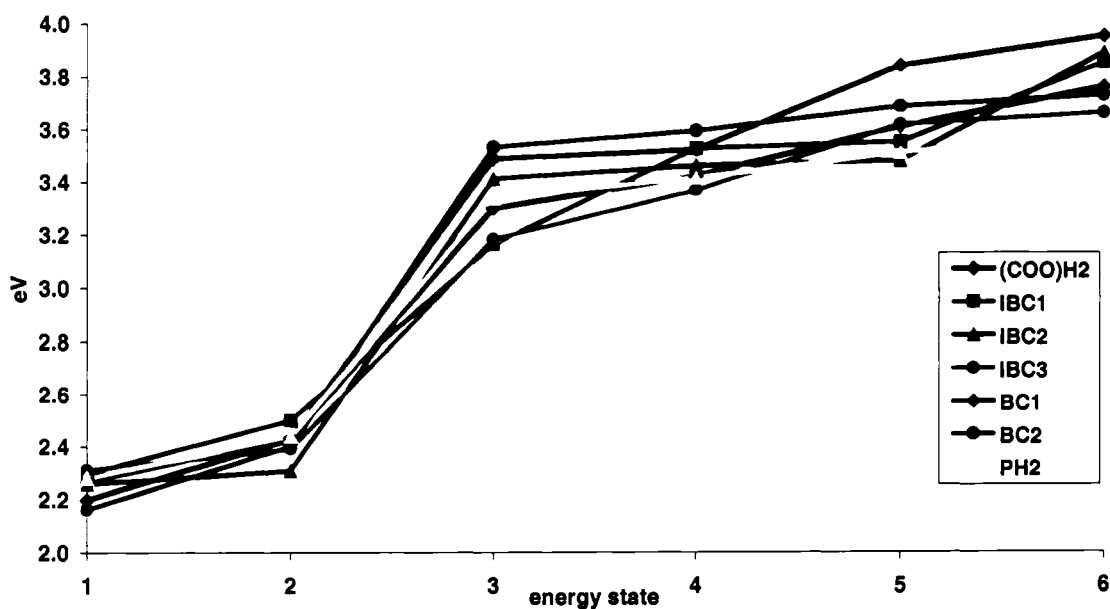
Figure 2.2 DFT/SCI excitation energies (in eV) of the six the lowest singlet energy states.

Table 2.2 DFT/SCI excitation energies (in nm) of the six the lowest singlet energy states.

Excited State (Wavelength)	PH2 (nm)	(COO)H2 (nm)	IBC1 (nm)	IBC2 (nm)	IBC3 (nm)	BC1 (nm)	BC2 (nm)
1	544	546	540	549	536	564	574
2	508	509	496	537	519	510	517
3	372	376	392	363	390	355	351
4	363	362	351	358	368	352	345
5	353	343	349	356	342	323	336
6	344	330	322	319	338	314	332
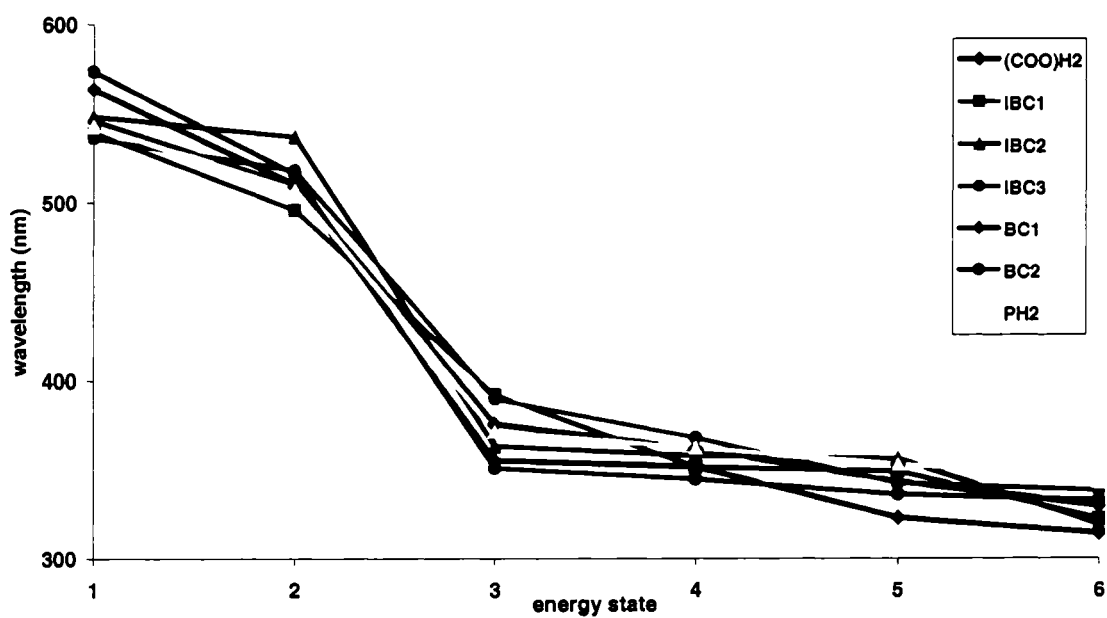
Figure 2.3 DFT/SCI excitation energies (in nm) of the six the lowest singlet energy states.

LDA calculations show that the bacteriochlorin dilactone isomers posses slightly bathochromically shifted spectra as compared to the isobacteriochlorin dilactone isomers. This trend is as expected. However, the bacteriochlorin dilactone do not induce a large bathochromic spectral shift in comparison to the spectra of the porphine and porpholactone.

2.1.c Conclusions

The computations provided us with data that encouraged us to pursue the rational syntheses of the novel dilactones, described in Sections 2.3 through 2.5. Section 2.7 will describe the experimentally determined photophysical properties of the dilactones and related derivatives. As will be detailed below, the computated optical spectra are much different from those that were obtained experimentally, highlighting the shortcomings of the DFT methods used for the prediction of the photophysical properties of porphyrinic molecules.

Section 2: Synthesis of Porpholactones

Of the several published porpholactone syntheses (see Section 1.2), we identified the stepwise approach developed by Brückner and co-workers as the most general and suitable for this project. Shown in Scheme 2.1, meso-tetraphenylporphyrin **2.1a** (TPPH$_2$) is oxidized with a stoichiometric amount of OsO$_4$ in the presence of pyridine. This reaction produces the osmate ester of diol **2.2a** (osmate-(OH)$_2$TPCH$_2$). The osmate ester **2.2a** is reduced to diol chlorin **2.4a** ((OH)$_2$TPCH$_2$) using gaseous H$_2$S. Subsequent MnO$_4^-$-induced cleavage of the diol **2.4a** under phase transfer catalysis presumably then generates the corresponding secochlorin biscarboxylate that, however, cannot be isolated. Instead it spontaneously decarboxylates and cyclizes to form the porpholactone (COO)TPLH$_2$ **2.5a** with a yield of up to 80%.[3, 22] The UV-Vis absorption spectra of **2.2a** and **2.4a** are shown in Figure 2.4.
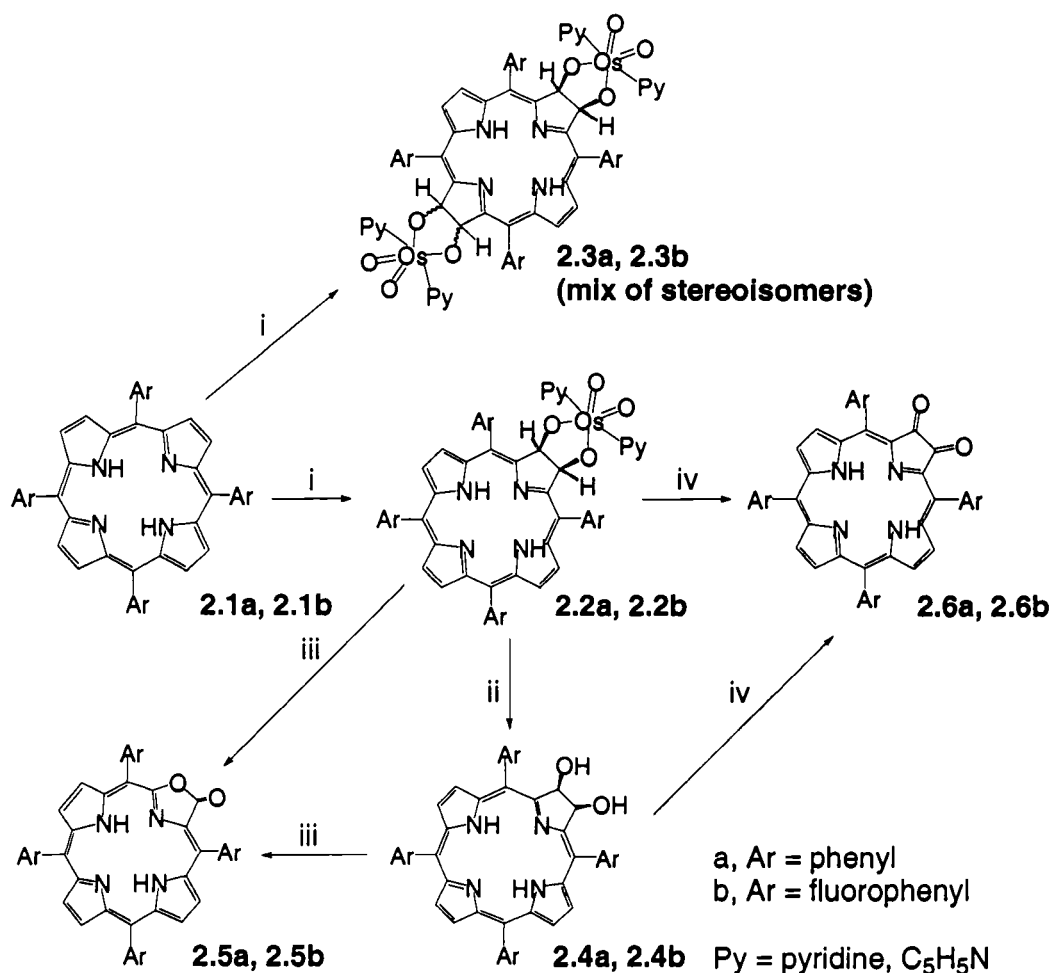
Scheme 2.1 Synthesis of the lactone adapted from Bruckner and co-workers. i) OsO₄/pyridine, ii) H₂S, iii) MnO₄⁻/phase transfer catalysis, iv) MNO.

This reaction sequence was deemed general and applicable to the synthesis of pentafluorophenylporpholactones. Thus, the oxidation reaction of *meso*-tetra(pentafluorophenyl)porphyrin **2.1b** (TFPPH₂) with OsO₄ generates the osmate ester of the diol **2.2b** (osmate-(OH)₂TFPCH₂) in yields of approximately 60%. The UV-vis spectrum of the product **2.2b** (Figure 2.5) shows the expected characteristics of a chlorin, in particular the broadened Soret band and the enhanced longest wavelength absorption band at 650 nm. The spectrum of **2.2b** compares well to the spectrum of the phenyl

substituted analogue **2.2a**. The resulting osmate ester is, like in the tetraphenyl-analogue, stable and can be isolated by chromatography.
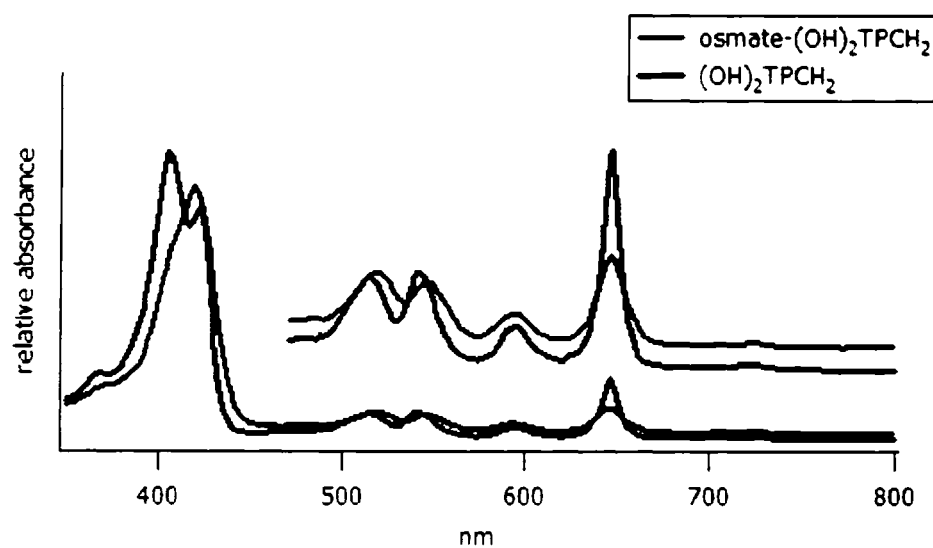
Figure 2.4 UV-Vis of the phenyl substituted diol **2.4a** and osmate ester of the diol **2.2a**.
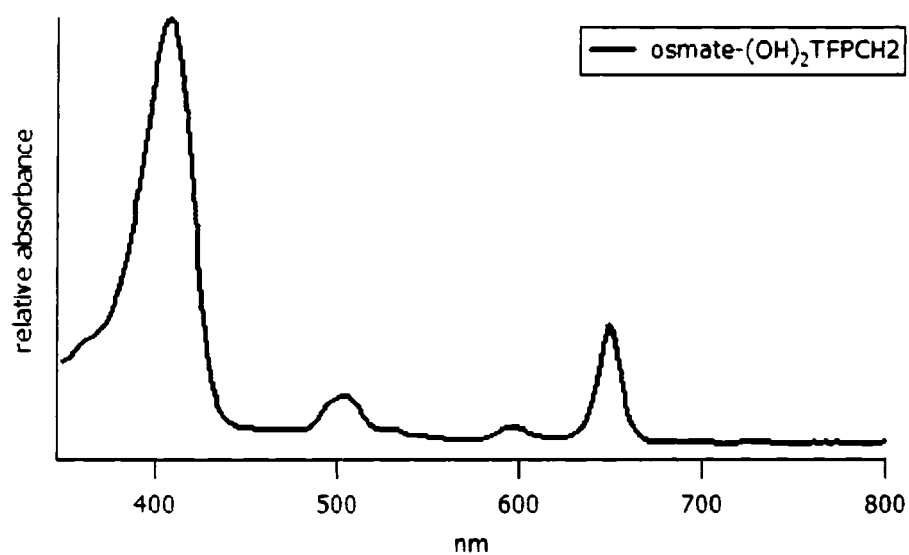
Figure 2.5 UV-Vis of the fluorophenyl substituted osmate ester of the diol **2.2b**.

The ^{1}H NMR of product **2.2b** confirms the presumed osmate ester structure (Figure 2.6). The interpretation of the spectrum is simplified by the absence of signals for the phenyl protons. Six signals are observed for the β-protons. These β-hydrogen signals exhibit the splitting pattern expected for the two-fold symmetry of **2.2b**: a pair of doublets at 8.7 and 8.4 ppm, and one singlet at 8.5 ppm all in a 1:1:1 intensity ratio. The pair of triplets at 7.6 and 7.3 ppm correspond to the two β-hydrogens of the pyridine of the osmate ester. Their inequivalency is due to the arrangement of the osmate ester above the porphyrin macrocycle. Three peaks equivalent to a single free pyridine are seen at 7.1, 7.5 and 8.5 ppm. The broad singlet at 6.9 ppm corresponds to the proton on the pyrrolidine ring. A broad singlet at -2.0 ppm corresponds to the pyrrole protons in the porphyrin core (not shown). There are two pyridine molecules complexed to the osmium, the *ortho-*, *meta-*, and *para*-hydrogen of each pyridine all have ^{4}J vicinal coupling observed in the corresponding order at 8.5, 7.3, and 7.8 ppm.
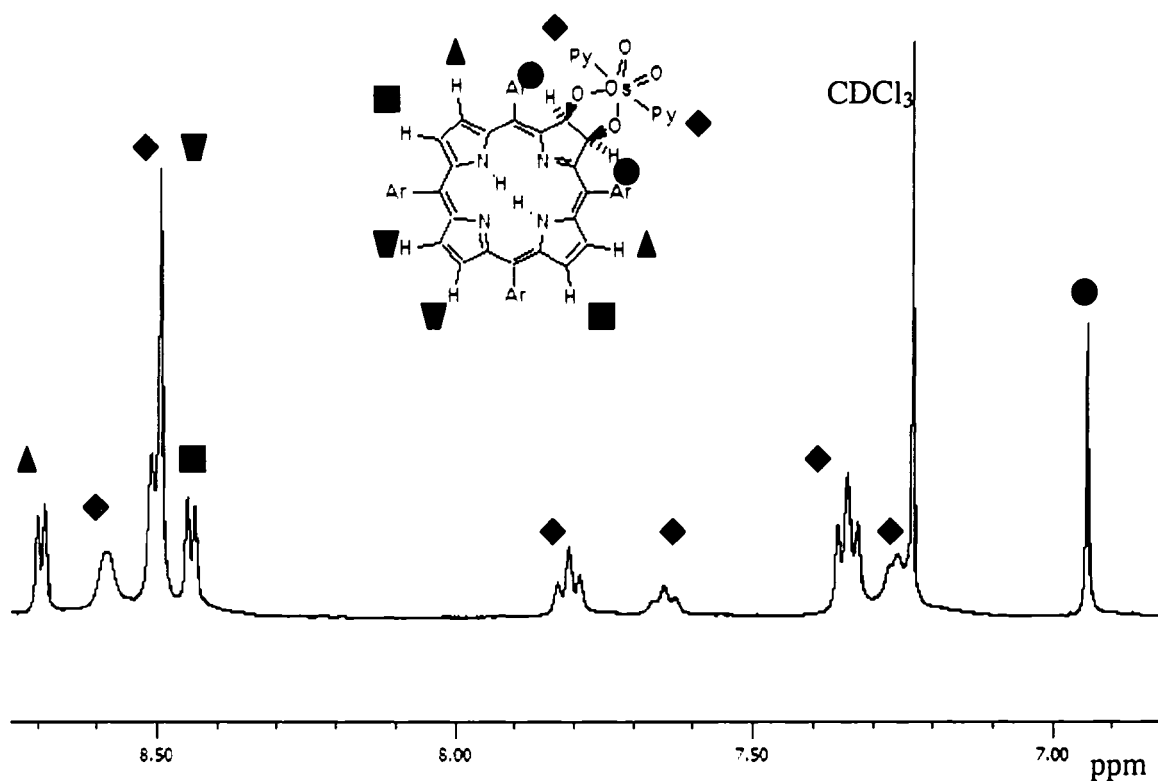
Figure 2.6 ¹H NMR of osmate-(OH)₂TFPCH₂ **2.2b** (Ar = C₆F₅). (The grey diamonds are representative of a single free pyridine molecule.)

Crystals suitable for a single crystal diffractometry study of the osmate-(OH)₂TFPCH₂ **2.2b** were grown by slow diffusion of petroleum ether into a saturated CHCl₃ solution of **2.2b**. The structure of **2.2b** is shown in Figure 2.7 and confirms the expected and spectroscopically derived structure. The *vic-cis* diol functionality, as its osmate ester, positioned above the mean plane of the porphyrin macrocycle is clearly evident. The osmium(VI) center is coordinated in an octahedral fashion. *Trans* to each diol oxygen atom are the coordinated pyridines, with the remaining coordination sites occupied by oxogroups. The structure of the osmate ester moiety is analogous to several other published osmate esters. The near perfect planarity of the porphyrin macrocycle is evident. As typically observed with *meso*-aryl substituted porphyrins, the fluorophenyl

substituents are arranged perpendicular to the macrocycle to reduce steric hinderance between the β-protons and the o-fluorine groups. We also observe clearly as expected, that the osmate ester and adjoined pyridines are also positioned above the mean plane of the porphyrin macrocycle.
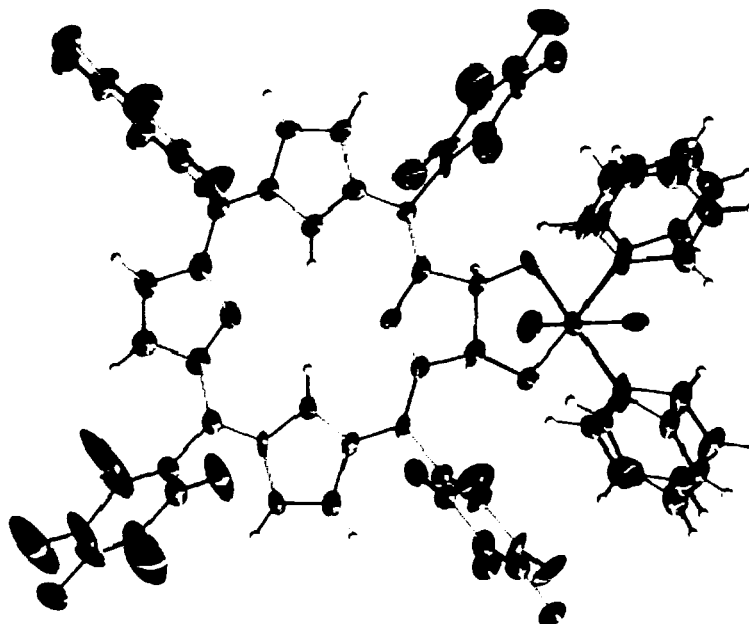
Figure 2.7 ORTEP representation of the single crystal X-ray structure of **2.2b**.[49]

The attempted H₂S-mediated reduction of the fluorophenyl substituted osmate-(OH)₂TFPCH₂ (**2.2b**) lead to the formation of a number of intractable products which showed chlorin-type UV-vis spectra. We surmise that the H₂S lead to a nucleophilic aromatic substitution reaction of the para-fluoro groups. Commonly using N- or S-nucleophiles, the pentafluorophenyl group can be used to regiospecifically introduce p-phenyl substituents. This reaction pattern has been well documented for pentafluorphenylporphyrins.[50-53]

Other reductive cleavage methods such as using a biphasic system consisting of a solution of **2.2b** in organic solvents agitated with aqueous bisulfite solutions lead to the formation of greatly emulsified mixtures. Cleavage of the osmate ester was also

attempted oxidatively using 4-methylmorpholine N-oxide (MNO). Instead of simple cleavage, however, MNO induces a cleavage and an oxidation of the diol moiety to a dione moiety **2.6b** (Scheme 2.1).

The oxidative cleavage of the phenyl substituted osmate ester (**2.2a**) with KMNO$_4$ under phase transfer conditions (THF/18-crown-6) lead directly, after chromatographic separation of the reaction mixture, to the desired porpholactones in high yields (80%). However, the overall yields of this reaction using the fluorophenyl substituted **2.2b** are lower (48%) than in the corresponding reaction using **2.2a**.

When the MnO$_4$-induced cleavage of the diol functionality is performed using KMnO$_4$ in THF, 18-crown-6 is used as the phase transfer catalyst in order to solubilize the oxidant. Nearly 100% conversion of the non-fluorinate diol **2.4a** to lactone **2.5a** is possible in relatively large scale (0.5 g) when excess KMnO$_4$ is added to the reaction mixture in small amounts (few mg at a time) over 1-5 days. The reaction is monitored by TLC and total conversion can be observed with minimal decomposition. To bypass the use of the highly toxic phase transfer catalyst, cetyltrimethylammonium permanganate (CTAP), an MnO$_4$ derivative soluble in most organic solvents, was synthesized and found very suitable to carry out the oxidation.[54]

The UV-Vis absorbance spectra of the phenyl and fluorophenyl substituted lactones are shown in Figure 2.8. Both have characteristic Soret bands around 400 nm, followed by four Q-bands between 500-650 nm. However, the phenyl substituted lactone **2.5a** maintains a porphyrin-like spectrum while the fluorophenyl substituted lactone **2.5b** has a more chlorin-like spectrum. IR spectra of both phenyl and fluorophenyl substituted lactones have a single strong absorption between 1750-1735 cm^{-1}, characteristic for the presence of a conjugated of C=O moiety.
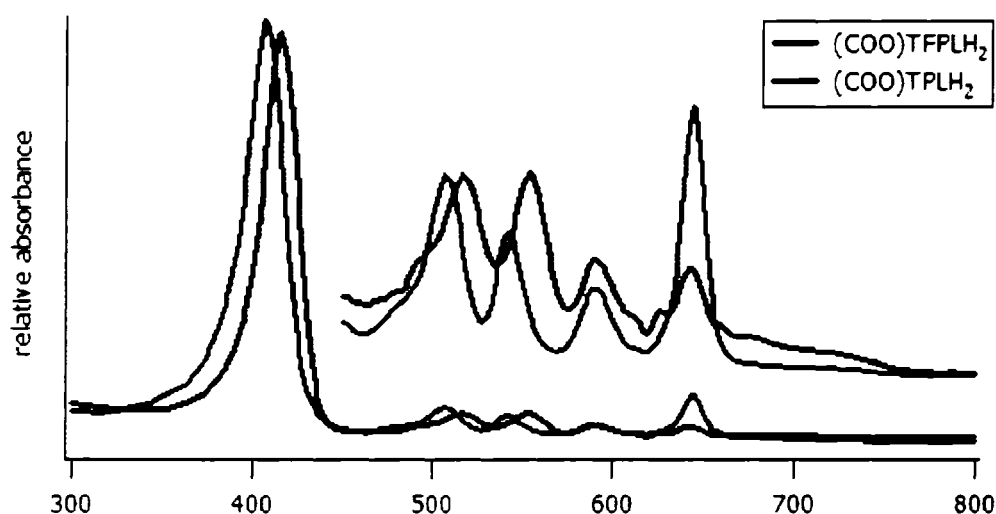
Figure 2.8 UV-Vis spectra of phenyl **2.5a** and fluorophenyl substituted **2.5b** free base lactone.

The ^{1}H NMR spectrum of the fluorophenyl substituted porpholactone **2.5a** is characteristic of a non-symmetric chlorin (Figure 2.9). Two broad singlets at -2.05 and -1.82 ppm correspond to the two pyrrole protons in the porphyrin core (not shown). Six signals correspond to the six non-equivalent protons observed for the β-protons. Two protons appear as doublets, due to the ^3J vicinal coupling, while the other four protons have both vicinal coupling as well as a ^4J coupling to the inner NH protons. The NMR of the phenyl substituted porpholactone is similar save for the addition of broad multiplets in the aromatic region (7-8 ppm) due to the twenty phenyl protons.
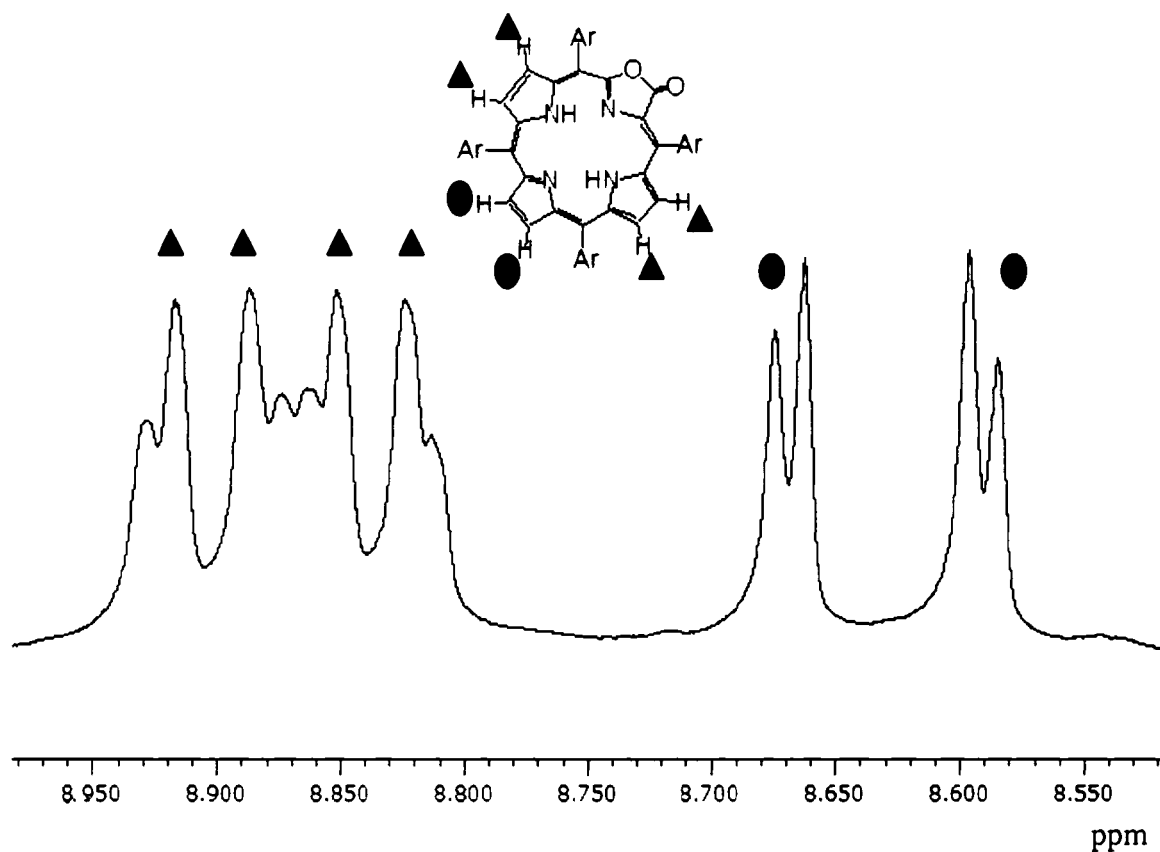
Figure 2.9 ^{1}H NMR of (COO)TFPLH$_2$ **2.5b** (Ar = C$_6$F$_5$).

Crystals suitable for a single crystal diffractometry study of the free base lactone **2.5a** were grown by slow diffusion of petroleum ether into a saturated CHCl$_3$ solution of **2.5a**. The structure of **2.5a** is shown in Figure 2.10 and confirms the expected and spectroscopically derived structure. Figure 2.11 shows the near perfect planarity of the porphyrin macrocycle. As typically observed, the phenyl substituents are arranged perpendicular to the macrocycle while the lactone moiety sits in the π-electron plane of the porphyrin macrocycle.
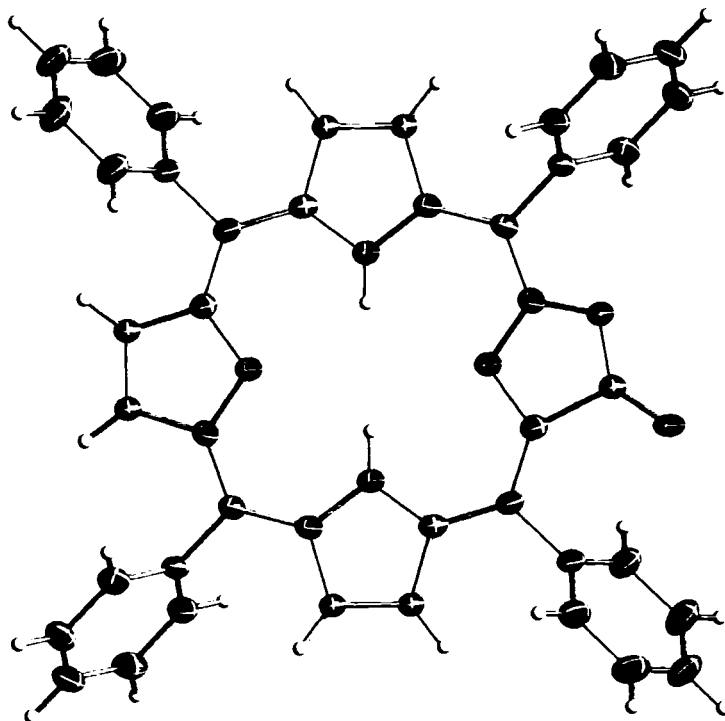
Figure 2.10 ORTEP top view representation of the single crystal X-ray structure of lactone **2.5a**.[49]
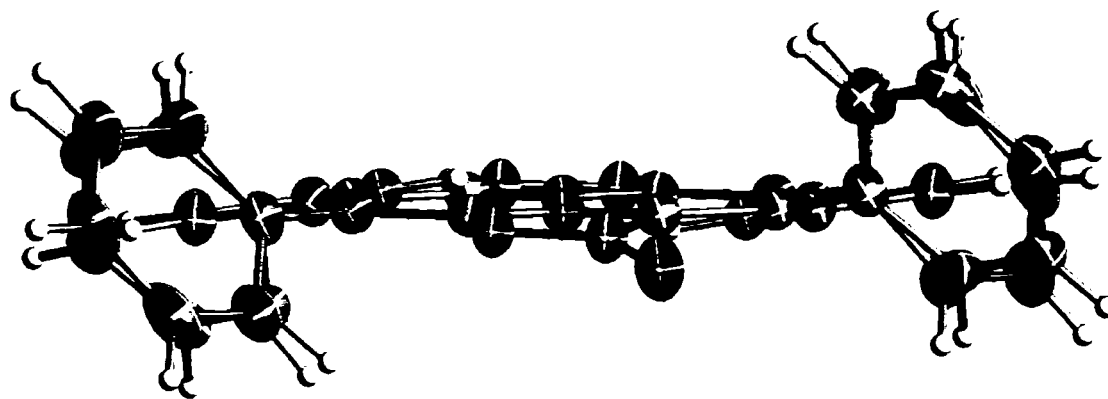
Figure 2.11 ORTEP side view representation of the single crystal X-ray structure of lactone **2.5a**.[49]

We also found that metalloporphyrins can undergo the MnO_4^- mediated oxidation of the diol to the lactone. One substantial difference between the metallated and free base

reactions is that oxidation of a metallo-fluorophenyl substituted osmate ester of the diol proceeds immediately with nearly 100% conversion to the lactone. We observe this using osmate-(OH)$_2$TFPC coordinated to Zn(II) and Pt(II).

An alternate route to metallo-lactones is the metallation of the free base lactones. Platinum insertion into (COO)TPLH$_2$ proceeds with relative ease with an 80% isolated yield. The reaction is accomplished using one of a variety of platinum salts (platinum(II) chloride, potassium tetrachloroplatinate, platinum(II) pentanedionate). The presence of platinum is observable in the shifts in the characteristic UV-vis spectrum of platinum porpholactones. The absorbance spectra of the platinum lactones are shown in Figure 2.12. In comparison to the absorbance spectra of the free base lactones (Figure 2.8), these display the characteristic metallo-lactone spectra with a broad band Soret around 400 nm and two Q-bands at approximately 560 nm.
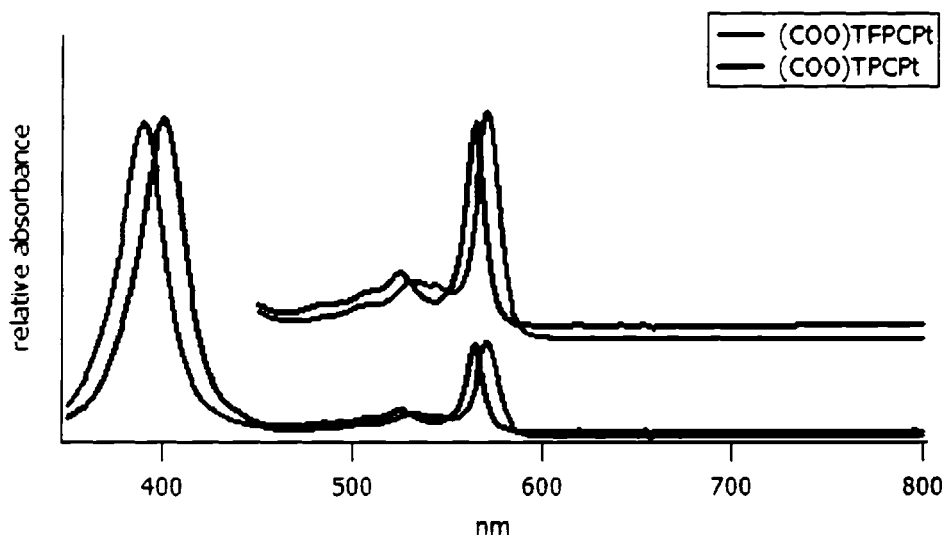
Figure 2.12 UV-Vis spectra of the phenyl and fluorophenyl substituted platinum lactone 2.5a, 2.5b.

The ^{1}H NMR of (COO)TPLPt **2.12a** is shown in Figure 2.13. The disappearance of the signals for the NH protons in the ^{1}H-NMR spectrum of platinum lactone also indicates the successful formation of the platinum complex. Further, ^{195}Pt is NMR active

and its resonance can be observed and used for verification of platinum insertion.[55] However, the sensitivity of ^{195}Pt is low, with a 3.36×10^{-3}-fold sensitivity of that of ^{1}H. In principle, a weak ^{4}J coupling of the ^{195}Pt nucleus to the β-protons is sometimes observed. However, in the work described here, this coupling was irrelevant or, when observed, ignored.
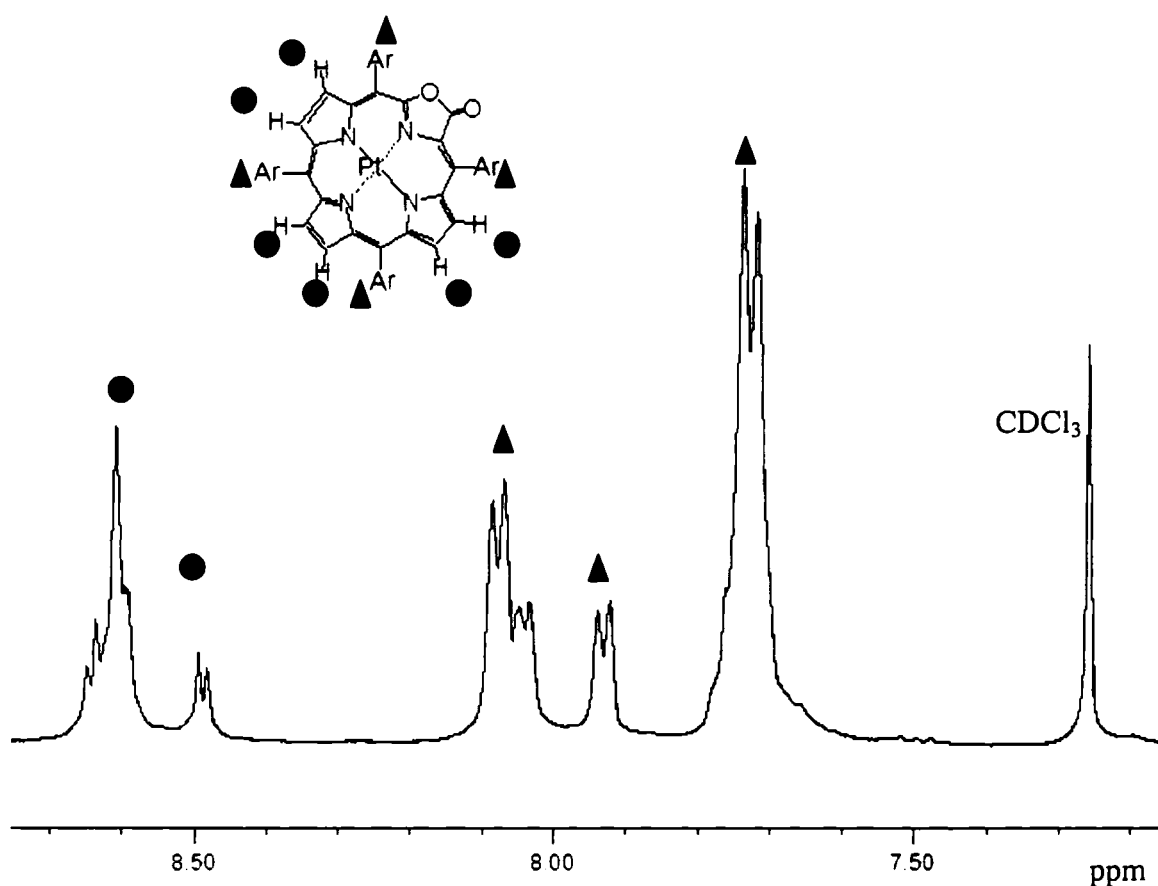
Figure 2.13 ^{1}H NMR of (COO)TPLPt **2.12a** (Ar = C_6H_5).

Mass spectroscopic data from the phenyl and fluorophenyl substituted lactones are detailed in Chapter 3.

Section 3: Acid/Base Characteristics of Porpholactones

Porphyrin are amphoteric, they have the ability to react as an acid or a base. This is due to the fact that its inner ring possesses two basic imino-type nitrogen atoms (=N–), and two (weakly) acidic pyrrole-type (–NH–) nitrogens. Of these several possible anions and cations, only five, the dianion, monoanion, neutral porphyrin, monocation, and dication, have been observed spectroscopically (Figure 2.14).[12]
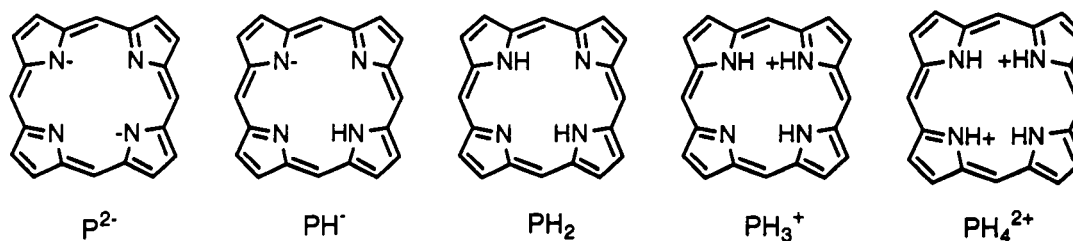
Figure 2.14 Possible neutral, anionic, and cationic species of porphyrin.

The acid/base characteristics of a porphyrin are affected by its side-chains, degree of reduction, and its conformation. The basicity of a porphyrin decreases as the electron-attracting power of its side-chains increases. The reduction of a porphyrin to a chlorin and the presence of an isocyclic ring, as in chlorophylls and their derivatives, both also tend to decrease the basicity of the pyrrole nitrogens.[12] In due course of our investigations, we found a number of peculiar acid-base properties of the porpholactones that prompted us to study these properties in some detail.

2.3.a Addition of Acid

Both the phenyl and fluorophenyl substituted porphyrins and lactones (2.1a, 2.1b, 2.5a, 2.5b) can be metallated as demonstrated in Section 1.3. The same substituents can also be protonated with the addition of acid and subsequently demetallated. However, we observe that a higher concentration of acid is needed to protonate the fluorophenyl substituted porphyrin 2.1b and lactone 2.5b in comparison to their phenyl substituted

derivatives (**2.1a, 2.5a**). The differences in acid/base reactivity of phenyl and fluorophenyl substituted porphyrin derivatives are largely due to the fact that fluorinated substituents are highly electron withdrawing, decreasing the basicity of the porphyrin.

As in the reduction of a porphyrin to a chlorin, both porpholactones, $(COO)TPLH_2$ and $(COO)TFPLH_2$, are less basic than their parent porphyrins. In porpholactones, one pyrrolic nitrogen formally becomes a vinylogous amide that is much less basic than the imines of a porphyrin. In comparison to each other, fluorophenyl substituted $(COO)TFPLH_2$ was again demonstrated to be less basic than the phenyl substituted $(COO)TPLH_2$ due to its electron withdrawing fluorinated substituents which render the porphyrin ring electron-deprived.

The addition of acid to $(COO)TPLH_2$ causes a bathochromatic shift in absorbance and changes the visible color of the solution from purple to bright green. The four characteristic Q-bands of the phenyl substituted lactone are transformed into a single band at 614 nm with a shoulder at 586 nm (Figure 2.15). Here $(COO)TPLH_2$ in CH_2Cl_2 is protonated with the addition of TFA (less than 1%). This reaction and subsequent shift in absorbance wavelength is reversible with the addition of base (TEA). In Figure 2.16, the careful titration of TFA into $(COO)TPLH_2$ in CH_2Cl_2 shows two isosbestic points at 480 nm and 567 nm. These isosbestic points give the wavelength at which the absorption coefficients of equimolar solutions of the lactone and new product are identical. Their observation is indicative for a one-step conversion of the starting porpholactone to the final protonated species.
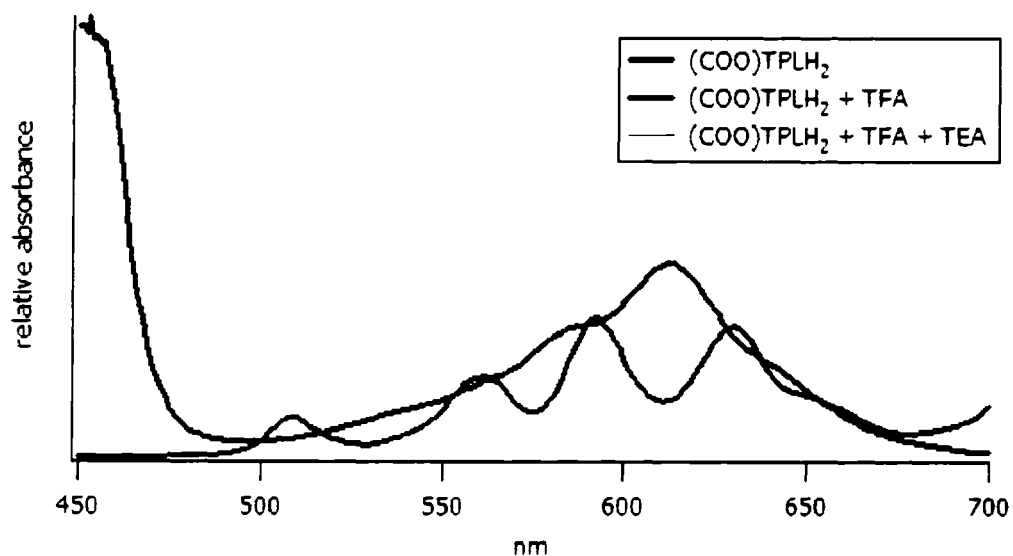
Figure 2.15 UV-Vis absorbance of (COO)TPLH$_2$ with the addition of TFA followed by the addition of TEA.
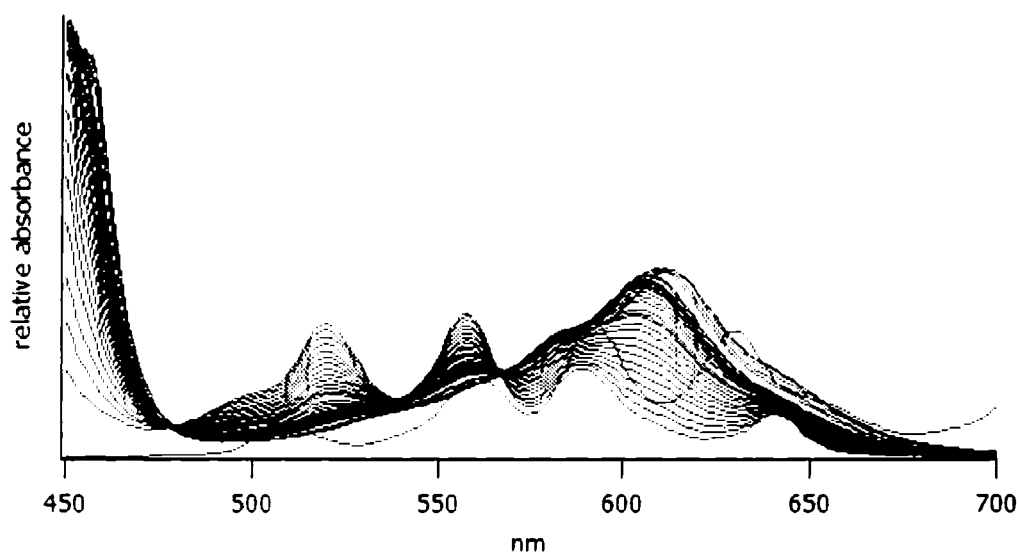
Figure 2.16 Titration of TFA into (COO)TPLH$_2$ in CH$_2$Cl$_2$ showing isosbestic points at 480 nm and 567 nm.

The addition of TFA to (COO)TFPLH$_2$ changes the four Q-bands of (COO)TFPLH$_2$ to a broad band ranging from 575 nm to 592 nm with side bands at 550

nm and 623 nm (Figure 2.17). The titration of TFA into (COO)TFPLH$_2$ in CH$_2$Cl$_2$ gives 4 isosbestic points at 525 nm, 536 nm, 550 nm, and 630 nm. A change in the (COO)TFPLH$_2$ solution visible color, from purple to bright blue, is observed with the addition of 100% TFA. Again, protonation is easily reversed with a few drops of base (TEA), restoring the original (COO)TFPLH$_2$ spectra as seen in Figure 2.17.
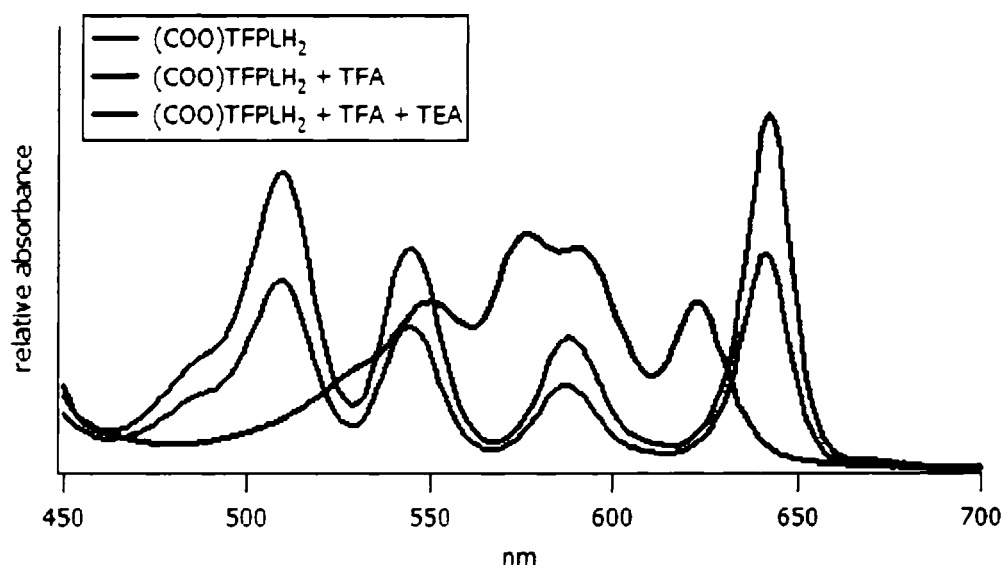
Figure 2.17 Change in UV-Vis absorbance of (COO)TFPLH$_2$ with the addition of TFA followed by the addition of TEA.

2.3.b Addition of Base

The generation of the anions of porphyrins generally requires the use of strong bases such as tBuLi or MeLi. Addition of bases such as NaOMe and NaOEt as well as non-nucleophillic bases like DBU to phenyl substituted TPP derivatives produces no or only negligible spectral changes. A similar reactivity to these bases is expected from the fluorophenyl substituted TFPP derivatives. However, Figure 2.18 shows that the addition of base to TFPPH$_2$ actually induces a blue shift in TFPPH$_2$ absorbance spectra.
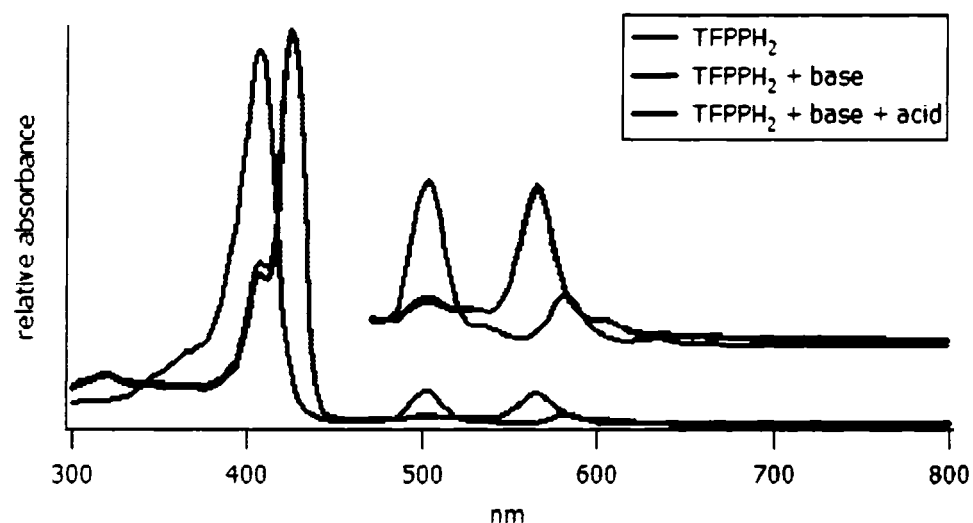
Figure 2.18 UV-Vis absorbance of TFPPH₂ with the addition of base (NaOMe) followed by the subsequent addition of acid (TFA).

Whereas the addition of base to free base or metallated (COO)TPL produced no reaction, the addition of a nucleophillic or non-nucleophillic base to the free base or metallated (COO)TFPL induces spectral changes. As shown in Figure 2.19, the addition of NaOMe or NaOEt, two nucleophillic bases, induces a red shift in the Soret band and transforms the four Q-bands of the lactone into one strongly bathrochromatically shifted broad band. With both (COO)TFPLH₂ and (COO)TFPLPt, the Soret band is shifted to approximately 430 nm while the longer wavelength Q-band is shifted to around 702 nm. This reaction is reversed upon the addition of an acid (HCl, H₂SO₄) to the solution. A variety of other metallated (COO)TFPL also show similar spectral characteristics with the addition of a base (Figure 2.20). While metallated porphyrin derivatives have two Q-bands around 550 nm, the Q-bands of the new base induced metallated species are red shifted to 650 nm to 725 nm.
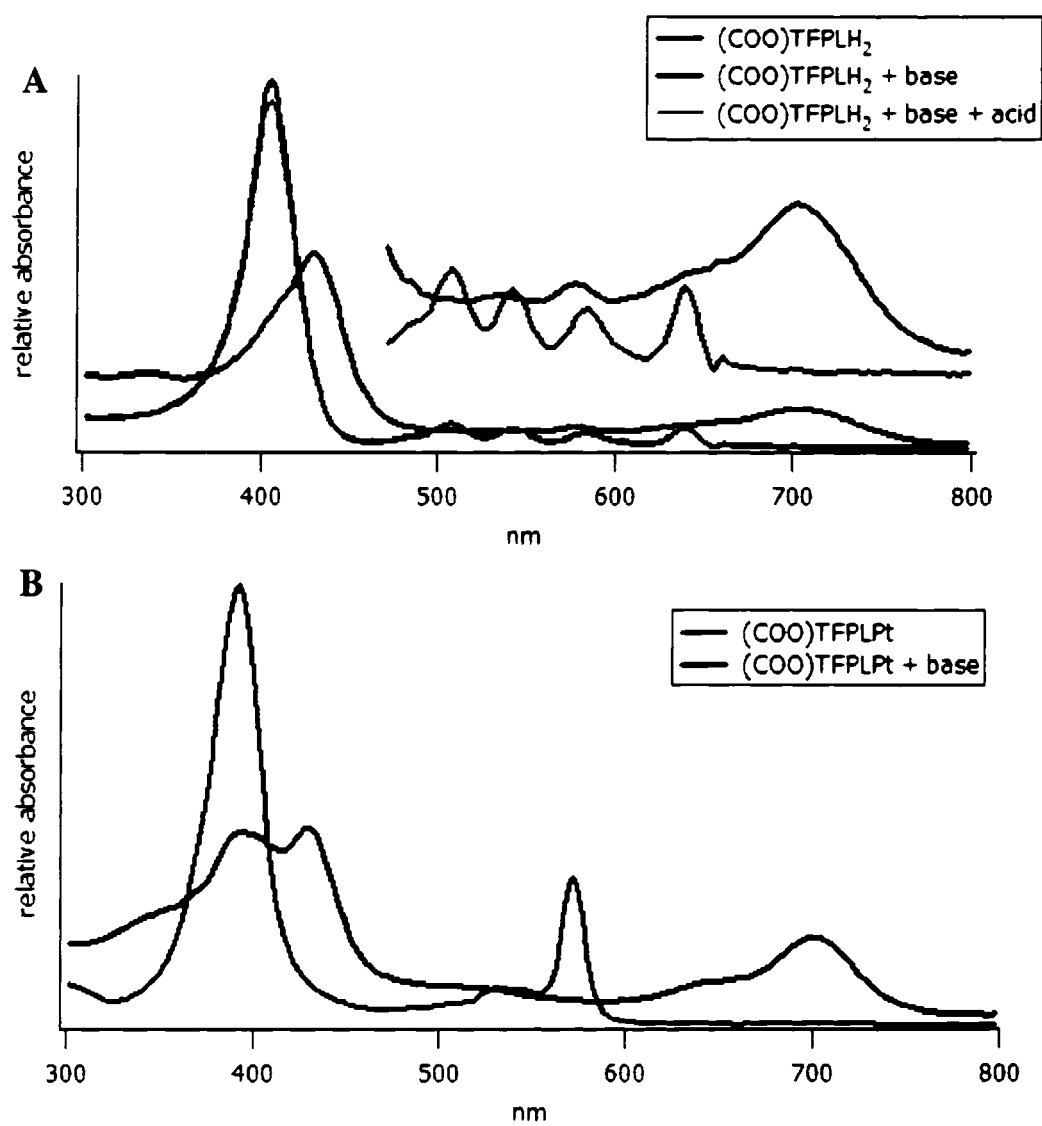
Figure 2.19 A) Change in UV-Vis absorbance of (COO)TFPLH₂ with the addition of a nucleophillic base followed by the subsequent addition of acid. B) Change in UV-Vis absorbance of (COO)TFPLPt with the addition of a nucleophillic base.
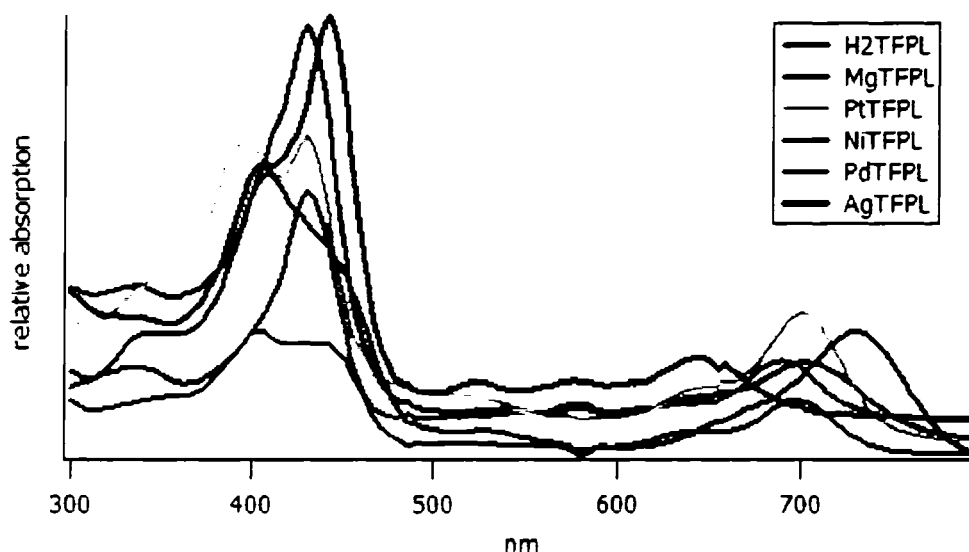
Figure 2.20 Bathochromic shift in UV-Vis absorbance of various metallated (COO)TFPL with the addition of NaOMe or NaOEt.

Exposure of the lactone to a nucleophillic base suggests that the spectrally observed new species is generated by a nucleophillic attack onto the lactone moiety. Considering that this reaction is reversible with the addition of acid, the breaking of the lactone ring is rather unlikely. In addition, deprotonation at a pyrrolic nitrogen is also highly unfavorable since both free base and metallolactones undergo these reactions. To differentiate between this unlikely ring opening mechanism and deprotonation at a β-position, the non-nucleophillic base 1,8-diaza-7-bicyclo[5.4.0]undecene (DBU) was used with free base and platinum (COO)TFPL in the following UV-Vis and NMR experiments.

Equal micromolar concentrations of (COO)TFPLPt and DBU (3 μM each) were combined in a 1mL cuvette and their reaction over time was monitored by UV-Vis. In a span of 30 minutes, the majority of (COO)TFPLPt is converted to a new species with a red shifted Soret band at 445 nm and a single broad Q-band around 725 nm. Figure 2.21 shows this progression over time. It is also noted that the use of the base DBU induces a further bathochromatically shifted spectra than NaOMe or NaOEt previously shown in Figure 2.19. The time course of the conversion of (COO)TFPLPt to the new species is

shown in Figure 2.22. We observe a one-step conversion of the starting porpholactone to the new base induced species.
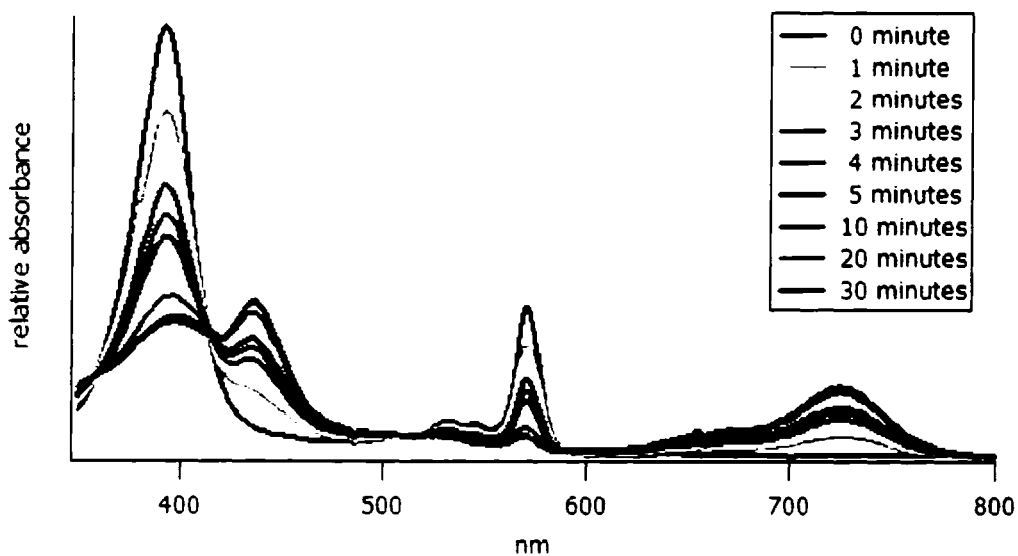
Figure 2.21 Reaction of (COO)TFPLPt to one equivalent of DBU monitored by UV-Vis with respect to time.
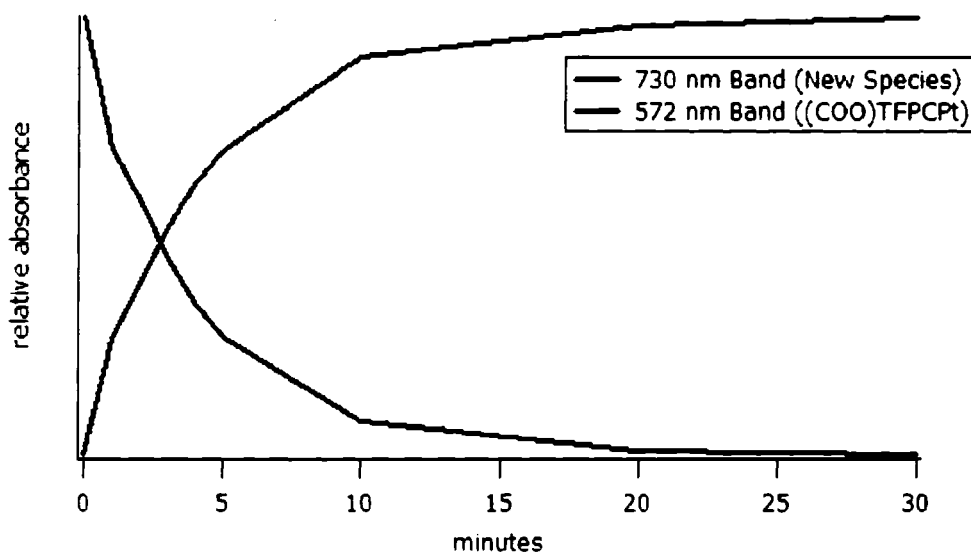
Figure 2.22 Rate of conversion from (COO)TFPLPt to the new base induced species calculated using Figure 2.21 above.

NMR titrations of free base and platinum (COO)TFPL with DBU were utilized in attempts to attempts to specify the location of the origin of deprotonation and/or the spectral change. Since opening of the lactone moiety and deprotonation of the inner pyrrole protons are unlikely, we hypothesize that the addition of base deprotonates a β-proton on the lactone macrocycle. Evaluation of this NMR data is still in progress. New peaks in the ^1H NMR of both free base and platinum (COO)TFPL were observed with the addition of DBU, however, the proton peaks at the β positions are overlapping which causes difficulties with integration. Accuracy and the integration is, however, needed as we are trying to observe the transition of 6 β-H to 5 β-H. The addition of DBU also changes the overall concentration of the NMR reaction solution, requiring the use of an internal reference.

2.3.c Conclusions

These observations suggest that the β-protons in (COO)TFPL are much more acidic in comparison to those in (COO)TPL and their parent porphyrins. Thus we hypothesize that the addition of the fluorinated substituents and lactone moiety make (COO)TFPL acidic enough to be readily deprotonated with the addition of base.

The acidity of the fluorophenyl substituted lactones allows them potential for sensor applications. We have shown that they are highly reactive under basic conditions, producing new species whose absorption and emission spectra are especially bathochromatically shifted in comparison to the usual lactone spectra. As with our already characterized PSPs described in Section 1.4, these new base induced derivatives can be detected and applied as possible novel pH sensors.

A significant application for a pH sensor would be its use in the detection of impending structural failure. Large structures such as buildings, bridges, and roads are made with concrete. It is known that a pH concrete of 10 or higher suggest corrosion or the onset of decay. If this increase in the basicity of concrete was detected at an early stage, repair or evacuation could be accomplished before any destruction of property or life. Less drastically, continual upkeep would be unnecessary as conditions could be

constantly monitored and amended. As with PSPs, such a pH sensor could be incorporated into a paint or polymer matrix and applied to a fiber optic sensor embedded in a concrete structure. Monitoring of this sensor could be accomplished with an external computer.

Section 4: Dihydroxylation of Diolchlorin and Porpholactones

As described in Section 2.3, the synthesis of the lactone relies on the oxidative cleavage of diol chlorins.[56] Since the tetraolbacteriochlorins and tetraolisobacteriochlorins are known, we surmised that this methodology could be employed for the one-step synthesis of porphodilactones. A second possible approach to the dilactone involves two steps, the dihydroxylation of a porpholactone followed by oxidative diol cleavage to establish a second lacone moiety. In this section we will discuss both the syntheses and characterization of the tetraols and the dihydroxylactones, as intermediary steps towards the synthesis of the porphodilactones.

In 1995, Brückner and Dolphin developed a method to specifically synthesize tetraolbacterio- or tetraolisobacteriochlorins (Scheme 2.2).[56] Parallel to the known reactivity of chlorins, they found that dihydroxylation of a free base diol, $(OH)_2TPCH_2$ **2.4a**, induces regiospecifically the pyrrolic β,β'-double bond opposite to the alredy established diol moiety to be osmylated , leading to the formation of a bacteriochlorin tetraol **2.7a**. On the other hand, the insertion of a metal into the porphyrin changes the preferred π-delocalization pathway, which makes the double bond in an adjacent pyrrolic unit more reactive.[56, 57] Thus, an isobacteriochlorin tetraol **2.8a** is formed.
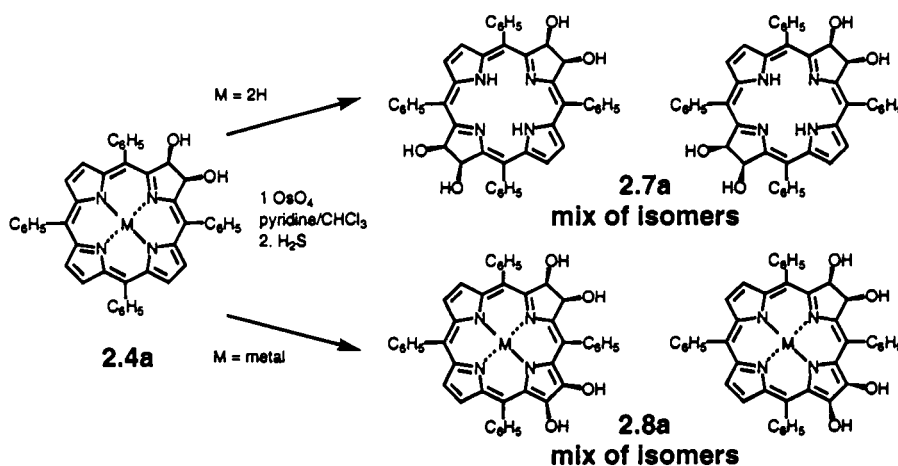
Scheme 2.2 Dihydroxylation of free base and metallated $(OH)_2TPC$ inducing bacterio- versus isobacteriochlorin formation.

2.4.a Dihydroxylation of the Diolchlorins

Phenyl and fluorophenyl substituted tetraolbacterio- (**2.3a**, **2.3b**, **2.7a**) and tetraolisobacteriochlorim (**2.8a**, **2.9a**, **2.9b**) regioisomers were synthesized as shown in Scheme 2.2. As mentioned in Section 2.3.a, we could not reduce the fluorophenyl substituted osmate esters **2.3b**, **2.9b** to the tetraol **2.7b**, **2.8b**, instead, the corresponding osmate esters (**2.3b**, **2.9b**) were isolated.

2.3a, 2.3b
(mix of isomers)

2.7a, 2.7b
(mix of isomers)

a, Ar = phenyl
b, Ar = fluorophenyl

Py = pyridine, C_5H_5N

2.9a, 2.9b
(mix of isomers)

2.8a, 2.8b
(mix of isomers)
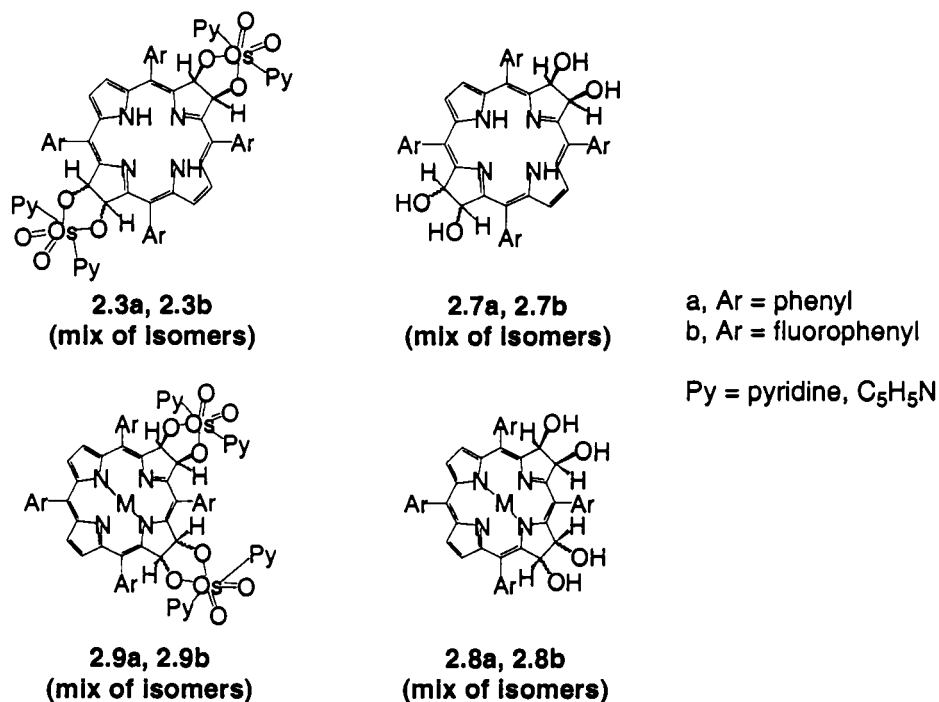
Scheme 2.3 Bacterio- and isobacteriochlorin regioisomers.

As expected, the absorbance spectra of osmate-(OH)$_4$TFPBCH$_2$ is bathochromically shifted while osmate-(OH)$_4$TFPiBCPt remains chlorin-like. As seen in Figure 2.23, the Soret and first Q-band of osmate-(OH)$_4$TFPBCH$_2$ occur respectively at 374 and 505 nm, however the second Q-band is red shifted to 704 nm. In comparison, the Soret band of osmate-(OH)$_4$TFPiBCPt is similar to that of osmate-(OH)$_4$TFPBCH$_2$ (380 nm) however; it has a single Q-band at 568 nm, with a shoulder at 529 nm. The

phenyl substituted bacterio- and isobacteriochlorin have been previously characterized.[56, 58]
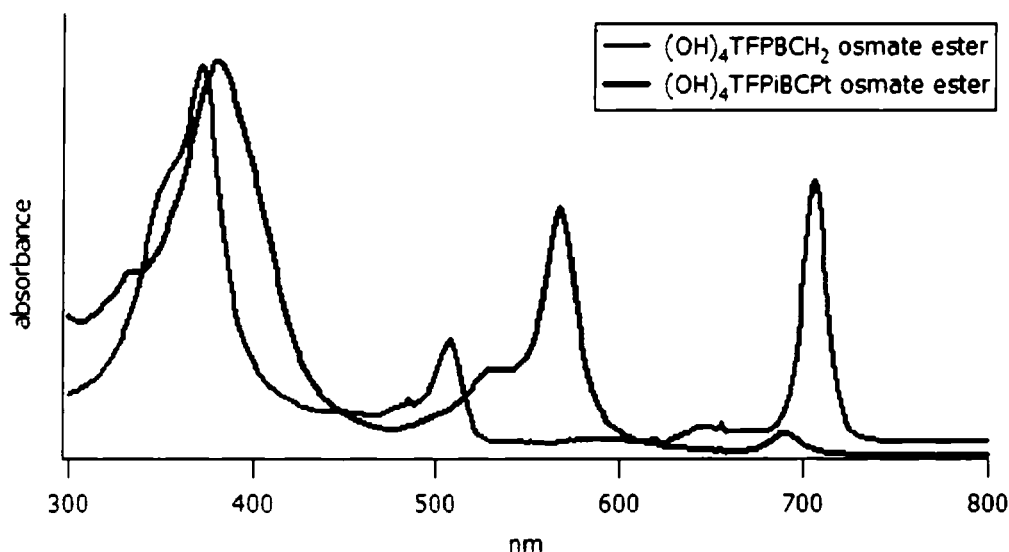
Figure 2.23 UV-Vis spectra of fluorophenyl substituted osmate bacterio- 2.3b and isobacteriochlorin 2.9b.

Crystalization of the fluorophenyl substituted osmate esters has proved to be surprisingly facile. Crystals suitable for a single crystal diffractometry study of bisosmate-(OH)$_4$TFPBCH$_2$ (2.3b) were grown by slow diffusion of petroleum ether into a CHCl$_3$ solution of 2.3b. The solid state of 2.3b is graphically represented in Figure 2.24 and confirms the expected and spectroscopically derived bacteriochlorin bisosmate ester structure. Its crystal structure shows a cis arrangement of the two osmate esters, with respect to their relative orientation to the mean plane of the porphyrin. The planarity of the porphyrin is only slightly disturbed through this substitution and the macrocycle is slightly twisted.
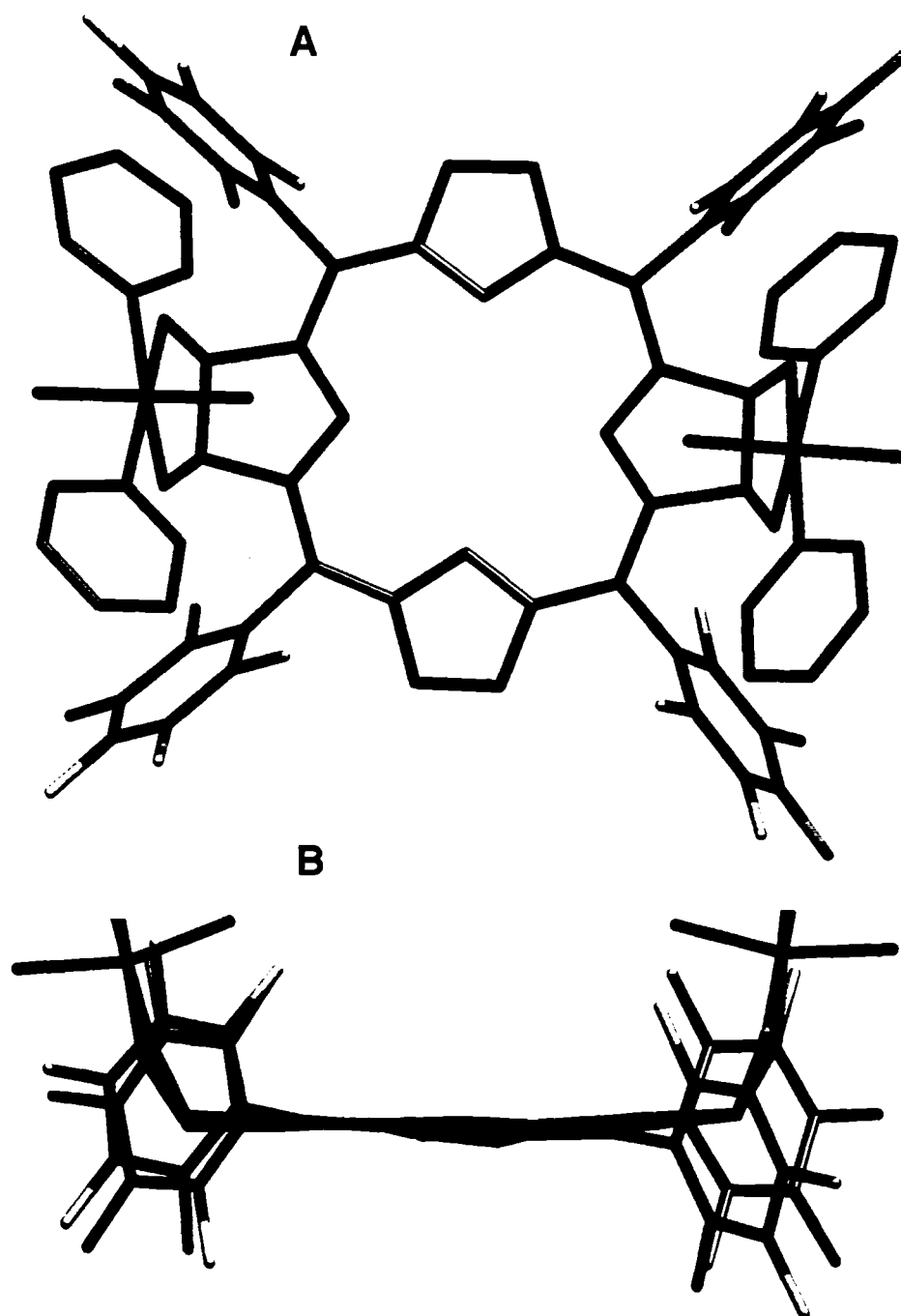
Figure 2.24 ORTEP representation of the single crystal X-ray structure of free base fluorophenyl substituted bacteriochlorin **2.3b**. A) Top view. B) Side view.[49]

Additionally, crystals suitable for a single crystal diffractometry study of osmate-(OH)$_4$TFPiBCZn (**2.9b**) were grown by slow diffusion of petroleum ether into a CHCl$_3$ solution of **2.9n**. The solid state of **2.9b** is graphically represented in Figure 2.25. The crystal structure of this isobacteriochlorin shows a *trans* arrangement of the two osmate esters, with respect to the plane of the porphyrin. Here, the plane of the porphyrin is maintained to be planar. The central zinc ion is coordinated with a fifths axial ligand, a ethanol moiety. The resulting square pyramidal coordination environment for the zinc ion is as frequently observed in zinc porphyrins.
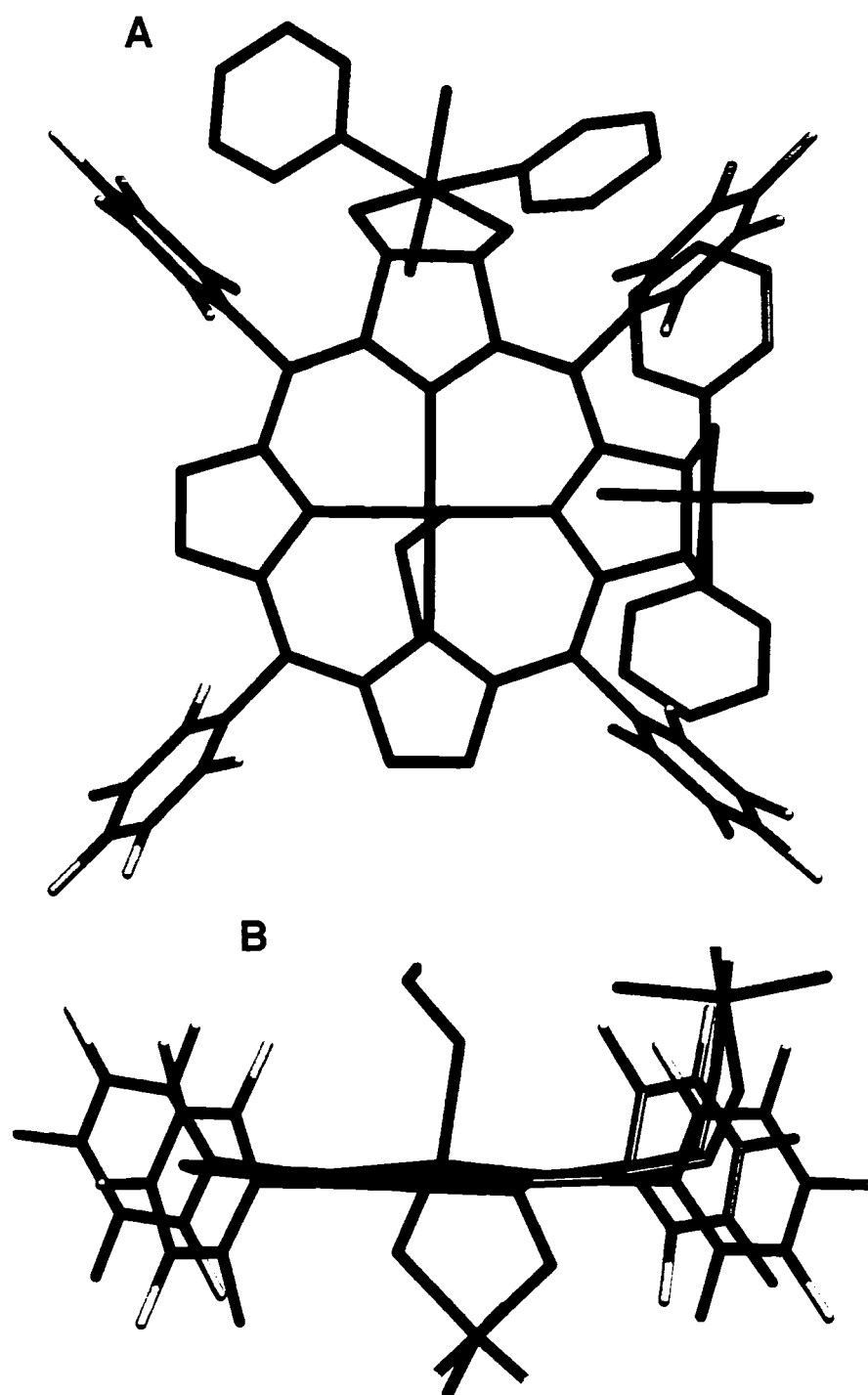
Figure 2.25 ORTEP representation of the single crystal X-ray structure of zinc fluorophenyl substituted isobacteriochlorin **2.9b**. A) Top view. B) Side view.[49]

The

The ^{1}H NMR of osmate-(OH)$_4$TFPBCH$_2$ **2.3b** shows the two-fold symmetry of the compound and indicates the presence of four pyridines represented by a series of three multiplets (Figure 2.26). The first multiplet at 8.4 ppm represents the eight *o*-hydrogen, the next at 8.0 ppm represents the four *p*-hydrogen, and the last at 7.5 ppm represents the eight *m*-hydrogen of the pyridines. The four equivalent β-hydrogen are observed as a multiplet at 8.6 ppm due to coupling to the inner imine protons and lack of N-H tautomerism while the multiplet at 6.6 ppm corresponds to the four pyrrolidine-hydrogens. No indication on the relative *cis* or *trans* arrangement of the osmate esters can be derived from the ^{1}H NMR.

Figure 2.26 ^{1}H NMR of osmate-(OH)$_4$TFPBCH$_2$ **2.3b** (Ar = C$_6$F$_5$).

The ^{1}H NMR of osmate-(OH)$_4$TFPiBCPt **2.9b** is very similar to that of osmate-(OH)$_4$TFPBCH$_2$ **2.3b**. Both compounds possess two-fold symmetry. The four pyridines are represented by multiplets at 8.5 ppm (*o*-hydrogen), 7.8 ppm (*p*-hydrogen), and 7.4 ppm (*m*-hydrogen). Four β-hydrogen have ^{3}J vicinal coupling and appear as doublets at 8.0 and 7.7 ppm while the multiplet at 6.4 ppm corresponds to the pyrrolidine hydrogens. The coupling of these hydrogens is the most diagnostic feature for the isobacteriochlorin structure.

2.4.b Oxidation of the Lactone

As shown in Scheme 2.4, dihydroxylation of (COO)TPLH$_2$ with OsO$_4$ in pyridine affords the osmate ester of the dihydroxyporpholactone **2.10a**. Subsequent cleavage of the osmate ester with H$_2$S gives **2.11a** in up to a 67% yield. The osmate ester of the fluorophenyl substituted dihydroxyporpholactone **2.10a** can be synthesized in up to a 33% yield.

2.5a, 2.5b   **2.10a, 2.10b**   **2.11a, 2.11b**

a, Ar = phenyl
b, Ar = fluorophenyl

Py = pyridine, C$_5$H$_5$N
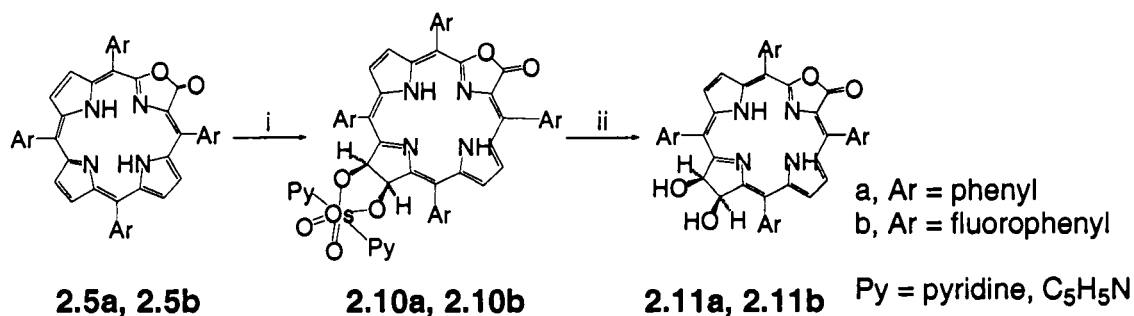
Scheme 2.4 Dihydroxylation of free base lactone. i) OsO$_4$/pyridine, ii) H$_2$S.

In similar yields, the formation of isobacteriochlorins can be directed through the oxidation of metallated lactones (Scheme 2.5).
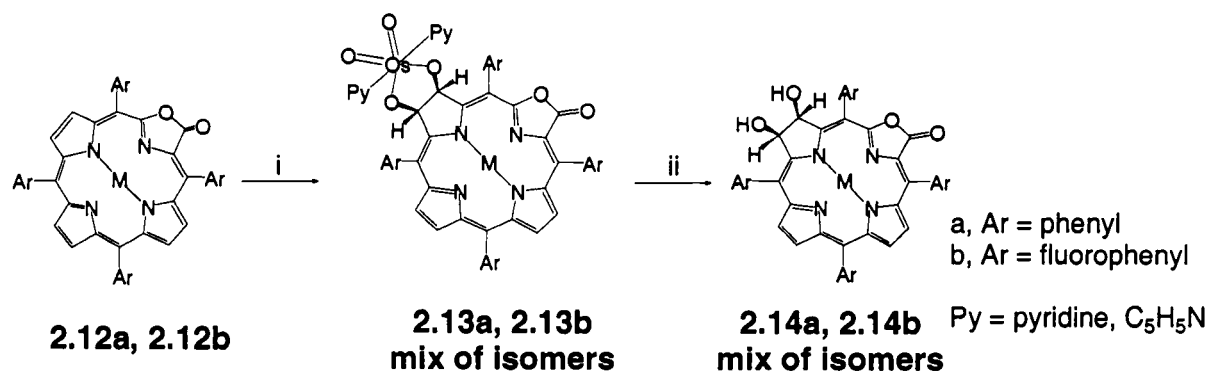
Scheme 2.5 Dihydroxylation of metalated lactone. i) OsO_4/pyridine, ii) H_2S.

In the UV-Vis spectra of the free base dihydroxyporpholactones **2.11a** and **2.10b** are shown in Figure 2.27. Instead of the expected bacteriochlorin peak, one broad Q-band, from 505-550 nm is observed in the UV-Vis spectra of osmate-$(OH)_2(COO)TFPBLH_2$ (**2.10b**).
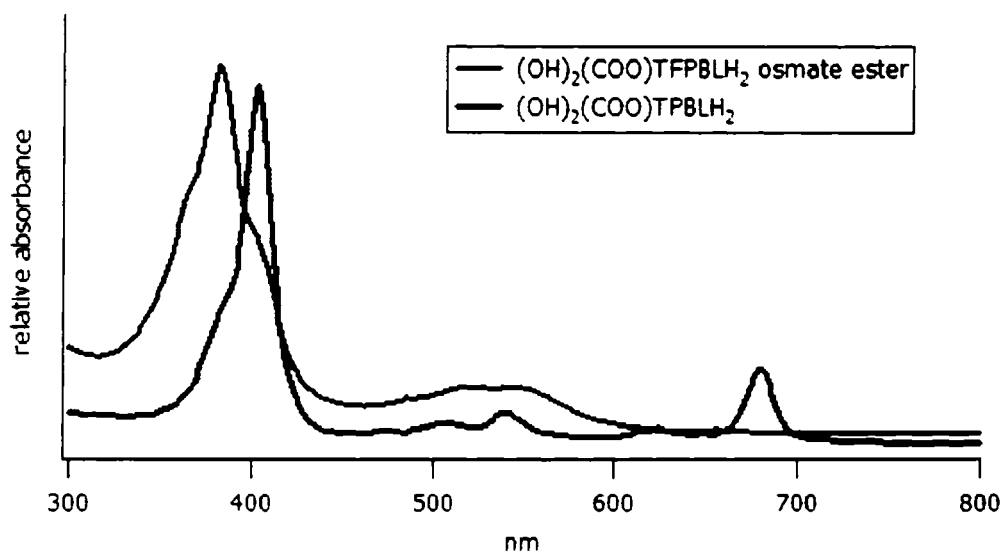
Figure 2.27 UV-Vis absorbance spectra of free base dihydroxylactone species **2.10b**, **2.11a**.

The UV-Vis absorbance spectra of the platinum dihydroxyporpholactones **2.13b** and **2.14a** are shown in Figure 2.28. Similar to typical metalloporphyrins which have two Q-bands instead of four; these platinum isobacteriochlorins all have a single Q-band at approximately 600 nm with a shoulder at around 550 nm. Also representative of chlorin-like spectra, these peaks are not red shifted in comparison to the bacteriochlorins.
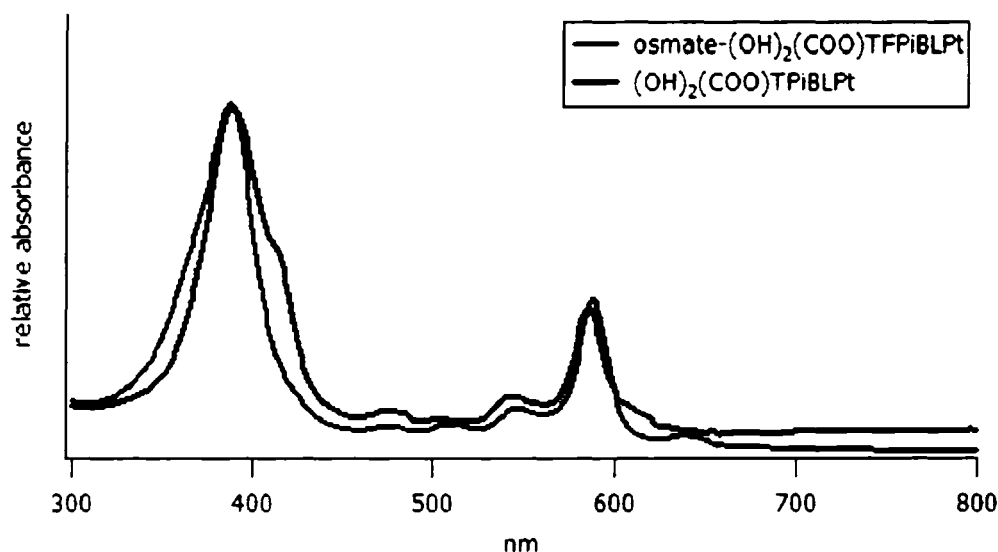
Figure 2.28 UV-Vis absorbance spectra of platinum isobacteriochlorin species **2.13b**, **2.14a**.

The IR spectra of both the free base and metallated dihydroxylactones show strong absorption between 1750-1735 cm^{-1}, characteristic of C=O ester stretching.

The ^{1}H NMR of $(OH)_2(COO)TPBLH_2$ **2.11a** shows broad multiplets in the aromatic region (7.5 - 8 ppm) representative of twenty phenyl protons (Figure 2.29). The four β-hydrogen signals consist of a double doublet (1H, δ = 8.5 ppm), a multiplet (2H, δ = 8.3 ppm), and a doublet (1H, δ = 8.1 ppm) caused by the asymmetry of the lactone moiety as well as small coupling to the NH protons. The two β-hydrogen adjoined to the OH carbon are seen as a doublet of doublets at 6.1 - 6.2 ppm. This complex coupling arises from the ^{3}J vicinal coupling of one β-hydrogen with the other, as well as ^{3}J and ^{4}J coupling with each of the hydrogen of the alcohol. The two hydrogen of the alcohol

consist of two doublets at 3.0 and 3.1 ppm while the imine hydrogen consists of two singlets at -1.1 and -1.5 ppm (not shown). The interpretation of the ^{1}H NMR of $(OH)_2(COO)TPBLH_2$ **2.11a** is confirmed by the addition of D_2O to the NMR tube. The addition of D_2O induces the exchange of deuterium with the hydrogen of the alcohol and imine. Hence, the OH and NH protons around 3 and -1 ppm disappear while the double of doublets around 6 ppm is simplified to a pair of doublets.
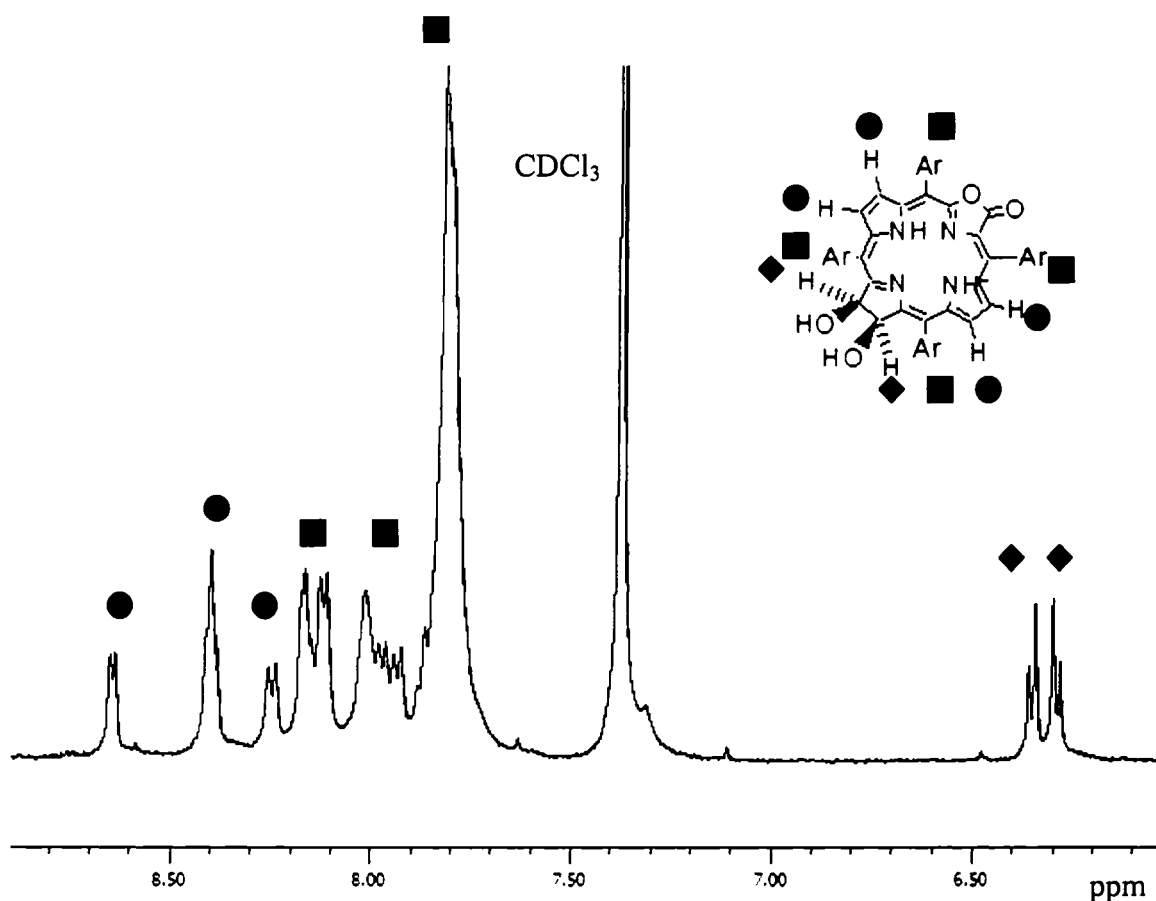
Figure 2.29 ^{1}H NMR of $(OH)_2(COO)TPBLH_2$ **2.11a** (Ar = C_6H_5).

The ^{1}H NMR of osmate-$(OH)_2(COO)TFPBLH_2$ **2.10b** is comparable to that of $(OH)_2(COO)TPBLH_2$ **2.11a**, save for the absence of phenyl protons and the addition of pyridine protons.

The ^{1}H NMRs of the platinum dihydroxylactones **2.13b** and **2.14a**, show a mixture of two isobacteriochlorin dihydroxylactone isomers that are formed by the relative orientation of the lactone moiety. One isomer carries the lactone carbonyl group next to the diol functionality, the other carries the lactone moiety away from it. However, the exact isomeric ratio of this mixture cannot be determined by ^{1}H NMR.

With all porpholactone oxidations, we consistently observe that the fluorophenyl substituted substrates provide much lower yields than the phenyl substituted substrates. Nonetheless, both the tetraols and dihydroxyporpholactones provide a stable intermediary towards the synthesis of the dilactone. As expected, the bacteriochlorins display a bathochromatic shift in spectral absorbance and could themselves be used towards sensor development. All photochemical results regarding the tetraols and novel dihydroxyporpholactones are presented in Section 2.7.

Section 5: Oxidation of Dihydroxyporpholactones and Tetraols

The two synthetic intermediates to dilactone, tetraol and dihydroxylactone, were described in Section 2.4. The MnO_4^- oxidation of both these species is thought to give rise to the novel porphodilactone. As described in Section 2.3.a, the method we chose for the MnO_4^--mediated diol oxidation includes $KMnO_4$ in THF, with 18-crown-6 as the phase transfer catalyst or the organically soluble cetyltrimethylammonium permanganate (CTAP). The oxidation of the free base dihydroxyporpholactones **2.10a**, **2.10b**, **2.11a** to dilactone **2.12a**, **2.12b** proceeds in satisfactory yields with the use of $KMnO_4$ in THF with 18-crown-6. (We did not attempt oxidation of the metallated dihydroxyporpholactones.) The phenyl substituted **2.11a** was oxidized to the dilactone in an approximately 50% yield while the fluorophenyl substituted reaction of **2.10b** to the dilactone proceeded at a lower yield of 37%.
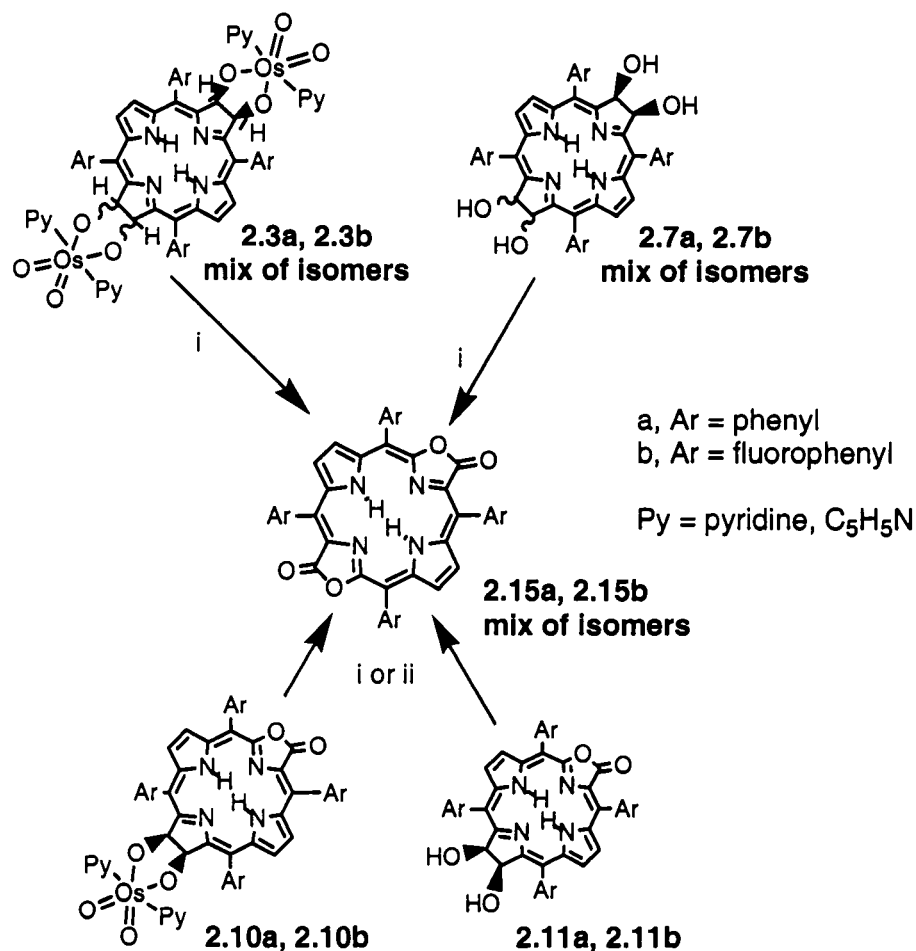
Scheme 2.6 Synthesis of bacteriochlorin dilactone. i) CTAP, ii) KMnO₄/THF, 18-crown-6.

The oxidization of the phenyl and fluorophenyl substituted tetraolbacterio- (**2.3a**, **2.3b**, **2.7a**) and tetraolisobacteriochlorin (**2.8a**, **2.9a**, **2.9b**) regioisomers was accomplished with the used of CTAP. Oxidation of the tetraolbacteriochlorin (OH)₄TPBCH₂ **2.7a** and osmate-(OH)₄TFPBCH₂ **2.3b**, produced spectroscopically comparable bacteriodilactone **2.15a**, **2.15b** in low yields. Platinum and zinc tetraolisobacteriochlorim **2.8a**, **2.9a**, **2.9b** were also successfully oxidized to their corresponding metallated dilactones with the use of CTAP.
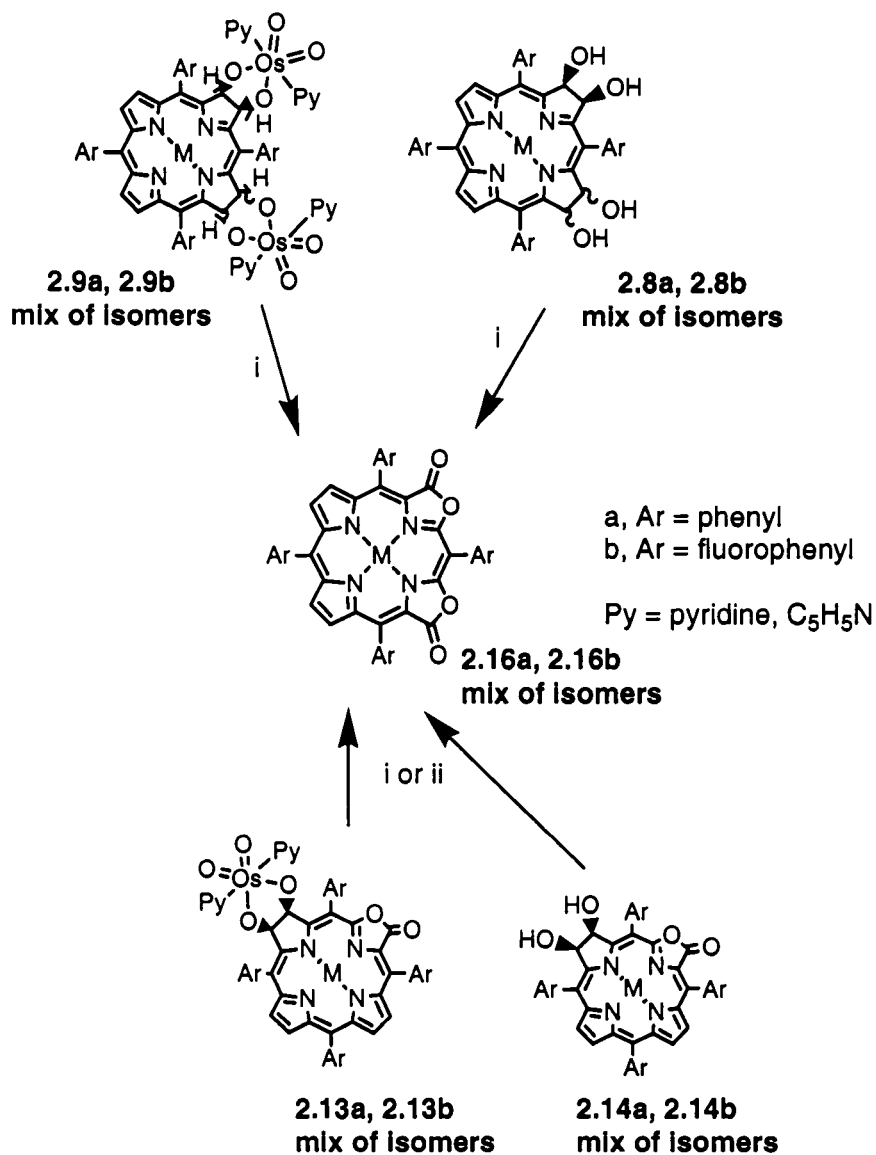
Scheme 2.7 Synthesis of isobacteriochlorin dilactone. i) CTAP, ii) KMnO$_4$/THF, 18-crown-6.

The UV-Vis absorbance spectra of the free base bacteriochlorin dilactones **2.15a**, **2.15b** are shown in Figure 2.30. The absorbance spectrum of (COO)$_2$TPBLH$_2$ **2.15a** has four Q-bands with the longest wavelength Q-band at 655 nm. The spectrum of (COO)$_2$TFPBLH$_2$ **2.15b** shows the longest wavelength Q-band at 664 nm.
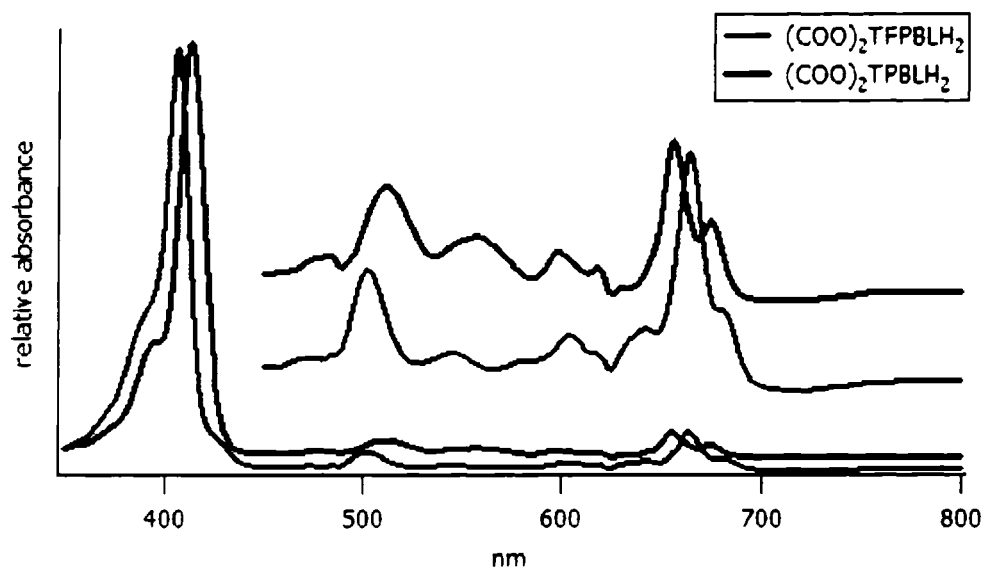
Figure 2.30 UV-Vis absorbance spectra of free base bacteriochlorin dilactones **2.15a**, **2.15b**.

The UV-Vis absorbance spectrum of the platinum fluorophenyl substituted isobacteriochlorin dilactone **2.16a**, **2.16b** is shown in Figure 2.31. The absorbance spectrum of $(COO)_2$TFPiBLPt has a broad band Soret at 390 nm and a single Q-band at 572 nm.
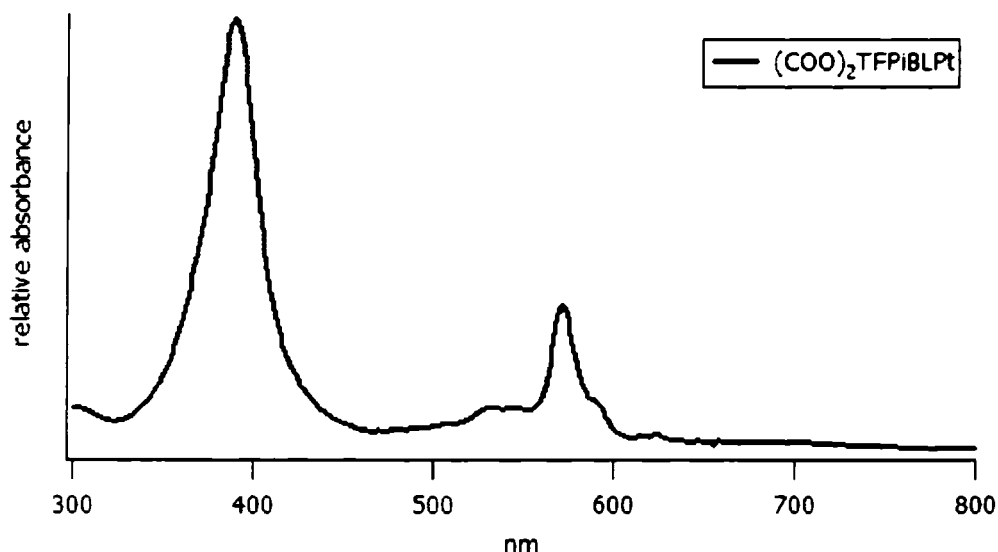
Figure 2.31 UV-Vis absorbance spectra of platinum fluorophenyl substituted isobacteriochlorin dilactone **2.16b.**

All dilactone IR spectra show a strong absorption attributed to the C=O lactone stretching $(1750\text{-}1735 \text{ cm}^{-1})$ mode and aromatic C=C stretching absorptions around 1500 cm^{-1}.

The free base dilactones are produced in an isomeric mixture (shown in Scheme 2.6). These two isomers can be visualized by TLC. While having approximately the same R_f values, $(COO)_2TPBLH_2$ **2.15a** ($R_f = 0.58$, silica-CHCl$_3$) is dark brown at the top of the TLC spot while grey/green at the bottom and $(COO)_2TFPBLH_2$ **2.15b** ($R_f = 0.93$, silica-CHCl$_3$) is dark purple at the top while light blue/green at the bottom. Chromatographic separation of the isomers could not be achived even using High Performance TLC plates (silica-CH$_2$Cl$_2$/hexanes 1:1).

Although we have not been able to separate them, the ratio of the regioisomers can be determined by ^1H NMR. In the ^1H NMR of $(COO)_2TPBLH_2$ **2.15a** an isomeric ratio of 1:3 C_{2h}- to C_{2v}- dilactone isomer is typically observed (Figure 2.32). Due to ^4J coupling to the inner imine protons, the two sets of C_{2h}-isomer β-hydrogen are consistent with two doublets at 8.6 and 8.2 ppm (J = 0.1 ppm), each equivalent to 3H. The β-hydrogen of the C_{2v}-isomer correspond to the pair of doublets of doublets (each 1H, δ =

7.6, 7.8) from ^3J vicinal coupling in addition to ^4J coupling to the inner imine protons. The m- and p-phenyl hydrogen are equivalent in both isomers and are observed as a broad multiplet in the aromatic region (24H, $\delta = 7.7$). However, the o-phenyl hydrogen are not equivalent in each isomer. Due to ^3J and ^4J vicinal coupling along the phenyl ring, each o-phenyl hydrogen is represented by a double doublet. The signals for the two o-phenyl hydrogen of the C_{2h}-isomer appear at 8.0 and 7.8 ppm each having an abundance of 3H. The signals for the C_{2v}-isomer o-phenyl hydrogen are at 8.1 and 7.9 ppm each having an abundance of 1H. There are no phenyl protons in the ^1H NMR of $(COO)_2TFPBLH_2$ **2.15b**, only four β-hydrogen in an isomeric ratio of 1:2 C_{2v}- to C_{2h}-dilactone isomer. Here we see no coupling to the inner imine protons. Two singlets at 8.7 and 8.5 ppm, each 2H, correspond to the C_{2h} β-hydrogen. Each C_{2v} β-hydrogen has ^3J vicinal coupling and corresponds to the possible pairs of doublets at 8.9 and 8.6 ppm, each 1H.
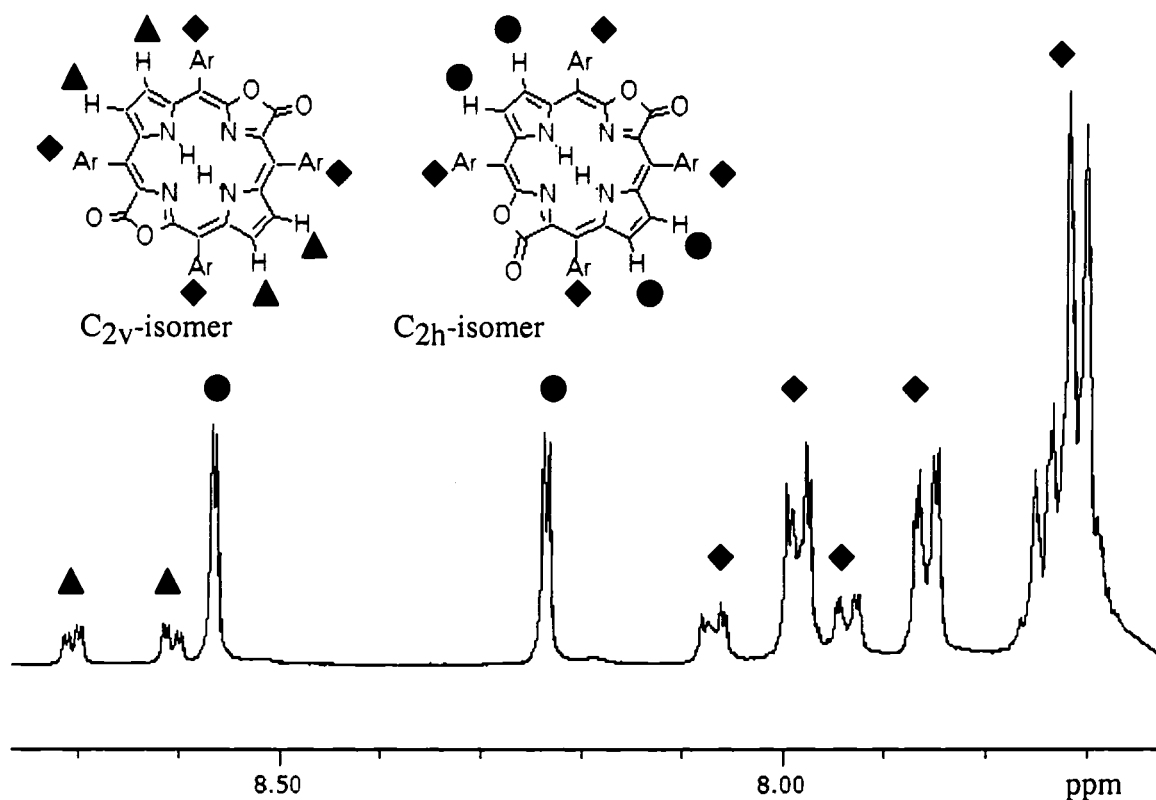
Figure 2.32 ^{1}H NMR of $(COO)_2TPBLH_2$ **2.15a** $(Ar = C_6H_5)$.

The isobacteriochlorin dilactones are produced as a mixture of three regioisomers as shown in Scheme 2.7. Separation of these regioisomers is not readily achieved but the possible formation of an isomeric mixture of dihydroxylactone intermediates is observed while monitoring the reaction by TLC. By TLC $(COO)_2TFPiBLZn$ appears light green in color and runs at a high polarity while the starting material $(OH)_4TFPiBCZn$ is dark green in color and runs at a low polarity. During the course of the reaction, a blue/green intermediary appears between the starting material and product. A similar intermediary is observed in the synthesis of $(COO)_2TFPiBLPt$. We are attempting to separate and characterize these proposed dihydroxylactone intermediates but no conclusive spectroscopic evidence is presented here.

Again we are not able to separate the regioisomers of the isobacteriochlorin dilactones but ^{1}H NMR allows us to determine the ratio of each regioisomer in the product mixture. The regioisomers of the metallated isobacteriochlorin dilactone form in a 1:1:1 ratio of the three isomers. It is possible to observe three different regioisomers, each with a total of four β-hydrogen, in the ^{1}H NMR of $(COO)_2$TFPiBLZn **2.16b**. A pair of doublets (δ = 8.1, 8.3 ppm), each 4H, represent the eight β-hydrogen of the two equivalent isomers. The non-equivalent isomer consists of a multiplet (2H, δ = 8.4) and two doublets (δ = 8.5, 8.7 ppm), each 1H. The ^{1}H NMR of $(COO)_2$TFPiBLPt **2.16b** is similar to the ^{1}H NMR of $(COO)_2$TFPiBLZn **2.16b** except weak Pt-H coupling is observed as described in Section 2.3.a.

As detailed in Sections 1.5 and 2.1, our prime synthetic goal was the bacteriochlorin dilactone platinum complex. Since we were able to separately direct the formation of bacteriochlorin and isobacteriochlorin using the methodology given in Section 2.4, we have been able to make free base bacteriochlorin dilactone **2.15a**, **2.15b**, and metallated isobacteriochlorin dilactone **2.16a**, **2.16b**. As shown in Scheme 2.8, we assume that the metallation of the free base **2.15a**, **2.15b** would produce our desired product while a demetallation of **2.16a**, **2.16b** would complete the series of the family of dilactones.
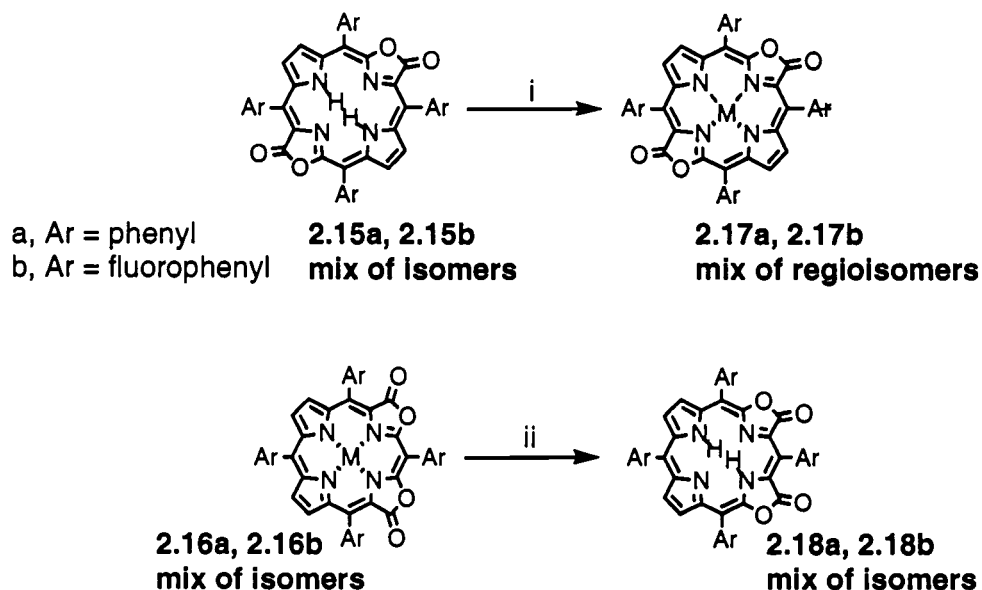
Scheme 2.8 Metallation of the bacteriochlorin dilactone i) Pt(II) salt/benzonitrile. Protonation and demetallation of the isobacteriochlorin dilactone ii) H⁺.

Platinum metalation of (COO)₂TPBLH₂ **2.15a** was attempted using a variety of platinum salts (platinum (II) chloride, potassium tetrachloroplatinate (II), platinum (II) pentanedionate). Whereas metalation of (COO)TPBLH₂ **2.5a** in this same manner had been successful as shown in Section 2.3.b, metalation of (COO)₂TPBLH₂ **2.15a** failed to produce one major product that was identifiable as the target species. The platinum metalation conditions induced the formation of a a slight amount of a new green product as seen by TLC, but the two species could not be separated by chromatography though we hypothesize this product to be the (COO)₂TPiBLPt **2.17a**. Longer reaction times did not increase the yield of this green product. With the metallation of (COO)₂TPBLH₂ **2.15a** unsuccessful, metallation of (COO)₂TFPBLH₂ **2.15b** was not attempted. Now write an explanation for the failed metalation (less acidic due to vinylogous lactame moieties, etc, connect to acid-base chapter.

Protonation and demetallation of (COO)₂TFPiBLZn **2.16b** was attempted using 100% TFA. This strong acid induced a slight color change from light green to blue. The UV-Vis absorbance spectra of this acid induced blue product shows a slight

bathochromic shift in Q-band but, surprisingly, no demetallation, even after two hour reaction time With the demetallation of $(COO)_2$TFPiBLZn **2.16b** being unsuccessful, demetallation of $(COO)_2$TFPiBLPt was not attempted.

As demonstrated in Section 2.3, monolactones are less basic than porphyrins. This is because one pyrrolic nitrogen of a porphyrin is converted to a vinylogous amide in the synthesis of porpholactone, thus accounting for the decreased basicity of porpholactones. Given this, dilactones should be even less basic than monolactones, with fluorophenyl substituted derivatives being yet less basic. Therefore we predict that protonation and subsequent demetallation is impossible with the dilactones.

Section 6: Non-related Porphyrin Macrocycles for use as Novel NIR Sensors

The triplet-emission of the platinum porphyrins are ligand-based. In other words, it is expected that a longer wavelength absorbing free base porphyrin derivative will lead also to a longer wavelength triplet emission. A number of other porphyrin derivatives with significantly red-shifted absorption spectra were reported in recent years. Among them, three derivatives are directly derived from diol chlorins, the starting material for the porpholactones investigated (Scheme 2.9).
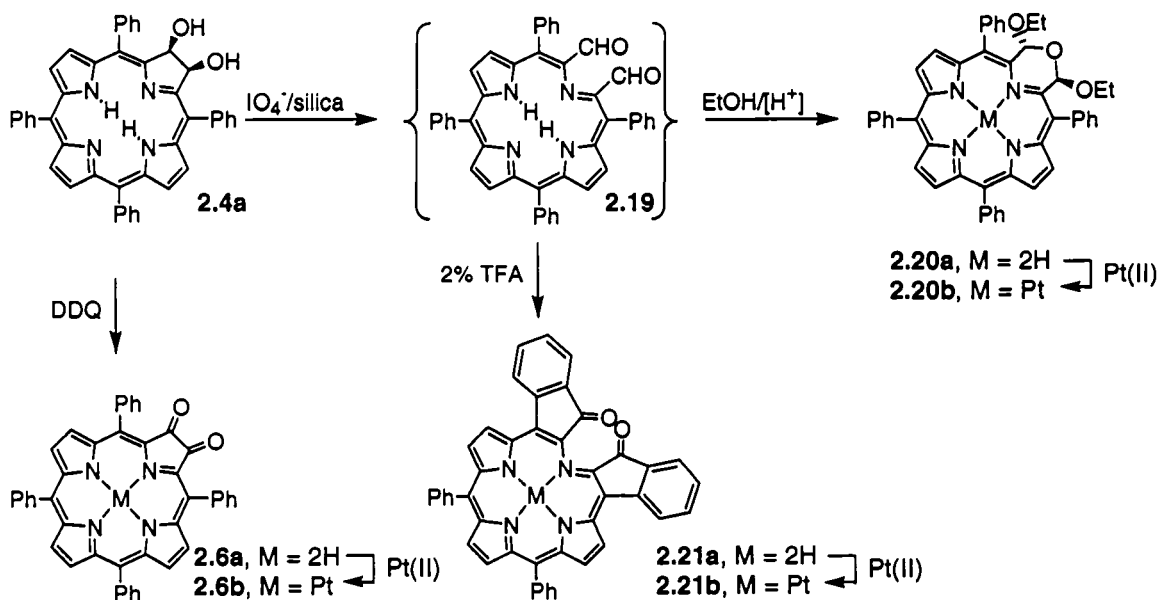
Scheme 2.9 Synthesis of porphyrins with red-shifted absorption spectra derived from diol chlorins.

Oxidation of diol chlorin **2.4a** using DDQ generates the dione ((O=)₂TPCH₂) **2.6a**.[59] As seen in Section 2.3.a (Scheme 2.1), the dione was also generated by MNO oxidation. This compound is characterized by a very broad and red-shifted Q-band as compared to porphyrins and chlorins. Diol cleavage using periodate fixed on silica gel forms the corresponding secochlorin bisaldehyde ((CHO)₂TPCH₂) **2.19a**.[60] This

chromophore is, however, not stable and is therefore not isolated but reacted *in situ*. Thus, reaction with a nucleophile such as EtOH generates the morpholinochlorin ((EtO)$_2$TPMH$_2$) **2.20a** (the name is derived from the morpholine moiety that is incorporated into a porphyrin-like framework).[60] The UV-vis spectrum of this pyrrole-modified porphyrin is chlorin-like with a λ_{max} of 680 nm. Reaction of **2.19a** under strongly acidic conditions and the absence of a nucleophile leads to a nucleophilic attack of the carbonyl groups on the *o*-positions of the neighboring *meso*-phenyl groups. The resulting primary product, bis-secondary alcohol, oxidizes spontaneously, and indaphyrin (DPIH$_2$) **2.21a** is the sole isolated product (the name indaphyrin is derived from the indanone units attached to the porphyrin).[60, 61] Indaphyrins have, owing to their two conjugated ketone groups and the two co-planar phenyl groups and their computed non-planarity, extremely modified UV-vis spectra as compared to most other porphyrinic chromophores. Key to their interest with respect to the creation of red-emitting chromophores, λ_{max} of **2.21a** is 812 nm.

As all three free base derivatives **2.6a**, **2.20a**, and **2.21a** were reported by the Bruckner group, they were readily available.[59-61] Furthermore, all three proved to be readily susceptible to platinum insertion using standard methods (PtCl$_2$ in hot PhCN) to provide **2.6c**, **2.20b**, and **2.21b**, respectively. All platinum compounds had the ^{1}H and ^{13}C NMR spectroscopic properties expected and they were comparable to those of the well known Ni(II) complexes.
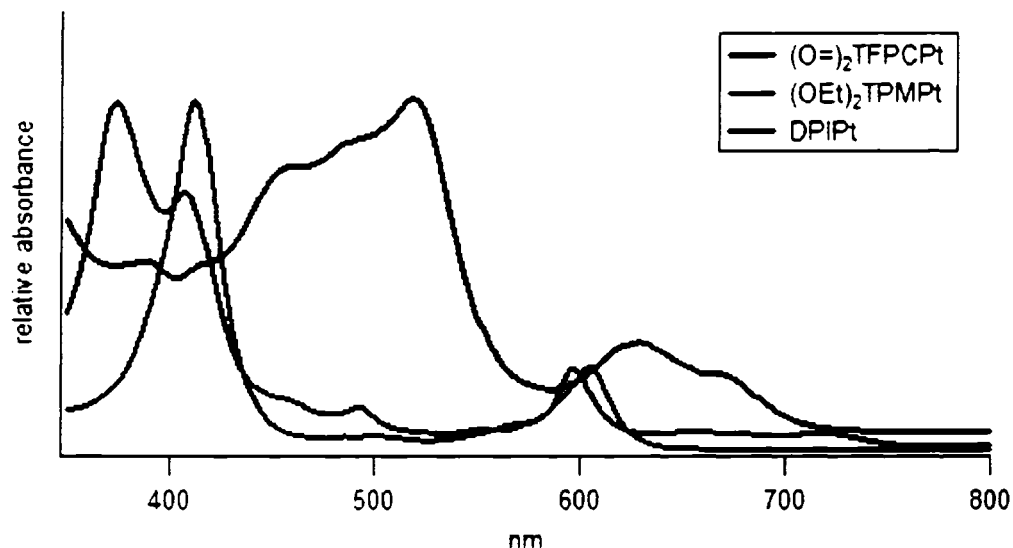
Figure 2.33 Absorbance spectra of the platinum dione **2.6c**, morpholino chlorin **2.20b**, and indaphyrin **2.21b**.

As seen in their absorbance spectra, each platinum complex has a broad band Soret and single Q-band, as expected for metallated porphyrins. While **2.6c** and **2.20b** absorb at anticipated wavelengths of approximately 400 and 60 nm, the indaphyrin **2.21b** has bathochromically shifted broad band emissions at 516 nm and 628 nm.

Crystals of **2.21b** suitable for single crystal diffractometry study were grown by gas-phase diffusion of MeCN into a saturated $CHCl_3$-solution of **2.21b**. The solid state structure confirms the spectroscopically derived connectivity of the compound, in particular the ketone linkage between the secoporphyrin framework and the (near co-planar) meso-phenyl groups. The structure also shows the twist of the mean plane of the macrocycle. It is worth noting that this twist is inherent to the macrocycle and was also predicted for the free base compound.[61] Irrespective of this twist, the Pt(II) center is coordinated in a perfect square planar arrangement and all Ni-N bond distances are within 0.02 Å identical to those observed in platinum porphyrin.
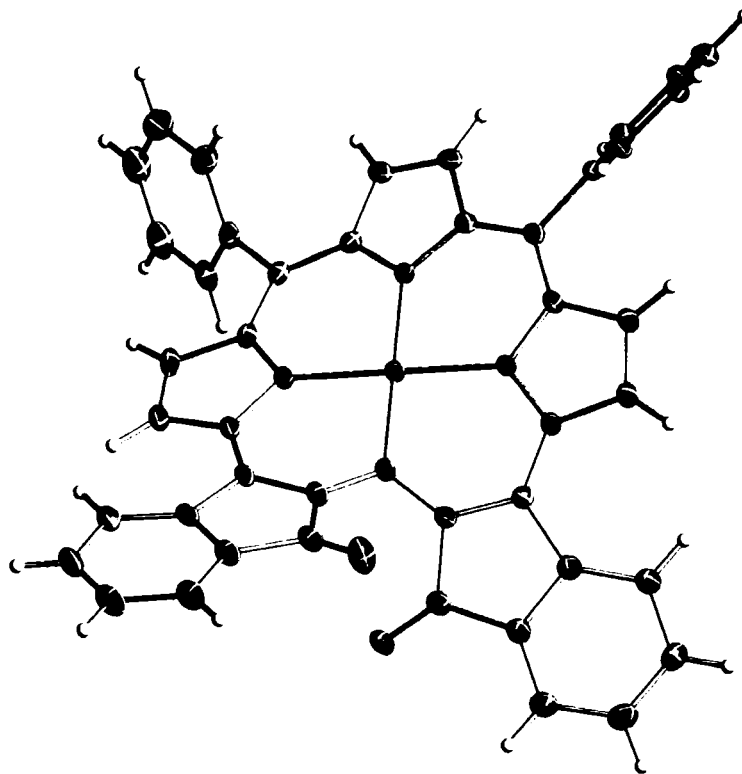
Figure 2.34 ORTEP representation of the single crystal X-ray structure of 2.21b.[49]

Section 7: Photophysical Measurements

2.7.a Introduction

As explained in detail in Section 1.4, porphyrins exhibit unique electronic and spectroscopic properties. Porphyrin absorption, which describes why blood is red and grass is green, is explained by Gouterman's four orbital theory.[23] Porphyrin luminescence which includes both fluorescence and phosphorescence, is quenched by diatomic oxygen.[29-32] These parameters (the rate of luminescence emission and the rate of radiation absorption) can be used to calculated quantum yield and emission lifetimes of various porphyrin derivatives.

The use of porphyrins in photodynamic therapy (PDT), which utilizes the O_2 quenching of the porphyrin and the creation of singlet O_2, has been a major accomplishment in porphyrin application. Our work with porphyrins involves their use as oxygen sensors, with our pressure sensitive paint (PSP) utilizing their ability to measure oxygen consumption and concentration via phosphorescence quenching of the porphyrin triplet state (Section 1.5). As described in Chapter 2, we are working towards the synthesis of a NIR oxygen sensor for the incorporation of multiple analyte detectors, as well as the creation of a chemosensor to be used in *in vivo* biological systems. A non-invasive, *in vivo* oxygen sensor would be of major importance since oxygen is a key metabolite, and tissue hypoxia is a critical parameter with respect to various tissue pathologies, such as retinal diseases, brain abnormalities and cancer. In addition, imaging technologies for mapping tissue oxygenation have yet to be adequately developed. However, researchers have found that phosphorescence quenching is exquisitely sensitive and selective to oxygen, possesses excellent temporal resolution and can be implemented for high-resolution hypoxia imaging in 2D.[62]

A porphyrin sensor that functions in the NIR is necessary because the depth of penetration of light into tissue is limited by optical absorption, due to endogeneous tissue chromophores, mainly hemoglobin, and by optical scattering within the tissue. To be used *in vivo*, the porphyrin sensor would need to absorb light strongly up to the near-IR

region (600-900 nm), where light has greater penetration into tissue. Detection of the porphyrin sensor would also need to be in the NIR region (700-1400 nm) to avoid the emission of water. In recent years InGaAs detectors have become readily available to detect emission in this region.

The phenyl substituted diol, tetraol, and lactone have been previously described by Brückner, Dolphin, and coworkers while the fluorophenyl substituted lactone was previously described by Gouterman, Khalil, and coworkers.[3, 20, 22, 56, 58] Additionally, the syntheses of the dione, indaphyrin, bisaldehyde tetraphenyl secochlorin, and diethyl tetraphenyl morpholino chlorin have also been previously detailed.[59-61] However, the majority of the fluorophenyl substituted and a few of the phenyl substituted porphyrin derivatives discussed in Chapter 2 are novel species. We present here for the first time the photophysical results from the novel porphyrin derivatives in the synthetic series presented in Chapter 2.

2.7.b Free Base Series

As seen in Table 2.3, the phenyl substituted free base porphyrin **2.1a** is comparable in absorption wavelength to the pyrrole reduced chlorins **2.2a**, **2.4a**, **2.5a**. However, when a second pyrrole group is reduced, forming a bacteriochlorin **2.7a**, **2.11a**, **2.15a**, the absorption wavelength is red shifted up to 60 nm, depending on the chemical substituents to the pyrrole ring. The emission wavelengths for these species range from approximately 650-750 nm and are given in Table 2.4. Figure 2.35 shows that there is minimal change in emission wavelength with the reduction of one or two pyrrole rings.

Table 2.3 Absorption Wavelengths of Free Base Phenyl Substituted Series.

Compound Name	Abbreviation	Absorption (nm)				
		B(0,0)	$Q_y(1,0)$	$Q_y(0,0)$	$Q_x(1,0)$	$Q_x(0,0)$
meso-tetrakisphenylporphyrin	TPPH$_2$	415	514	545	587	645
meso-tetrakisphenyl-2,3-dihydroxychlorin	(OH)$_2$TPCH$_2$	404	514	539	593	646
meso-tetrakisphenyl-2,3-dihydroxychlorin osmate ester	osmate - (OH)$_2$TPCH$_2$	418	518	545	594	648
meso-tetrakisphenyl-2-oxa-3-oxoporphyrin; porpholactone	(COO)TPLH$_2$	415	517	554	590	642
meso-tetrakisphenyl-2,3-*cis*-dihydroxy-12-oxa-13-oxochlorin	(OH)$_2$(COO) TPBLH$_2$	404	Q(1,0) 540	Q(0,0) 679		
meso-tetrakisphenyl-2,12-dioxa-3,13-dioxoporphyrin (C$_{2v}$-isomer) and *meso*-tetrakisphenyl-2,13-dioxa-3,12-dioxoporphyrin (C$_{2h}$-isomer), bacteriodilactone, mix of isomers	(COO)$_2$TPBLH$_2$	406	Q(1,0) 511	Q(1,0) 656		
meso-tetrakisphenyl-2,3,12,13-tetrahydroxybacteriochlorin osmate ester, (believed to be the trans isomer)	osmate-(OH)$_4$TPBCH$_2$	420	Q(1,0) 534	Q(0,0) 706		
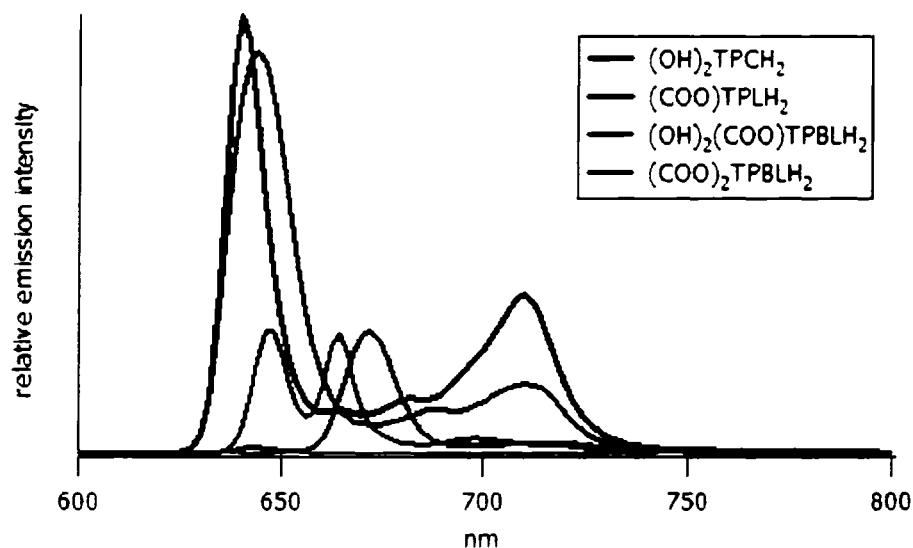
Figure 2.35 Emission spectra of phenyl substituted free base porphyrin derivatives.

Table 2.4 Emission, Lifetime, and Quantum Yield of Free Base Phenyl Substituted Series.

Abbreviation	Emission (nm) in EtOH fluorescence		Quantum Yield	
			Φ_f	Φ_p
TPPH$_2$	652	718	0.11	10^{-4}
(OH)$_2$TPCH$_2$	644	710		
osmate - (OH)$_2$TPCH$_2$	644	710		
(COO)TPLH$_2$	640	708		
(OH)$_2$(COO)TPBLH$_2$	672	716		
(COO)$_2$TPBLH$_2$	648	664		

The absorption wavelengths of the fluorophenyl substituted free base porphyrin derivatives are given in Table 2.5. The only derivative that shows a significant red shifted absorption is the tetrahydroxybacteriochlorin osmate ester **2.3b** (Q(0,0) = 712 nm). The dihydroxylactone bacteriochlorin **2.15a** is actually hypsochromically shifted to a Q(0,0) of 545 nm. The emission wavelengths for these species range from approximately 650-708 nm and are listed in Table 2.6. Figure 2.36 shows emission from the majority of these species at approximately 640 nm and 708 nm.

Table 2.5 Absorption Wavelengths of Free Base Fluorophenyl Substituted Series.

Compound Name	Abbreviation	Absorption (nm)				
		B(0,0)	$Q_y(1,0)$	$Q_y(0,0)$	$Q_x(1,0)$	$Q_x(0,0)$
meso-tetrakis(pentafluoro-phenyl)porphyrin	TFPPH$_2$	410	505	535	582	635
meso-tetrakis(pentafluoro-phenyl)-2,3-dihydroxychlorin osmate ester	osmate - (OH)$_2$TFPCH$_2$	408	505	535	598	650
meso-tetrakis(pentafluoro-phenyl)-2-oxa-3-oxoporphyrin; porpholactone	(COO) TFPLH$_2$	416	512	546	592	644
meso-tetrakis(pentafluoro-phenyl)-2,3-*cis*-dihydroxy-12-oxa-13-oxochlorin; dihydroxy bacteriolactone	osmate-(OH)$_2$(COO) TFPBLH$_2$	382	Q(1,0) 505	Q(0,0) 545		
meso-tetrakis(pentafluoro-phenyl)-2,12-dioxa-3,13-dioxoporphyrin and -2,13-dioxa-3,12-dioxoporphyrin, bacteriodilactone, mix of isomers	(COO)$_2$ TFPBLH$_2$	406	Q(1,0) 500	Q(0,0) 663		
meso-tetrakis(pentafluoro-phenyl)-2,3,12,13-tetrahydroxybacteriochlor in osmate ester, (trans isomer)	osmate-(OH)$_4$TPBCH$_2$	378	Q(1,0) 509	Q(0,0) 712		

relative emission intensity

Legend:
- osmate-(OH)₂TFPCH₂
- (COO)TFPLH₂
- osmate-(OH)₂(COO)TFPBLH₂
- (COO)₂TFPBLH₂
- osmate-(OH)₄TFPBCH₂

600   650   700   750   800
nm
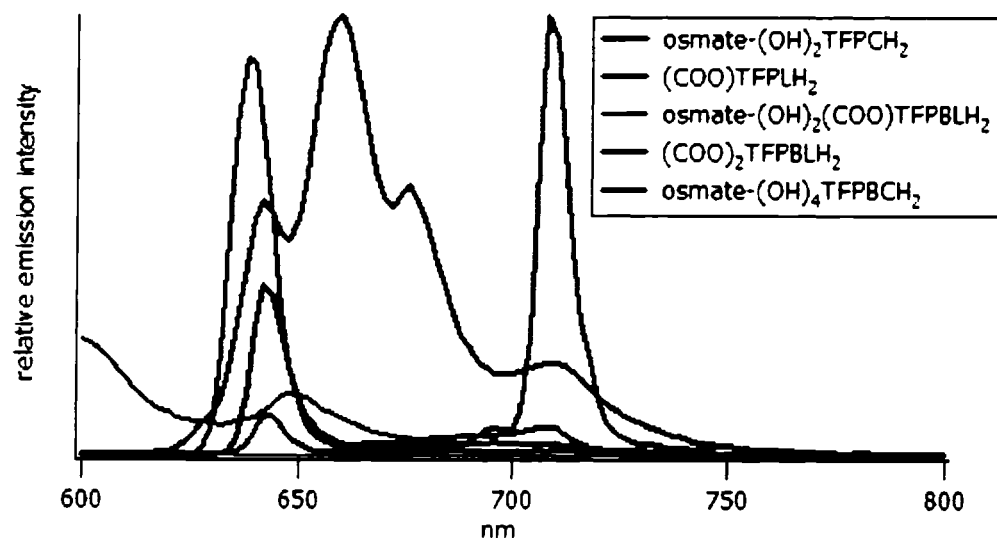
Figure 2.36 Emission spectra of fluorophenyl substituted free base porphyrin derivatives.

Table 2.6 Emission, Lifetime, and Quantum Yield of Free Base Fluorophenyl Substituted Series.

Abbreviation	Emission (nm) in EtOH				Lifetime		Quantum Yield	
	fluorescence	phosphorescence			τ_f(ns)	τ_p	Φ_f	Φ_p
TFPPH₂	631	698			9.8			
osmate-(OH)₂TFPCH₂	642	708						
(COO)TFPLH₂	640	708			6.7		0.07	
osmate-(OH)₂(COO)TFPBLH₂	556	598	648					
(COO)₂TFPBLH₂	642	660	676	708				
osmate-(OH)₄TFPBCH₂	642	708						

The phenyl substituted porphyrin derivatives behave as expected, with the bacteriochlorin species displaying a bathochromatic shift in absorption and emission wavelength. However, the fluorophenyl substituted porphyrin derivatives show only

minimal changes in absorption and emission wavelength upon reduction of the pyrrole rings.

In both the phenyl and fluorophenyl substituted synthetic series, related derivatives show overlapping spectral emissions. It is likely that common derivatives will have similar photophysical characteristics; however, overlapping emissions may be due to sample impurities. The gadolinium excitation detector has a high sensitivity to impurities and in some spectra, the excitation of a compound's starting material is also observed. Therefore, excitation spectra for all porphyrin derivatives were measured at their various emission wavelengths. In most case, emission wavelengths accordingly mirror the absorbance spectra of the given derivative.

2.7.c Platinum Metallated Series

The phenyl substituted platinum derivatives have very similar absorption wavelengths. As expected, the reduction of a second pyrrole ring, forming the isobacteriochlorin **2.8a**, produces a spectral absorption much similar in wavelength to the chlorin and porphyrin (Table 2.7). However, Figure 2.37 and Table 2.8 show that emission wavelengths of the new phenyl substituted platinum derivatives are shifted into the near-IR region.

Table 2.7 Absorption Wavelengths of Platinum Phenyl Substituted Series.

Compound Name	Abbreviation	Absorption (nm)		
		B(0,0)	Q(1,0)	Q(0,0)
[*meso*-tetrakisphenylporphyrinato]Pt(II)	TPPPt	403	539	510
[*meso*-tetrakisphenyl-2,3-dihydroxychlorinato]Pt(II)	(OH)₂TPCPt	397	585	
[*meso*-tetrakisphenyl-2-oxa-3-oxoporphyrinato]Pt(II); Pt-porpholactone	(COO)TPLPt	400	525	564
[*meso*-tetrakisphenyl-2,3-*cis*-dihydroxy-7-oxa-8-oxochlorinato]Pt(II); Pt-dihydroxyporpholactone	(OH)₂(COO)TPiBLPt	387	542	584
[*meso*-tetrakisphenyl-2,3,7,8-*tetra*hydroxyisobactiochlorinato]Pt(II); Pt-tetrahydroxyisobacteriochlorin	(OH)₄TPiBLPt	380	531	568
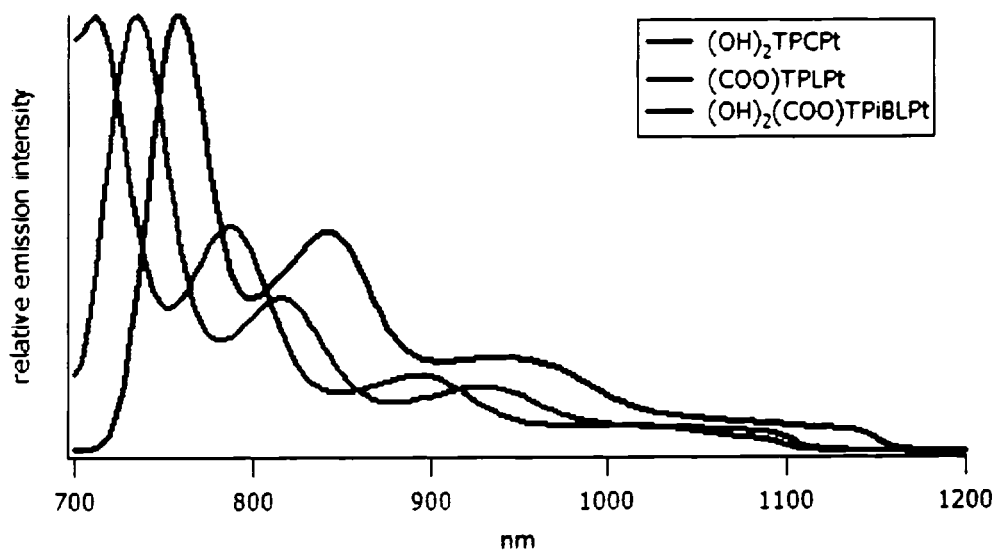
Figure 2.37 Emission spectra of phenyl substituted platinum porphyrin derivatives.

Table 2.8 Emission, Lifetime, and Quantum Yield of Platinum Phenyl Substituted Series.

| Abbreviation | Emission (nm) in EtOH | | Lifetime | Quantum Yield |
	fluorescence	phosphorescence	τ_p	Φ_p
TPPPt			0.249 ms	0.45
(OH)$_2$TPCPt	734		92 μs (734 nm)	
(COO)TPLPt	712			
(OH)$_2$(COO) TPiBLPt	758	850		
(OH)$_4$TPiBLPt	380	531		

The absorption wavelengths for the fluorophenyl substituted platinum derivatives are again characteristic to isobacteriochlorin species (Table 2.9). Despite this lack of change in absorption, we observe a bathochromic shift in emission wavelength. While the fluorophenyl substituted platinum lactone emits around 733 nm, Table 2.10 shows that the emission wavelengths of all of the new fluorophenyl substituted platinum derivatives are shifted into the near-IR region. The phosphorescent lifetime decay of the new platinum derivatives, measured at 77 K in ethanol, ranges from 40-78 μs. This is comparable to TFPPPt (120 μs). Figure 2.38 shows the emission spectrum of the fluorophenyl substituted platinum lactone in comparison to the emission spectra of the new fluorophenyl substituted platinum derivatives.

Table 2.9 Absorption Wavelengths of Platinum Fluorophenyl Substituted Series.

Compound Name	Abbreviation	Absorption (nm)		
		B(0,0)	Q(1,0)	Q(0,0)
[meso-tetrakis(pentafluorophenyl) porphyrinato]Pt(II)	TFPPPt	390	506	540
[meso-tetrakis(pentafluorophenyl)-2,3-dihydroxychlorinato]Pt(II) osmate ester	osmate-(OH)$_2$ TFPCPt	391	590	
[meso-tetrakis(pentafluorophenyl)-2-oxa-3-oxoporphyrinato]Pt(II); Pt-porpholactone	(COO)TFPLPt	396	536	574
[meso-tetrakis(pentafluorophenyl)-2,3-cis-dihydroxy-7-oxa-8-oxochlorinato]Pt(II); Pt-dihydroxyporpholactone	osmate-(OH)$_2$(COO) TFPiBLPt	386	545	586
[meso-tetrakis(pentafluorophenyl)-diporpholactonato]Pt(II) (mix of regioisomers)	(COO)$_2$TFPiBLPt	380	532	572
[meso-tetrakis(pentafluorophenyl)-2,3,7,8-tetrahydroxyisobacterio-chlorinato]Pt(II)	osmate-(OH)$_4$ TFPiBLPt	382	525	568
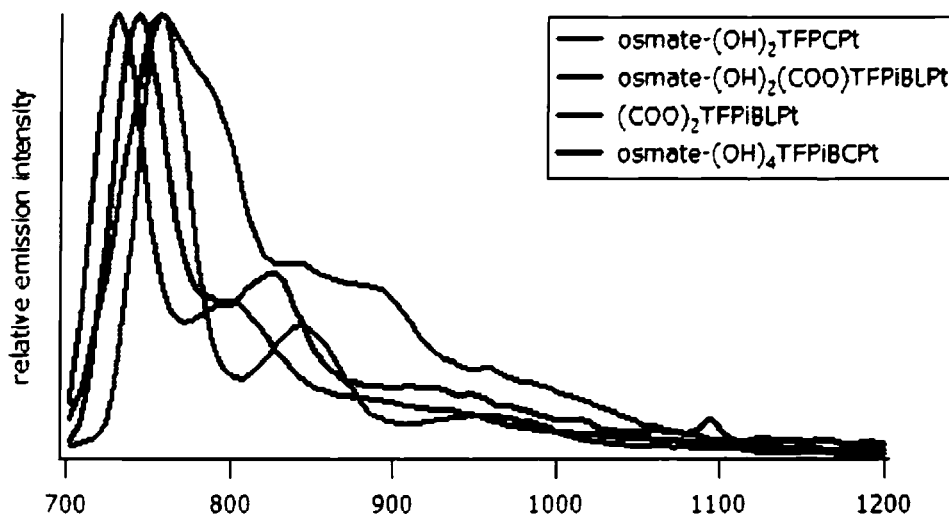
Figure 2.38 Emission spectrum of novel fluorophenyl substituted platinum porphyrin derivatives.

Table 2.10 Emission, Lifetime, and Quantum Yield of Platinum Fluorophenyl Substituted Series.

Abbreviation	Emission (nm) in EtOH				Lifetime
	fluorescence		phosphorescence		τp
TFPPPt			651	712	120 μs
osmate-(OH)₂TFPC Pt	758	844	964		59 μs (758 nm)
(COO)TFPLPt			733		75 μs (733 nm)
osmate-(OH)₂(COO) TFPiBLPt	758	790	892		42 ± 1 μs (758 nm)
(COO)₂TFPiBLPt	732	800			69 ± 1 μs (800 nm)
osmate-(OH)₄TFPiBLPt	742	824			~78 μs (742 nm)

Various other free base and platinum porphyrin species were also synthesized along side the lactone series **2.6c**, **2.20b**, **2.21b**. Their absorption wavelengths are listed in Table 2.11. The photophysical characterization of the platinum derivatives of these

species has not been previously determined. In addition, sensor viability of these derivatives has not been probed. We discover that these platinum porphyrin derivatives have bathochromically shifted emission wavelengths. As listed in Table 2.12, Figure 2.39 also shows these wavelengths reach into the near IR. At approximately 141-118 µs, the platinum morpholinochlorin **2.20b** has a phosphorescent lifetime decay comparable to TFPPPt. Additionally, the fluorophenyl substituted platinum dione **2.6c** has a phosphorescent decay comparable to the novel platinum fluorophenyl substituted bacteriochlorin derivatives.

Table 2.11 Absorption Wavelengths of Non-Related Platinum Fluorophenyl substituted Series.

Compound Name	Abbreviation	Absorption (nm)		
		B(0,0)	Q(1,0)	Q(0,0)
[*meso*-tetrakisphenyl-2,3-dioxo-oxoporphyrinato]	(O=)₂TPPH₂	395	676	730
[diethoxymorpholinochlorinato]Pt	(OEt)₂TPMPt	412	605	
[diphenylindaphyrinato]Pt	DPIPt	519	629	676
[*meso*-tetrakisphenyl-2,3-dioxo-oxoporphyrinato]Pt(II)	(O=)₂TFPPPt	374/408	490	597
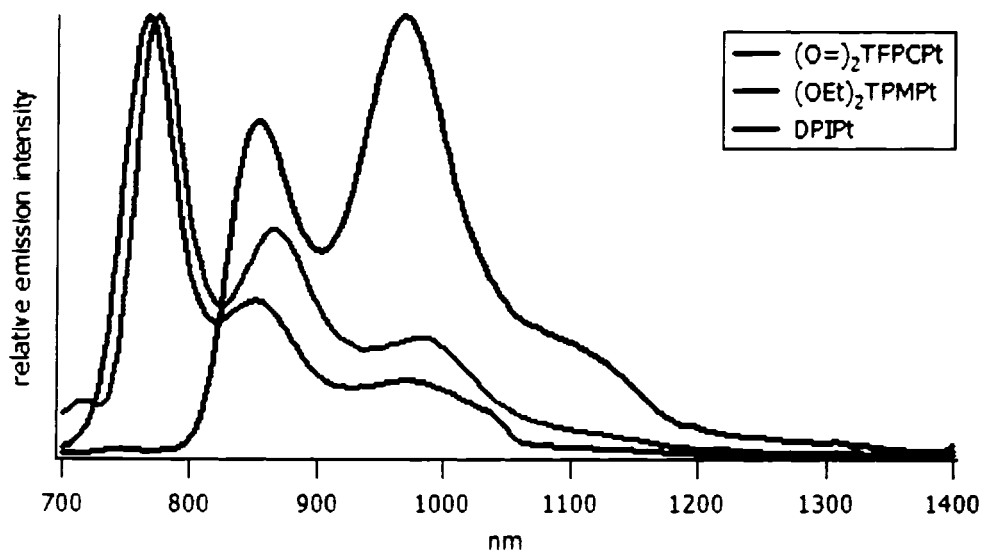
Figure 2.39 Emission spectrum of fluorophenyl substituted platinum derivatives.

Table 2.12 Emission, Lifetime, and Quantum Yield of Non-Related Platinum Fluorophenyl substituted Series.

Abbreviation	Emission (nm) in EtOH		Lifetime
	fluorescence	phosphorescence	τp
$(O=)_2TPPH_2$	666	678	
$(OEt)_2TPMPt$	772	864	988	141 μs (864 nm)
DPIPt	852	968		2.0 ± 0.1 μs (968 nm)
$(O=)_2TFPPPt$	764	852	976	~79 μs (768 nm)

Section 8: Conclusions

We have described two synthetic pathways toward the formation of isobacteriochlorin **2.16a**, **2.16b** and bacteriochlorin dilactones **2.15a**, **2.15b**. The first pathway involves the two step oxidation of the tetraolbacterio- **2.3b**, **2.7a** or tetraolisobacteriochlorin **2.8a**, **2.9b** or to the bacterio- **2.15a**, **2.15b** or isobacteriochlorin dilactone **2.16a**, **2.16b**. The alltemate pathway involves the two step synthesis of porpholactone followed by oxidation to dihydroxylactone and MnO_4^--induced oxidation yielding porphodilactone **2.15**, **2.16**. Although both synthtesis are viable, the former is the most simplified process.

Unique acid/base properties of the fluorophenyl substituted porpholactone have made it impossible to metalate the free base dilactone or conversely, protonate a metal porphodilactone (Section 2.5). One pyrrolic nitrogen of a porphyrin is converted to a vinylogous amide in the synthesis of porpholactone, thus accounting for the decreased basicity of porpholactones. Additionally, the electron withdrawing fluorines from the fluorophenyl substituted porphyrin derivative induce an electron deprived porphyrin ring, increasing the acidity of the fluorophenyl substituted derivatives. Due to this circumstance, we were not able to synthesize our target species, the fluorophenyl substituted platinum bacteriodilactone. We were however able to synthesize various phenyl and fluorophenyl substituted derivatives of free base lactones and bacteriochlorins, and metallated lactones and isobacteriochlorins.

Using DFT approximations (Section 2.2), we had hypothesized that the absorption and emission spectra of the bacteriodilactones **2.15** would be bathochromically shifted in comparison to the spectra of parent porphyrins **2.1** and lactones **2.5**. Due to the unique acid/base characteristics of the porphodilactones **2.15**, platinum insertion proved unsuccessful. Without the platinum heavy atom effect, transfer of energy from the singlet excited state to the triple state was not optimized, and no phosphorescent emission was measured. This is observed in the fluorescent emissions (shorter wavelengths) and shorter lifetime decays of both the phenyl and fluorophenyl substituted derivatives (Section 2.7).

However, the platinum isobacteriochlorin derivatives, in addition to a few other platinum species (**2.6c, 2.20b, 2.21b**), were found to exhibit near IR spectral characteristics (Section 2.7). With platinum incorporated into the porphyrin ring, the quantum yield of the singlet to triplet excitation state transition is close to a 100% and phosphorescent porphyrin emission is thus maximized. We found these species to have emission wavelengths spanning from 700 nm to close to 1000 nm. Many of these platinum derivatives also had lifetime decays between 40 – 80 μs, comparable to previously developed porphyrin PSP sensors.

As to a first observation, we believe that the osmium (of the osmate esters) does not have any effect on the spectral characteristics of these porphyrin compounds. The osmium lies outside of the porphyrin π-electron plane, thus eliminating any interaction with the porphyrin macrocycle. We observe no heavy atom effect, as seen with the addition of platinum to the porphyrin inner core, nor do we observe any quenching effects.

We are currently in the process of fully evaluating each novel species described in this chapter. We hope to find many of these species viable for use in sensor development.

Notes to Chapter 2:

1.   Gouterman, M.; Hall, R. J.; Khalil, G. E.; Martin, P. C.; Shankland, E. G.; Cerny, R. L., Tetra(pentafluorophenyl)porpholactone. *Journal of the American Chemical Society* 1989, 111, (10), 3702-7.

2.   McCarthy, J., R.; Jenkins, Hilary, A.; Bruckner, Christian, Free Base meso-Tetraaryl-morpholinochlorins and Porpholactone from meso-Tetraaryl-2,3-dihydroxy-chlorin. *Organic Letters* 2003, 5, (1), 19-22.

3.   McCarthy, J. R. Novel Macrocycles by Modification of the beta, beta'-Position of Porphyrins. PhD, University of Connecticut, Storrs, 2003.

4.   Zeller, M., In Youngstown State University, Ohio, 2006.

5.   Chen, X.; Hui, L.; Foster, D. A.; Drain, C. M., Efficient Synthesis and Photodynamic Activity of Porphyrin-Saccharide Conjugates: Targeting and Incapacitating Cancer Cells. *Biochemistry* 2004, 43, (34), 10918-10929.

6.   Elgie, K. J.; Scobie, M.; Boyle, R. W., Application of combinatorial techniques in the synthesis of unsymmetrically substituted 5,15-diphenylporphyrins. *Tetrahedron Lett.* 2000, 41, (15), 2753-2757.

7.   Pasetto, P.; Chen, X.; Drain, C. M.; Franck, R. W., Synthesis of hydrolytically stable porphyrin C- and S-glycoconjugates in high yields. *Chem. Commun.* 2001, 81-82.

8.   Shaw, S. J.; Elgie, K. J.; Edwards, C.; Boyle, R. W., Mono-(pentafluorophenyl)porphyrins - useful intermediates in the regioselective synthesis of multifunctionalized porphyrins. *Tetrahedron Lett.* 1999, 40, (8), 1595-1596.

9.   Furniss, B. S. H., A.J.; Smith, P.W.G.; Tatchell, A.R, *Vogel's Textbook of Pratical Organic Chemistry*. 5 ed.; Longman: 1989; p 549.

10.   Minaev, B. A., H., Spin uncoupling in molecular hydrogen activation by platinum clusters. *J. Mol. Catalysis A: Chemical* 1999, 148, (1), 179-195.

11.   Falk, J. E., *Porphyrins and Metalloporphyrins*. Elsevier Publishing Company: Amsterdam, 1964.

12.   Bruckner, C. D., D., beta,beta'-Dihydroxylation of meso-Tetraphenylchlorins an dMetallochlorins. *Tetrahedron Letters* 1995, 36, (52), 9425-9428.

13. Chang, C. K. S., C.; Wu, W., *J. Chem. Soc., Chem. Commun.* 1986, 1213-1215.

14. Bruckner, C. D., D., 2,3-vic-Dihydroxy-meso-tetraphenylchlorins from the Osmium Tetroxide Oxidation of meso-Tetraphenylporphyrin. *Tetrahedron Letters* 1995, 36, (19), 3295-3298.

15. Daniell, H. W.; Williams, S. C.; Jenkins, H. A.; Brückner, C., Oxidation of meso-tetraphenyl-2,3-dihydroxychlorin: simplified synthesis of ß,ß'-dioxochlorins. *Tetrahedron Lett.* 2003, 44, (21), 4045-4049.

16. McCarthy, J. R.; Melfi, P. J.; Capetta, S. H.; Brückner, C., Use of Ag(II) as a removable template in porphyrin chemistry: diol cleavage products of [meso-tetraphenyl-2,3-cis-diolchlorinato]silver(II). *Tetrahedron* 2003, 59, (46), 9137-9146.

17. McCarthy, J. R.; Hyland, M. A.; Brückner, C., Synthesis of indaphyrins: meso-tetraarylsecochlorin-based porphyrinoids containing direct o-phenyl-to-ß-linkages. *Org. Biomol. Chem.* 2004, 2, (10), 1484-1491.

18. Gouterman, M., Study of the Effects of Substituents on the Absorption Spectra of Porphyrins. *The Journal of Chemical Physics* 1959, 30, (5), 1139-1161.

19. Bowen, E. J., *Trans. Faraday Soc.* 1954, 50, (2), 97.

20. Cox, G. S. W., D.G., *Chem. Phys. Lett.* 1979, 67, (2,3), 511.

21. Phillips, D., *Polymer Photophysics.* Chapman and Hall: London, 1985; p 12.

22. Stern, O. V., M, *Phys. Z.* 1919, 20, 183.

23. Brinas, R. P. T., T.; Hochstrasser, R.M.; Vinogradov, S.A., Phosphorescent Oxygen Sensor with Dendritic Protection and Two-Photon Absorbing Antenna. *J. Am. Chem. Soc.* 2005, 127, 11851-11862.

Chapter 3 - Detailed Mass Spectrometric Analysis

Section 1: Overview

In this chapter we show the detailed mass spectrometric analysis of *meso*-phenyl- and pentafluorophenyl-substituted porphyrins, porpholactones, and corroles using positive and negative mode tandem ESI mass spectrometry (Figure 3.1). In Section 3.2, we illustrate that the typical fragmentation of *meso*-phenyl- and *meso*-pentafluorophenyl-substituted porphyrins. We elucidate the fragmentation pattern for *meso*-phenyl- and *meso*-pentafluorophenyl-substituted porpholactones in Section 3.3. The fragmentation pathways of the porpholactones highlight the substantial perturbance the partially oxidized pyrrole unit introduces into the porphyrinic macrocycle. As a comparison species, we also discuss in Section 3.4 the results of positive and negative mode tandem ESI collision-induced fragmentations of *meso*-tetrakis(heptafluoropropyl)porphyrin.

These results will facilitate the interpretation of MS spectra of *meso*-pentafluorophenyl-substituted porphyrinic compounds using ESI mass spectrometry while also potentially provide tools to distinguish *o*-fluorophenyl substituted derivatives from other isomers. The fragmentations pattern observed may also point to strategies towards the bulk synthesis of novel porphyrinoid structures.

Porphyrins   **Porpholactones**   **Corroles**

TPP   TPL   TPC

X = NH, all R = ⟨phenyl⟩

X = NH, all R = ⟨pentafluorophenyl⟩   T^{F}PP   T^{F}PL   T^{F}PC

X = S, all R = ⟨tolyl⟩—CH$_3$ TTSL
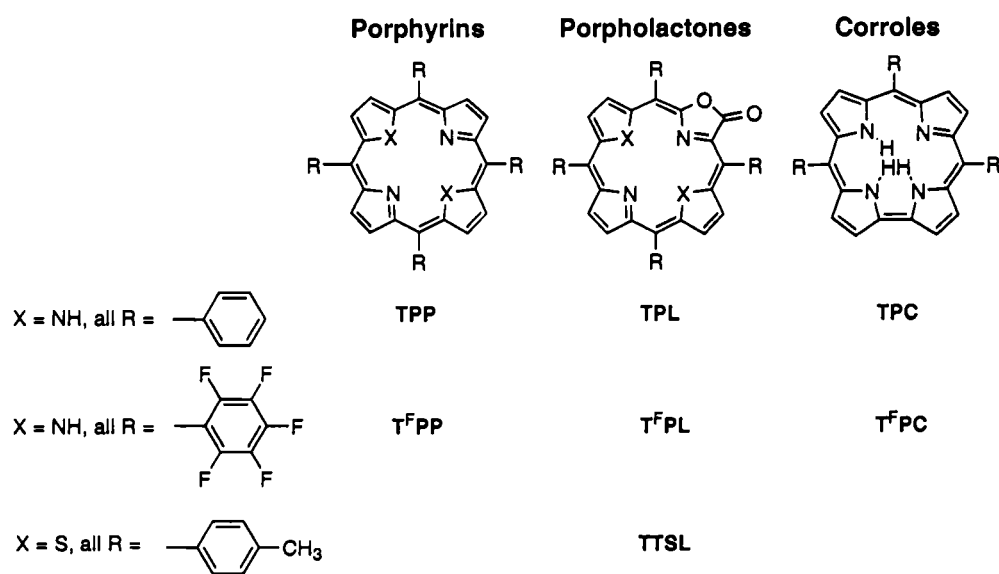
Figure 3.1 Structure and naming convention of the porphyrinic macrocycles investigated.

Section 2: Tandem Electrospray Ionization (ESI) Mass Spectrometric Analysis of *meso*-Tetrakisphenyl Porphyrin and *meso*-Pentafluorophenyl Porphyrin and Corrole

3.2.a Introduction

meso-Tetraarylporphyrins, the parent compound of which is *meso*-tetrakisphenylporphyrin (**TPP**), are the most widely studied class of synthetic porphyrins (Figure 3.1). Their popularity as, for instance, model compounds for naturally occurring co-factors arises from their straight forward syntheses and the option to widely vary the type of substituents on the aryl rings.[63] One particular *meso*-aryl group, the electron-withdrawing pentafluorophenyl group **TFPP**, is commonly utilized when chemical inertness is to be imparted onto the porphyrinic macrocycle, such as increased stability toward oxidative degradation.[64-68] Metalloporphyrins and metallocorroles (based on the ligand *meso*-tris(pentafluorophenyl)corrole, **TFPC**) used in group transfer catalyses also take advantage of the stabilizing effects of the pentafluorophenyl moiety.[67-69] The *meso*-pentafluorophenyl group was introduced into porphyrin isomers (*N*-confused porphyrins),[70, 71] as well as into expanded porphyrins.[72]

While the protection from undesired reactions on the porphyrinic macrocycle is the impetus for the use of the pentafluorophenyl group in the following examples, the *p*-position of pentafluorophenyl group is activated toward a nucleophilic aromatic substitution reaction. Commonly using *N*- or *S*-nucleophiles, the pentafluorophenyl group can therefore be used to regiospecifically introduce *p*-phenyl substituents.[50-53] In addition, the pentafluorophenyl groups mediates the solubility of porphyrins in fluorinated solvents and supercritical CO_2.[73, 74] Further, **TFPP** was suggested as a chemically inert and strongly light-absorbing matrix in MALDI-TOF mass spectrometry.[75] Lastly, ^{19}F is NMR active, and the pentafluorophenyl group offers a convenient NMR tag to elucidate the structure of complex porphyrinic derivatives.[65, 76] The many uses for *meso*-pentafluorophenyl groups make efficient analysis of these

compounds desirable. Electrospray ionization (ESI) mass spectrometry (MS) is becoming a popular technique for the analyses of porphyrins.[60, 77-86]

During the mass spectrometric analysis of variously β-substituted *meso*-phenylporphyrins, ring-closure reactions involving the *meso*-phenyl group have been observed before. For instance, β-nitro- and β-vinyl-substituted porphyrins form, under FAB conditions, fragment ions enclosing six-membered rings, such as structures 3.1 and 3.2, respectively (Figure 3.2).[82] Conversely, *p*-nitrophenyl-substituted porphyrins do not undergo this type of cyclization. Hence, this reaction can be utilized for the determination of these regioisomers of nitroporphyrins by tandem mass spectrometry.[87]
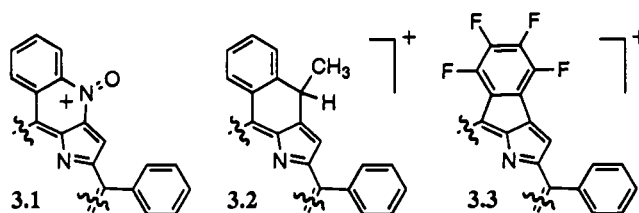
Figure 3.2 *meso*-Phenyl-fused structures previously observed during the mass spectrometric analysis of porphyrins.

We show here the results of single and tandem ESI mass spectrometry investigations of a *meso*-pentafluorophenyl-substituted porphyrin (TFPP) and -corrole (TFPC) in comparison to their non-fluorinated analogues TPP and TPC. Well-defined fragmentation patterns characteristic for the presence of *meso*-tetrafluorophenyl groups that are evocative of the formation of fragments with covalent *o*-phenyl-to-β-linkages are observed. Equivalent HF-elimination-mediated *o*-to-β-linkage formations enclosing a five-membered ring between the *meso*-aryl group and the porphyrin ring, were recently reported by the groups of Cavaleiro and Santana-Marques.[84] They reported the occurrence of these linkages of type 3 in the collision-induced ESI-MS spectra of *meso*-pentafluorophenyl derivatized cationic pyrrolidine-fused chlorins and isobacterio-chlorins.[84] A limited number of these cyclization reactions were found among a host of

other fragmentations characteristic for pyrrolidine-fused systems. We demonstrate here that formation of β-to-o-linkages during the tandem mass spectrometric analysis of *meso*-tetrafluorophenylporphyrins follows predictable and rational patterns. In certain cases, all theoretically conceivable ring-closures can be observed, and the reaction appears to be general for *meso*-pentafluorophenyl-substituted porphyrinoids.

3.2.b Results and Discussion

Single and Tandem ESI(+) Mass Spectra of TPP and TPC

The ESI spectrum of **TPP** ($C_{44}H_{30}N_4$), recorded in the positive ion mode, is shown in Figure 3.3A. The sole species formed is the expected monoprotonated parent compounds [**TPP** + H]$^+$ with a m/z value of 615. Protonation is likely taking place at one of the inner, basic imine nitrogens. The ESI-MS/MS spectrum of the species [**TPP** + H]$^+$ is shown in Figure 3.3B. Collision-induced fragmentation of the singly protonated **TPP** results predominantly in the loss of one phenyl group as a $C_6H_5^\bullet$ radical, forming the protonated triphenyl radical species **3.4** of m/z 538 (Scheme 3.1). The loss of a second phenyl group (expected m/z of 461.2) is of relatively low abundance. In general, these findings have been amply described before and serve here simply as benchmark data against which we evaluate the behavior of the pentafluorophenyl-derived analogue.[77, 81, 83]
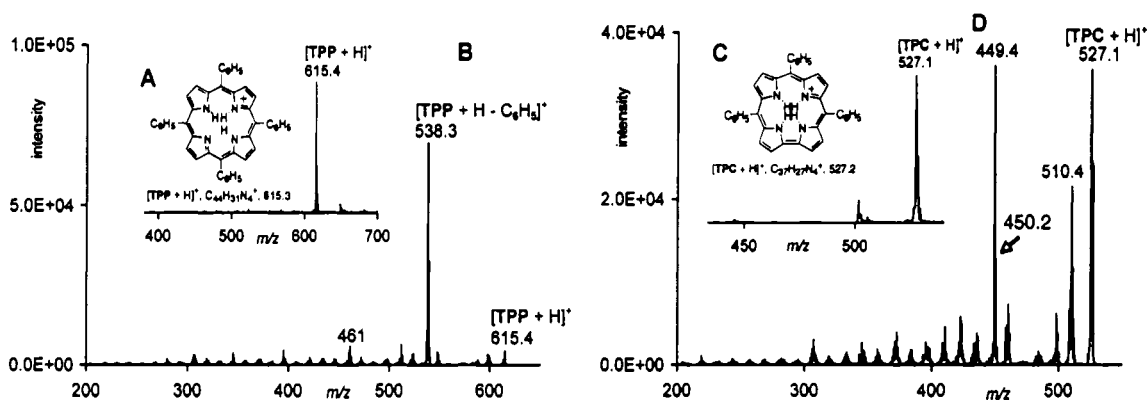
Figure 3.3 ESI(+) spectra of TPP and TPC. A) ESI(+) mass spectrum of TPP. B) Collision induced fragmentation spectrum of the species [TPP + H]⁺ (m/z 615). C) ESI(+) mass spectrum of TPC. D) Collision induced fragmentation spectrum of the species [TPC + H]⁺ (m/z 527). The interpretation of the spectra is presented in Scheme 3.1.
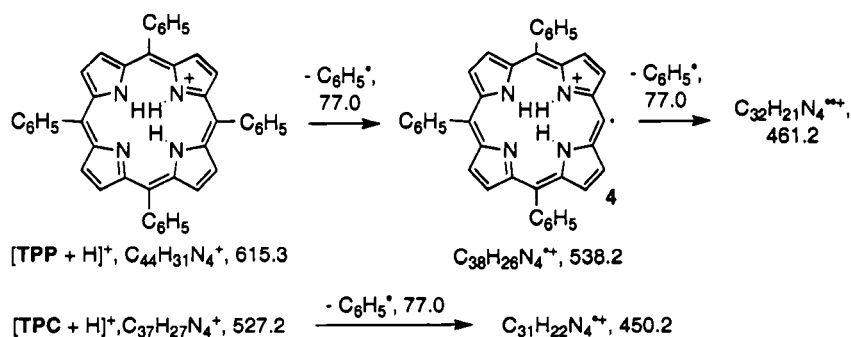
Scheme 3.1 Interpretation of the spectra shown in Figures 3.3A-D.

The full scan ESI(+) mass spectra of triphenylcorrole **TPC** (Figure 3.3C) parallels that of **TPP**. The major species present are the respective MH⁺ ions. Likewise, the tandem ESI(+) spectra of the respective MH⁺ species (Figure 3.3D) can be interpreted along the same lines as that for **TPP** (Scheme 3.1). The loss of one *meso*-substituent radical is the major fragmentation pathway that is accompanied by a minor pathway attributed to the breakup of the macrocycle. The peaks resulting from this breakup are broad and point toward the successive loss of C- and N-fragments with varying numbers of hydrogens.

We were not able to record interpretable spectra for any of these two macrocycles under ESI(-) conditions. This result is surprising for **TPC** as its acidity is reportedly much higher than that of porphyrins.[88]

Single and Tandem ESI(+) and ESI(-) Mass Spectrometric Analysis of TFPP

When subjecting the fluorinated porphyrin **TFPP** to the same ESI(+) ionization conditions as its non-fluorinated counterpart **TPP**, we recorded spectra that were not as well defined (cf. Figure 3.4A with Figure 3.3A). Presumably the electron-withdrawing *meso*-pentafluorophenyl substituents increase the acidity of the porphyrin and prevent efficient protonation. Hence, we tested the recording of the spectra in negative ionization mode (Figure 3.4E).

Essentially only one ion at *m/z* 973 is detected, corresponding to the species [**TFPP** – H]⁻. Ionization is thus brought about by efficient deprotonation, presumably of one of the inner pyrrole-type nitrogens. The collision-induced fragmentation of the [**TFPP** - H]⁻ species is shown in Figure 3.4F. Four major and several minor fragments are detected. Notably, the species corresponding to the loss of a pentafluorophenyl group (expected at *m/z* 806) is absent. As the predominant fragmentation pattern, a successive loss of HF (20 amu) is observed whereby four high-intensity fragmentation are followed by four low-intensity fragmentations. Since a *cis*-elimination of HF cannot take place in **TFPP**, we surmise that the elimination is, under concomitant formation of an *o*-to-β-single bond, due to the loss of one H from the pyrrolic β-positions and the loss of one F from the *o*-position of a flanking pentafluorophenyl group. This finding mirrors a report by Santana-Marques and co-workers who also observed, amidst other fragmentations, the occurrence of HF-elimination in the collision-induced ESI-MS spectra of *meso*-pentafluorophenyl derivatized cationic pyrrolidine-fused chlorins and isobacteriochlorins that were also interpreted as the formation of β-to-*o*-linkages.[84] In contrast, however, **TFPP** possesses a much simpler structure that enables the HF elimination to occur as the sole fragmentation pathway. The simplicity of the parent ion and the purported elimination products allows a reliable molecular modeling of the process and a detailed

prediction of their structures that point toward a generalization of the findings (see below).
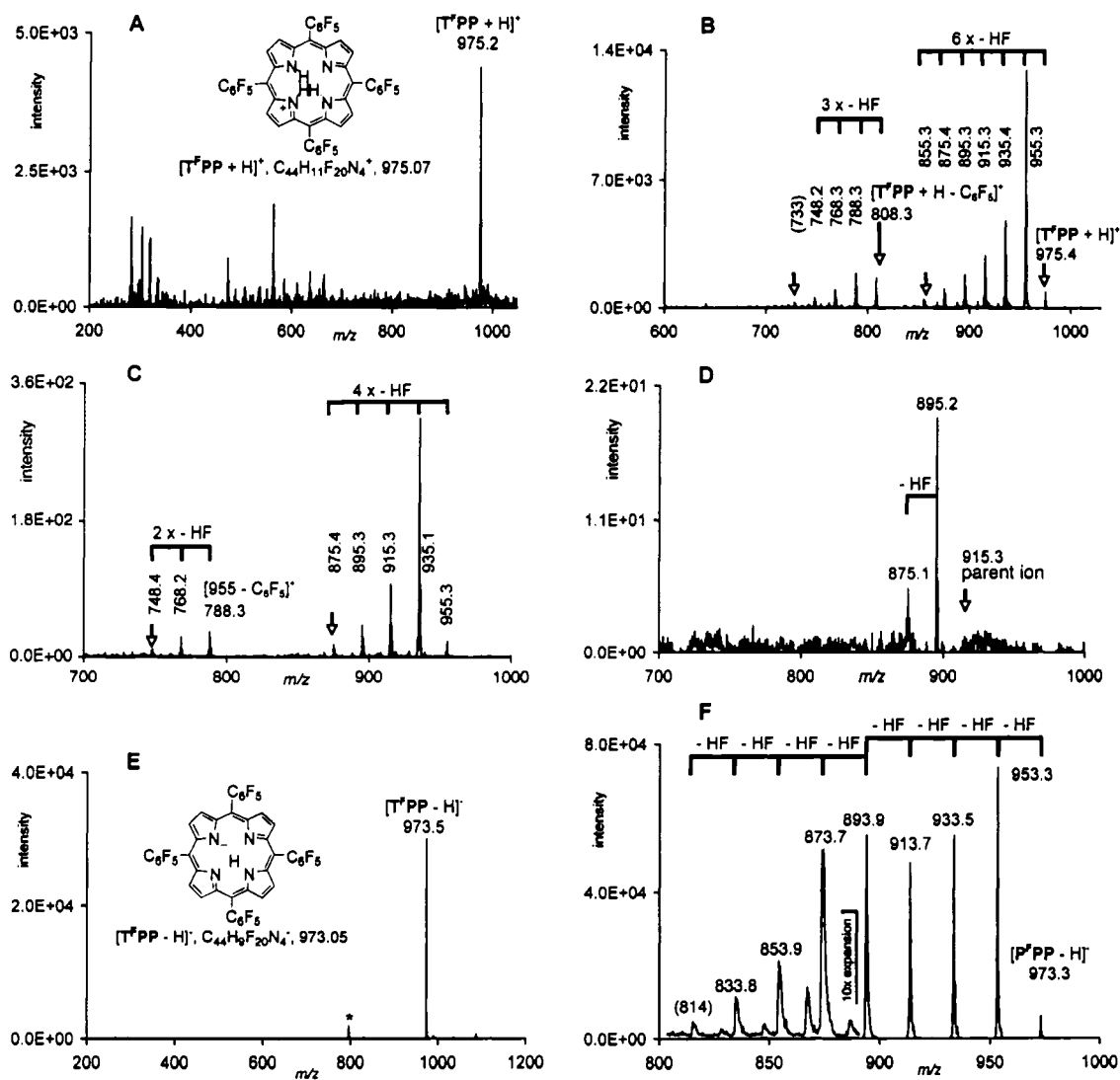
Figure 3.4 ESI mass spectra of TFPP. A) Full scan ESI(+) mass spectrum. B) Collision induced fragmentation spectrum of the species [TFPP + H]$^+$ (m/z 975). An interpretation of the spectrum is provided in Scheme 3.3. C) ESI(+) MS^3 spectrum of the species m/z 955 (see in Fig. 3.5B). D) ESI(+) MS^3 spectrum of the species m/z 915 (see in Fig. 3.5B). E) Full scan ESI(-) mass spectrum. The peak marked * (at m/z 795) is an impurity of TFPC originating from the preparation of TFPP (for a discussion of the origin and the tandem mass spectrum of this species, see below). F) Collision induced fragmentation spectrum of the species [TFPP - H]$^-$ (m/z 973). An interpretation of these spectra is shown in Scheme 3.2.

meso-Aryl groups attached to porphyrins are, in the solution and solid state, arranged approximately perpendicular to the mean plane of the porphyrin. This is because of a steric interaction between the β-hydrogen and the *o*-phenyl substituents (Structure A, Figure 3.5). A direct linkage between these two positions allows the phenyl group to be arranged nearly co-planar to the porphyrin but forces the opposite *o*-atom into closer proximity to the adjacent β-hydrogen. The latter interaction is perceivably alleviated by a ruffling distortion of the macrocycle (**B**). The resulting extension of the porphyrinic π-system, together with the liberation of HF, are the likely driving forces for the formation of such a linkage.
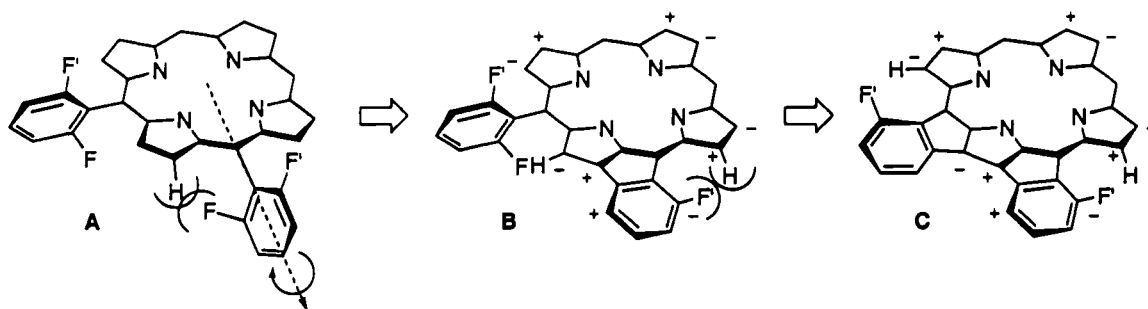
Figure 3.5 Illustration of the steric interaction between the ß-hydrogen and the *o*-phenyl substituent in *meso*-phenylporphyrin (A), *o*-to-ß-fused porphyrin (B), and bis-fused porphyrin (C). The + and - indicate the ruffled conformation of the porphyrinic macrocycle, i.e., the relative position of the atoms with respect to the mean plane of the macrocycle.

The mechanism of the elimination reaction is likely that of a nucleophilic aromatic substitution (S_{NAr}), a reaction type common for the electron-poor pentafluorophenyl group (Scheme 3.2).[50-53] The elimination can be repeated four times, linking each aryl group. A cooperative interaction between the linkages that orients the direction of the subsequent fusions seems plausible. If one linkage causes a ruffling distortion of the macrocycle, the ruffled conformation facilitates the formation of a second linkage in a unidirectional fashion because this does not introduce any (or only minor) additional steric interaction between the *o*-atom of the second linked aryl group and the adjacent β-hydrogen (Structure C, Figure 3.5). In fact, they are, as a direct result

of the ruffling that translates throughout the entire macrocycle, already pre-oriented away from each other. Inversely, a non-unidirectional linkage goes 'against the grain' and introduces additional steric interactions. Thus, the first elimination (to form **3.5**) enables the subsequent eliminations to take place in the regioselective, unidirectional manner shown (**3.5** to **3.6**, **3.7**, and finally **3.8**, Scheme 3.2). Molecular mechanics calculations corroborate this proposition.
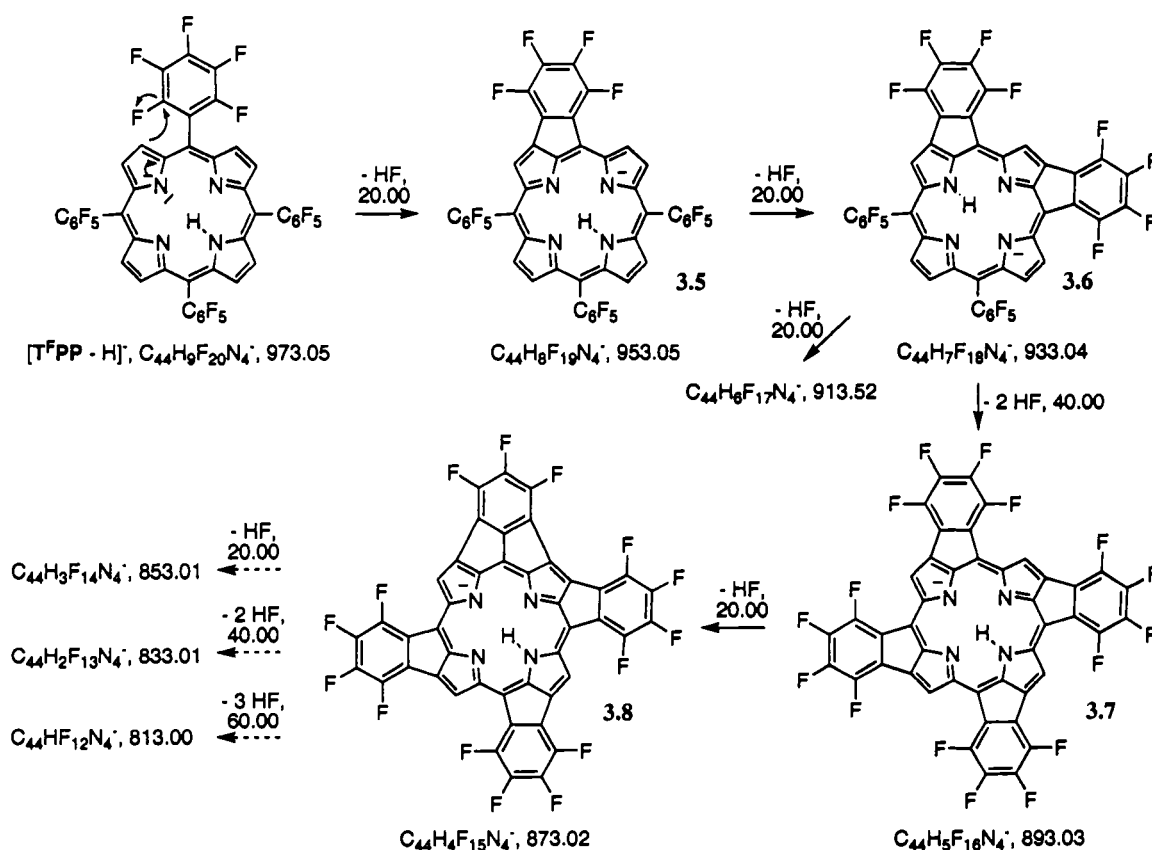
Scheme 3.2 Interpretation of the collision-induced fragmentation mass spectrum of [TFPP - H]⁻ (Figure 3.5D).

We computed the total energy of **TFPP** in comparison to most of the possible isomers containing one to eight *o*-to-β-linkages. The results of the computations are summarized in Figure 3.6. The formation of one β-to-*o*-linkage (species **II**) increases the overall (strain) energy of the system only by 10% compared to the energy of the parent

compound (**I**). In fact, up to four linkages increase the overall strain energy by only 50% (**IX**) if the linkages are connected in a unidirectional fashion. If the linkages are not established in a unidirectional fashion, as in **V** or in **X** and **XI**, the energy of the system is 10-15% higher as compared to the unidirectional isomers **IV** and **IX**, respectively. If even one phenyl group is linked on both o-positions (**VI**), the energy nearly doubles. Thus, all isomers of the species containing four linkages (**X** - **XIV**) in a non-unidirectional fashion have significantly higher energies than **IX**. Those bearing two doubly-linked phenyl groups possess up to three-fold the energy of **IX**. The fifth to eighth consecutive linkages necessarily involve such doubly-linked phenyl groups and, consequently, their energies are significantly elevated. Whether these high-energy ring-fusions occur also in a unidirectional fashion could not be made out clearly.

This result correlates well with the observed relative peak intensities in the fragmentation spectrum of [**TFPP** - H]⁻ (Figure 3.4F). The fifth and subsequent eliminations proceed with low efficiency, and the corresponding fragment peaks are minor compared to the peaks resulting from the first four eliminations (note the 10-fold intensity enhancement of the spectrum below m/z 890). It is, therefore, not surprising that literature precedence for the bulk-phase formation of o-,o'-linked phenyl groups in the solution phase are rare and involve only one phenyl group and two enclosed six-membered rings or one five- and one six-membered ring.[89, 90] Porphyrinoids containing direct β-to-o-linkages enclosing five-membered rings between the phenyl and the porphyrin macrocycle are also known, though their establishment follow different routes than presumed here.[91, 92]
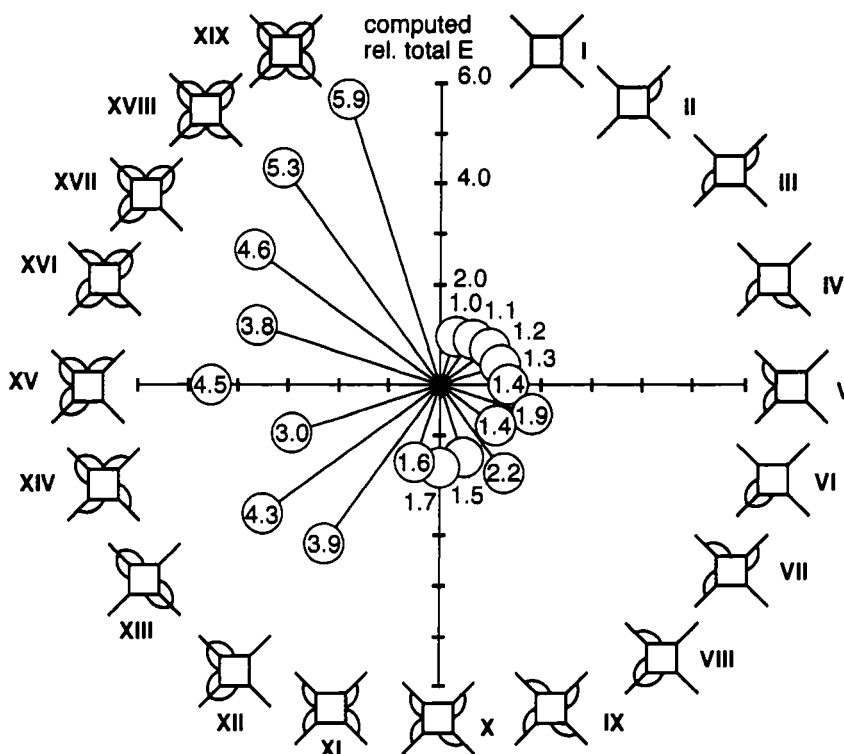
Figure 3.6 Computed relative (strain) energy increases upon successive formations of select β-to-o-linkages in TFPP (Chem3D, MM2 basis set). Overall energy computed for I is 63 kJ/mol. The compounds computed are indicated in a stylized fashion: The squares represent the porphyrin macrocycle, the straight lines the *meso*-phenyl groups, and the o-to- β-linkages are indicated by the connections between these two elements.

In light of the foregoing, the fragmentation ESI(+) mass spectrum of [TFPP + H]$^+$ (Figure 3.4B) can qualitatively be interpreted in a similar fashion as the ESI(-) spectrum, with two notable differences (Scheme 3.3). Firstly, two HF elimination series can be distinguished: One series of six eliminations beginning with the species [TFPP + H]$^+$ (at *m/z* 975) and ending with the fragment **3.9** (*m/z* 855, shown is the isomer with opposite double linkages as the computations have shown this arrangement to be energetically more favorable), and one series beginning with the species **3.10** (*m/z* 808). Fragment **3.10** is derived from [TFPP + H]$^+$ by a loss of a C$_6$F$_5$$^•$ radical. Since this fragment contains less pentafluorophenyl groups that can lead to ring-closure, only a maximum of three HF eliminations, to presumably form species **3.11**, are observed. A fourth elimination that requires a highly strained, doubly-fused aryl group, cannot be made out

clearly. Secondly, the mechanism of the elimination is much less clear since an intramolecular nucleophilic substitution mechanism is much less likely operating within a cationic pseudomolecular species, though it does not rule it out entirely. The driving forces for the reactions are identical in either cases and may drive an even unfavorable reaction pathway. Further, as the loss of aryl radical fragments demonstrates, radical pathways also cannot be excluded. We have also observed the HF-elimination in *meso*-heptafluoropropyl-substituted porphyrins under ESI conditions that is, under ESI(+) conditions, intermingled with a radical fragmentation pathway of the *meso*-alkyl groups.[86]

Scheme 3.3 Interpretation of the collision-induced fragmentation mass spectrum of [TFPP + H]$^+$ (Figure 3.4B). For clarity, the interpretation of Figures 3.4C and 3.4D were omitted.

The fact that two competing fragmentation pathways (HF and C_6F_5˙ losses) are observed allows further insight into the regio-selectivity of the sequential HF losses.

The MS^3 spectra of the species that have lost 1 to 3 HF fragments, the loss of a C$_6$F$_5$$^{\bullet}$ fragment is observed in addition to further HF-losses. Representative for this case, Figure 3.4C shows the MS^3 spectrum of the m/z 955 species ([TFPP + H - HF]$^+$). The spectrum looks like the spectrum for [TFPP + H]$^+$ truncated by the first HF loss. Inversely, only one or two HF losses are observed in the daughter ions that have already lost 3 or 4 HF molecules, respectively. Figure 3.4D, the MS^3 spectrum of the m/z 915 species ([TFPP + H - 3 HF]$^+$) shows such a case. Only two further HF-losses are observed while there are no indications for any loss of an aryl group. The first fusion makes the loss of an aryl group through a simple *meso-ipso* single bond breakage impossible. Hence, this finding supports further the supposition that firstly HF fragmentations occur that fuse all the phenyl groups with a single bond to the macrocycle before a second fusion is established.

Tandem ESI(-) Mass Spectra of the m/z 796 Species Assigned to TFPC

The porphyrin **TFPP** is made by acid-catalyzed condensation of pyrrole and pentafluorobenzaldehyde. It is well known that this reaction also generates the corresponding corrole **TFPC**.[93, 94] Inspection of the mass spectra of a commercial sample of **TFPP** clearly shows the presence of this impurity (see Figure 3.4E).

The collision-induced fragmentation spectra of the parent ion of the trifluorophenylcorrole **TFPC** in the ESI(+) and ESI(-) modes are shown in Figures 3.7A and 3.7B, respectively. The ESI(+) spectrum allows the observation of five HF eliminations, leading to the formation of species **3.12**, and the loss of one pentafluorophenyl group from the parent ion (m/z 797) (Scheme 3.4). Again, the ESI(-) spectrum provides the clearest spectrum. Three consecutive HF eliminations are visible, presumably one for each pentafluorophenyl group of **TFPC**, forming species **3.13**. This compares to the four high-intensity eliminations corresponding to the four fluorophenyl groups in **TFPP** and the three eliminations for the three fluorophenyl groups in the porphyrin radical species **3.11** (Scheme 3.3). Hence, the number of HF eliminations observable in the ESI(-) spectra is diagnostic for the number of pentafluorophenyl groups

attached to the porphyrinic framework. Similarly important, this observation lends further credence to the validity of the interpretation of the mass spectra.
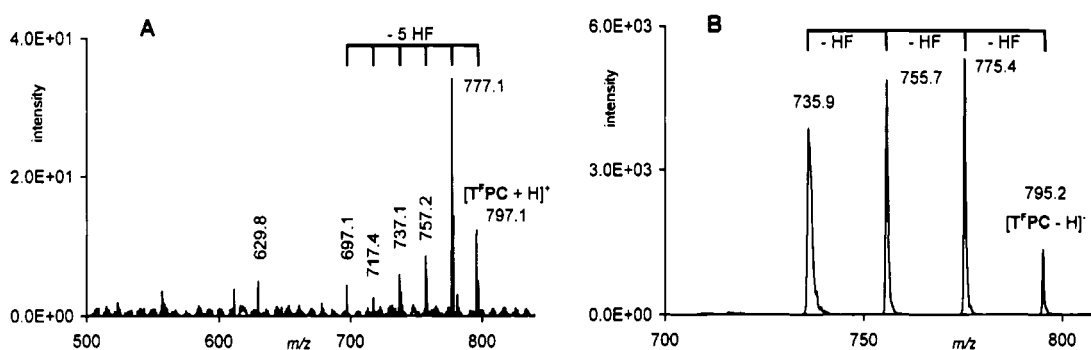
Figure 3.7 A) Collision-induced ESI(+) spectrum of the m/z 797 species that is detectable in the full scan spectrum of TFPP and that is assigned to $[TFPC + H]^+$. B) Collision-induced ESI(-) spectrum of the m/z 795 species visible in the full scan spectrum of TFPP (Figure 3.4C) and that is assigned to $[TFPC - H]^-$. An interpretation of the spectra is provided in Scheme 3.4.
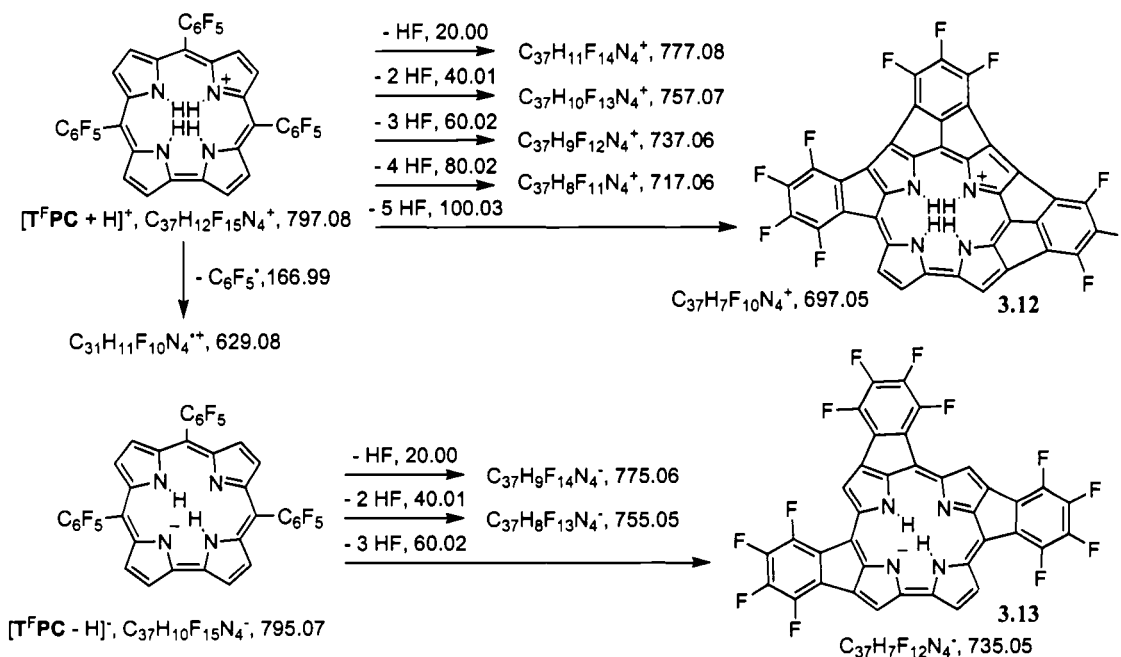
Scheme 3.4 Interpretation of the collision-induced fragmentation mass spectrum of $[TFPC + H]^+$ (Figure 3.6).

3.2.cConclusions

We have shown the detailed mass spectrometric analysis of *meso*-phenyl- and pentafluorophenyl-substituted porphyrins and corroles using positive and negative mode tandem ESI mass spectrometry. The typical and known fragmentation of the phenyl-substituted macrocycles in the positive mode is the loss of phenyl side chains. *meso*-Pentafluorophenyl-substitution allows also the recording of spectra in the negative mode whereby this derivatization also changes the MS behavior of porphyrinic macrocycles in a fundamental way in both ionization modes when compared to their *meso*-phenyl-substituted counterparts. As the predominant fragmentation pattern we have identified the successive loss of HF. We attribute this to the formation of fragment ions with direct *o*-phenyl-to-β-linkages. This observation, taken together with the observations reported before,[84] establish this fragmentation pathway as likely to be general for *meso*-pentafluorophenyl-substituted porphyrinoids. The results will facilitate the interpretation of MS spectra of *meso*-pentafluorophenyl-substituted porphyrinic compounds using ESI mass spectrometry. Whether the observed fragmentation modes can also be adopted for the solution phase bulk synthesis of porphyrins containing co-planarized *meso*-aryl groups by chemically induced HF eliminations is currently a subject of investigations in our laboratories.

Section 3: Tandem Electrospray Ionization (ESI) Mass Spectrometric Analysis of Porpholactones

3.3.a Introduction

First discovered by serendipity, *meso*-tetrakisphenylporpholactone (**TPL**) and *meso*-tetrakis(pentafluorophenyl)porpholactone (**TFPL**) are as discussed in the introduction as discussed in the introduction, now available along a number of complementary routes. ESI-MS/MS analyses of the fragmentation pathways of **TPL** shown here prove its fragmentation pattern to be uniquely different from those of the other macrocycles investigated. The fragmentation modes can be traced to the partially oxidized porphyrin ring in the porpholactone and are attributed to the formation of an unprecedented pyrrolo[2,3*c*]pyrrole-containing, 'contracted' porphyrin. This fragmentation pattern was also observed for dithiaporpholactone **TTSL** (a) K. K. Lara, C. R. Rinaldo, C. Brückner, Tetrahedron Lett. 2003, 44, 7793. (b) K. K. Lara, C. K. Rinaldo, C. Brückner, Tetrahedron 2005, 61, 2529. The analyses of the *meso*-perfluorinated porpholactone analogue **TFPL** show the fragmentation typical of porpholactones, combined with the effects of the pentafluorophenyl group discussed in the preceding section. The results are relevant to the better analyses of porphyrinic compounds using ESI-MS, highlight their reactivity and may point toward methods for the preparation of novel porphyrinic macrocycles.

3.3.b Results and Discussion

Single and Tandem ESI(+) Mass Spectra of TPL

The ESI(+) spectrum of **TPL** is shown in Figure 3.8A. As expected, the predominant ion formed is the monoprotonated species [**TPL** + H]$^+$ with a *m/z* value of 633 ($C_{43}H_{28}N_4O_2$). In stark contrast to **TPP** and the other *meso*-arylporphyrinoids studied, however, the ESI(+) collision-induced fragmentation spectrum of this species

does not show a loss of a *meso*-phenyl radical (Figure 3.8B). Instead, components out of the oxazolidone moiety are excised. While the predominant fragmentation pattern is the sequential losses of CO (for a detailed discussion of the formation of this fragment, see below), small peaks corresponding to the loss of a single O and CO_2 are also detectable. The proposed structures of the resulting species are shown in Scheme 3.5.
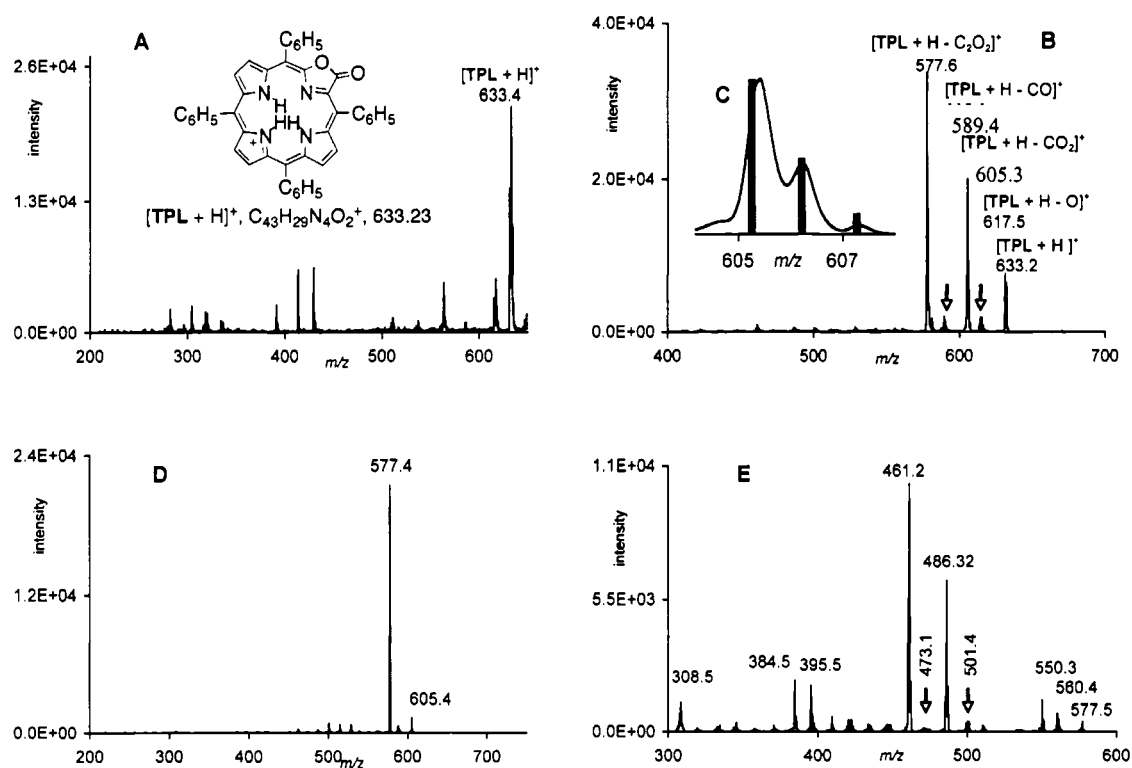
Figure 3.8 A) Full scan ESI(+) mass spectrum of TPL. B) Collision induced fragmentation spectrum of the species [TPL + H]$^+$ (*m/z* 633). The interpretation of the fragmentation pattern is shown in Scheme 3.5. C - insert) Peak expansion of the *m/z* 605 cluster; the bars represent the calculated isotope pattern for $C_{42}H_{29}N_4O^+$. D) Collision induced spectrum of the species *m/z* 605 (from spectrum 3.8B), collision energy was chosen to minimize the parent ion peak. The interpretation of this spectrum is shown in Scheme 3.6. E: Collision induced spectrum of the species *m/z* 577 (from spectrum 3.8B). The proposed fragmentation scheme is shown in Scheme 3.7.
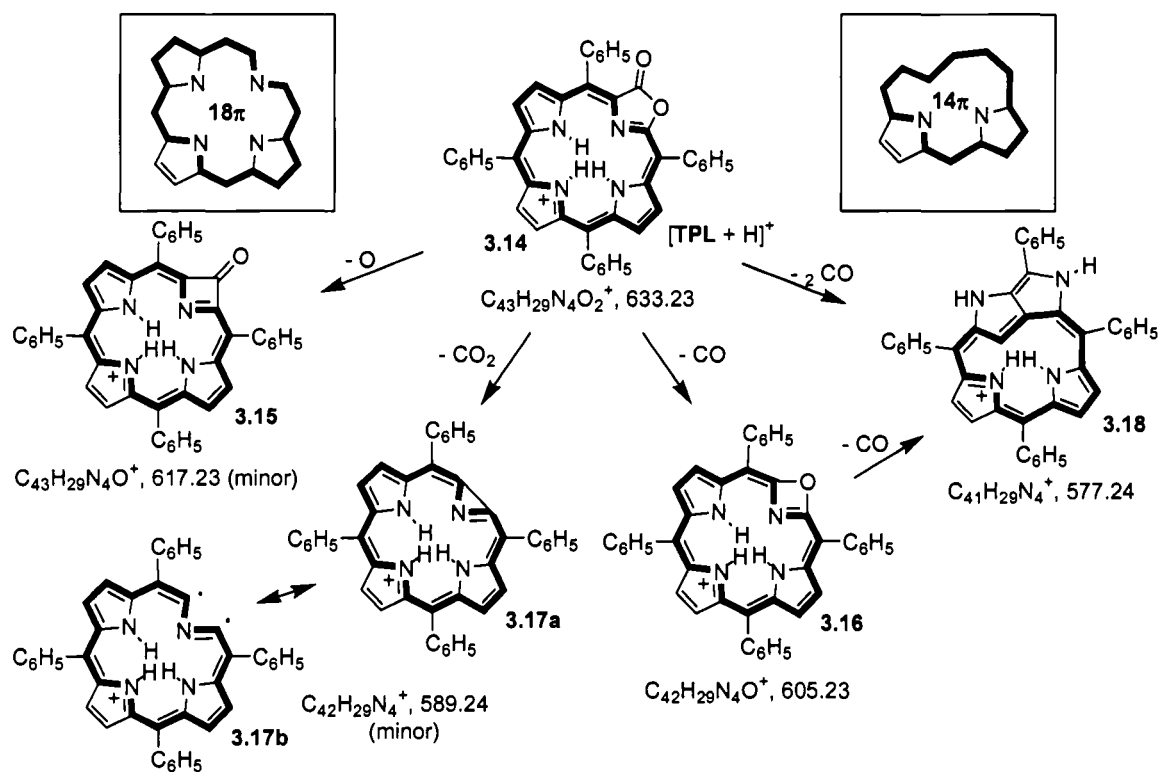
Scheme 3.5 Interpretation of the collision-induced fragmentation mass spectrum of [TPL + H]$^+$ (Figure 3.1B).

The proposed structures of the compounds **3.15** - **3.17** are within expectations for the fragmentation of [**TPL** + H]$^+$ when considering that the aromatic 18π-electron system characteristic of porphyrinic compounds (cross-conjugated with another β, β'-double bond) of the parent ion is maintained. A possible structure for the azirene-containing system **3.17a** may also be the corresponding chlorophin diradical species **3.17b**. Chlorophins are known porphyrinic compounds. Evidently, the break-down of the oxazolidone moiety and the generation of closed-shell compounds represent lower energy pathways than the loss of a phenyl radical. This is an indication for the lesser stability of the partially oxidized porphyrin derivative **TPL** as compared to **TPP** itself. Considering that the spectroscopic properties of **TPL** are in many aspects similar to those of **TPP**,[20, 60] and that the replacement of a β, β'-double bond in TPP by a lactone moiety does not introduce any steric strain or interrupts the 18π-electron system, the drastic effects of this

replacement with respect to the observed fragmentation pattern is astounding. Parallel to the findings with **TPP**, the ESI(-) spectrum of **TPL** could not be recorded.

The proposed structure of fragmentation product **3.18** is not immediately evident but is supported by a number of findings. Its m/z value of 577 corresponds to the loss of 56 amu (or, formally, a C_2O_2 fragment) from $[\mathbf{TPL} + H]^+$. The loss of the hypothetical species C_2O_2 in one step is not likely. Instead, the sequential loss of two COs is more probable. Indeed, the tandem mass spectrum of species **3.16**, formed from $[\mathbf{TPL} + H]^+$ by loss of one CO, shows near-exclusive formation of **3.18** by means of loss of another CO (Figure 3.8D). A macrocycle ring-opened product corresponding to the mass of **3.18** would be expected to rapidly fragment further. This, however, is not observed. How, then, can the oxazete ring (the only source of O) in **3.16** loose CO, involving the loss of a ring-carbon, while concomitantly forming the evidently stable, likely ring-closed and aromatic pseudomolecular species **3.18**? Scheme 3.6 offers an explanation.
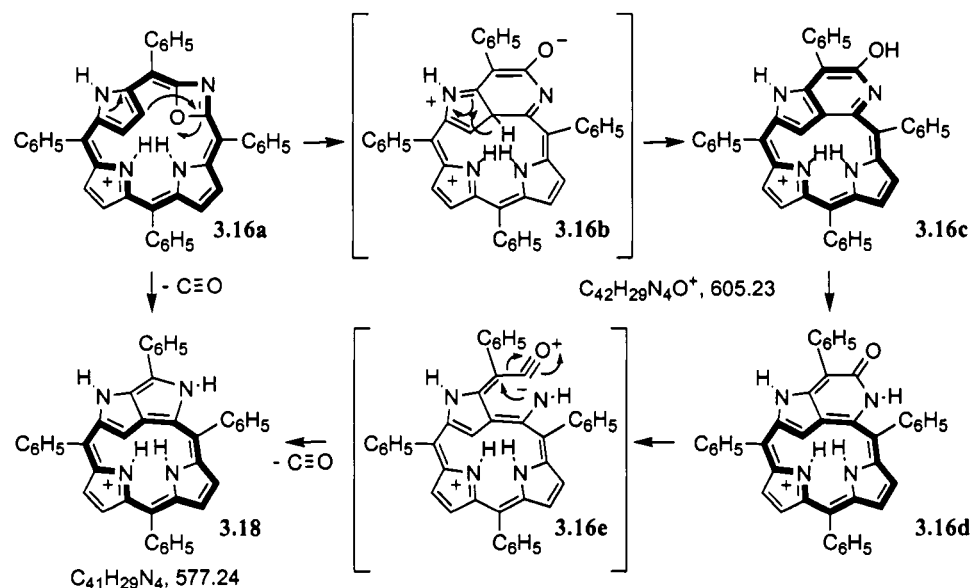
Scheme **3.6** Mechanism of the formation of **3.18** by decarbonylation of **3.16a**.

Ring opening of the (strained) oxazete ring of **3.16a** by means of a nucleophilic attack by a pyrrolic β-position generates a fused pyrrolopyridine system (**3.16a** → **3.16b**

→ **3.16c**). This reaction may occur in a stepwise or concerted fashion. Inverted pyrrolic units are common in expanded oligopyrrolic macrocycles. In fact, comparable β-ring-to-pyrrole nitrogen bonds were reported in 'N-fused' porphyrins and pentaphyrins, though the latter were formed in oxidative processes. The resulting pyrrolopyridine system **3.16c**, or its more likely tautomeric pyrrolo-pyridinone form **3.16d**, feature 18π or 14π aromatic systems, respectively, and are not sterically constricted. All of the structures **3.16a** – **3.16d** are isomers of each other and, solely based on the observed m/z value, one cannot tell which represents the stable form of the species of m/z 605 (though an investigation of the mass spectrum of the pentafluorophenyl derivative **TFPL** provides additional clues, see below). Intramolecular CO loss from **3.16d** along a McLafferty-type cleavage typical for amides finally generates (via **3.16e**) the species **3.18**. The overall result of the fragmentation is that one *meso*-phenyldipyrrin building block of a porphyrin is formally replaced by a phenyl-substituted pyrrolo[2,3c]pyrrole moiety. Its structure represents a hitherto unreported contracted 14π-porphyrinoid.

The collision induced fragmentation spectrum of **3.18** (MS^3-spectrum) is shown in Figure 3.8. The rich features of the spectrum and the occurrence of fragments of relatively low m/z values suggest a break-up of the porphyrinic macrocycle. Especially the peak clusters below m/z 500 are broad and indicative of a number of overlaying species, preventing a conclusive interpretation. Nonetheless, some of the peaks provide support for the structure assigned to **3.18**. However, it must be noted that the large number of possible isomeric structures that correspond to the m/z values measured limit the diagnostic value of the peaks. An interpretation of the fragmentation spectrum of **3.18** is presented in Scheme 3.7, whereby only one possible isomer of the fragments is shown that, based on the structure of **3.18**, can reasonably be expected. Protonation is shown to occur on the central imine-type nitrogens although some species can also be protonated at other sites. Further, Scheme 3.7 does not attempt to provide a genealogy of the fragments.

The interpretation rests on the following rationale: The 14π-aromatic system of **3.18** is deemed the most stable core structure and is maintained in the fragmentations

corresponding to the loss of a single phenyl group (**3.19**), NH₃ (**3.20**), or HCN (**3.21**). Two species are most prominent in the fragmentation spectrum, those of *m/z* 486 and 461. For the heavier fragment, it is tempting to propose the deconstruction of the phenyl-derivatized pyrrolopyrrole building block that maintains the 14π-system (**3.22**). Its structure can be formulated in two isomeric forms, the cyclobutenopyrrole form **3.22a** or as azepine **3.22b**. However, a ring-opened isomer of the same *m/z* can also be formulated (**3.22c**). Further fragmentation of this species on either end under the loss of pyrroles or benzyl groups are expected (**3.23** – **3.26**), and the corresponding fragment peaks are indeed observed. Whether the particular structures shown represent the actual species remains, however, speculative. It is nevertheless significant that this analysis accounts for all major and most of the minor peaks observed, many of which incorporate the pyrrolopyrrole moiety or are derived from the loss of the entire moiety. Further indications for the structure of **3.18** are provided by the ESI(+) MS analysis of the dithiaporpholactone **TTSL** and the ESI(-) MS analysis of pentafluoro-phenylporpholactone **TFPL** (see below).
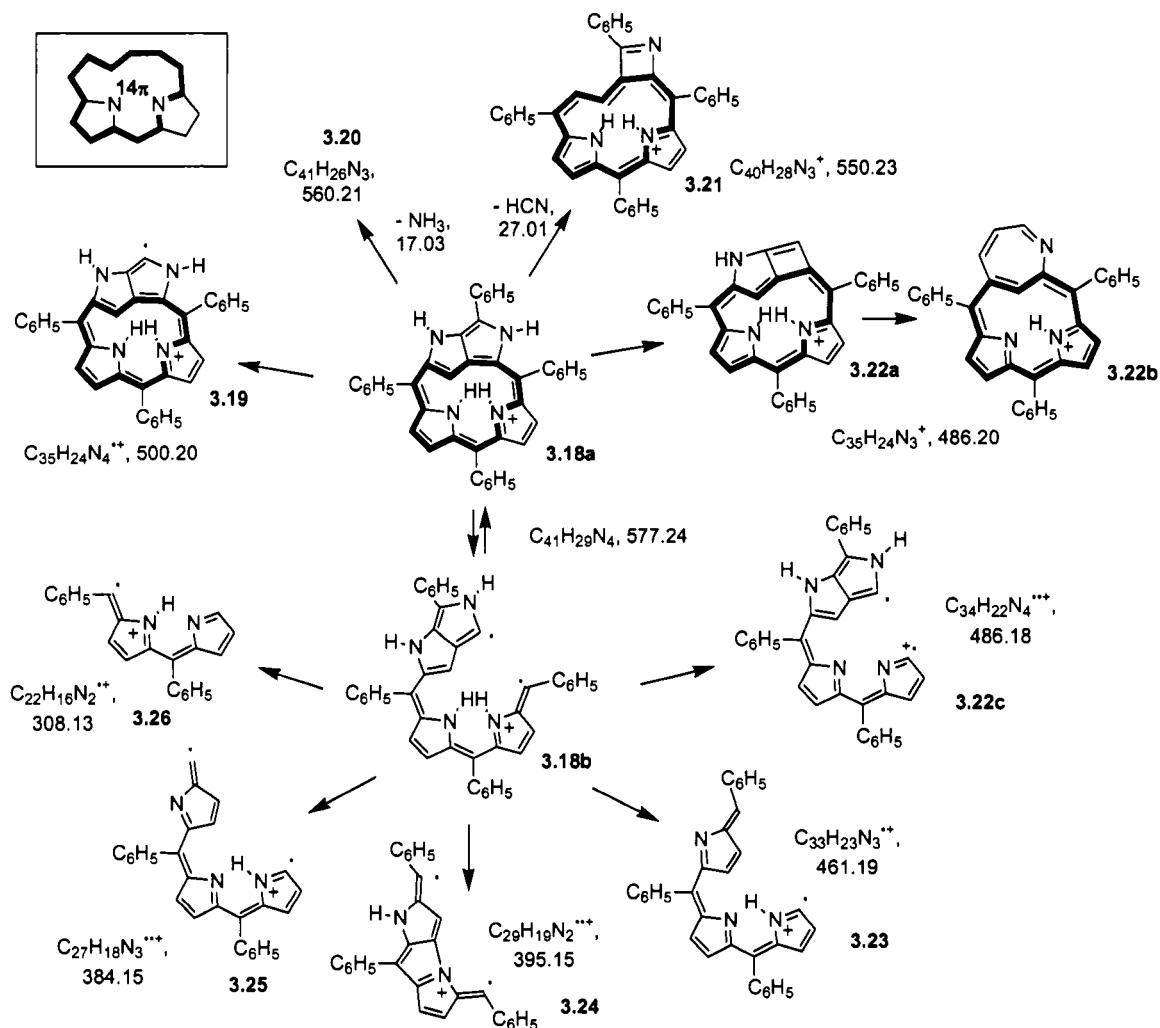
Scheme 3.7 Interpretation of the collision-induced mass spectrum of **3.18** (Figure 3.8E).

Single and Tandem ESI(+) Mass Spectrometric Analysis of TTSL

The full scan ESI(+) spectrum of **TTSL** shows, as expected, the protonated parent ion at m/z 723 (Figure 3.9A). The fragmentation mass spectrum of this ion is shown in Figure 3.9B. Parallel to the observations made with **TPL**, no loss of any aryl groups is observed. Instead, the only break-down products detected are those corresponding to two consecutive losses of m/z 28 fragments (CO).
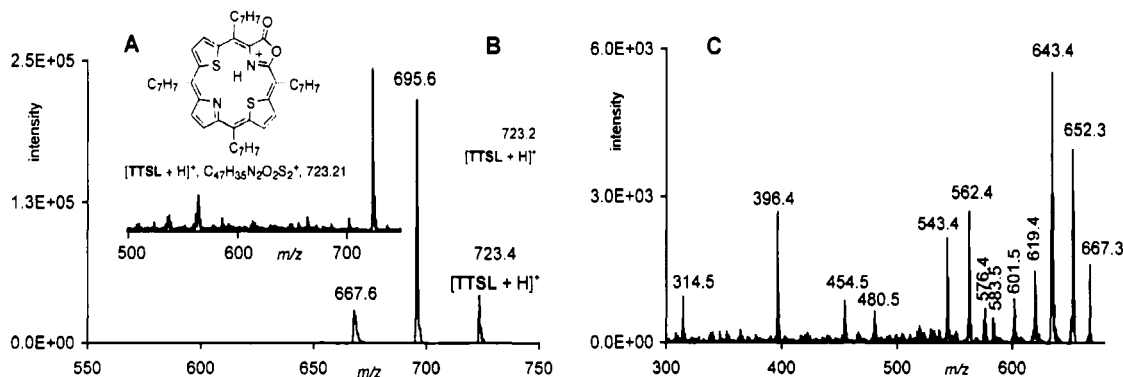
Figure 3.9 A) Full scan ESI(+) spectrum of TTSL. B) Collision induced fragmentation spectrum of the species [TTSL + H]⁺ (*m/z* 723). An interpretation of the spectrum is provided in Scheme 3.8. C) Collision-induced fragmentation spectrum of the *m/z* 667 species (from spectrum 3.9B). An interpretation of the spectrum is provided in Scheme 3.9.
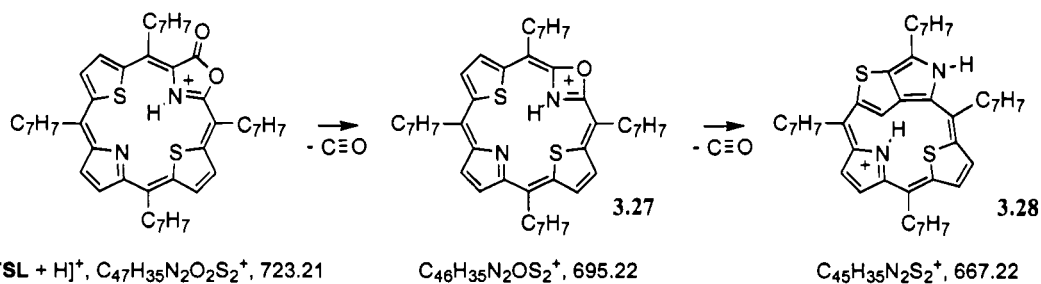
Scheme 3.8 Interpretation of the collision-induced fragmentation mass spectrum of [TTSL + H]+ (Figure 3.9B).

Scheme 3.8 provides an interpretation of the spectrum that parallels the interpretation of the spectrum of the all-aza species **TPL**. Loss of the first CO leads to the formation of the oxazete-containing species **3.27**, the dithiaanalogue to **3.16**. The subsequent loss of CO forms the thiophenolo[2,3c]pyrrole-containing species **3.28**, the dithiaanalogue to **3.18**. Evidently, species **3.28** is a stable pseudomolecular species as no consecutive fragmentations are measured.
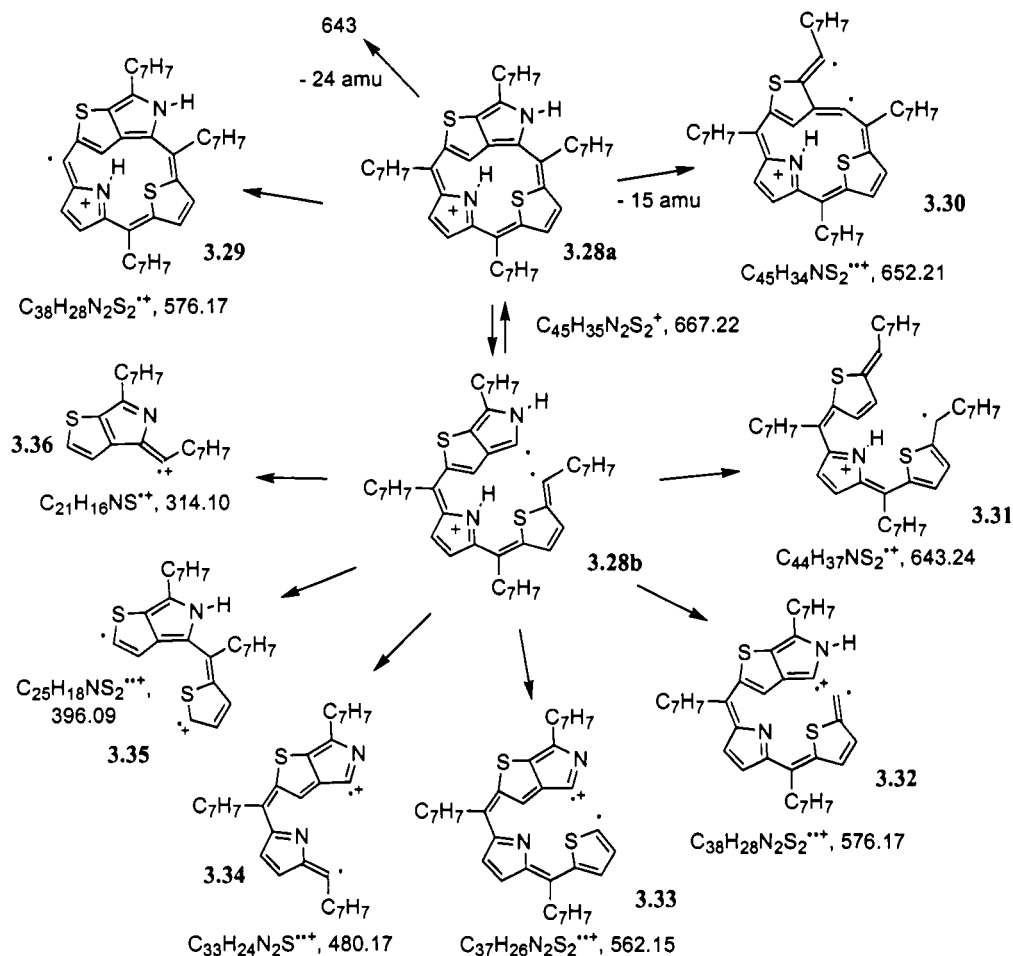
Scheme 3.9 Interpretation of the collision-induced fragmentation mass spectrum of **3.28** (Figure 3.10C).

The collision-induced fragmentation spectrum of species **3.28** (MS^3-spectrum) is shown in Figure 3.9C. Again, parallel to the observations made for the all-aza species **3.18**, a series of small fragment losses are observed, followed by a rich fragmentation pattern suggestive of macrocycle ring-opened products. The interpretation of the spectrum is shown in Scheme 3.9 whereby the same rationales were used, and the same caveats as to its validity apply that were detailed above. Within these limits, however, most peaks find an explanation. Some species proposed, such as **3.29** and **3.30**, are the dithia-, tolyl-analogues to the all-aza-phenyl-species **3.19** and **3.22**, respectively. It is also of note that many species contain the intact thiophenolopyrrole moiety. Due to its fused ring system structure, it possesses a high heteroatom:hydrogen ratio (especially

those of low *m/z* ratios such as **3.35** and **3.36**). This limits the number of possible isomeric structures not evoking this moiety. We interpret this as a further indication for the reality of the proposed structures.

Single and Tandem ESI(+) and ESI(-) Mass Spectrometric Analysis of TFPL

The ESI(+) mass spectrum of **TFPL** is shown in Figure 3.10A, its corresponding ESI(-) spectrum in Figure 3.10D. In analogy to the observations made with **TFPP** and **TFPC**, the negative mode spectrum is very clean and shows almost exclusively the deprotonated ion [**TFPL** – H]⁻ (*m/z* 991). The tandem mass spectrum of this species is shown in Figure 3.10E. The most intense fragment of [**TFPL** – H]⁻ is that of the parent ion [**TFPL** – H]⁻ – CO_2 (at *m/z* 947) for which we propose azirene structure **3.37** (Scheme 3.10). It is the fluorinated analogue to the **TPL** fragment **3.17** (Scheme 3.5). Unlike this minor fragment from **TPL**, **3.37** is the major (if not sole) fragmentation product resulting from the collapse of the pyrrolidinone moiety in **TFPL**, an effect likely due to the electronic influence of the pentafluorophenyl groups.
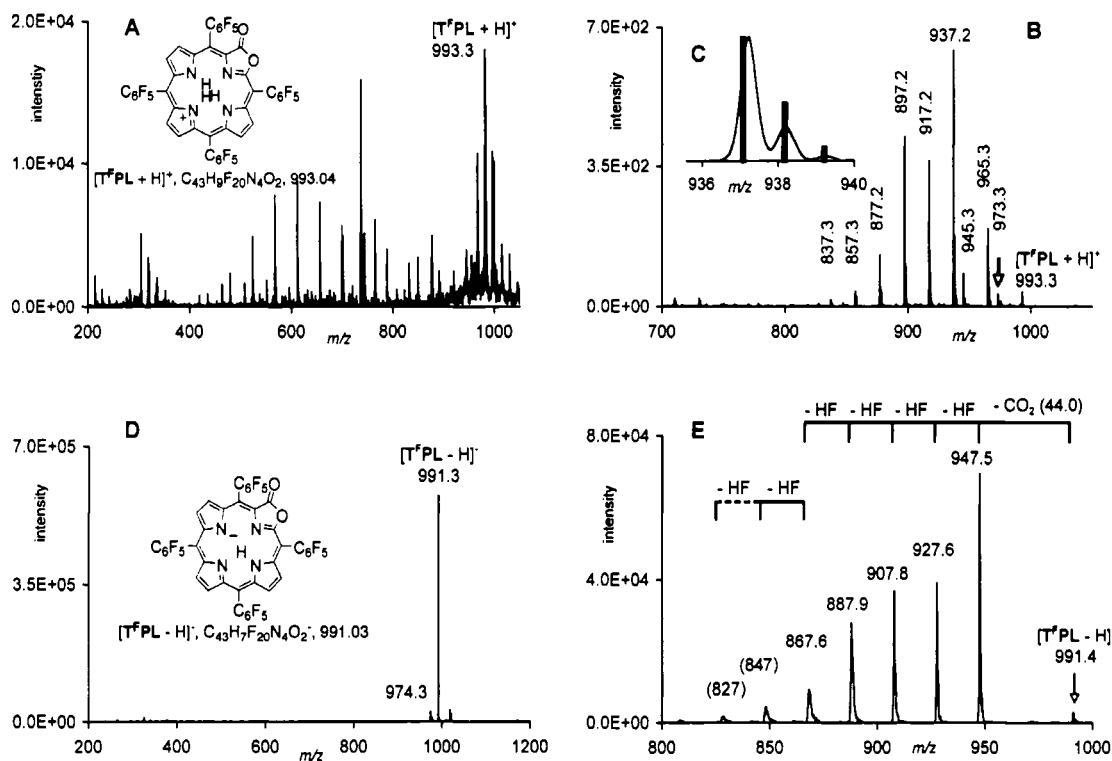
Figure 3.10 A) Full scan ESI(+) spectrum of TFPL. B) Collision induced fragmentation spectrum of the species [TFPL + H]$^+$ (m/z 993). The spectrum is interpreted in Scheme 3.11. C) Expansion of peak cluster of m/z 937, bars represent the computed isotope pattern for the species $C_{41}H_9F_{20}N_4^+$. D) Full scan ESI(-) spectrum of TFPL. E) Collision induced fragmentation spectrum of the species [TFPL - H]$^-$ (m/z 991). An interpretation of the spectra is presented in Scheme 3.10.

The subsequent fragmentation of **3.37** is the successive loss of up to five HF molecules, presumably forming singly and multiply o-to-β-linked macrocycles such as **3.38** and **3.39**. The peak intensity tapers off with each successive HF loss, although the first three losses appear to be efficient. We believe this is significant and related to the azirine (or the corresponding chlorophin diradical) structure of **3.37**. Only three pyrrolic subunits are intact allowing linkages to three aryl groups each. Linkages to the azirine ring would form highly strained four-membered ring structures and are deemed unlikely. The fourth and fifth linkages thus imply the double-linkage of one or two aryl groups,

respectively. As detailed above, that leads to higher energy structures such as **3.37** and are, therefore, occurring to a much lesser extent.
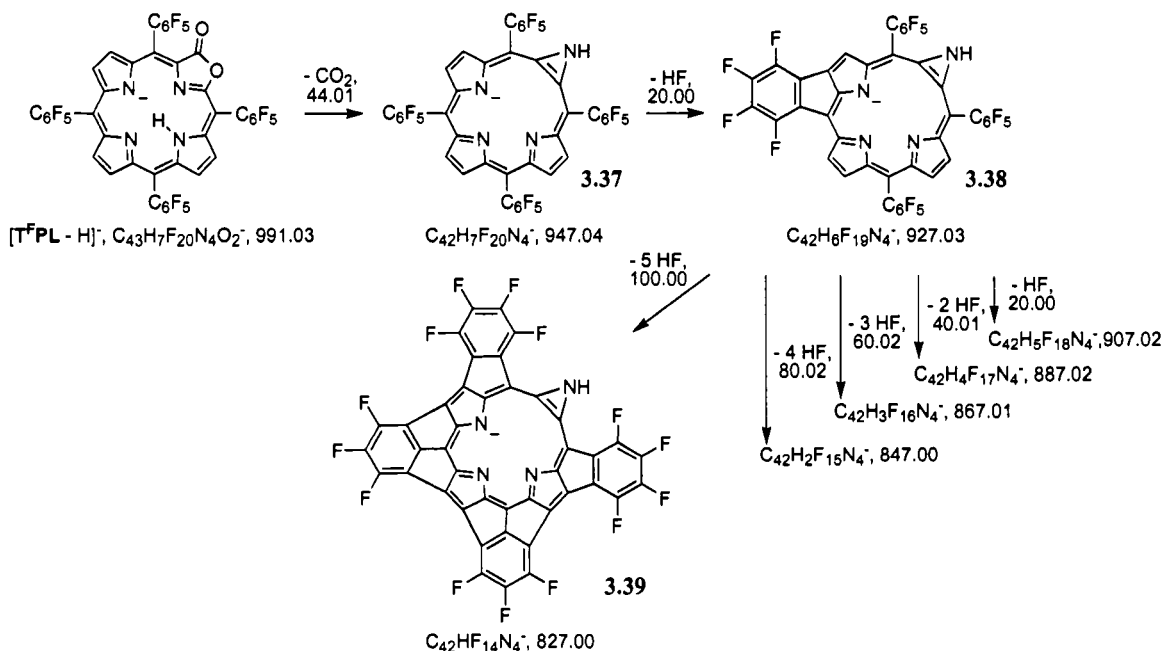
Scheme 3.10 Interpretation of the collision-induced fragmentation mass spectrum of [TFPL – H]⁻ (Figure 3.10E)

The ESI(+) fragmentation spectrum of the protonated species $[\mathbf{TFPL} + \mathbf{H}]^+$ is complex but very instructive (Figure 3.10B). Scheme 3.11 shows our interpretation of the spectrum which, in general, combines the elements of the interpretation of the ESI(+) spectrum of $[\mathbf{TPL} + \mathbf{H}]^+$ with those delineated for *meso*-pentafluorophenyl substituted porphyrins (Schemes 3.8 and 3.9). We have shown that $[\mathbf{TPL} + \mathbf{H}]^+$ is prone to excising O (minor), CO (major), CO_2 (minor) and two consecutive CO (major). Qualitatively, these trends are preserved for the fragmentation of $[\mathbf{TFPL} + \mathbf{H}]^+$. Thus, minor peaks corresponding to the loss of O (at *m/z* 977) or CO_2 (at *m/z* 949) from the parent ion $[\mathbf{TFPL} + \mathbf{H}]^+$ (*m/z* 993) are detectable. The sequential loss of two CO groups (resulting in the formation of the species at *m/z* 965 and 937, respectively) constitute the predominant fragmentation pathway, forming species **3.41** (or its rearranged product

3.43) and **3.45**, respectively. A minor peak at *m/z* 973, corresponding to the loss of HF from the parent ion [**TFPL** + H]$^+$, is evidence for the formation of *o*-to-β-cyclized species **3.40**.

The loss of HF from the species **3.41/3.43**, forms **3.42** or its rearranged product **3.44** (*m/z* 945). However, no further losses of HF from **3.40**, **3.41/3.43**, or **3.42/3.44** are observed. We do not believe that this is due to the small peak intensity for these species. Instead, we interpret the finding as an indication for the rapid isomerization of **3.41** or **3.42** to **3.43** or **3.44**, respectively, followed by efficient CO expulsion. The resulting species **3.45** (at *m/z* 937) and **3.46** (at *m/z* 917) are the major species in the spectrum. Their difference is a HF-loss mediated aryl-to-pyrrole linkage. It is attractive to assume the *N*-phenyl linkage shown for structure **3.46** as the location for this linkage because nitrogen is a better nucleophile than carbon. Such a linkage would also assist in the CO expulsion from **3.44** according to the mechanism shown in Scheme 3.6. Further, and most compelling for the structure of **3.46**, this species is set up to lose a maximum of 4 HF groups under the formation of aryl-to-β linkages to form **4.47** (isomeric structures, particularly one involving a link to the peripheral pyrrole-nitrogen, are possible), all of which are observed. Once again, the first linkages are evidently facile, and the last, forming a doubly-linked phenyl group takes place with the lowest efficiency. It is interesting to note that ring-opened fragments are not dominating the spectrum and that the pattern indicative of the sequential losses of single heteroatoms is absent, both perhaps the result of the stabilizing effects of the pentafluorophenyl groups.

All considered, the fragmentation of [**TFPL** + H]$^+$ follows the findings described for the fragmentation of porpholactone **TPL**, modulated by the presence of *meso*-pentafluorophenyl groups. Thus, the spectrum of [**TFPL** + H]$^+$ provides some further, independent and persuasive support for the soundness of the proposed pyrrolopyrrole species **3.18**(and **3.28**, **3.45/3.46**) and further insight in its formation.

[TFPL + H]⁺, $C_{43}H_9F_{20}N_4O_2^+$, 993.04

$C_{43}H_8F_{19}N_4O_2^+$, 973.03 (minor)

- CO, 28.01

- CO, 28.01

3.40

3.41

$C_{42}H_9F_{20}N_4O^+$, 965.05

3.42

$C_{42}H_8F_{19}N_4O^+$, 945.04 (minor)

- HF, 20.00 → not observed

3.43

$C_{42}H_9F_{20}N_4O^+$, 965.05

3.44

$C_{42}H_8F_{19}N_4O^+$, 945.04

- CO, 28.01

- CO, 28.01

- HF, 20.00 → $C_{41}H_7F_{18}N_4^+$, 897.04

- 2 HF, 40.01 → $C_{41}H_6F_{17}N_4^+$, 877.03

- 3 HF, 60.02 → $C_{41}H_5F_{16}N_4^+$, 857.03

- 4 HF, 80.02

3.45

$C_{41}H_9F_{20}N_4^+$, 937.05 (major)

3.46

$C_{41}H_8F_{19}N_4^+$, 917.04 (major)

3.47

$C_{41}H_4F_{15}N_4^+$, 837.02

Scheme 3.11 Interpretation of the collision-induced fragmentation mass spectrum of [TFPL + H]⁺ (Figure 3.10B).

3.3.c Conclusions

We have further elucidated the fragmentation pattern for *meso*-phenyl- and *meso*-pentafluorophenyl-substituted porpholactones and dithiaporpholactones. The fragmentation pathways highlight the substantial perturbance the partially oxidized pyrrole unit introduces into the porphyrinic macrocycle. Whereas porphyrins are very robust under the conditions investigated, the porpholactones show exceedingly rich fragmentations, all originating in the collapse of the oxazolidone moiety. In as far as these gas-phase reactions can inspire the total synthesis of novel 14π-porphyrinoids, such as pyrrolo[2,3c]pyrrole containing contracted porphyrins such as **3.18**, is also a subject of current investigations.

Section 4: Tandem Electrospray Ionization (ESI) Mass Spectrometric Analysis of *meso*-Tetrakis(Heptafluoropropyl)Porphyrin

3.4.a Introduction

Meso-Tetraarylporphyrins are the most widely studied class of synthetic porphyrins.[63] Much less investigated are their parent compounds, *meso*-tetrakis-alkylporphyrins (Figure 3.11), and the corresponding *meso*-perfluoroalkylporphyrins.[42, 96-98] In particular, the *meso*-perfluoroalkylporphyrins have proved useful in, for example, the design of synthetic monooxygenase mimicks.[99] In addition, their potential in both photodynamic therapy and in the in vivo imaging by fluorescence and ^{19}F NMR (nuclear magnetic resonance) spectroscopy was evaluated.[100]
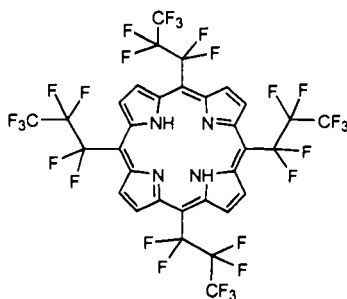
Figure 3.11 Structure of the *meso*-tetrakis-alkylporphyrin (TFHP).

Recently, the groups of Guo and Chen described, inter alia, the functionalization of *meso*-arylporphyrins with *meso*-fluoroiodo-alkanes **3.48** or fluorochloro-alkanes **3.49**. Radical-induced deiodination or debromination resulted in the formation of terminal radicals that efficiently ring-closed with the neighboring β-positions to form products **3.50** and **3.51**, respectively (Scheme 3.12).[101, 102] Thus, a range of fused ring products enclosing five- and six-membered rings were prepared. These findings prompted the question whether *meso*-perfluoroalkylporphyrins such as *meso*-

tetrakis(heptafluoropropyl)- porphyrin (**TFHP**) also undergo similar cyclizations. Our findings answer this question affirmatively.
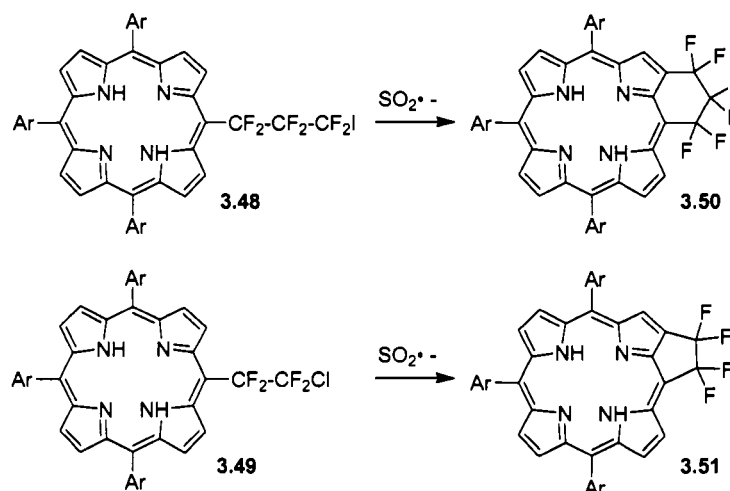
Scheme 3.12 The functionalization of *meso*-arylporphyrins with *meso*-fluoroiodo-alkanes **3.48** and fluorochloro-alkanes **3.49**.

We show the analysis of **TFHP** by tandem electrospray ionization (ESI) mass spectrometry in the positive and negative mode. Using collision-induced fragmentation techniques, we find that rich fragmentation patterns in positive and negative ionization modes are observed. Next to the expected losses of radical fragments, HF eliminations are observed, which we attribute to the formation of polycyclic systems containing *meso*-alkyl-to-β-fusions. A detailed analysis of the spectra allows some conclusions to be drawn as to the nature of these products.

3.4.b Results and Discussion

ESI mass spectrometry is becoming a popular technique for the analyses of porphyrins and metalloporphyrins.[60, 77, 78, 81, 84, 103, 104] Free base porphyrins are readily protonated.[81, 84] Thus, ESI(+) is commonly used for the analysis of porphyrins and proves also to be suitable for the analysis of **TFHP** (see the following section). For the

simplicity and clarity of the resulting spectra and their interpretation, we will, however, first discuss our findings using the ESI in the negative ion detection mode (ESI(-)).

Single and Tandem ESI(-) Mass Spectrometry Spectra of **TFHP**

The ESI(-) spectrum of **TFHP** ($C_{32}H_{10}F_{28}N_4$, exact mass: 982.0458 amu), recorded in the negative ion mode, shows as the major species one peak at m/z 981.3, corresponding to the species [**TFHP** - H]⁻. Ionization is thus brought about by deprotonation, presumably of one of the inner pyrrole-type nitrogens. The electronwithdrawing *meso*-perfluoroalkyl substituents increase the acidity of the porphyrin and make deprotonation possible. As expected for the soft ESI method, no fragment ions are observed.[105]

Figure 3.12 shows the collision-induced fragmentation spectrum of the species at m/z 981. As the sole fragmentation pattern, the successive loss of six equivalents of HF (20 amu) is observed. Because a *cis*-elimination of HF (hydrogen fluoride) cannot take place in **TFHP**, we surmise that the elimination is, under concomitant formation of a single bond, due to the loss of one H from the pyrrolic β-positions and the loss of one F from a flanking perfluoroalkyl group (Scheme 3.12). It can not be conclusively derived whether this reaction is due to a nucleophilic attack of a β-carbon at the fluoroalkyl chain or due to a radical-mediated process, but the absence of any radical fragmentations (cf. below to the corresponding fragmentation spectrum in the ESI(+) mode) suggests a substitution mechanism. This mechanism is also assisted by the negatively charged porphyrinic macrocycle. We, and others, have observed the formation of such linkages under mass spectrometry conditions in *meso*-perfluoroaryl-substituted porphyrins.[84, 106]
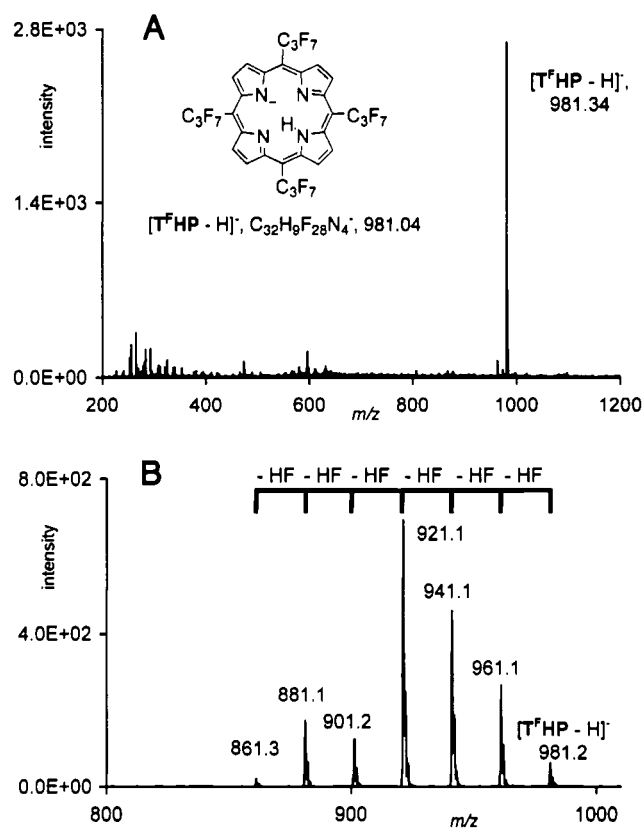
Figure 3.12 A) Full scan ESI(-) spectrum of TFHP. B) Collision induced fragmentation spectrum of the species [TFHP - H]⁻ (m/z 981). An interpretation of the spectra is presented in Scheme 3.13.
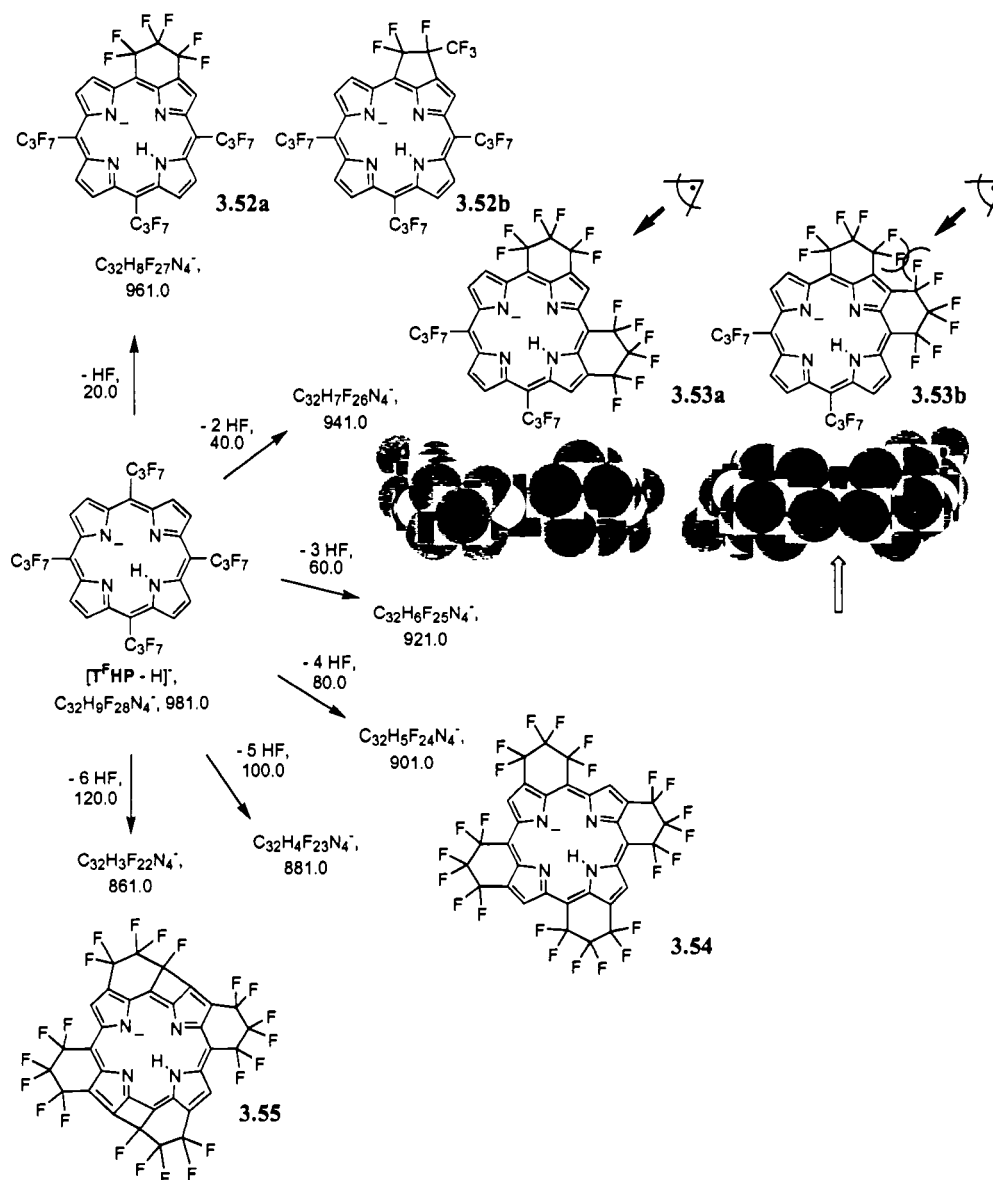
Scheme 3.13 Interpretation of the collision-induced fragmentation spectrum of [TFHP - H]⁻ (Figure 3.12). Open arrow indicates steric interactions; the solid arrows indicate the view direction of the molecular model of **3.53a/b** (energy-minimized, MM2 level, CS Chem 3D Pro, v. 5.0), shown in space-filling representation, atoms at 100% van der Waals radii: solid gray: carbon, dotted: fluorine, solid white: hydrogen.

The structure of the species at *m/z* 961 resulting from one loss of HF from [**TFHP** - H]⁻ could be species **3.52a**, enclosing a six-membered ring, or **3.52b**, enclosing a five-membered ring. The ESI(-) spectrum does not provide any indications of which species

is formed. However, as we will show later, the ESI(+) spectrum provides clues that preferentially the six-membered ring is formed. Hence, the consecutive fragmentation products are formulated in Scheme 3.13 as the fused six-membered ring species. The second and subsequent two HF losses can result in the formation of numerous isomers. We surmise that the cyclizations occur in an unidirectional orientation. Instead of forming products such as **3.53b**, in which the two alkyl chains are linked to the same pyrrolic building block, isomer **3.53a** is formed, in which the two alkyl chains are linked to two different pyrrolic units. We base this on a molecular modeling study (CS Chem 3D Pro, MM2 basis set). A space-filling representation of the energy minimized isomers **3.53a** and **3.53b** was generated and is shown in Scheme 3.13. Although isomer **3.53a** is not sterically encumbered, significant overlap of the van der Waals radii of two fluorine atoms is clearly present in isomer **3.53b**. Hence, accounting for the cooperative interaction between the linkages, we have formulated the species **3.54** that resulted from the loss of four equivalents of HF as the symmetrically linked isomer.

The fifth and sixth loss of HF implies the formation of two more linkages, presumably forming fused four-membered rings, as shown for **3.55**. The position of the four-membered rings was, as shown, positioned to be opposite to each other but there is no experimental evidence to exclude the formation of these fusions in pyrrolic subunits adjacent to each other. Molecular modeling studies have revealed the metric possibility of these linkages although the porphyrin assumes a slightly domed conformation. This high-energy deformation is likely the reason the intensity of the ion peaks corresponding to the fifth and especially the sixth HF loss are small. No further fragmentations are observed in the tandem ESI(-) spectrum of [**TFHP** - H]⁻.

Single and Tandem ESI(+) Mass Spectrometry Spectra of **TFHP**

The single ESI mass spectrum of **TFHP**, recorded in the positive ion mode, shows one predominant species at m/z 983.4 that corresponds to the expected monoprotonated species [**TFHP** + H]$^+$ ($C_{32}H_{11}F_{28}N_4{}^+$, exact mass: 983.0531). The collision-induced fragmentation ESI(+) spectrum of the species [**TFHP** + H]$^+$ (Figure

3.13) shows, in principal, similar HF-loss patterns as the ESI(-) spectrum, which we interpret in a similar fashion (Scheme 3.14). However, the spectrum is complicated by the fact that radical fragmentations are observed and that the fragments each undergo HF loss-mediated cyclization reactions.
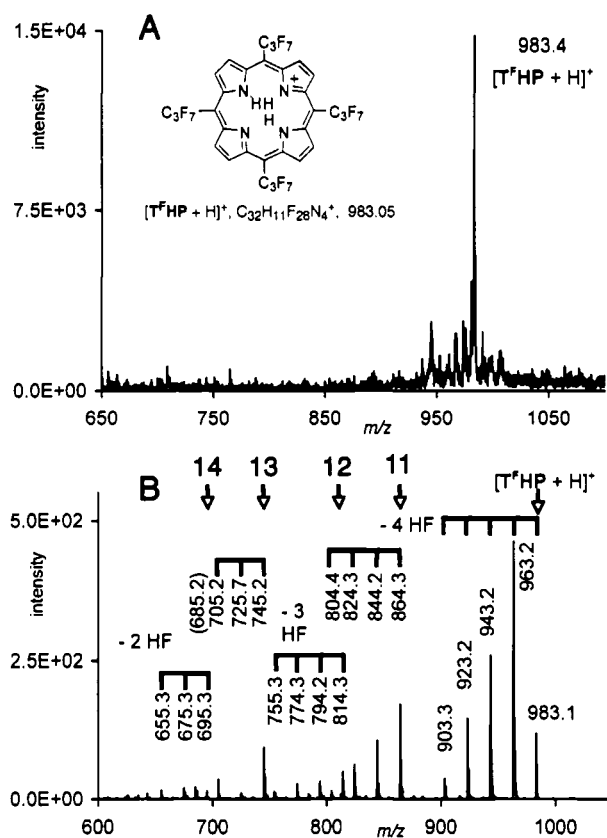
Figure 3.13 A) Full scan ESI(+) spectrum of TFHP. B): Collision induced fragmentation spectrum of the species [T^F HP + H]^+ (m/z 983). An interpretation of the spectra is presented in Scheme 3.14.
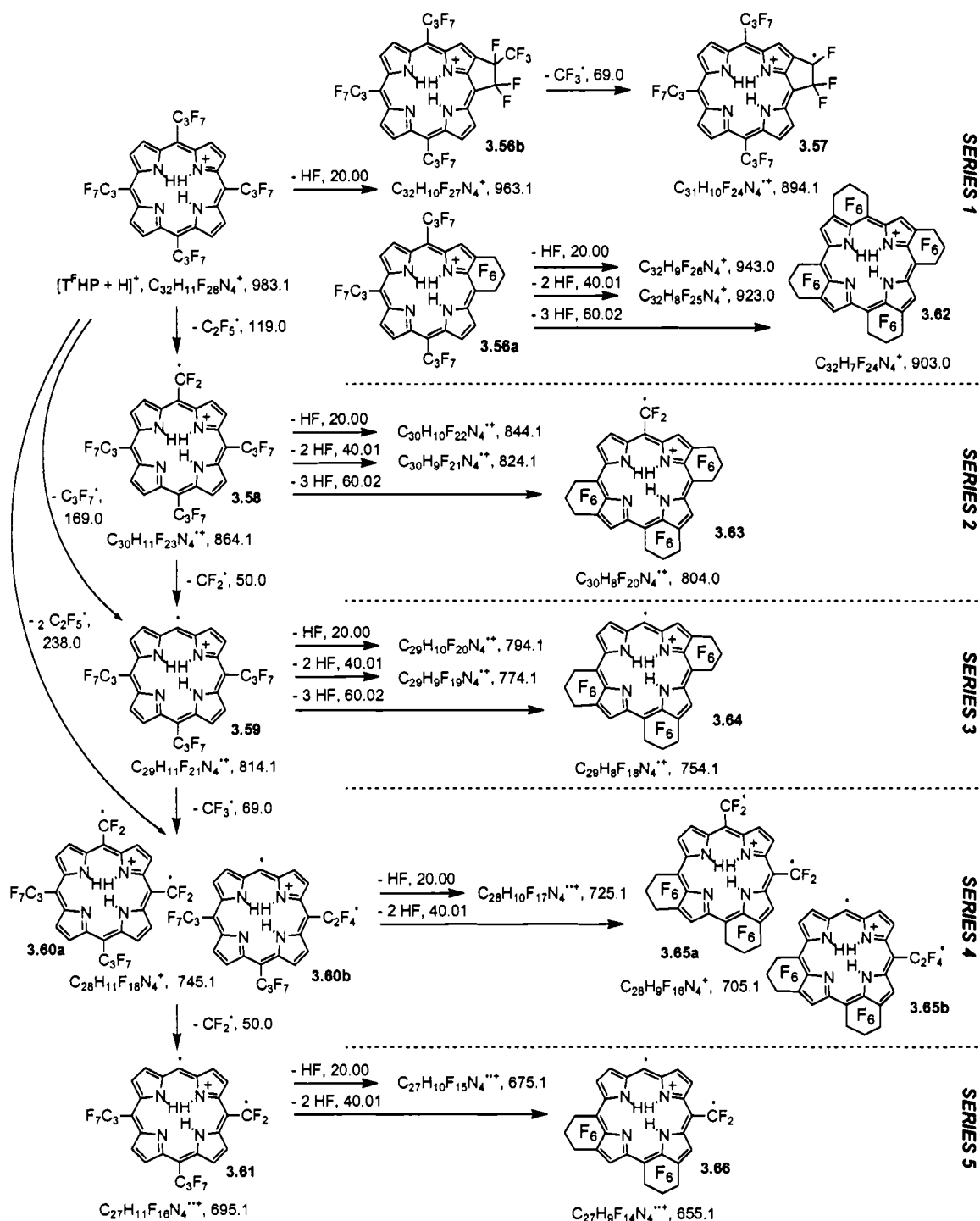
Scheme 3.14 Interpretation of the collision-induced fragmentation spectrum of [TFHP + H]$^+$ (Figure 3.13).

The heaviest fragment is species **3.56** of *m/z* 963, derived from [**TFHP** + H]$^+$ by loss of HF. Analogous to the negative ion mode spectrum, two possible structures can be formulated for this product, **3.56a** and **3.56b**. The six-membered product **3.56a** is set up for three more equivalent losses of HF, all of which are observed, ultimately forming species **3.62**. The five-membered ring species **3.56b** is not a likely structure for the ion of *m/z* 963. This is because the ESI(+) spectrum is characterized by the occurrence of many radical fragmentations of the heptafluoropropyl substituents (see in the following paragraph). This should make the formation of the highly stabilized radical **3.57** through loss of a CF$^{\bullet}_3$ radical likely. That fragment, however, is not observed. The mechanism for the cyclization reactions are, because of the observation of extensive radical fragmentations, of radical nature, although the very electron-rich nature of even a monoprotonated porphyrin ring may still allow nucleophilic substitution reactions to take place.

The tandem ESI(+) spectrum of [**TFHP** + H]$^+$ is, in contrast to its ESI(-) spectrum, rich of fragmentations of the heptafluoropropyl substituents. This circumstance provides valuable indications for the structure of the products. The spectrum allows the identification of five independent series of peaks, which are all derived from the parent ion [**TFHP** + H]$^+$ by different radical fragmentations of the heptafluoropropyl group(s): Series **1** through **5**, origination in the species **3.58**, **3.59**, **3.60**, and **3.61**, respectively. Each peak series is related through sequential losses of up to four molecules of HF (Figure 3.13). All expected radical fragments from [**TFHP** + H]$^+$ are found: loss of C$_2$F$_5^{\bullet}$ from [**TFHP** + H]$^+$ leads to the formation of the stable benzylic radical species **3.58**. Loss of one entire *meso*-group (C$_3$F$_7^{\bullet}$) from [**TFHP** + H]$^+$ (or loss of CF$_2$ from **3.58**) generates the aromatic radical species **3.59**. Further loss of a CF$_3^{\bullet}$ radical from **3.59** forms **3.60b**. Alternatively, the diradical isomeric structure **3.60b**, resulting from two sequential losses of C$_2$F$_5^{\bullet}$ from [**TFHP** + H]$^+$, is also a likely structure for the species of *m/z* 745. The final alkyl-fragmentation product that can be traced is species **3.61** for which multiple origins can be assumed.

Fragment **3.58** undergoes all three expected HF losses with concomitant formation of six-membered rings. Once again, no product resulting from the loss of a $CF_3{}^{\bullet}$ from **3.58** or any of its HF condensation products are detected, supporting the benzylic radical structure **3.63** containing fused six-membered rings as the structure for the final product. For the same steric arguments provided previously, we show the symmetric condensation products derived from unidirectional ring fusions. An analogous analysis can be made for **3.59**, leading to porphyrin radical **3.64**.

An analysis of the fragmentation of species **3.60** does not allow its identification as either **3.60a** or **3.60b** because both structures are set up to undergo the observed two HF-mediated six-membered ring closures to form the two isomers of **3.65** shown. Finally, fragment **3.61** can undergo two subsequent HF extrusions, forming **3.66**. In addition, HF losses from fragments **3.65** and **3.66** are observed, suggestive of the formation of four-membered rings (cf. to Scheme 3.13). This, and whether **3.65** and **3.66** undergo internal radical recombination processes, however, remains speculative.

3.4.c Conclusions

We have shown the detailed mass spectrometric analysis of a *meso* perfluoroalkylporphyrin. The overriding pattern observed in the positive and negative ion mode spectra are a series of HF eliminations we attribute to the formation of *meso*-alkyl to-β-position fusion products. We are not aware of any reports describing this fragmentation pattern for *meso*-perfluoroalkylporphyrins. The results will facilitate the interpretation of mass spectrometry spectra of *meso*-perfluoroalkyl-substituted porphyrinic compounds using ESI mass spectrometry. The findings provide an understanding of the behavior of fluoro-substituted *meso*-alkylporphyrins under ESI mass spectrometry conditions. Whether the observed fragmentation modes also can be adopted for the solution-phase bulk synthesis of porphyrins containing fused perfluorinated ring systems is currently a subject of investigations in our laboratories.

Notes to Chapter 3:

1.   Lindsey, J. S., Synthesis of *meso*-Substituted Porphyrins. In *The Porphyrin Handbook*, Guilard, R., Ed. Academic Press: San Diego, 2000; Vol. 1, pp 45-118.

2.   Mahammed, A.; Goldberg, I.; Gross, Z., Highly Selective Chlorosulfonation of Tris(pentafluorophenyl)corrole as a Synthetic Tool for the Preparation of Amphiphilic Corroles and Metal Complexes of Planar Chirality. *Org. Lett.* **2001**, 3, (22), 3443-3446.

3.   Silva, A. M. G.; Tome, A. C.; Neves, M. G. P. M. S.; Silva, A. M. S.; Cavaleiro, J. A. S., meso-Tetraarylporphyrins as dipolarophiles in 1,3-dipolar cycloaddition reactions. *Chem. Commun.* **1999**, 1767-1768.

4.   Fujii, H., Electronic structure and reactivity of high-valent oxo iron porphyrins. *Coord. Chem. Rev.* **2002**, 226, 51-60.

5.   Simkhovich, L.; Galili, N.; Saltsman, I.; Goldberg, I.; Gross, Z., Coordination Chemistry of the Novel 5,10,15-Tris(pentafluorophenyl)corrole: Synthesis, Spectroscopy, and Structural Characterization of Its Cobalt(III), Rhodium(III), and Iron(IV) Complexes. *Inorg. Chem.* **2000**, 39, (13), 2704-2705.

6.   Witowska-Jarosz, J.; Gorski, L.; Malinowska, E.; Jarosz, M., Mass spectrometric investigation of gallium and zirconium complexes with octaethylporphyrin and tetraphenylporphyrin. *Journal of Mass Spectrometry* **2002**, 37, (12), 1236-1241.

7.   Rosenthal, J.; Pistorio, B. J.; Chng, L. L.; Nocera, D. G., Aerobic Catalytic Photooxidation of Olefins by an Electron-Deficient Pacman Bisiron(III) -Oxo Porphyrin. *J. Org. Chem.* **2005**, 70, (5), 1885 - 1888.

8.   Furuta, H.; Maeda, H.; Osuka, A., Doubly N-Confused Porphyrin: A New Complexing Agent Capable of Stabilizing Higher Oxidation States. *J. Am. Chem. Soc.* **2000**, 122, (5), 803-807.

9.   Maeda, H.; Osuka, A.; Ishikawa, Y.; Aritome, I.; Hisaeda, Y.; Furuta, H., N-Confused Porphyrin-Bearing meso-Perfluorophenyl Groups: A Potential Agent That Forms Stable Square-Planar Complexes with Cu(II) and Ag(III). *Org. Lett.* **2003**, 5, (8), 1293-1296.

10.   Shin, J.-Y.; Furuta, H.; Osuka, A., N-Fused Pentaphyrin. *Angew. Chem. Int. Ed.* **2001**, 40, (3), 619-621.

11.   Shaw, S. J.; Elgie, K. J.; Edwards, C.; Boyle, R. W., Mono-(pentafluorophenyl)porphyrins - useful intermediates in the regioselective synthesis of multifunctionalized porphyrins. *Tetrahedron Lett.* **1999**, 40, (8), 1595-1596.

12.   Elgie, K. J.; Scobie, M.; Boyle, R. W., Application of combinatorial techniques in the synthesis of unsymmetrically substituted 5,15-diphenylporphyrins. *Tetrahedron Lett.* **2000**, 41, (15), 2753-2757.

13.   Pasetto, P.; Chen, X.; Drain, C. M.; Franck, R. W., Synthesis of hydrolytically stable porphyrin C- and S-glycoconjugates in high yields. *Chem. Commun.* **2001**, 81-82.

14.   Chen, X.; Hui, L.; Foster, D. A.; Drain, C. M., Efficient Synthesis and Photodynamic Activity of Porphyrin-Saccharide Conjugates: Targeting and Incapacitating Cancer Cells. *Biochemistry* **2004**, 43, (34), 10918-10929.

15.   DiMagno, S. G.; Dussault, P. H.; Schultz, J. A., Fluorous Biphasic Singlet Oxygenation with a Perfluoroalkylated Photosensitizer. *J. Am. Chem. Soc.* **1996**, 118, (22), 5312-5313.

16.   Birnbaum, E. R.; Le Lacheur, R. M.; Horton, A. C.; Tumas, W., Metalloporphyrin-catalyzed homogeneous oxidation in supercritical carbon dioxide. *J. Mol. Catal. A* 139, (1), 11-24.

17.   Ayorinde, F. O.; Hambright, P.; Porter, T. N.; Q. L. Keith, J., Use of meso-Tetrakis(pentafluorophenyl)porphyrin as a Matrix for Low Molecular Weight Alkylphenol Ethoxylates in Laser Desorption/Ionization Time-of-flight Mass Spectrometry. *Rapid Commun. Mass Spectrom.* **1999**, 13, 2474–2479.

18.   Birnbaum, E. R.; Schaefer, W. P.; Labinger, J. A.; Bercaw, J. E.; Gray, H. B., Electronic Structures of Halogenated Ruthenium Porphyrins. Crystal Structure of RuTFPPCl8(CO)H2O (TFPPCl8 = Octa-.beta.-chlorotetrakis(pentafluorophenyl)porphyrin). *Inorg. Chem.* **1995**, 34, (7), 1751-1755.

19.   Van Berkel, G. J.; McLuckey, S. A.; Glish, G. L., Electrospray ionization of porphyrins using a quadrupole ion trap for mass analysis. *Anal. Chem.* **1991**, 63, (11), 1098-1109.

20.   Vandell, V. E.; Limbach, P. A., Electrospray ionization mass spectrometry of metalloporphyrins. *J. Mass Spectrom.* **1998**, 33, (3), 212-220.

21.   Berkel, G. J. V.; Quinones, M. A.; Quirke, J. M. E., Geoporphyrin analysis using electrospray ionization-mass spectrometry. *Energy & Fuels* **1993**, 7, (3), 411 - 419.

22.   Airs, R. L.; Keely, B. J., A novel approach for sensitivity enhancement in atmospheric pressure chemical ionisation liquid chromatography/mass spectrometry of chlorophylls. *Rapid Commun. Mass Spectrom.* **2000**, 14, (3), 125-128.

23.   Quirke, J. M. E., Mass Spectrometry of Porphyrins and Metalloporphyrins. In *The Porphyrin Handbook*, Guilard, R., Ed. Academic Press: San Diego, 2000; Vol. 7, pp 371-426.

24.   Domingues, M. R. M.; Marques, M. G. O. S.; Alonso, C. M. A.; Neves, M. G. P. M. S.; Cavaleiro, J. A. S.; Ferrer-Correia, A. J.; Nemirovskiy, O. V.; Gros, M. L., Unexpected fragmentation of b-substituted meso-tetraphenylporphyrins induced by high-energy collisional activation. *J. Am. Soc. Mass Spectrom.* **2002**, 13, (12), 1427-1431.

25.   McCarthy, J. R.; Melfi, P. J.; Capetta, S. H.; Brückner, C., Use of Ag(II) as a removable template in porphyrin chemistry: diol cleavage products of [meso-tetraphenyl-2,3-cis-diolchlorinato]silver(II). *Tetrahedron* **2003**, 59, (46), 9137-9146.

26.   Domingues, M. R. M.; Domingues, P.; Reis, A.; Ferrer-Correira, A. J.; Tomé, J. P. C.; Tomé, A. C.; Neves, M. G. P. M. S.; Cavaleiro, J. A. S., Structural characterization of glycoporphyrins by electrospray tandem mass spectrometry. *J. Mass. Spectrom.* **2004**, 39, (2), 158 - 167.

27.   Izquerido, R. A.; Barros, C. M.; Santana-Marques, M. G.; Correia, A. J. F.; Silva, A. M. G.; Tome, A. C.; Silva, A.; Neves, M. G. P. M. S.; Cavaleiro, J. A. S., Cycloreversion and other gas-phase reactions of neutral and cationic pyrrolidine-fused chlorins and isobacteriochlorins under ion bombardment and electrospray. *Rapid Commun. Mass Spectrom.* **2004**, 18, 2601-2611.

28.   Silva, E. M. P.; Domingues, M. R. M.; Barros, C.; Faustino, M. A. F.; Tomé, J. P. C.; Neves, M. G. P. M. S.; Tomé, A. C.; Santana-Marques, M. G.; Cavaleiro, J. A. S.; Ferrer-Correia, A. J., Characterization of dinitroporphyrin zinc complexes by electrospray ionization tandem mass spectrometry. Unusual fragmentations of -(1,3-dinitroalkyl) porphyrins. *J. Mass. Spectrom.* **2005**, 40, (1), 117-122.

29.   Lau, K. S. F.; Sadilek, M.; Khalil, G. E.; Gouterman, M.; Brückner, C., Tandem ESI Mass Spectrometric Analysis of meso-Tetrakis(heptafluoropropyl)-porphyrin. *J. Am. Soc. Mass Spectrom.* **2005**, 16, (12), 1915-1920.

30.   Domingues, M. R. M.; S.-Marques, M. G. O.; Domingues, P.; Graça Neves, M.; Cavaleiro, J. A. S.; Ferrer-Correia, A. J., Differentiation of Positional Isomers of Nitro Meso-Tetraphenylporphyrins by Tandem Mass Spectrometry. *Am. Soc. Mass. Spectrom.* **2001**, 12, 381-384.

31.   Mahammed, A.; Weaver, J. J.; Gray, H. B.; Abdelas, M.; Gross, Z., How acidic are corroles and why? *Tetrahedron Lett.* **2003**, 44, 2077-2079.

32.   Barloy, L.; Dolphin, D.; Dupré, D.; Wijesekera, T. P. J., Anomalous Double Cyclization Reactions of β-Formylporphyrins. *J. Org. Chem.* **1994**, 59, (26), 7976-7985.

33.   Aihara, H.; Jaquinod, L.; Nurco, D. J.; Smith, K. M., Multicarbocycle Formation Mediated by Arenoporphyrin 1,4-Diradicals: Synthesis of Picenoporphyrins. *Angew. Chem. Int. Ed.* **2001**, 40, (18), 3439-3441.

34.   Daniell, H. W.; Brückner, C., Enantiomeric resolution of a ruffled porphyrinoid. *Angew. Chem., Int. Ed.* **2004**, 43, (13), 1688-1691.

35.   Fox, S.; Boyle, R. W., First examples of intramolecular Pd(0) catalyzed couplings on ortho-iodinated meso-phenyl porphyrins. *Chem. Commun.* **2004**, (11), 1322-1323.

36.   Gross, Z.; Galili, N.; Saltsman, I., The first direct synthesis of corroles from pyrrole. *Angew. Chem., Int. Ed.* **1999**, 38, (10), 1427-1429.

37.   Paolesse, R.; Mini, S.; Sagone, F.; Boschi, T.; Jaquinod, L.; Nurco, D. J.; Smith, K. M., 5,10,15-Triphenylcorrole: a product from a modified Rothemund reaction. *Chem. Commun.* **1999**, (14), 1307-1308.

38.   (a) K. K. Lara, C. R. Rinaldo, C. Brückner, Tetrahedron Lett. 2003, 44, 7793. (b) K. K. Lara, C. K. Rinaldo, C. Brückner, Tetrahedron 2005, 61, 2529

39.   Gouterman, M.; Hall, R. J.; Khalil, G. E.; Martin, P. C.; Shankland, E. G.; Cerny, R. L., Tetra(pentafluorophenyl)porpholactone. *Journal of the American Chemical Society* **1989**, 111, (10), 3702-7.

40.   DiMagno, S. G.; Williams, R. A.; Therien, M. J., Facile Synthesis of *meso*-Tetrakis(perfluoroalkyl)porphyrins: ... *J. Org. Chem.* **1994**, 59, 6943-6948.

41.   DiMagno, S. G.; Wertsching, A. K.; Ross2, C. R., Electronic Consequences of Nonplanar Core Conformations in Electron-Deficient Porphyrins: The Structure and Spectroscopic Properties of [5,10,15,20-Tetrakis(heptafluoropropyl)porphinato]cobalt(II). *J. Am. Chem. Soc.* **1995**, 117, (31), 8279-8280.

42.   Goll, J. G.; Moore, K. T.; Ghosh, A.; Therien, M. J., Synthesis, Structure, Electronic Spectroscopy, Photophysics, Electrochemistry, and X-ray Photoelectron Spectroscopy of Highly-Electron-Deficient [5,10,15,20-Tetrakis(perfluoroalkyl)porphinato]zinc(II) Complexes and Their Free Base Derivatives. *J. Am. Chem. Soc.* **1996**, 118, (35), 8344-8354.

43.	Moore, K. T.; Fletcher, J. T.; Therien, M. J., Syntheses, NMR and EPR Spectroscopy, Electrochemical Properties, and Structural Studies of [5,10,15,20-Tetrakis(perfluoroalkyl)porphinato]iron(II) and -iron(III) Complexes. *J. Am. Chem. Soc.* **1999**, 121, (22'), 5196-5209.

44.	Tsuchiya, S. J.; Seno, M., *Chem. Lett.* **1989**, 236.

45.	Grancho, J. C. P.; Pereira, M. M.; Miguel, M. D. G.; Gonsalves, A. M. R.; Burrows, H. D., Synthesis, spectra and photophysics of some free base tetrafluoroalkyl and tetrafluoroaryl porphyrins with potential applications in imaging. *Photochem. Photobiol.* **2002**, 75, (2), 249-256.

46.	Chen, L.; Jin, L.-M.; Guo, C.-C.; Chen, Q.-Y., Fluoroalkylation of Porphyrins: generation of 2- and 20-Perfluoroalkyl-5,10,15-triarylporphyrin Radicals and their Intramolecular Cyclizations. *Synlett* **2005**, (6), 963-970.

47.	Zeng, Z.; Liu, C.; Jin, L.-M.; Guo, C.-C.; Chen, Q.-Y., Unexpected Intramolecular Cyclization of 2-(Perfluoroalkyl)tetraarylporphyrin Radicals: Approaches for the Intramolecular Cyclization of 2-(Perfluoroalkyl)tetraarylporphyrin Radicals. *Eur. J. Org. Chem.* **2005**, (2), 306-316.

48.	Van Berkel, G. J.; McLuckey, S. A.; Glish, G. L., Electrochemical origin of radical cations observed in electrospray ionization mass spectra. *Anal. Chem.* **1992**, 56, 1586 - 1593.

49.	Rosell-Melé, A.; Carter, J. F.; Maxwell, J. R., High-Performance Liquid Chromatography-Mass Spectrometry of Porphyrins by Using an Atmospheric Pressure Interface. *J. Am. Soc. Mass Spectrom.* **1996**, 7, (9), 965-971.

50.	Cole, R. B., Some tenets pertaining to electrospray ionization mass spectrometry. *J. Mass. Spectrom.* **2000**, 35, 763-772.

51.	Lau, K. S. F.; Sadilek, M.; Khalil, G. E.; Gouterman, M. P.; Brückner, C., Observation of Novel Porphyrinoid Structures During the ESI Mass Spectrometric Analysis of meso-Phenylporpholactone and meso-Pentafluorophenyl-substituted Porphyrins, Porpholactones, and Corroles. *Chem. – Eur. J.* **2005**, submitted.

Chapter 4 - Experimental

Section 1: General

The analytical TLC plates were Silicycle ultra pure silica gel 60 (aluminum backed, 250 μm); preparative TLC plates (500 μm silica gel on glass) and the flash column silica gel (standard grade, 60Å, 32-63 μm) used were provided by Sorbent Technologies, Atlanta, GA. ^{1}H and ^{13}C NMR spectra were recorded on a Bruker DRX400 and were referenced to residual solvent peaks. UV-vis spectra were recorded on Cary 50 spectrophotometer and on a Hewlett Packard 8452A Diode Array spectrophotometer. IR spectra were recorded on a Perkin-Elmer Model 834 FT-IR. X-ray crystallography was done by Matthias Zeller of Youngstown State University, Ohio.

TPPH$_2$ X,[15] **TTSL X,**(a) K. K. Lara, C. R. Rinaldo, C. Brückner, Tetrahedron Lett. 2003, 44, 7793. (b) K. K. Lara, C. K. Rinaldo, C. Brückner, Tetrahedron 2005, 61, 2529. and **TPCH$_2$ X**[108] were synthesized according to literature methods. **TFPPH$_2$ X** and **TFPPPt X** were purchased from Frontier Science, Inc., Logan, UT, USA.

Section 2: Density Functional Theory

This work was assisted by Professor Wes Borden and Dr. Dave Hrovat (formerly University of Washington, currently University of North Texas). All molecular geometries were optimized at the local DFT level (LDA or GGA). Beckke's time dependent hybrid exchange-correlation functional, DFT(B3LYP)/6-31G*, was used to calculate the lowest excited singlet states of the new porphyrin and lactone derivatives. The calculations have been preformed in the *ikazkiol* network at the University of Washington using the program *Gaussian 03*. Data visualization was accomplished using the Molden visualization program.

Section 3: Near-IR Spectrometry

This work was done in collaboration with Dr. Steffen Jockusch and Dr. Nicholas Turro of Columbia University New York. All porphyrin compounds were synthesized as described in Chapters 2.

Near IR emission spectra were recorded on a modified SPEX Fluorolog 2 (J. Y. Horiba, Edison, NJ) equipped with a liquid nitrogen cooled Ge diode detector (EO817L; North Coast Scientific Corp.). As excitation source a 450 W Xe-lamp (Osram) in conjunction with a double-grating monochromator was used. Emission spectra were recorded at 77 K employing a liquid nitrogen filled dewar and pyrex NMR tubes (4 mm diameter).

Section 4: Phosphorescent Lifetime

This work was done in collaboration with Dr. Steffen Jockusch and Dr. Nicholas Turro of Columbia University New York. All porphyrin compounds were synthesized as described in Chapters 2

Phosphorescence lifetimes were measured using the pulses from a Lambda Physik dye laser (FL3002; Laser dyes: Stilbene 3 or BiBuQ), which was pumped with a Lambda Physik Excimer laser (Lextra). The phosphorescence was collected and isolated using lenses and monochromators (H10 for Vis spectral range and 1681B for NIR spectral range; Jobin-Yvon Inc.) and focused into Hamamatzu photomultiplier tubes (PMT) (R928 for Vis spectral range and H9170-45 for NIR spectral range). The photocurrent from the PMT was amplified (SR 560, Stanford Research Systems) and stored on a digital oscilloscope (TDS 360, Tektronix). The lifetimes were determined at 77 K employing a liquid nitrogen filled dewar and pyrex NMR tubes (4 mm diameter).

Section 5: Mass Spectrometry

All mass spectrometry data were obtained using an ion trap mass spectrometer EsquireLC (Bruker Daltonics, Billerica, MA, USA) with electrospray ionization source. Samples were dissolved in spectral grade CH_2Cl_2 and diluted in CH_3CN to approximate

μM concentrations. This solution was directly infused into the ion source at a flow rate of 1 μL/min. Spectra were collected in both positive and negative ionization mode using identical solutions. The standard tune parameters were similar for both modes: Capillary voltage 3500 - 4000 V, Δ endplate 500 V, capillary offset 70 V, skimmer 1 set to 30 V, skimmer 2 set to 4 V, octupole 3 V and octupole Δ 2 V, trap drive 55-75 V, ion charge control (ICC) on and target 25,000 (10,000 in negative mode for better isotope resolution), nebulizer gas (N_2) 12 psi, drying gas (N_2) 5 l/min, drying temperature 250 °C. The fragmentation spectra of the analytes were collected with an isolation width of 4 amu, fragmentation amplitude set to 1 volt and SmartFrag On (amplitude automatically varies to 30-200 % of the set fragmentation amplitude of 1 V). The accuracy of the data is ± 0.3 amu.

Section 6: Dihydroxychlorin and Tetrahydroxybacterio- and isobacteriochlorin via OsO₄ Oxidation

meso-tetrakisphenyl-2,3-dihydroxychlorin osmate ester, osmate-(OH)₂TPCH₂ (2.2a) was synthesized in 50% yield according to literature methods.[109] **2.2a** appears brown-purple in color: R_f (silica- CH_2Cl_2/2.5% MeOH) 0.4; UV-vis (CHCl₃) λ_{max} 418, 518, 545, 594, 648 nm; fluorescence (MCH, 77K) at 642, 706 nm (excitation at 405 nm).

meso-Tetrakisphenyl-2,3-dihydroxychlorin, (OH)₂TPCH₂ (2.4a), was synthesized in 50% yield according to literature methods.[109] **2.4a** appears brown-purple in color when wet, upon drying brown: R_f (silica- CH_2Cl_2) 0.2, (silica- CH_2Cl_2/2.5% MeOH) 0.86; ¹H NMR (400 MHz, CDCl₃) δ ppm -1.76--1.87 (m, 1H), -0.03 (s, 1H), 0.91-0.81 (m, 1H), 1.20 (dd, J = 21.14, 14.12 Hz, 1H), 1.54 (s, 1H), 2.06-1.97 (m, 1H), 2.14 (s, 1H), 3.19-3.08 (m, 1H), 3.50-3.41 (m, 1H), 3.69 (q, J = 7.00, 6.99, 6.99 Hz, 1H), 4.36-4.28 (m, 1H), 6.39-6.29 (m, 1H), 7.01-6.92 (m, 1H), 7.23 (s, 1H), 7.78-7.59 (m, 1H), 7.97-7.85 (m, 1H), 8.20-7.99 (m, 1H), 8.35-8.24 (m, 1H), 8.45 (s, 1H), 8.66-8.55 (m, 1H); UV-vis (CHCl₃) λ_{max} 404, 514, 539, 593, 646 nm; fluorescence (MCH, 77K) at 644, 710 nm (excitation at 406 nm); MS (ESI(+), 250 °C) 663 m/z.

meso-tetrakisphenyl-2,3,12,13-tetrahydroxybacteriochlorin   osmate   ester,
(trans isomer) osmate-(OH)₄TPBCH₂ (2.3a). 2.3a was prepared in 100% yield from
the oxidation of 2.1a. 2.3a was also prepared in lower yields from 2.1a following the
elution of 2.2a.[56] 2.3a appears brown-green in color: R_f (silica- CH_2Cl_2/2.5% MeOH)
0.28; UV-vis (CHCl₃) λ_{max} 420, 534, 706 nm.

meso-tetrakis(pentafluorophenyl)-2,3-dihydroxychlorin   osmate   ester,
osmate-(OH)₂TFPCH₂ (2.2b). TFPPH₂ 2.1b (1.0 g, 1.03 X 10⁻³ mol) was dissolved in
freshly distilled, ethanol-stabilized CHCl₃/20% pyridine (30 mL) and was treated with
OsO_4 (500 mg, 2 equiv.). The reaction flask was stoppered, stirred at ambient
temperature, and shielded from ambient light with aluminum foil for 3 days. The
reaction was then quenched by rotary evaporation to dryness. The product was
redissolved in CHCl₃ and purified by flash chromatography. The first fraction, osmate-
(OH)₂TFPCH₂ (2.2b), was eluted with CHCl₃ (1.01 g, 7.03 X 10⁻⁴ mol, 71% yield). Slow
diffusion of petroleum ether into a CHCl₃ solution of (2.2b) yielded olive-green crystals
for x-ray crystallography: R_f (silica- CH_2Cl_2/2.5% MeOH) 0.1; ¹H NMR (400 MHz,
CDCl₃) δ ppm -2.03 (s, 1H), -0.02 (s, 1H), 0.92-0.77 (m, 1H), 1.24 (s, 1H), 1.66 (s, 1H),
2.06-1.98 (m, 1H), 2.19-2.10 (m, 1H), 2.63-2.55 (m, 1H), 6.94 (s, 1H), 7.42-7.12 (m,
1H), 7.54-7.45 (m, 1H), 7.65 (s, 1H), 7.81 (t, J = 7.51, 7.51 Hz, 1H), 8.76-8.35 (m, 1H);
¹³C NMR (400 MHz, CDCl₃) δ ppm 93.3, 95.3, 96.1, 100.5, 102.4, 105.1, 107.4, 108.5,
109.6, 113.5, 123.7, 124.0, 125.0, 127.4, 128.4, 132.2, 135.3, 136.0, 140.2, 140.5, 141.3,
141.8, 141.9, 149.3, 149.7, 150.9, 152.6, 154.0, 155.7, 158.2, 165.9; UV-vis (CHCl₃) λ_{max}
408, 505, 535, 598, 650 nm; fluorescence (EtOH, 77K) at 642, 708 nm (excitation at 400
nm).

meso-tetrakis(pentafluorophenyl)-2,3,12,13-tetrahydroxybacteriochlorin
osmate ester, (trans isomer) osmate-(OH)₄TFPBCH₂ (2.3b). 2.3b was prepared in
100% yield from the oxidation of 2.1b. 2.3b was also prepared in lower yields from 2.1b

following the elution of **2.2b**. Slow diffusion of petroleum ether into a CHCl₃ solution of **(2.3b)** yielded light-green crystals for x-ray crystallography: R_f (silica- CH_2Cl_2/2.5% MeOH) 0.03; ^1H NMR (400 MHz, CDCl₃) δ ppm -2.08--2.22 (m, 1H), -0.16--0.25 (m, 1H), 0.03--0.15 (m, 1H), 0.13-0.05 (m, 1H), 0.89-0.76 (m, 1H), 1.07-0.93 (m, 1H), 1.18 (s, 1H), 1.75-1.66 (m, 1H), 1.97-1.81 (m, 1H), 2.03 (s, 1H), 2.45 (td, J = 3.66, 1.81, 1.81 Hz, 1H), 2.72-2.64 (m, 1H), 2.88-2.80 (m, 1H), 2.99-2.89 (m, 1H), 3.63-3.03 (m, 1H), 4.06 (q, J = 5.25, 5.25, 5.25 Hz, 1H), 4.31 (t, J = 5.08, 5); UV-vis (CHCl₃) λ_{max} 378, 509, 712 nm; fluorescence (EtOH, 77K) at 642, 708 nm (excitation at 372 nm).

[*meso*-tetrakisphenyl-2,3-dihydroxychlorinato]Pt(II), (OH)₂TPCPt (2.4a). **2.4a** was synthesized according to literature methods.[109] **2.4a** appears dark pink in color: R_f (silica- CH_2Cl_2/2.5% MeOH) 0.77; ^1H NMR (400 MHz, CDCl₃) δ ppm -0.03 (s, 1H), 1.29-1.10 (m, 1H), 1.52 (s, 1H), 2.14 (s, 1H), 3.14-3.03 (m, 1H), 3.69 (dd, J = 13.74, 6.78 Hz, 1H), 6.27 (d, J = 1.68 Hz, 1H), 7.23 (s, 1H), 7.53-7.44 (m, 1H), 7.65 (ddd, J = 13.07, 11.41, 7.57 Hz, 1H), 8.22-7.92 (m, 1H), 8.46-8.33 (m, 1H), 8.72 (s, 1H); UV-vis (CHCl₃) λ_{max} 397, 585 nm; phosphorescence (EtOH, 77K) at 652, 734 nm (excitation at 397 nm); τ_p (EtOH, 77 K) 92 μs (734 nm); MS (ESI(+), 250 °C) 844 m/z.

[*meso*-tetrakisphenyl-2,3,7,8-tetrahydroxyisobactiochlorinato]Pt(II); Pt-tetrahydroxyisobacteriochlorin, (OH)₄TPiBCPt (2.8a). **2.8a** was prepared in 100% yield from the oxidation of TPPPt. **2.8a** was also prepared in lower yields from TPPPt following the elution of platinum **2.2b**.[56] R_f (silica- CH_2Cl_2/2.5% MeOH) 0.38; UV-vis (CHCl₃) λ_{max} 380, 531, 568 nm; phosphorescence (EtOH, 77K) at 758, 844, 964 nm (excitation at 391 nm).

[*meso*-tetrakis(pentafluorophenyl)-2,3-dihydroxychlorinato]Pt(II) osmate ester, osmate-(OH)₂TFPCPt (2.4b). TFPPPt (0.4 g, 3.48 X 10⁻⁴ mol) was dissolved in freshly distilled, ethanol-stabilized CHCl₃/20% pyridine (20 mL) and was treated with OsO₄ (50 mg, 5.7 equiv.). The reaction flask was stoppered, stirred at ambient

temperature, and shielded from ambient light with aluminum foil for 4 days. The reaction was then quenched by rotary evaporation to dryness. The product was redissolved in CH_2Cl_2 and purified by flash chromatography. The first fraction, TFPPPt, was eluted witht 100% CH_2Cl_2. Crimson-red osmate-$(OH)_2$TFPCPt (**2.4b**), was eluted in the third fraction with 0.5% MeOH/CH_2Cl_2 (0.34 g, 2.18 X 10^{-4} mol, 63% yield): R_f (silica- CH_2Cl_2/2.5% MeOH) 0.6; ^{1}H NMR (400 MHz, CDCl$_3$) δ ppm 0.09 (s, 1H), 1.32-1.22 (m, 1H), 1.53 (s, 1H), 2.21-2.13 (m, 1H), 5.34-5.25 (m, 1H), 6.61-6.53 (m, 1H), 6.82-6.74 (m, 1H), 6.92 (s, 1H), 7.57-7.14 (m, 1H), 7.83 (t, J = 7.50, 7.50 Hz, 1H), 8.65-8.18 (m, 1H), 8.90-8.76 (m, 1H); UV-vis (CHCl$_3$) λ_{max} 391, 590 nm; phosphorescence (EtOH, 77K) at 758, 844, 964 nm (excitation at 391 nm); τ_p (EtOH, 77 K) 59 μs (758 nm).

[*meso*-tetrakis(pentafluorophenyl)-2,3,7,8-tetrahydroxyisobacterio-chlorinato]Pt(II) osmate ester, osmate-(OH)$_4$TFPiBCPt (2.8b). **2.8b** was prepared in 100% yield from the oxidation of TFPPPt. **2.8b** was also prepared in lower yields from TFPPPt following the elution of platinum **2.2a**. Slow diffusion of petroleum ether into a CHCl$_3$ solution of **2.8b** yielded cherry-red crystals for x-ray crystallography: R_f (silica-CH_2Cl_2/2.5% MeOH) 0.3; ^{1}H NMR (400 MHz, CDCl$_3$) δ ppm 0.08 (s, 1H), 1.26 (s, 1H), 1.55 (s, 1H), 2.21-2.12 (m, 1H), 3.69-3.60 (m, 1H), 6.43 (dd, J = 16.45, 7.14 Hz, 1H), 6.70-6.59 (m, 1H), 6.85-6.76 (m, 1H), 7.49-7.08 (m, 1H), 7.92-7.64 (m, 1H), 8.01 (d, J = 4.66 Hz, 1H), 8.26-8.16 (m, 1H), 8.54 (dd, J = 12.87, 5.30 Hz, 1H), 8.79-8.68 (m, 1H); ^{13}C NMR (400 MHz, CDCl$_3$) δ ppm 91.1 92.0, 93.6, 95.5, 96.7, 98.0, 98.2, 98.6, 98.8, 101.5, 102.0, 102.4, 103.8, 104.2, 105.2, 105.6, 105.8, 109.0, 110.6, 112.4, 116.8, 117.1, 120.3, 125.0, 125.0, 127.3, 131.5, 140.5, 142.5, 148.2, 149.4, 149.5, 150.0, 150.1, 151.2, 152.0, 152.6, 155.3, 159.5; UV-vis (CHCl$_3$) λ_{max} 382, 525, 568 nm; phosphorescence (EtOH, 77K) at 742, 824 nm (excitation at 380 nm); τ_p (EtOH, 77 K) 78 μs (742 nm).

Section 7: Porpholactones

meso-tetrakisphenyl-2-oxa-3-oxoporphyrin; porpholactone, (COO)TPLH$_2$ (2.5a), was synthesized in 80% yield according to literature methods.[22] 2.5a appears bright-purple in color: R$_f$ (silica- CH$_2$Cl$_2$) 0.88, (silica- CH$_2$Cl$_2$/20% pet ether) 0.54; UV-vis (CHCl$_3$) λ_{max} 415, 517, 554, 590, 642 nm; fluorescence (EtOH, 77K) at 640, 708 nm (excitation at 415 nm); MS (ESI(+), 250 °C) 633 m/z.

meso-tetrakis(pentafluorophenyl)-2-oxa-3-oxoporphyrin; porpholactone, (COO)TFPLH$_2$ (2.5b).[20] A mixture of meso-tetra(pentafluorophenyl)porphyrin 2.1b (0.5 g, 5.19x10^{-4} mol), silver nitrate (2.5 g, 1.47x10^{-2} mol), oxalic acid (5.16 g, 5.73x10^{-2} mol), and glacial acetic acid (417 mL, 7.29 mol) was brought to reflux in a round-bottom flask equipped with a magnetic stir bar and shielded from ambient light using a photochemical box. The reaction was allowed to reflux for approximately 6 hours while monitored by TLC (silica, [3:1/hexanes:CH$_2$Cl$_2$]), which produced a solution blood red in color. The solvent, glacial acetic acid, was then evaporated off by rotary evaporation. The product was dissolved in CH$_2$Cl$_2$, washed with deionized water, 10% (w/w) Na$_2$CO$_3$, then saturated NaCl. After drying, filtering, and rotary evaporation, the dark red solid residue was purified by chromatography on a silica gel column and eluted with hexanes. Hexanes/CH$_2$Cl$_2$ then eluted multiple products, including 2.5b. A second purification using silica gel column chromatography and the same solvent system gave 2.5b (0.1617 g, 1.62x10^{-4} mol, 32% yield).

Light reactions were prepared in the same fashion using a separate photochemical box, which allowed for irradiation of the reaction vessel with different wavelengths of light. The light source was a Zenon lamp, to which 400 nm, 500 nm, and 706 nm interference filters were attached in order to allow for varying wavelengths.

(COO)TFPLH$_2$ (2.5b) was also prepared in 48% yield by MnO$_4^-$ oxidation of 2.1b with CTAP in CH$_2$Cl$_2$.[22] On silica, 2.5b appears pink-red in color: ^{1}H NMR (400 MHz,

CDCl₃) δ ppm -2.09 (s, 1H), -1.80 (s, 1H), 0.13-0.04 (m, 1H), 0.88 (s, 1H), 1.40-1.16 (m, 1H), 1.56 (s, 1H), 2.18 (s, 1H), 2.45-2.32 (m, 1H), 3.88-3.79 (m, 1H), 5.71 (s, 1H), 7.26 (s, 1H), 8.63 (dd, J = 31.13, 4.67 Hz, 1H), 8.87 (ddd, J = 24.23, 15.97, 4.44 Hz, 1H); ^{13}C NMR (400 MHz, CDCl₃) δ ppm 87.34, 99.9, 102.5, 105.2, 108.8, 125.9, 127.7, 127.8, 129.9, 131.7, 133.7, 135.2, 136.3, 138.7, 138.4, 141.1, 144.9, 144.9, 145.0, 145.0, 145.0, 145.1, 147.4, 147.4, 147.5, 147.5, 154.4, 154.6, 157.0, 165.7; UV-vis (CHCl₃) λ_{max} 416, 512, 546, 592, 644 nm; fluorescence (EtOH, 77K) at 640, 708 nm (excitation at 407 nm); τ_f 6.7 ns; Φ_f 0.07 sec⁻¹; MS (ESI(-), 250 °C) 991 m/z.

[*meso*-tetrakisphenyl-2-oxa-3-oxoporphyrinato]Pt(II); Pt-porpholactone, (COO)TPLPt (2.12a). To a stirring solution of **2.5a** (150 mg, 2.37 X 10⁻⁴ mol) in 30 mL benzonitrile was added PtCl₂ (63 mg, 2.37 X 10⁻⁴ mol, 1 equiv.).(ref) Platinum insertion into (COO)TPLH₂ **2.5a** proceeded with relative ease at an 80% yield. This reaction can be accomplished using one of a variety of platinum salts (platinum (II) chloride, potassium tetrachloroplatinate (II), platinum (II) pentanedionate). **2.12a** can also be produced by MnO₄⁻ oxidation of platinum **2.4a** according to literature methods.[22] **2.12a** appears orange-red in color: R_f (silica- CH₂Cl₂/20% pet ether) 0.5; ^{1}H NMR (400 MHz, CDCl₃) δ ppm 0.01 (s, 1H), 0.98-0.87 (m, 1H), 1.26 (s, 1H), 1.55 (s, 1H), 2.18 (s, 1H), 3.54-3.44 (m, 1H), 7.26 (s, 1H), 7.56-7.43 (m, 1H), 7.84-7.56 (m, 1H), 8.17-7.86 (m, 1H), 8.72-8.41 (m, 1H); UV-vis (CHCl₃) λ_{max} 400, 525, 564 nm; fluorescence (EtOH, 77K) at 712 nm (excitation at 400 nm); MS (ESI(+), 250 °C) 826 m/z.

[*meso*-tetrakis(pentafluorophenyl)-2-oxa-3-oxoporphyrinato]Pt(II); Pt-porpholactone, (COO)TFPLPt (2.12b) was prepared by MnO₄⁻ oxidation of platinum **2.4b** with CTAP in CH₂Cl₂.[22] **2.12b** appears dark fuchsia in color: R_f (silica- CH₂Cl₂) 0.95, (silica- CH₂Cl₂/20% pet ether) 0.87; UV-vis (CHCl₃) λ_{max} 396, 536, 574 nm; fluorescence (EtOH, 77K) at 733 nm (excitation at 389 nm); τ_p 75 µs (733 nm); MS (ESI(-), 250 °C) 1184 m/z.

Section 8: Oxidation of Porpholactone to Dihydroxyporpholactone

meso-tetrakisphenyl-2,3-cis-dihydroxy-12-oxa-13-oxochlorin;

dihydroxybacteriolactone, $(OH)_2(COO)TPBLH_2$ (2.11a). $(COO)TPLH_2$ 2.5a (0.3 g, 5.0 X 10^{-4} mol) was dissolved in freshly distilled, ethanol-stabilized $CHCl_3$/20% pyridine (100 mL) and was treated with OsO_4 (250 mg, 1 X 10^{-3} mol, 2 equiv.). The reaction flask was stoppered, stirred at ambient temperature, and shielded from ambient light with aluminum foil for 2 days. The reaction was then quenched with gaseous H_2S (5.6 X 10^{-3} L) and dried under N_2. The product was redissolved in $CHCl_3$ and purified by flash chromatography. Starting material 2.5a was eluted in the first fraction with 100% $CHCl_3$. The desired product 2.11a was eluted in the second fraction with $CHCl_3$/1% MeOH and recrystalized in EtOH (approx. 100 mg, 33% yield). 2.11a appears magenta in color when wet and dries brown: R_f (silica- CH_2Cl_2/2.5% MeOH) 0.63; ^1H NMR (400 MHz, $CDCl_3$) δ ppm -1.44--1.54 (m, 1H), -1.01--1.12 (m, 1H), -0.000 (s, 1H), 0.97 (dd, J = 2.10, 1.26 Hz, 1H), 1.24 (t, J = 7.00, 7.00 Hz, 1H), 1.58 (s, 1H), 2.17 (s, 1H), 3.10-2.99 (m, 1H), 3.23-3.13 (m, 1H), 3.49 (s, 1H), 3.80-3.64 (m, 1H), 6.30-6.13 (m, 1H), 7.26 (s, 1H), 8.19-7.60 (m, 1H), 8.29 (s, 1H), 8.59-8.48 (m, 1H); UV-vis $(CHCl_3)$ λ_{max} 404, 540, 679 nm; fluorescence (MCH, 77K) at 672, 716 nm (excitation at 403 nm); MS (ESI(+), 250 °C) 889 m/z.

meso-tetrakis(pentafluorophenyl)-2,3-cis-dihydroxy-12-oxa-13-oxochlorin

osmate ester; dihydroxybacteriolactone, osmate-$(OH)_2(COO)TFPBLH_2$ (2.11b) In the same manner as 2.11a, 2.11b was prepared by OsO_4 oxidation of 2.5b. 2.11b was not quenched with gaseous H_2S but was instead rotary evaporated to dryness. The product was redissolved in $CHCl_3$ and purified by preparatory TLC (500 μM silica on glass-$CHCl_3$/2% MeOH). X appears bright red-pink in color: R_f (silica- CH_2Cl_2/2.5% MeOH) 0.28; ^1H NMR (400 MHz, $CDCl_3$) δ ppm -0.01--0.13 (m, 1H), 1.36-0.73 (m, 1H), 1.61-1.46 (m, 1H), 2.11 (s, 1H), 3.73-2.81 (m, 1H), 3.82-3.74 (m, 1H), 5.13-4.99 (m, 1H), 6.02-5.62 (m, 1H), 6.80-6.66 (m, 1H), 7.16-7.03 (m, 1H), 7.27 (d, J = 5.75 Hz, 1H), 7.99-7.59 (m, 1H), 8.49 (s, 1H); ^{13}C NMR (400 MHz, $CDCl_3$) δ ppm 90.7, 91.0, 91.7,

95.6, 95.8, 112.1, 115.8, 121.1, 123.7, 123.7, 123.8, 123.9, 125.0, 125.2, 125.3, 125.3, 130.9, 136.5, 137.3, 140.6, 140.7, 140.8, 141.0, 148.8, 148.9, 148.9, 149.0, 149.2, 149.4, 149.5, 152.1, 154.4, 156.1, 158.4, 165.0, 174.5; UV-vis (CHCl$_3$) λ_{max} 382, 505, 545 nm; fluorescence (EtOH, 77K) at 556, 598, 648 nm (excitation at 382 nm).

[*meso*-tetrakisphenyl-2,3-cis-dihydroxy-7-oxa-8-oxochlorinato]Pt(II);   Pt-dihydroxyisobacteriolactone, (OH)$_2$(COO)TPiBLPt (2.14a). 2.14a was prepared in the same way as 2.11 via OsO$_4$ oxidation of 2.12a followed by cleavage of osmate ester with H$_2$S. The product was redissolved in CHCl$_3$ and purified by preparatory TLC (2 X 500 μM silica on glass- 100% CHCl$_3$). 2.14a appears grey-blue in color: R$_f$ (silica-CH$_2$Cl$_2$/2.5% MeOH) 0.16; UV-vis (CHCl$_3$) λ_{max} 387, 542, 584 nm; phosphorescence (EtOH, 77K) at 758 nm (excitation at 397 nm); MS (ESI(-), 250 °C) 1082 m/z.

[*meso*-tetrakis(pentafluorophenyl)-2,3-cis-dihydroxy-7-oxa-8-oxochlorinato]Pt(II)   osmate   ester;   Pt-dihydroxyisobacteriolactone,   osmate-(OH)$_2$(COO)TFPiBLPt (2.14b). 2.14b was prepared in the same way as 2.14a via OsO$_4$ oxidation of 2.12b followed by rotary evaporation to dryness. The product was redissolved in CHCl$_3$ and purified by preparatory TLC (100 μM silica on glass- 100% CHCl$_3$). 2.12b appears pink-purple in color: ^{1}H NMR (400 MHz, CDCl$_3$) δ ppm 0.07 (s, 1H), 0.98-0.84 (m, 1H), 1.26 (s, 1H), 1.55 (s, 1H), 2.21-2.13 (m, 1H), 3.68-3.60 (m, 1H), 6.33-6.03 (m, 1H), 7.26 (s, 1H), 7.71-7.57 (m, 1H), 7.97-7.80 (m, 1H), 8.69-8.44 (m, 1H), 8.92-8.81 (m, 1H);   UV-vis (CHCl$_3$) λ_{max} 386, 545, 586 nm; phosphorescence (EtOH, 77K) at 758, 790, 892 nm (excitation at 387 nm); τ$_p$ (EtOH, 77K) 42 ± 1 μs (758 nm).

Section 9: Porphodilactones

meso-tetrakisphenyl-2,12-dioxa-3,13-dioxoporphyrin (C2v-isomer) and meso-tetrakisphenyl-2,13-dioxa-3,12-dioxoporphyrin   (C2h-isomer);   bacteriodilactone, mix of isomers, (COO)$_2$TPBLH$_2$ (2.15a). To a stiring solution of X (0.20 g, 3.03 X 10⁻

[4] mol) in 20 mL THF was added 18-crown-6 (13.2 mg, 4.99 X 10^{-5} mol, 0.16 equiv.). $KMnO_4$ (0.56 g, 3.54 X 10^{-3} mol, 10 equiv.) was added to the solution and the reaction mixture was allowed to stir at ambient temperature for 1 hour. The solution was filtered through a short plug of silica gel and the filter cake was washed with $CHCl_3$. The product was recrystallized in EtOH to provide 0.12 g (60% yield) of **2.15a** as a dark brown-purple solid. R_f (silica- $CHCl_3$) 0.58; ^1H NMR (400 MHz, $CDCl_3$) δ ppm -1.02--1.14 (m, 1H), -0.25--0.37 (m, 1H), -0.16 (s, 1H), 0.81-0.73 (m, 1H), 1.16-0.98 (m, 1H), 1.77-1.68 (m, 1H), 1.92-1.83 (m, 1H), 2.09-1.99 (m, 1H), 3.21 (s, 1H), 3.82 (d, J = 135.50 Hz, 1H), 7.26 (s, 1H), 7.58 (d, J = 13.07 Hz, 1H), 8.16-8.05 (m, 1H), 8.64-8.39 (m, 1H), 11.79-11.67 (m, 1H); UV-vis ($CHCl_3$) λ_{max} 406, 511, 656 nm; fluorescence (EtOH, 77K) at 648, 664 nm (excitation at 413 nm); MS (ESI(-), 250 °C) 651 m/z.

meso-tetrakis(pentafluorophenyl)-2,12-dioxa-3,13-dioxoporphyrin (C2v-isomer) and meso-tetrakis(pentafluorophenyl)-2,13-dioxa-3,12-dioxoporphyrin (C2h-isomer); bacteriodilactone, mix of isomers, $(COO)_2TFPBLH_2$ (2.15b). **2.3b** (0.21 g, 1.15 X 10^{-4} mol) was dissolved in 25 mL CH_2Cl_2. Stirring at ambient temperature and monitoring by TLC, CTAP (0.12 g, 2.90 X 10^{-4} mol, 2.5 equilv.) was added to the solution over 1 hour. The resulting solution was filtered through a short silica plug with a layer of sand on the top. The first fraction was collected separately yielding a grey-green solution. R_f (silica- $CHCl_3$) 0.93; ^1H NMR (400 MHz, $CDCl_3$) δ ppm -0.10 (s, 1H), 0.89-0.78 (m, 1H), 1.11 (s, 1H), 1.68-1.60 (m, 1H), 1.85-1.70 (m, 1H), 1.98-1.89 (m, 1H), 2.13-2.03 (m, 1H), 2.47-2.37 (m, 1H), 2.68-2.60 (m, 1H), 2.82-2.74 (m, 1H), 2.92-2.84 (m, 1H), 3.72-3.01 (m, 1H), 4.01-3.93 (m, 1H), 4.23-4.14 (m, 1H), 6.05-5.95 (m, 1H), 6.29-6.15 (m, 1H), 7.25 (s, 1H), 7.63-7.33 (m, 1H), 8.02-7.83 (m, 1H), 8.56-8.44 (m, 1H), 9.91-9.81 (m, 1H); UV-vis ($CHCl_3$) λ_{max} 406, 500, 663 nm; fluorescence (EtOH, 77K) at 642, 660, 676, 708 nm (excitation at 407 nm); MS (ESI(-), 250 °C) 1009 m/z.

[*meso*-tetrakis(pentafluorophenyl)-diporpholactonato]Pt(II) (mix of regioisomers), **(COO)₂TFPiBLPt (2.16b)**. An excess amount of CTAP is added to a stirring solution of **2.9b** dissolved in CH₂Cl₂. This reaction was allowed to stir at ambient temperature overnight. The resulting solution was filtered through a short celite plug and purified by preparatory TLC (1000 μm silica on glass- CH₂Cl₂/2.5% MeOH). **2.16b** appears light-purple in color: R_f (silica- CH₂Cl₂/2.5% MeOH) 0.87; UV-vis (CHCl₃) λ_{max} 380, 532, 572 nm; phosphorescence (EtOH, 77K) at 732, 800 nm (excitation at 389 nm); τ_p (EtOH, 77K) 69 ± 1 μs (800 nm); MS (ESI(-), 250 °C) 1201 m/z.

Notes to Chapter 4:

1. Adler, A. D. L., F.R.; Finarelli, J.D.; Goldmacher, J.; Assour, J.; Korsakoff, L., A Simplified Synthesis for meso-Tetraphenylporphyrin. *J. Org. Chem.* 1967, 32, 476.

2. (a) K. K. Lara, C. R. Rinaldo, C. Brückner, Tetrahedron Lett. 2003, 44, 7793. (b) K. K. Lara, C. K. Rinaldo, C. Brückner, Tetrahedron 2005, 61, 2529.

3. Briñas, R. P.; Brückner, C., Triarylcorroles by oxidative coupling of triaryltetrapyrranes. *Synlett* 2001, (3), 442-444.

4. Bruckner, C. R., S.J.; Dolphin, D., Formation of a meso-Tetraphenylsecochlorin and a Homoporphyrin with a Twist. *J. Org. Chem.* 1998, 63, 2094-2098.

5. Bruckner, C. D., D., beta,beta'-Dihydroxylation of meso-Tetraphenylchlorins an dMetallochlorins. *Tetrahedron Letters* 1995, 36, (52), 9425-9428.

6. McCarthy, J., R.; Jenkins, Hilary, A.; Bruckner, Christian, Free Base meso-Tetraaryl-morpholinochlorins and Porpholactone from meso-Tetraaryl-2,3-dihydroxy-chlorin. *Organic Letters* 2003, 5, (1), 19-22.

7. Gouterman, M.; Hall, R. J.; Khalil, G. E.; Martin, P. C.; Shankland, E. G.; Cerny, R. L., Tetra(pentafluorophenyl)porpholactone. *Journal of the American Chemical Society* 1989, 111, (10), 3702-7.

List of References

1.   *Singlet Oxygen: Reactions with Organic Compounds and Polymers*. Wiley: Winchester, 1978; p 331.

2.   *Phthalocyanine Properties and Applications*. VHC: New York, 1989.

3.   *The Porphyrin Handbook*. 1 ed.; Academic Press: New York, 2000; Vol. 6, 7.

4.   Adler, A.; Longo, F. R.; Finarelli, J. D.; al., e., *Journal of Organic Chemistry* **1967**, 32, 476.

5.   Adler, A. D.; Longo, F. R.; Finarelli, J. D.; Goldmacher, J.; Assour, J.; Korsakoff, L., A simplified synthesis for TPP. *J. Org. Chem.* **1967**, 32, 476.

6.   Adler, A. D. L., F.R.; Shergalis, W.J., *J. Am. Chem. Soc.* **1964**, 86, 3145-3149.

7.   Adler, A. D. L., F.R.; Finarelli, J.D.; Goldmacher, J.; Assour, J.; Korsakoff, L., A Simplified Synthesis for meso-Tetraphenylporphyrin. *J. Org. Chem.* **1967**, 32, 476.

8.   Aihara, H.; Jaquinod, L.; Nurco, D. J.; Smith, K. M., Multicarbocycle Formation Mediated by Arenoporphyrin 1,4-Diradicals: Synthesis of Picenoporphyrins. *Angew. Chem. Int. Ed.* **2001**, 40, (18), 3439-3441.

9.   Airs, R. L.; Keely, B. J., A novel approach for sensitivity enhancement in atmospheric pressure chemical ionisation liquid chromatography/mass spectrometry of chlorophylls. *Rapid Commun. Mass Spectrom.* **2000**, 14, (3), 125-128.

10.   Anderson, S.; Anderson, H. L.; Sanders, J. K. M., Selective templates: synthesis and electrospray mass spectrometry of a linear porphyrin octamer. *Angewandte Chemie* **1992**, 104, (7), 921-4 (See also Angew. Chem., Int. Ed. Engl., 1992, 31(7), 907-10).

11.   Arai, S.; Ishihara, S.; Takeoka, S.; Ohkawa, H.; Shibue, T.; Nishide, H., Stability of porphyrin-calix[4]arene complexes analyzed by electrospray ionization mass spectrometry. *Rapid communications in mass spectrometry: 2004* 18, (18), 2065-8.

12.   Arai, S.; Ishihara, S.; Takeoka, S.; Ohkawa, H.; Shibue, T.; Nishide, H., Stability of porphyrin-calix[4]arene complexes analyzed by electrospray ionization mass spectrometry. *Rapid Communications in Mass Spectrometry* **2004**, 18, (18), 2065-2068.

13.   Atkins, P. W. F., R.S., *Molecular Quantum Mechanics*. 3 ed.; Oxford University Press: Oxford, 1997; p 202-239.

14.   Ayorinde, F. O.; Hambright, P.; Porter, T. N.; Q. L. Keith, J., Use of meso-Tetrakis(pentafluorophenyl)porphyrin as a Matrix for Low Molecular Weight Alkylphenol Ethoxylates in Laser Desorption/Ionization Time-of-flight Mass Spectrometry. *Rapid Commun. Mass Spectrom.* **1999,** 13, 2474–2479.

15.   Barloy, L.; Dolphin, D.; Dupré, D.; Wijesekera, T. P. J., Anomalous Double Cyclization Reactions of β-Formylporphyrins. *J. Org. Chem.* **1994,** 59, (26), 7976-7985.

16.   Batinic-Haberle, I.; Stevens, R. D.; Fridovich, I., Electrospray mass spectrometry of isomeric tetrakis(N-alkylpyridyl)porphyrins and their manganese(III) and iron(III) complexes. *Journal of Porphyrins and Phthalocyanines* **2000,** 4, (3), 217-227.

17.   Bell, J. H.; Schairer, E. T.; Hand, L. A.; Mehta, R. D., *Ann. Rev. Fluid Mechanic* **2001,** 33, 155.

18.   Berkel, G. J. V.; Quinones, M. A.; Quirke, J. M. E., Geoporphyrin analysis using electrospray ionization-mass spectrometry. *Energy & Fuels* **1993,** 7, (3), 411 - 419.

19.   Birnbaum, E. R.; Le Lacheur, R. M.; Horton, A. C.; Tumas, W., Metalloporphyrin-catalyzed homogeneous oxidation in supercritical carbon dioxide. *J. Mol. Catal. A* 139, (1), 11-24.

20.   Birnbaum, E. R.; Schaefer, W. P.; Labinger, J. A.; Bercaw, J. E.; Gray, H. B., Electronic Structures of Halogenated Ruthenium Porphyrins. Crystal Structure of RuTFPPCl8(CO)H2O (TFPPCl8 = Octa-.beta.-chlorotetrakis(pentafluorophenyl)porphyrin). *Inorg. Chem.* **1995,** 34, (7), 1751-1755.

21.   Bowen, E. J., *Trans. Faraday Soc.* **1954,** 50, (2), 97.

22.   Bowen, E. J., *Luminescence in Chemistry.* Van Nostrand: London, 1968; p 13-14.

23.   Briñas, R. P.; Brückner, C., Triarylcorroles by oxidative coupling of triaryltetrapyrranes. *Synlett* **2001,** (3), 442-444.

24.   Brinas, R. P. T., T.; Hochstrasser, R.M.; Vinogradov, S.A., Phosphorescent Oxygen Sensor with Dendritic Protection and Two-Photon Absorbing Antenna. *J. Am. Chem. Soc.* **2005,** 127, 11851-11862.

25.   Bruckner, C.; Rettig, S. J.; Dolphin, D., Formation of a meso-Tetraphenylsecochlorin and a Homoporphyrin with a Twist. *Journal of Organic Chemistry* **1998,** 63, 2094-2098.

26.   Bruckner, C. D., D., beta,beta'-Dihydroxylation of meso-Tetraphenylchlorins an dMetallochlorins. *Tetrahedron Letters* **1995**, 36, (52), 9425-9428.

27.   Bruckner, C. D., D., 2,3-vic-Dihydroxy-meso-tetraphenylchlorins from the Osmium Tetroxide Oxidation of meso-Tetraphenylporphyrin. *Tetrahedron Letters* **1995**, 36, (19), 3295-3298.

28.   Bruckner, C. R., S.J.; Dolphin, D., Formation of a meso-Tetraphenylsecochlorin and a Homoporphyrin with a Twist. *J. Org. Chem.* **1998**, 63, 2094-2098.

29.   Chang, C. K. S., C.; Wu, W., *J. Chem. Soc., Chem. Commun.* **1986**, 1213-1215.

30.   Chen, L.; Jin, L.-M.; Guo, C.-C.; Chen, Q.-Y., Fluoroalkylation of Porphyrins: generation of 2- and 20-Perfluoroalkyl-5,10,15-triarylporphyrin Radicals and their Intramolecular Cyclizations. *Synlett* **2005**, (6), 963-970.

31.   Chen, X.; Hui, L.; Foster, D. A.; Drain, C. M., Efficient Synthesis and Photodynamic Activity of Porphyrin-Saccharide Conjugates: Targeting and Incapacitating Cancer Cells. *Biochemistry* **2004**, 43, (34), 10918-10929.

32.   Chillier, X. F. D.; Monnier, A.; Bill, H.; Guelacar, F. O.; Buchs, A.; McLuckey, S. A.; Van Berkel, G. J., A mass spectrometry and optical spectroscopy investigation of gas-phase ion formation in electrospray. *Rapid Communications in Mass Spectrometry* **1996**, 10, (3), 299-304.

33.   Cole, R. B., Some tenets pertaining to electrospray ionization mass spectrometry. *J. Mass. Spectrom.* **2000**, 35, 763-772.

34.   Cox, G. S. W., D.G., *Chem. Phys. Lett.* **1979**, 67, (2,3), 511.

35.   Crossley, M. J.; King, L. G., *J. Chem. Soc. Commun.* **1984**, 920.

36.   Crossley, M. J. H., Trevor W.; King, Lionel G., Conversion of a porphyrin into a 5,6-dihydroporphyrin. Synthesis and X-ray crystal structure of (5RS, 6SR)-5,6-dihydro-6-(methoxycarbonyl)-8-oxo-5,10,15,20-tetraphenyl-8H-7-oxaporphyrin. *Bull. Soc. Chim. Fr.* **1996**, 133, 735-742.

37.   Crossley, M. J. K., Lionel G., Novel Heterocyclic Systems from Selective Oxidation at the beta-Pyrrolic Position of Porphyrins. *J. Chem. Soc., Chem. Commun.* **1984**, 920-922.

38.   Daniell, H. W.; Brückner, C., Enantiomeric resolution of a ruffled porphyrinoid. *Angew. Chem., Int. Ed.* **2004**, 43, (13), 1688-1691.

39.   Daniell, H. W.; Williams, S. C.; Jenkins, H. A.; Brückner, C., Oxidation of meso-tetraphenyl-2,3-dihydroxychlorin: simplified synthesis of ß,ß'-dioxochlorins. *Tetrahedron Lett.* **2003**, 44, (21), 4045-4049.

40.   Danton, M.; Lim, C. K., Identification of monovinyl tripropionic acid porphyrins and metabolites from feces of patients with hereditary coproporphyria by high-performance liquid chromatography/electrospray ionization quadrupole time-of-flight tandem mass spectrometry. *Rapid Communications in Mass Spectrometry* **2004**, 18, (19), 2309-2316.

41.   DiMagno, S. G.; Dussault, P. H.; Schultz, J. A., Fluorous Biphasic Singlet Oxygenation with a Perfluoroalkylated Photosensitizer. *J. Am. Chem. Soc.* **1996**, 118, (22), 5312-5313.

42.   DiMagno, S. G.; Wertsching, A. K.; Ross2, C. R., Electronic Consequences of Nonplanar Core Conformations in Electron-Deficient Porphyrins: The Structure and Spectroscopic Properties of [5,10,15,20-Tetrakis(heptafluoropropyl)porphinato]cobalt(II). *J. Am. Chem. Soc.* **1995**, 117, (31), 8279-8280.

43.   DiMagno, S. G.; Williams, R. A.; Therien, M. J., Facile Synthesis of *meso*-Tetrakis(perfluoroalkyl)porphyrins: ... *J. Org. Chem.* **1994**, 59, 6943-6948.

44.   Domingues, M. R. M.; Domingues, P.; Reis, A.; Ferrer-Correira, A. J.; Tomé, J. P. C.; Tomé, A. C.; Neves, M. G. P. M. S.; Cavaleiro, J. A. S., Structural characterization of glycoporphyrins by electrospray tandem mass spectrometry. *J. Mass. Spectrom.* **2004**, 39, (2), 158 - 167.

45.   Domingues, M. R. M.; Marques, M. G. O. S.; Alonso, C. M. A.; Neves, M. G. P. M. S.; Cavaleiro, J. A. S.; Ferrer-Correia, A. J.; Nemirovskiy, O. V.; Gros, M. L., Unexpected fragmentation of b-substituted meso-tetraphenylporphyrins induced by high-energy collisional activation. *J. Am. Soc. Mass Spectrom.* **2002**, 13, (12), 1427-1431.

46.   Domingues, M. R. M.; S.-Marques, M. G. O.; Domingues, P.; Graça Neves, M.; Cavaleiro, J. A. S.; Ferrer-Correia, A. J., Differentiation of Positional Isomers of Nitro Meso-Tetraphenylporphyrins by Tandem Mass Spectrometry. *Am. Soc. Mass. Spectrom.* **2001**, 12, 381-384.

47.   Dougherty T., J., Photodynamic Therapy. *Photochemistry and Photobiology* **1993**, 58, (6), 895-900.

48.   Drabkin, D. L., Selected Landmarks in the History of Porphyrins and their Biological Functional Derivatives. In *The Porphyrins*, Dolphin, D., Ed. Academic Press: New York, 1978; Vol. 1, pp 29-83.

49.   Drain, C. M.; Gong, X.; Ruta, V.; Soll, C. E.; Chicoineau, P. F., Combinatorial Synthesis and Modification of Functional Porphyrin Libraries: Identification of New, Amphipathic Motifs for Biomolecule Binding. *Journal of Combinatorial Chemistry* **1999**, 1, (4), 286-290.

50.   D'Souza, F.; Deviprasad, G. R.; Zandler, M. E.; Hoang, V. T.; Klykov, A.; Van Stipdonk, M.; Perera, A.; El-Khouly, M. E.; Fujitsuka, M.; Ito, O., Spectroscopic, Electrochemical, and Photochemical Studies of Self-Assembled via Axial Coordination Zinc Porphyrin-Fulleropyrrolidine Dyads. *Journal of Physical Chemistry A* **2002**, 106, (13), 3243-3252.

51.   Dupont, A.; Gisselbrecht, J.-P.; Leize, E.; Wagner, L.; Van Dorsselaer, A., Electrospray mass spectrometry of electrochemically ionized molecules: application to the study of fullerenes. *Tetrahedron Letters* **1994**, 35, (33), 6083-6.

52.   Ege, S. N., *Organic Chemistry; Structure and Reactivity*. D.C. Health and Company: Lexington, 1994.

53.   Elgie, K. J.; Scobie, M.; Boyle, R. W., Application of combinatorial techniques in the synthesis of unsymmetrically substituted 5,15-diphenylporphyrins. *Tetrahedron Lett.* **2000**, 41, (15), 2753-2757.

54.   Falk, J. E., *Porphyrins and Metalloporphyrins*. Elsevier Publishing Company: Amsterdam, 1964.

55.   Fox, S.; Boyle, R. W., First examples of intramolecular Pd(0) catalyzed couplings on ortho-iodinated meso-phenyl porphyrins. *Chem. Commun.* **2004**, (11), 1322-1323.

56.   Fujii, H., Electronic structure and reactivity of high-valent oxo iron porphyrins. *Coord. Chem. Rev.* **2002**, 226, 51-60.

57.   Fukushima, K.; Funatsu, K.; Ichimura, A.; Sasaki, Y.; Suzuki, M.; Fujihara, T.; Tsuge, K.; Imamura, T., Synthesis and Properties of Rhodium(III) Porphyrin Cyclic Tetramer and Cofacial Dimer. *Inorganic Chemistry* **2003**, 42, (10), 3187-3193.

58.   Funatsu, K.; Imamura, T.; Ichimura, A.; Sasaki, Y., Novel Cofacial Ruthenium(II) Porphyrin Dimers and Tetramers. *Inorganic Chemistry* **1998**, 37, (19), 4986-4995.

59.   Furniss, B. S. H., A.J.; Smith, P.W.G.; Tatchell, A.R, *Vogel's Textbook of Pratical Organic Chemistry*. 5 ed.; Longman: 1989; p 549.

60.   Furuta, H.; Maeda, H.; Osuka, A., Doubly N-Confused Porphyrin: A New Complexing Agent Capable of Stabilizing Higher Oxidation States. *J. Am. Chem. Soc.* **2000,** 122, (5), 803-807.

61.   Ghosh, A., Ab-Initio Hartree-Fock and Local Density Functional Calculations on Prototype Halogenated Porphyrins. Do Electrochemically Measured Substituent Effects Reflect Gas-Phase Trends? *J. Phys. Chem.* **1994,** 98, 11004-11006.

62.   Ghosh, A. V., Torgil, Valence ionization potentials and cation radicals of prototype porphyrins. The remarkable performance of nonlocal density functional theory. *Theor. Chem. Acc.* **1997,** 97, 143-149.

63.   Giovannetti, R.; Bartocci, V.; Pucciarelli, F.; Ricciutelli, M., Reactions of anionic porphyrin with group 11 elements: a spectrophotometric and electrospray ionization mass spectrometry study. *Talanta* **2004,** 63, (4), 857-864.

64.   Goll, J. G.; Moore, K. T.; Ghosh, A.; Therien, M. J., Synthesis, Structure, Electronic Spectroscopy, Photophysics, Electrochemistry, and X-ray Photoelectron Spectroscopy of Highly-Electron-Deficient [5,10,15,20-Tetrakis(perfluoroalkyl)porphinato]zinc(II) Complexes and Their Free Base Derivatives. *J. Am. Chem. Soc.* **1996,** 118, (35), 8344-8354.

65.   Gouterman, M., Study of the Effects of Substituents on the Absorption Spectra of Porphyrins. *The Journal of Chemical Physics* **1959,** 30, (5), 1139-1161.

66.   Gouterman, M., *Optical spectra and electronic structure of porphyrins and related rings.* Academic Press: New York, 1978; Vol. 3, p 1-165.

67.   Gouterman, M., Oxygen quenching of luminescence of pressure sensitive paint for wind tunnel research. *Journal of Chemical Education* **1997,** 74, (6), 697-702.

68.   Gouterman, M.; Callis, J.; Dalton, L.; Khalil, G.; Mebarki, Y.; Cooper, K. R.; Grenier, M., Dual luminophor pressure-sensitive paint: III. Application to automotive model testing. *Meas. Sci. Technol.* **2004,** 15, (10), 1986-1994.

69.   Gouterman, M.; Hall, R. J.; Khalil, G. E.; Martin, P. C.; Shankland, E. G.; Cerny, R. L., Tetra(pentafluorophenyl)porpholactone. *Journal of the American Chemical Society* **1989,** 111, (10), 3702-7.

70.   Gouterman, M.; Hall, R. J.; Khalil, G. E.; Martin, P. C.; Shankland, E. G.; Cerny, R. L., Tetrakis(pentafluorophenyl)porpholactone. *Journal of the American Chemical Society* **1989,** 111, (10), 3702-7.

71.   Grancho, J. C. P.; Pereira, M. M.; Miguel, M. D. G.; Gonsalves, A. M. R.; Burrows, H. D., Synthesis, spectra and photophysics of some free base tetrafluoroalkyl and tetrafluoroaryl porphyrins with potential applications in imaging. *Photochem. Photobiol.* **2002,** 75, (2), 249-256.

72.   Greenwood, N. N. E., A, *Chemistry of the Elements.* Pergamon Press: Oxford, 1984; p 14.

73.   Gross, Z.; Galili, N.; Saltsman, I., The first direct synthesis of corroles from pyrrole. *Angew. Chem., Int. Ed.* **1999,** 38, (10), 1427-1429.

74.   Han, G.; Yang, P., Synthesis and characterization of water-insoluble and water-soluble dibutyltin(IV) porphinate complexes based on the tris(pyridinyl)porphyrin moiety, their anti-tumor activity in vitro and interaction with DNA. *Journal of inorganic biochemistry 2002* 91, (1), 230-6.

75.   Han, G.; Yang, P., Synthesis and characterization of water-insoluble and water-soluble dibutyltin(IV) porphinate complexes based on the tris(pyridinyl)porphyrin moiety, their anti-tumor activity in vitro and interaction with DNA. *Journal of Inorganic Biochemistry* **2002,** 91, (1), 230-236.

76.   Im, S. H. K., G.; Callis, J.; Ahn, B.H.; Xia, Y., Synthesis of Polystyrene Beads Loaded with Dual Luminophors for Self Referenced Oxygen Sensing. *Talanta* **2005,** 67, 492-497.

77.   Izquerido, R. A.; Barros, C. M.; Santana-Marques, M. G.; Correia, A. J. F.; Silva, A. M. G.; Tome, A. C.; Silva, A.; Neves, M. G. P. M. S.; Cavaleiro, J. A. S., Cycloreversion and other gas-phase reactions of neutral and cationic pyrrolidine-fused chlorins and isobacteriochlorins under ion bombardment and electrospray. *Rapid Commun. Mass Spectrom.* **2004,** 18, 2601-2611.

78.   Izquierdo, R. A.; Barros, C. M.; Santana-Marques, M. G.; Correia, A. J. F.; Silva, A. M. G.; Tome, A. C.; Silva, A.; Neves, M. G. P. M. S.; Cavaleiro, J. A. S., Cycloreversion and other gas-phase reactions of neutral and cationic pyrrolidine-fused chlorins and isobacteriochlorins under ion bombardment and electrospray. *Rapid Communications in Mass Spectrometry* **2004,** 18, (22), 2601-2611.

79.   Karunaratne, V.; Dolphin, D., Scavenger templates: synthesis and electrospray mass spectroscopy of a linear porphyrin octamer. *Chemtracts: Organic Chemistry* **1994,** 7, (2), 88-91.

80.   Kavandi, J. C., J.; Gouterman, M.; Khalil, G.; Wright, D.; Green, E.; Burns, D.; McLachlan, B., *Review of Scientific Instruments* **1990,** 61, 3340.

81.   Kavandi, J. L. Doctoral, University of Washington, Seattle, 1990.

82.   Khalil, G., Gouterman, M., and Green, E. Method for Measuring Oxygen Concentration. 1989.

83.   Khalil, G.; Gouterman, M.; Ching, S.; Costin, C.; Coyle, L.; Gouin, S.; Green, E.; Sadilek, M.; Wan, R.; Yearyean, J.; Zelelow, B., Synthesis and spectroscopic characterization of Ni, Zn, Pd and Pt tetra(pentafluorophenyl)porpholactone with comparison to Mg, Zn, Y, Pd and Pt metal complexes of tetra(pentafluorophenyl)porphine. *J. Porphyrins Phthalocyanines* **2002**, 6, (2), 135-145.

84.   Khalil, G. C., C.; Crafton, J.; Grenoble, S.; Gouterman, M.; Callis, J.; Dalton, L.R., *Sensor and Actuators* **2002**, (97), 13-21.

85.   Khalil, G. E.; Costin, C.; Crafton, J.; Jones, G.; Grenoble, S.; Gouterman, M.; Callis, J. B.; Dalton, L. R., Dual-luminophor pressure-sensitive paint I. Ratio of reference to sensor giving a small temperature dependency. *Sens. Actuators, B* **2004**, 97, (1), 13-21.

86.   Khalil, G. E.; Lau, K.; Phelan, G. D.; Carlson, B.; Gouterman, M.; Callis, J. B.; Dalton, L. R., Europium beta-diketonate temperature sensors: Effects of ligands, matrix, and concentration. *Review of Scientific Instruments* **2004**, 75, (1), 192-206.

87.   Kimura, F. K., G.; Zettsu, N.; Xia, Y.; Callis, J.; Gouterman, M.; Dalton, L.; Dabiri, D.; Rodriguez, M., Dual Luminophore Polystyrene Microspheres for Pressure Sensitive Luminescent Imaging. *Measurent Sci. Tech.* **2006**, in press.

88.   Koch, W. H., Max C., *A Chemist's Guide to Density Functional Theory*. 2nd ed.; Wiley-VCH: New York, 2000.

89.   Lau, K. S. F.; Sadilek, M.; Khalil, G. E.; Gouterman, M.; Brückner, C., Tandem ESI Mass Spectrometric Analysis of meso-Tetrakis(heptafluoropropyl)-porphyrin. *J. Am. Soc. Mass Spectrom.* **2005**, 16, (12), 1915-1920.

90.   Lau, K. S. F.; Sadilek, M.; Khalil, G. E.; Gouterman, M. P.; Brückner, C., Observation of Novel Porphyrinoid Structures During the ESI Mass Spectrometric Analysis of meso-Phenylporpholactone and meso-Pentafluorophenyl-substituted Porphyrins, Porpholactones, and Corroles. *Chem. – Eur. J.* **2005**, submitted.

91.   Lau, R. L. C.; Jiang, J.; Ng, D. K. P.; Chan, T. W. D., Fourier transform ion cyclotron resonance studies of lanthanide(III) porphyrin-phthalocyanine heteroleptic sandwich complexes by using electrospray ionization. *Journal of the American Society for Mass Spectrometry* **1997**, 8, (2), 161-169.

92.   Lindsey, J. S., Synthesis of *meso*-Substituted Porphyrins. In *The Porphyrin Handbook*, Guilard, R., Ed. Academic Press: San Diego, 2000; Vol. 1, pp 45-118.
93.   Lindsey, J. S. S., I.C., *Tetrahedron Lett.* **1986,** 27, (4969-4970).

94.   Lindsey, J. S. S., I.C.; Hsu, H.C.; Kearney, P.C.; Marguerettaz, A.M., *J. Org. Chem.* **1987,** 52, 827-836.

95.   Ma, L.; Song, F.; Liu, Z.; Liu, S., Investigation of metalloporphyrins and their imidazole complexes using electrospray ionization mass spectrometry. *Fenxi Huaxue* **2001,** 29, (5), 573-576.

96.   Maeda, H.; Osuka, A.; Ishikawa, Y.; Aritome, I.; Hisaeda, Y.; Furuta, H., N-Confused Porphyrin-Bearing meso-Perfluorophenyl Groups: A Potential Agent That Forms Stable Square-Planar Complexes with Cu(II) and Ag(III). *Org. Lett.* **2003,** 5, (8), 1293-1296.

97.   Mahammed, A.; Goldberg, I.; Gross, Z., Highly Selective Chlorosulfonation of Tris(pentafluorophenyl)corrole as a Synthetic Tool for the Preparation of Amphiphilic Corroles and Metal Complexes of Planar Chirality. *Org. Lett.* **2001,** 3, (22), 3443-3446.

98.   Mahammed, A.; Weaver, J. J.; Gray, H. B.; Abdelas, M.; Gross, Z., How acidic are corroles and why? *Tetrahedron Lett.* **2003,** 44, 2077-2079.

99.   McCarthy, J., R.; Jenkins, Hilary, A.; Bruckner, Christian, Free Base meso-Tetraaryl-morpholinochlorins and Porpholactone from meso-Tetraaryl-2,3-dihydroxy-chlorin. *Organic Letters* **2003,** 5, (1), 19-22.

100.   McCarthy Jason, R.; Jenkins Hilary, A.; Bruckner, C., Free base meso-tetraaryl-morpholinochlorins and porpholactone from meso-tetraaryl-2,3-dihydroxy-chlorin. *Organic letters* **2003,** 5, (1), 19-22.

101.   McCarthy, J. R. Novel Macrocycles by Modification of the beta, beta'–Position of Porphyrins. PhD, University of Connecticut, Storrs, 2003.

102.   McCarthy, J. R.; Hyland, M. A.; Brückner, C., Indaphyrin, a meso-tetraphenylsecochlorin-derived chromophore incorporating o-phenyl-to-ß-linkages. *Chem. Commun.* **2003,** (14), 1738-1739.

103.   McCarthy, J. R.; Hyland, M. A.; Brückner, C., Synthesis of indaphyrins: meso-tetraarylsecochlorin-based porphyrinoids containing direct o-phenyl-to-ß-linkages. *Org. Biomol. Chem.* **2004,** 2, (10), 1484-1491.

104. McCarthy, J. R.; Melfi, P. J.; Capetta, S. H.; Brückner, C., Use of Ag(II) as a removable template in porphyrin chemistry: diol cleavage products of [meso-tetraphenyl-2,3-cis-diolchlorinato]silver(II). *Tetrahedron* **2003,** 59, (46), 9137-9146.

105. McGraw, C., et al., *Rev. Sci. Instruments* **2003,** 74, 5260-66.

106. Mebarki, Y., In The Institute for Aerospace Research, NRC.: Ottawa, Canada, 2004.

107. Milgrom, L. R., *The Colors of Life.* Oxford University Press: Oxford, 1997.

108. Minaev, B. A., H., Spin uncoupling in molecular hydrogen activation by platinum clusters. *J. Mol. Catalysis A: Chemical* **1999,** 148, (1), 179-195.

109. Moore, K. T.; Fletcher, J. T.; Therien, M. J., Syntheses, NMR and EPR Spectroscopy, Electrochemical Properties, and Structural Studies of [5,10,15,20-Tetrakis(perfluoroalkyl)porphinato]iron(II) and -iron(III) Complexes. *J. Am. Chem. Soc.* **1999,** 121, (22`), 5196-5209.

110. Pandey, R. K., Recent advances in photodynamic therapy. *Journal of Porphyrins and Phthalocyanines* **2000,** 4, 368-373.

111. Paolesse, R.; Mini, S.; Sagone, F.; Boschi, T.; Jaquinod, L.; Nurco, D. J.; Smith, K. M., 5,10,15-Triphenylcorrole: a product from a modified Rothemund reaction. *Chem. Commun.* **1999,** (14), 1307-1308.

112. Parusel, A. B. J. G., Abhik, Density Functional Theory Based Configuration Interaction Calculations on the Electronic Spectra of Free-Base Porphyrin, Chlorin, Bacteriochlorin, and cis- and trans-Isobacteriochlorin. *J. Phys. Chem. A* **2000,** 104, 2504-2507.

113. Pasetto, P.; Chen, X.; Drain, C. M.; Franck, R. W., Synthesis of hydrolytically stable porphyrin C- and S-glycoconjugates in high yields. *Chem. Commun.* **2001,** 81-82.

114. Phillips, D., *Polymer Photophysics.* Chapman and Hall: London, 1985; p 12.

115. Quirke, J. M. E., Mass Spectrometry of Porphyrins and Metalloporphyrins. In *The Porphyrin Handbook,* Guilard, R., Ed. Academic Press: San Diego, 2000; Vol. 7, pp 371-426.

116. Rodgers, R. P.; Hendrickson, C. L.; Emmett, M. R.; Marshall, A. G.; Greaney, M.; Qian, K., Molecular characterization of petroporphyrins in crude oil by electrospray ionization Fourier transform ion cyclotron resonance mass spectrometry. *Canadian Journal of Chemistry* **2001,** 79, (5/6), 546-551.

117.   Rosell-Mele, A.; Carter, J. F.; Maxwell, J. R., High-performance liquid chromatography-mass spectrometry of porphyrins by using an atmospheric pressure interface. *Journal of the American Society for Mass Spectrometry* **1996**, 7, (9), 965-971.

118.   Rosell-Melé, A.; Carter, J. F.; Maxwell, J. R., High-Performance Liquid Chromatography-Mass Spectrometry of Porphyrins by Using an Atmospheric Pressure Interface. *J. Am. Soc. Mass Spectrom.* **1996**, 7, (9), 965-971.

119.   Rosenthal, J.; Pistorio, B. J.; Chng, L. L.; Nocera, D. G., Aerobic Catalytic Photooxidation of Olefins by an Electron-Deficient Pacman Bisiron(III) -Oxo Porphyrin. *J. Org. Chem.* **2005**, 70, (5), 1885 - 1888.

120.   Rothemund, P. J., *J. Am. Chem. Soc.* **1936**, 58, 625-627.

121.   Ryeng, H. G., Abhik, Do Nonplanar Distortions of Porphyrins Bring about Strongly Red-Shifted Electronic Spectra? Controversy, Consensus, New Developments, and Relevance to Chelatases. *J. Am. Chem. Soc.* **2002**, 124, 8099-8103.

122.   Shaw, S. J.; Elgie, K. J.; Edwards, C.; Boyle, R. W., Mono-(pentafluorophenyl)porphyrins - useful intermediates in the regioselective synthesis of multifunctionalized porphyrins. *Tetrahedron Lett.* **1999**, 40, (8), 1595-1596.

123.   Shin, J.-Y.; Furuta, H.; Osuka, A., N-Fused Pentaphyrin. *Angew. Chem. Int. Ed.* **2001**, 40, (3), 619-621.

124.   Siegel, M. M.; Tabei, K.; Tsao, R.; Pastel, M. J.; Pandey, R. K.; Berkenkamp, S.; Hillenkamp, F.; de Vries, M. S., Comparative mass spectrometric analyses of Photofrin oligomers by fast atom bombardment mass spectrometry, UV and IR matrix-assisted laser desorption/ionization mass spectrometry, electrospray ionization mass spectrometry and laser desorption/jet-cooling photoionization mass spectrometry. *Journal of mass spectrometry:* **1999**, (6), 661-9.

125.   Siegel, M. M.; Tabei, K.; Tsao, R.; Pastel, M. J.; Pandey, R. K.; Berkenkamp, S.; Hillenkamp, F.; De Vries, M. S., Comparative mass spectrometric analyses of photofrin oligomers by fast atom bombardment mass spectrometry, UV and IR matrix-assisted laser desorption/ionization mass spectrometry, electrospray ionization mass spectrometry and laser desorption/jet-cooling photoionization mass spectrometry. *Journal of Mass Spectrometry* **1999**, 34, (6), 661-669.

126.   Silva, A. M. G.; Tome, A. C.; Neves, M. G. P. M. S.; Silva, A. M. S.; Cavaleiro, J. A. S., meso-Tetraarylporphyrins as dipolarophiles in 1,3-dipolar cycloaddition reactions. *Chem. Commun.* **1999**, 1767-1768.

127. Silva, E. M. P.; Domingues, M. R. M.; Barros, C.; Faustino, M. A. F.; Tomé, J. P. C.; Neves, M. G. P. M. S.; Tomé, A. C.; Santana-Marques, M. G.; Cavaleiro, J. A. S.; Ferrer-Correia, A. J., Characterization of dinitroporphyrin zinc complexes by electrospray ionization tandem mass spectrometry. Unusual fragmentations of -(1,3-dinitroalkyl) porphyrins. *J. Mass. Spectrom.* **2005,** 40, (1), 117-122.

128. Simkhovich, L.; Galili, N.; Saltsman, I.; Goldberg, I.; Gross, Z., Coordination Chemistry of the Novel 5,10,15-Tris(pentafluorophenyl)corrole: Synthesis, Spectroscopy, and Structural Characterization of Its Cobalt(III), Rhodium(III), and Iron(IV) Complexes. *Inorg. Chem.* **2000,** 39, (13), 2704-2705.

129. Skoog, D. A. H., J.F.; Nieman, T.A., *Principles of Instrumental Analysis.* 5 ed.; Harcourt Brace and Company: Philadelphia, 1998; p 365-376.

130. Spellane, P. J.; Gouterman, M.; Antipas, A.; Kim, S.; Liu, Y. C., Porphyrins. 40. Electronic spectra and four-orbital energies of free-base, zinc, copper, and palladium tetrakis(perfluorophenyl)porphyrins. *Inorganic Chemistry* **1980,** 19, (2), 386-91.

131. Stern, O. V., M, *Phys. Z.* **1919,** 20, 183.

132. Sternberg, E. D.; Dolphin, D.; Bruckner, C., Porphyrin-based photosensitizers for use in photodynamic therapy. *Tetrahedron* **1998,** 54, (17), 4151-4202.

133. Sternberg, E. D.; Dolphin, D.; Brückner, C., Porphyrin-based photosensitizers for use in photodynamic therapy. *Tetrahedron* **1998,** 54, (17), 4151-4202.

134. Stilts, C. E. N., M.I.; Hilmey, D.G.; Davies, S.R.; Gollnick, S.O.; Oseroff, A.R.; Gibson, S.L.; Hilf, R.; Detty, M.R., Water-Soluble, Core-Modified Porphyrins as Novel, Longer-Wavelength-Absorbing Sensitizers for Photodynamic Therapy. *J. Med. Chem* **2000,** 43, 2403-2410.

135. Sweet, I., In Univ. of Washington: Seatte, WA, 2004.

136. Tomazela, D. M.; Gozzo, F. C.; Mayer, I.; Engelmann, F. M.; Araki, K.; Toma, H. E.; Eberlin, M. N., Electrospray mass and tandem mass spectrometry of homologous and isomeric singly, doubly, triply and quadruply charged cationic ruthenated meso-(phenyl)m-(meta- and para-pyridyl)n (m + n = 4) macrocyclic porphyrin complexes. *Journal of Mass Spectrometry* **2004,** 39, (10), 1161-1167.

137. Tsuchida, E.; Komatsu, T.; Yanagimoto, T., Molecular environment effect on O2 binding to lipidporphyrinatoiron(II) complexes in aqueous media. *Journal of Porphyrins and Phthalocyanines* **2000,** 4, (1), 81-87.

138. Tsuchiya, S. J.; Seno, M., *Chem. Lett.* **1989,** 236.

139. Van Berkel, G. J.; McLuckey, S. A.; Glish, G. L., Electrospray ionization of porphyrins using a quadrupole ion trap for mass analysis. *Anal. Chem.* **1991,** 63, (11), 1098-1109.

140. Van Berkel, G. J.; McLuckey, S. A.; Glish, G. L., Electrochemical origin of radical cations observed in electrospray ionization mass spectra. *Anal. Chem.* **1992,** 56, 1586 - 1593.

141. Van Berkel, G. J.; Quinones, M. A.; Quirke, J. M. E., Geoporphyrin analysis using electrospray ionization-mass spectrometry. *Energy & Fuels* **1993,** 7, (3), 411-19.

142. Vandell, V. E.; Limbach, P. A., Characterization of the electrospray mass spectrometry behavior of porphyrins. *Book of Abstracts, 211th ACS National Meeting, New Orleans, LA, March 24-28* **1996,** ANYL-052.

143. Vandell, V. E.; Limbach, P. A., Electrospray ionization mass spectrometry of metalloporphyrins. *J. Mass Spectrom.* **1998,** 33, (3), 212-220.

144. Witowska-Jarosz, J.; Gorski, L.; Malinowska, E.; Jarosz, M., Mass spectrometric investigation of gallium and zirconium complexes with octaethylporphyrin and tetraphenylporphyrin. *Journal of Mass Spectrometry* **2002,** 37, (12), 1236-1241.

145. Witowska-Jarosz, J.; Gorski, L.; Malinowska, E.; Jarosz, M., Electrospray mass spectrometric investigation of the influence of the nature of mobile phase on the ionization of gallium and zirconium porphyrins. *Journal of Mass Spectrometry* **2003,** 38, (12), 1265-1266.

146. Zelelow, B., Memorandum. In Seattle, 2002.

147. Zelelow, B.; Khalil, G. E.; Phelan, G.; Carlson, B.; Gouterman, M.; Callis, J. B.; Dalton, L. R., Dual luminophor pressure sensitive paint II. Lifetime based measurement of pressure and temperature. *Sensors and Actuators, B: Chemical* **2003,** B96, (1-2), 304-314.

148. Zeller, M., In Youngstown State University, Ohio, 2006.

149. Zeng, Z.; Liu, C.; Jin, L.-M.; Guo, C.-C.; Chen, Q.-Y., Unexpected Intramolecular Cyclization of 2-(Perfluoroalkyl)tetraarylporphyrin Radicals: Approaches for the Intramolecular Cyclization of 2-(Perfluoroalkyl)tetraarylporphyrin Radicals. *Eur. J. Org. Chem.* **2005,** (2), 306-316.

150. Zhao, L. *Singlet Oxygen*; B-180 ML; University of Iowa, Department of Radiology: Iowa City, February 8, 2001, 2001; 1-10.

Appendix A: Density Functional Theory

Gaussian 03 is the most recent version of the *Gaussian* series of electronic structure programs. Using DFT, *Gaussian* predicts the energies, molecular structures, and vibrational frequencies of molecular systems, along with numerous molecular properties derived from these basic computation types. These programs can be used to study molecules and reactions under a wide range of conditions, including both stable species, and compounds that are difficult or impossible to observe experimentally such as short-lived intermediates and transition structures.

The quantum mechanical approach to describe an atom uses the Schrödinger wave equation. This equation describes the kinetic and potential energies of the atom. The solution to this equation is the wavefunction Ψ. Ψ can be used to determine the energy states of the atom as well as other useful quantities. In general, Ψ is very complicated since it depends on 4N variables, 3 spatial and one spin variable for each N electron. Time is separated out for steady state solutions. One also has to account for interactions between electrons. Many chemistry, biology, and material science systems contain very large numbers of atoms and electrons making the calculation of the wavefunction too complicated. Therefore, approximations to the wave equation are chosen to handle these types of systems.

The main idea of Density Functional Theory (DFT) is to describe this more complicated type of interacting system via its density $\rho\left(\vec{r}\right)$, and not via its many-body wavefunction Ψ. For N electrons in a solid, which obey the Pauli principle and repulse each other via the Coulomb potential, this means that the basic variable of the system depends only on three degrees of freedom, the spatial coordinates x, y, and z, rather than 3*N degrees of freedom.

While DFT in principle gives a good description of ground state properties, practical applications of DFT are based on approximations for the so-called exchange-correlation potential. The exchange-correlation potential describes the effects of the Pauli principle and the Coulomb potential beyond a pure electrostatic interaction of the

electrons. Possessing the exact exchange-correlation potential means that one would have solved the many-body problem exactly, which is not feasible in solids.

Where as a *function* is the mapping of one variable onto another (e.g. $y = f(x)$, is a function mapping the variable x to y), a *functional* can be considered as a function whose argument is itself a function (e.g. $F[f(x)]$ where $F[f]$ is a functional of the function f). In DFT the "unknown universal functional" $E_{xc}[\rho]$, includes all unknown parts: the non-classical portion of the electron-electron interaction, the correction for the self-interaction, and the component of the kinetic energy covered by interacting reference frames. The quality of the DFT calculation relies on the accuracy of the chosen approximation to the unknown universal functional. With *Gaussian*, a qualitative hierarchy of functionals of ascending complexity and accuracy are chosen in order to give the best estimation of what the user wishes to calculate.[110] The three groups of functionals in this program include:

1. Local density approximations (LDA) yield accurate structural properties but frequently fails to calculate binding energies due to overbinding,

2. Gradient-corrected exchange-correlation functionals provide fairly accurate results indicated by absolute average errors (approx 5 kcal/mol for atomization energies with respect to G2 data base),

3. Hybrid functionals show the best results in many applications.

Local density approximation (LDA) locally substitutes the exchange-correlation energy density of an inhomogeneous system by that of an electron gas evaluated at the local density. While many ground state properties (lattice constants, bulk moduli, etc.) are well described in the LDA, the dielectric constant is overestimated by 10-40% in LDA compared to experiment. This overestimation stems from the neglect of a polarization-dependent exchange correlation field in LDA compared to DFT. Nonlocal density functional theory (NLDFT) is also referred to as the generalized gradient approximation (GGA). Here the local density is supplemented with information about

the gradient of the charge density to account for the non-homogeneity of the true electron density.[110]

Despite its discrepancies, LDA has been employed in numerous porphyrin electronic calculations. In agreement to electrochemical data, LDA calculations proved more favorable than Hartree-Fock theory in the calculation of valence ionization potentials of polyhalogenoporphyrins.[111] In addition, NLDFT was successfully used to calculate the valence ionization potentials of cation radicals of porphyrin type molecules of biochemical and synthetic importance.[112] Of particular interest, Ghosh and co-workers used DFT to determine if nonplanar distortions induce a bathochromatic shift in the porphyrin electron absorption spectra.

As demonstrated by Ghosh and co-workers, density functional theory based configuration interaction single calculations (DFT/SCI) has the ability to provide a reasonably accurate description of the electronic spectra of prototype porphyrin-type molecules at modest computational costs.[113] Using DFT/SCI, they were able to simulate the electronic spectra of low symmetry, complexly substituted porphyrin-type molecules. Their calculated results compared well with experiment, proving that DFT-based investigations can possibly predict many optical and photochemical properties of prototype porphyrin species. Using this methodology, we believed that DFT could help resolve our synthetic goal of designing bathochromically shifted novel porphyrin emitters.

Notes to Appendix A:

1.   Koch, W. H., Max C., *A Chemist's Guide to Density Functional Theory*. 2nd ed.; Wiley-VCH: New York, 2000.

2.   Ghosh, A., Ab-Initio Hartree-Fock and Local Density Functional Calculations on Prototype Halogenated Porphyrins. Do Electrochemically Measured Substituent Effects Reflect Gas-Phase Trends? *J. Phys. Chem.* **1994,** 98, 11004-11006.

3.   Ghosh, A. V., Torgil, Valence ionization potentials and cation radicals of prototype porphyrins. The remarkable performance of nonlocal density functional theory. *Theor. Chem. Acc.* **1997,** 97, 143-149.

4.   Parusel, A. B. J. G., Abhik, Density Functional Theory Based Configuration Interaction Calculations on the Electronic Spectra of Free-Base Porphyrin, Chlorin, Bacteriochlorin, and cis- and trans-Isobacteriochlorin. *J. Phys. Chem. A* **2000,** 104, 2504-2507.

Curriculum Vitae

EDUCATION:

2001 – 2006	**University of Washington** (Seattle, WA) Ph.D. in Organic Chemistry, March 2006 M.S. in Chemistry, June 2003
1997 – 2001	**University of Puget Sound** (Tacoma, WA) B.S. in Chemistry May 2001 Minors in Math and Biology
1993 – 1997	**Hudson's Bay High School** (Vancouver, WA) GPA 4.00, Class Rank 1 of 375

EXPERIENCE:

Fall 2003	**Head Teacher's Assistant, general chemistry, UW**
Summer-Fall 2002	**Teacher's Assistant, general chemistry, UW**
Spring 2004	**Teacher's Assistant, Instrumental Analysis, UW**
Winter 2005	**Teacher's Assistant, Instrumental Analysis, UW**
Summer 2005	**Teacher's Assistant, Quantitative Analysis, UW**
Oct. 2001-April 2002	**Lab Technician, Gouterman/Khalil group, Chemistry Dept., UW**
2000-2001	**Teacher's Assistant, general and organic chemistry, UPS**

AWARDS:

July 2004	3rd International Conference on Porphyrins and Phthalocyanines Student Scholarship
Summer 2000	Caputo Research Award
1997 – 2001	Presidential Scholarship, UPS

SELECTED PRESENTATIONS:

"Highly Stable Porphyrin Sensors," Northwest Biomechanics Symposium, Seattle, WA, May 2005.

"Highly Stable NIR Dyes for Photonic Applications: Effects of light and oxygen on the synthesis of tetra(pentafluorophenyl)porphodilactone," 3rd International Conference on Porphyrins and Phthalocyanines, New Orleans, LA, July 2004.

"Measuring oxygen pressure indirectly and directly: platinum porphyrin phosphorescence quenching and oxygen luminescence," Regional ACS Convention: Northwest Regional Meeting (NORM), Bozeman, MT, June 2003.

"Eu beta-diketonate temperature sensors: Effects of ligands, matrix, and concentration," National ACS Convention, New Orleans, LA, March 2003.

"Synthesis of a Substrate for T4 Lysozyme," Nation ACS Convention, San Diego, CA, March 2001.

PUBLICATIONS:

Lau, K. S. F.; McCarthy, J. R.; Zeller, M.; Sadilek, M.; Khalil, G. E.; Gouterman, M.; Brückner, C. "meso-Tetraphenylporpholactones II. Syntheses, Structures and Chemical Properties of Mono- and Dilactones" To be submitted to *J. Am. Chem. Soc.*

Lau, K. S. F.; Jockusch, S.; Turro, N.; McCarthy, J. R.; Frank; Birge; Khalil, G. E.; Gouterman, M.; Brückner, C. "meso-Tetraphenylporpholactones III. Photophysical Properties of Mono- and Dilactones and their Platinum(II) Complexes" To be submitted to *J. Am. Chem. Soc.*

Lau, K. S. F.; Sadilek, M.; Khalil, G. E.; Gouterman, M.; Brückner, C. "Observation of Novel Porphyrinoid Structures During the ESI Mass Spectrometric Analysis of meso-Pentafluorophenyl-substituted Porphyrins and –Corroles" submitted to *J. Am. Soc. Mass Spectrom.* Feb. 2005.

Lau, K.S.F.; Sadilek, M.; Khalil, G.E.; Gouterman, M.; Brückner, C. "Tandem ESI Mass Spectrometric Analysis of meso-Tetrakis(heptafluoropropyl)porphyrin" *J. Am. Soc. Mass Spectrom.* **2005**, 16, 1915-1920.

Khalil G.; Lau K.; Phelan G.; Carlson B.; Gouterman M.; Callis J.; Dalton L.R. "Eu beta-diketonate temperature sensors: Effects of ligands, matrix, and concentration" *Rev. Sci. Instrument* **2003**, 75, 1: 192-206.